The study of on-line process analytical methods for the determination of sodium, potassium, magnesium and calcium for the production of sterile liquid pharmaceuticals

A dissertation
submitted towards the degree
Doctor of Natural Sciences (Dr. rer. nat.)
of the Faculties of Natural Sciences and Technology of
Saarland University

submitted by
Dipl.-Chem. Afua Serwah

Saarbrücken, November 2015

Date of the defence:	July 29, 2016
Dean:	Prof. Dr.-Ing. Dirk Bähre
Examiner:	Prof. Dr. Holger Kohlmann
	PD Dr. Ralf Kautenburger
Chair:	Prof. Dr. Kaspar Hegetschweiler
Member of academic staff:	Dr. Angelika Ullrich

Declaration of original authorship

I hereby declare that this dissertation is my own original work except where otherwise indicated. All data or concepts drawn directly or indirectly from other sources have been correctly acknowledged. This dissertation has not been submitted in its present or similar form to any other academic institution either in Germany or abroad for the award of any other degree.

Saarbrücken, November 2015

Afua Serwah

Acknowledgements

My sincere gratitude goes to Prof. Dr. Holger Kohlmann, PD Dr. Ralf Kauteburger, my family and friends, Mr. Achim Rauch, all the workers in the following laboratories at Fresenius Medical Care Deutschland GmbH in St. Wendel: chemical-pharmaceutical development product and packaging, in-process control and final control, and finally, to the different companies (Deutsche Metrohm Prozessanalytik GmbH & Co. KG, Spectro Analytical Instruments GmbH, Agilent Technologies, Medizin- und Labortechnik Engineering GmbH Dresden, Analytik Jena AG, Thermo Fisher Scientific GmbH), in whose labs several measurements were carried out for this work. Thank you all for your encouragement, cooperativeness, assistance and patience, which have made this dissertation a success.

I AM VERY GRATEFUL AND GOD BLESS YOU ALL!!!

“I often say that when you can measure what you are speaking about, and express it in numbers, you know something about it; but when you cannot measure it, when you cannot express it in numbers, your knowledge is a meagre and unsatisfactory kind; it may be the beginning of knowledge, but you have scarcely, in your thoughts, advanced to the stage of Science, whatever the matter may be.” (1883)

Lord William Thomson Kelvin (1824-1907)

Contents

Abbreviations and Acronyms

(F)-AAS	(flame) atomic absorption spectrometry
AcAc	acetylacetone
AES	atomic emission spectrometry
AFS	atomic fluorescence spectrometry
c	concentration
CCD	charge-coupled device
CID	charge injection device
CIs	confidence intervals
cps	counts per second
EDL	electrodeless discharge lamp
EDTA	ethylenediamintetraacetate
EGTA	ethyleneglycoltetraacetate
EP	equivalence point
FDA	Food and Drug Administration
FIA	flow injection analysis
FMC	Fresenius medical Care
HCL	hollow-cathode lamp
HPLC	high performance liquid chromatograpy
HR-CS	high-resolution continuum-source
Hz	hertz
GDCh	German Chemical Society (Ger.: “Gesellschaft Deutscher Chemiker“)
GMP	Good Manufacturing Practice
ICAL	Intelligent Calibration Logic
ICH	International Conference of Harmonization
ICP-MS	inductively coupled plasma mass spectrometry
ICP-OES	inductively coupled plasma optical emission spectrometry
IPC	in-process control
IR	infrared
IS	internal standard
ISE	ion-selective electrode

IUPAC	International Union of Pure and Applied Chemistry
L	liter
LCL	lower control limit
LOD	low detection limit
LSL	lower specification limit
K	Kelvin
QbD	quality by design
max	maximum
min	minimum
min	minutes
mM	millimolar
mmol	millimole
mV	millivolt
NAZ	normal analytical zone
NIR (S)	near-infrared (spectroscopy)
nm	nanometer
PA	Process analytic
PAC	Process analytical chemistry
PAT	Process analytical technology
Ph. Eur.	European Pharmacopoeia
QC	quality control
RSD	Relative standard deviation
RTR	Real-time-release
SIA	sequential injection analysis
std. dev.	standard deviation
T	temperature
Tris	tris(hydroxymethyl)aminomethane
THz	terahertz
U	potential changes
UCL	upper control limit
USL	upper specification limit
UV	ultra-violet
V	volume
WFI	water for injection

1. Abstract

In this work, inductively coupled plasma optical emission spectrometry (ICP-OES) is applied for the determination of the alkaline (sodium and potassium) and the earth alkaline (calcium and magnesium) metals in dialysis solutions. In this type of samples, the above mentioned analytes are surrounded by matrix components, such as the organic substances glucose and lactate, which can interfere. Moreover, inter-element effects from the individual elements of interest are also possible.

Since the samples in this work have to be diluted and an internal standard (IS) is also necessary due to the higher precision required, a sample preparation unit is absolutely essential. With this system, the sampling and the introduction of the sample into the analytical instrument can also be carried out.

Based on these requirements, an on-line process analysis system, which consists of a sample preparation unit and the analytical instrument ICP-OES, is set up. Since the main tasks are carried out by the sample preparation unit and the analytical instrument, the applicability of these systems are to be examined individually, in compliance with the given requirements, in order to evaluate the error of each unit for a proper optimization of the on-line process analysis system.

The online process analysis system as a whole produced satisfactory results with the help of the so-called QC-standardization, i.e. correcting the measured values with a quality control (QC) standard.

1.1 Zusammenfassung

In dieser Arbeit wird die optische Emissionsspektrometrie mit induktiv gekoppeltem Plasma (ICP-OES) für die Bestimmung der alkalischen (Natrium und Kalium) und der erdalkalischen (Calcium und Magnesium) Metalle in Dialyselösungen eingesetzt. Bei dieser Art von Proben sind die oben genannten Analyten durch Matrixkomponenten wie beispielsweise die organischen Substanzen Glukose und Laktat umgeben, die sich störend auf die Analyse auswirken können. Außerdem können sich die zu bestimmenden Ionen untereinander beeinflussen.

Da die zu analysierenden Proben verdünnt werden müssen, und wegen der hohen Präzision mit einem internen Standard (IS) versehen werden müssen, ist ein Probenvorbereitungssystem unbedingt erforderlich. Mit diesem System wird außerdem die Probenahme bzw. deren Einführung in das Analysensystem realisiert.

Basierend auf diesen Anforderungen wird ein online-prozessanalytisches System aufgebaut, das aus einem Probenvorbereitungssystem und dem Analysegerät ICP-OES besteht. Da die Hauptaufgaben von dem Probenvorbereitungssystem und dem Analysegerät durchgeführt werden, wird die Anwendbarkeit dieser beiden Einheiten, unter Einhaltung der Anforderungen dieser Arbeit, einzeln untersucht, um den Fehler der jeweiligen Einheit abzuschätzen und so das Onlinesystem besser optimieren zu können.

Unter Anwendung der sog. QC-Standardisierung, Korrektur mit einem Qualitätskontrollstandard, wurden mit dem Onlineprozessanalysensystem sehr zufriedenstellende Ergebnisse erzielt.

2. Introduction and definition of task

The discovery and development of new drugs, especially for incurable diseases, which is associated with huge costs as well as patent expiries leading to lower sale prices are some of the recent challenging issues in the pharmaceutical industry. It is therefore necessary to reduce the time and cost of manufacturing in order to survive the ever-increasing competition in the global market. Moreover, due to the application of pharmaceuticals on human beings and/or animals, high quality standards such as the GMP guidelines, ICH guidelines and Ph. Eur. specifications are set by health authorities to regulate the quality assurance and the equalization of assessment criteria of these products. Consequently, the main principle by the production of pharmaceuticals is to ensure, secure and optimize the product quality. Right from the development of pharmaceuticals, analysis like the test of stability, identity and purity as well as the validation of the analytical methods are required before the products can be approved. Therefore, the quality control of drug products requires not only this regulated environment but additionally, analytical methods with higher reliability, accuracy and precision.

In view of this strict regulatory system, manufacturers in the pharmaceutical field mostly prefer the batch production process followed by an off-line analysis in the laboratory which is normally preformed at the end of the production. This method is usually time-consuming and can be very expensive under certain circumstances, especially, when the products are out of specification and have to be destroyed [1]. Therefore, a process that can be monitored and controlled in all stages is desirable.
Moreover, reducing manufacturing costs is a great possibility to cover up some development and regulatory approval costs as well as lower sales prices after patent expiries since the discovery and development of new products which helps to secure patents, is a long-lasting, complicated and very expensive process. The lifetime of a drug product from its discovery through development to a registered commercial product can last for about 10-15 years and cost over US $ 800 million to 1 billion [2]–[4].

Process analytical technology (PAT), which has been approved by the Food and Drug Administration (FDA) as a significant opportunity to facilitate and support the improvement in pharmaceutical development, manufacturing, and quality assurance through innovation in product and process development, process analysis, and process control, is a best innovation tool [5]. With the introduction of their guideline for industrial PAT as a regulatory framework in 2004, the FDA encourages the voluntary implementation of PAT into the pharmaceutical industry [5]. Moreover, process analytical chemistry (PAC) is the best alternative method to build quality into a product without applying all the principles of PAT.

The historical definition of process analytics as the chemical and physical analysis of materials in the process stream through the use of an on-line or in-line analyzer describes the analysis in a process fully automated to monitor and control it in all stages, provide constant information and thus facilitate the understanding of that process and the improvement of product quality as well as increase production rate without or with very little manual interference [3]. This is consistent with the drug quality system of the FDA which is also the first draft of the definition of QbD in the ICH Q8(R2) guideline: *quality* cannot *be tested into products; it should be built-in or should be by design* [3], [5].

Therefore, the best way to achieve high quality objectives in pharmaceutical production is with the additional implementation of effective principles and methods of innovation.

Beside the manufacturing of filter membranes, which are used in dialyzers, with a leading position worldwide, Fresenius Medical Care (FMC) also produces dialysis solutions for millions of patients around the world. Its plant in St. Wendel, which also manufactures both products, contributes greatly, with the numerous transfers of technology, innovations and product developments, to the well-being of many patients and to the success of the company.

To comply with the main principle by the production of pharmaceuticals, reduce costs and improve the global competitiveness of the company in the field of dialysis solutions, integrating PAC into the manufacturing process is one of the recent challenges of the FMC plant in St. Wendel.

Up to the present, the daily production of about 180,000 L dialysis solutions is carried out, firstly, as in a conventional pharmaceutical industry, with the batch process followed by a time-consuming off-line analysis (see Figure 2-1), which is associated with high labor costs.

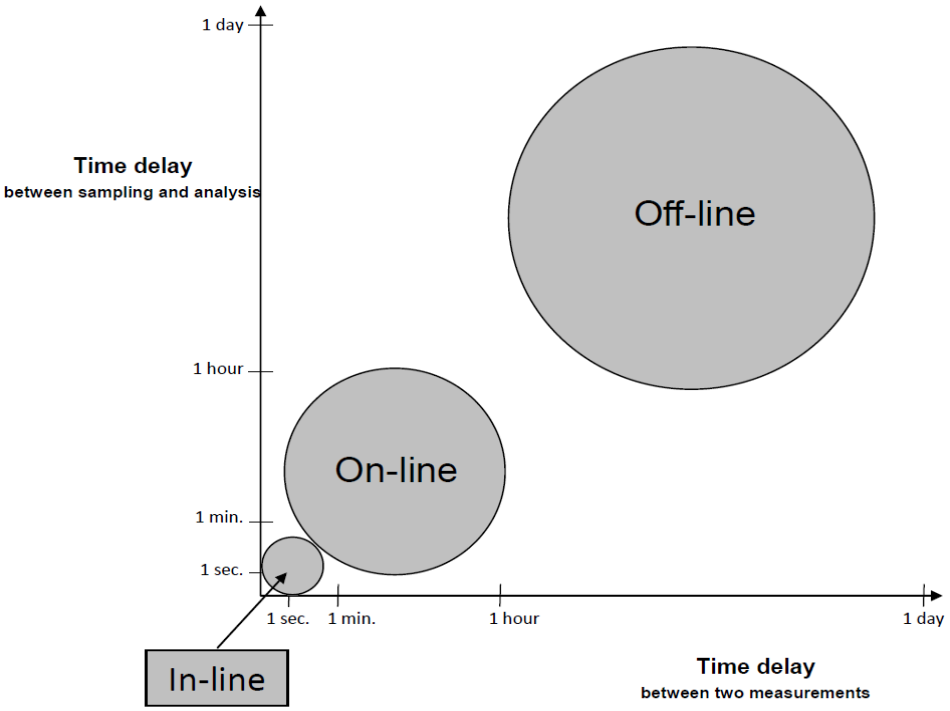

Figure 2-1: Time-consume between off-line, on-line and in-line [1]

Afterwards, they are filled automatically into solution bags, analyzed again, sterilized and then assayed finally for the batch release (see Figure 2-2).

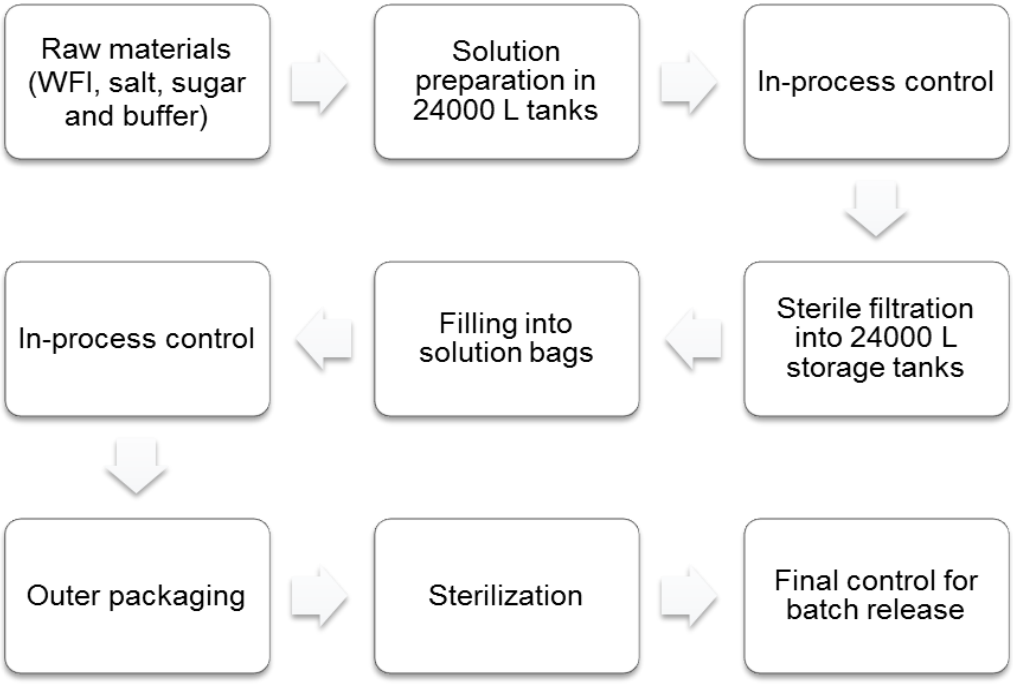

Figure 2-2: The production process of the dialysis solution

The goal of this work is therefore, the feasibility study of on-line analytical methods to replace the current laboratory analysis and so permanently monitor and control the product quality from its manufacturing till the last filling process and finally, motivate to a continuous production process. This should be accomplished in compliance with some given requirements (see Table 2-1). In this way, a time and cost efficient production together with an improvement in product quality and finally a parametric release can be achieved.

Table 2-1: Requirements to be met by the on-line process analysis system

Within the specification limits of the in-process control (IPC) for the release of a solution
Precision (relative standard deviation (RSD)) of < 1 %
Measuring time of max. 6 min for each analyte
Long-term stability
Highly robust method
Fulfill the laws for the production of pharmaceuticals (Ph. Eur., GMP, ICH guidelines, etc.)

In my diploma thesis, the on-line determination of chloride and hydrogen carbonate were studied and optimized successfully. Thus the determination of the remaining analytes (sodium, potassium, calcium, magnesium, glucose, lactate, phosphate, pH and density (see Table 2-2)) in an on-line process should be studied and evaluated [6].

The focus of this work is, therefore, on the determination of the metal ions sodium, potassium, calcium and magnesium with a suitable on-line process analysis system (Figure 2-3), which in this case, consists of an analytical instrument and a sample preparation unit.

In view of the composition of the sample (see Table 2-2), which can influence the analysis; the determination of matrix effect should be one of the main focuses of this work since matrix interference can affect both the accuracy and the precision of the method. Moreover, due to the application of the ICP-OES in an on-line system, the determination of its long-term stability should also be examined.

Although sampling normally carries the greatest error in the analytical chemistry and not the sample preparation or the sample analysis, the error from the sampling can be neglected in this work since the area of sampling is directly integrated in a form of a ring system into the production process and so regularly cleansed with distilled water and sterilized with steam as the production tanks. Moreover, the samples are homogenous mixtures.

Apart from leakages in the ten-way selector-valve that can influence the measurement negatively, the error from the sample transfer can be assumed as negligible.

An error analysis based on the sample dilution and the addition of reagents should therefore be performed to examine the precision of the sample preparation since this part is proposed to carry the greatest error in the sample preparation unit.

Since the two main parts of the on-line system have to accomplish different tasks, they have to be examined individually in compliance with the given specifications and requirements (Table 2-1) and then combined together. To achieve the goal of this work, an analytical method for the simultaneous determination of these ions is required.

Table 2-2: The components of dialysis solutions, beside WFI, and their measuring ranges (according to declaration)

Analytes	**Measuring range [mmol L^{-1}]**
Chloride	57.00 – 209.00
Hydrogen carbonate	21.16 – 72.00
Sodium	69.30 – 198.00
Potassium	1.05 – 80.00
Calcium	1.00 – 30.00
Magnesium	0.25 – 20.00
Glucose (anhydrous)	5.55 – 471.70
Lactate	35.00 – 70.00
Phosphate	1.05 – 25.00
pH	2.40 – 8.60
Density	1.0025 – 1.0390

Figure 2-3: The on-line process analysis system consisting of a sample preparation unit connected to an ICP-OES

Since the main analytical method used in this work (ICP-OES) and some of the methods which were tested at the beginning (see Table 2-3 and chapter 5.1) are based on atomic spectroscopy, this technique is explained into details in chapter 3.2.

Table 2-3: Examined methods and their detected elements

Examined methods	Detected elements	Requirements fulfilled?
Ion-selective electrode (ISE)	Na	no
Complexmetric titration with potentiometric indication	Ca and Mg	no
Flow injection analysis (FIA) with photometric detection	Ca and Mg	no
Flame photometry	Na, K and Ca	no
Flame-atomic absorption spectroscopy (F-AAS)	Na, K, Ca and Mg	no
Inductively coupled plasma optical emission spectroscopy (ICP-OES)	Na, K, Ca and Mg	yes

3. Theoretical Fundamentals

3.1 Process analytical chemistry (PAC)

Process analytical chemistry is a special form of the traditional analytical chemistry. In the PAC, the analysis is performed in the manufacturing process and not in the laboratory and so an economy of time is achieved. This differentiates the idea of PAC from that of the conventional analytical chemistry [7]. Thus, PAC was historically defined as the chemical and physical analysis of materials in the process stream through the use of an on-line or in-line analyzer, which can also be describe as analysis in the process [3]. PAC is also the origin of the widespread innovative concept, process analytical technology (PAT). PAT encompasses process analytical methods and other principles to enhance the understanding and control a manufacturing process [3], [5]. Whereas process analytical chemistry is essential to accomplish the concept of PAT, the former can work independently. In Table 3-1 is a list of some requirements for process analytical methods differentiated according to their level of importance and their areas of application.

Since PAC and PAT continue to develop in many fields and their goal becomes clearer as to ensure a constant product quality, the definition of PA or PAC has been broadened to include all factors contributing to the achievement of this goal.

The process analytic work group of GDCh defines PA or PAC as follows [8]:
“The purpose of process analytic is chemical, physical, biological and mathematical techniques and methods for the promptly assessment of critical parameters of chemical, physical, biological and environmental processes."
"The goal of process analytic is to provide relevant information and data for process optimization, automation, control and regulation to ensure a constant product quality in safe, environmentally sustainable and cost-efficient processes.”

This corresponds to the definition of PAT by the FDA as:
“a system for designing, analyzing, and controlling manufacturing through timely measurements (i.e., during processing) of critical quality and performance attributes of raw and in-process materials and processes, with the goal of ensuring final product quality. It is important to note that the term analytical in PAT is viewed broadly to

include chemical, physical, microbiological, mathematical, and risk analysis conducted in an integrated manner. The goal of PAT is to enhance understanding and control the manufacturing process, which is consistent with our current drug quality system: *quality cannot be tested into products; it should be built-in or should* ***be*** *by design* [5]."

Table 3-1: Ratings of the relative importance of various performance characteristics of on-line analyses in academic research, process development and industry (+/+++[a] Process-dependent, +++ very important, ++ important, + not very important) [9]

Characteristic	**Academic research**	**Process development**	**Manufacturing**
Good accuracy	+++	+++	+++
Good precision	+++	+++	+++
Good reproducibility	+++	+++	+++
Good selectivity	+++	+++	+++
Good sensitivity	+++	+++	+++
Extended linearity	+++	+++	+++
Good stability	++	+++	+++
Robust	++	+++	+++
High analysis frequency	++	+++	+/+++[a]
Short time delay of result	++	++	+++
Low price	+++	++	+
Multi-analyte analysis	+++	+++	+
Ease of use	+	+++	+++
Ease of validation	+	++	+++
High flexibility	+	+++	+
Ease of implementation	+	+++	++
Low maintenance	+	+++	+++

In short, the definitions above can be described as achieving a Real-time analytic with the PAC and a Real-time release (RTR) or a parametric release with the PAT [3].

The advantages of the implementation of PAC and PAT into a manufacturing process can be summarized as follows [1], [3], [5], [10]–[12]:

- Ensure and improve product quality (manufacture quality by design (QbD))
- Understand, control and the regulate the process
- Achieve a time- and cost-efficient production process
- Minimize labor cost
- Real-time analytic and Real-time release of batches
- Improve process safety
- Increase production rate and product yield
- Constant information on the status of the process
- Maintain sample integrity and reduce analytical error through automated sampling and sample preparation
- Minimize the use of energy

These objectives contribute to the most essential factors for the success and the global competitiveness of a company.

The above stated definitions clarify the fact that the implementation of PAT, and in some cases that of PAC, into a process requires an expertise team since it is an interdisciplinary field. This can sometimes result in a drawback for PAT implementation beside higher investments and maintenance costs. Moreover, it is required of the techniques involved in this process to operate under safe conditions, be highly reliable and robust to constantly produce precise and accurate analytical results.

Although it is well known through numerous publications that the chemical industry and other fields have been benefiting from the implementation of PAT for decades, the strictly regulated pharmaceutical industries has been hesitant to establish this concept till the introduction of the FDA guidance for industry PAT in 2004 [3], [5], [11]–[19]. Since then, the pharmaceutical field has realized the necessity and objectives and has been encouraged to apply this concept as an alternative to the

GMP guidelines to ensure an innovative pharmaceutical development, manufacturing, and quality assurance [5], [13], [14], [20]–[25].

The different ways of performing an analytical control is revealed in the difference between PAC and the tradition analytical chemistry as well as through its historical definition. This includes off-line, at-line, on-line, in-line and non-invasive in-line. These techniques are summarized under the five eras of process analytical chemistry although they did not develop systematically (see Figure 2-1).

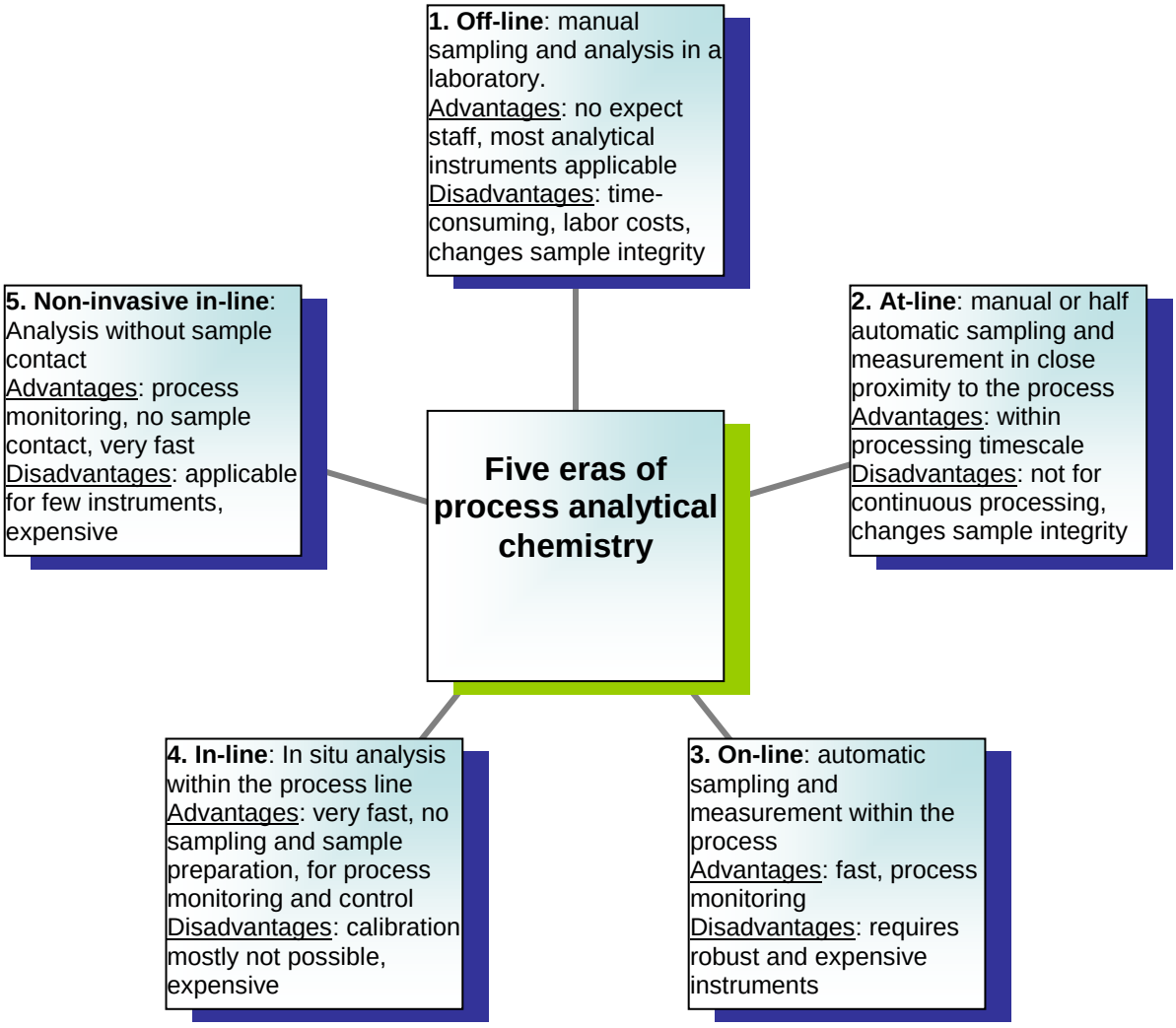

Figure 3-1: The five ways of performing the analytical control of a process [1], [3], [6], [10], [26]

As the degree of automation increases, the time-efficiency of the process also increase (Figure 3-2) whereas labor cost is saved at the same time. Moreover, the analytical error of the process will decrease when sampling and sample preparation system are fully automated or avoided and the sample integrity is maintained. Therefore, on-line and in-line are the most suitable techniques for the monitoring and control of a continuous process as well as for a real-time quality assurance [1], [5].

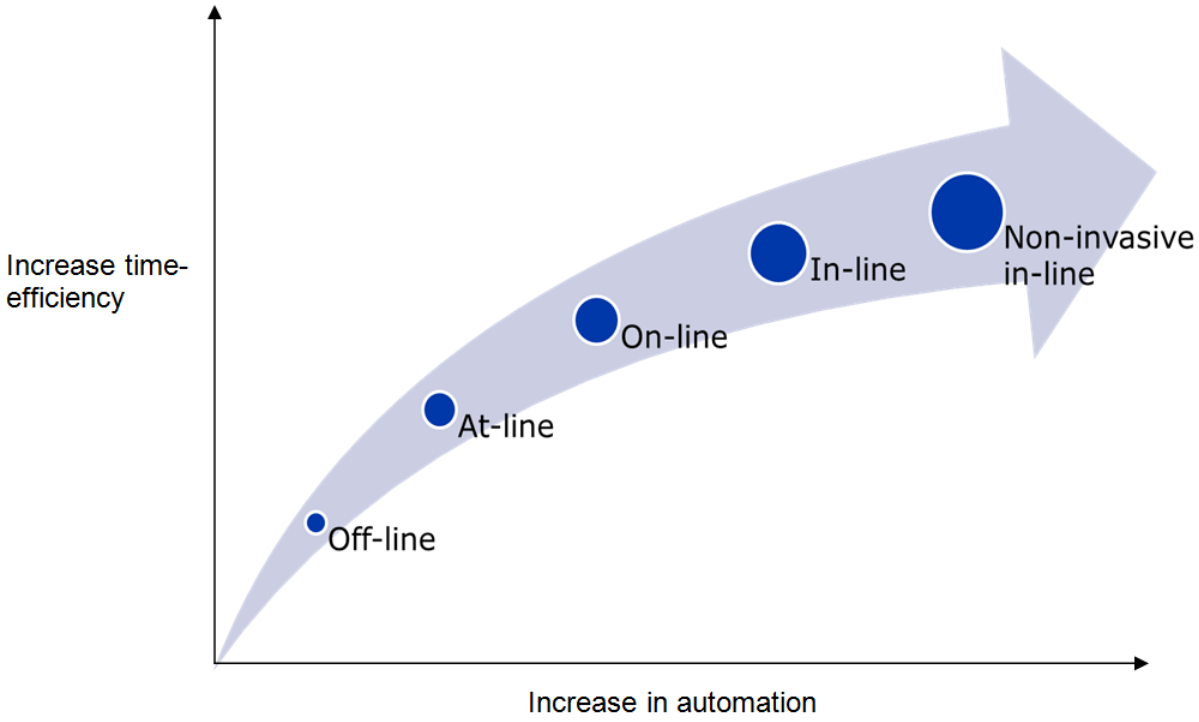

Figure 3-2: Time-efficiency increases with an increase in the degree of automation [1], [3], [10]

Spectroscopic techniques in combination with multivariate data analysis are the most popular process analytical methods applied in the PAT. In particular, molecular spectroscopic techniques, such as UV-Vis, NIR, IR, Raman, and THz, also known as far-IR, are widespread due to their facile application as in-line methods [1], [3], [10], [12]–[14], [19], [26], [27]. Among these techniques, NIR spectroscopy is clearly playing the predominant role followed by Raman spectroscopy [1], [28]–[49].

For multivariate data analysis and process control, chemometrics is applied since some parameters cannot be measured directly. With the help of this method, the calibration curves of complex data can be created [1], [3], [12]–[14], [19], [50]–[53].

Moreover, miniaturization is gaining much attention with the increase in automation since it is a way to enhance and improve the activities of high-throughput experimentation and process intensification [13]. In future, many research focuses as well as the prospects of PAT will mainly concentrate on the miniaturization of many analytical methods, so-called “lab on a chip”, and on chemometrics as well as on in-line methods, in particular, NIR [1], [3], [12]–[14], [19], [54].

GC or process-GC, FIA and SIA are gaining much attention in process analytic as on-line methods [1], [3], [12], [13], [55], [56].

HPLC and MS methods are widespread and commonly used methods in analytical chemistry, especially in medicine and drug delivery, their connection to the process

has still not been enforced because HPLC is not fast enough for process analytics and the interface for the sampling of the MS method is still difficult [1], [3], [13].

Due to the possibility of miniaturization, CE will soon become an interesting method in the PAT, such as GC and FIA, although it is in a period of development [1], [3], [13], [14], [54], [57], [58].

Moreover, at-line and on-line NMR methods are also well-known, particularly, due to their time-efficiency since quantitative analysis can be carried out with this method without calibration [1], [12], [13], [59].

Furthermore, sensors or process-sensors will be mostly applied in process analytics since they are cheaper and can be automated easily [12]–[14], [19], [60].

In addition, other analytical methods, such as X-ray analysis, laser spectroscopy and laser-induced plasma spectroscopy, are also been applied in the PAC and in the PAT [13], [61]–[63].

3.2 Atomic spectroscopy

Atomic spectroscopy is an analytical technique by which an electromagnetic spectrum, resulting from the absorption and/or emission of radiation by atoms or ions in the UV/visible range (160 - 780 nm), or a mass spectrum, derived from the number of single charged ions, is used to determine the composition of a sample [64]–[66]. Since every atom absorbs or emits light at a characteristic wavelength, the identification of an element in a sample or the analysis of the qualitative of a sample is based on this principle. Quantitative information or the concentration of an element in a sample is obtained from the amount of light intensity absorbed or emitted by an atom or ion since the light intensity is proportional to the concentration.

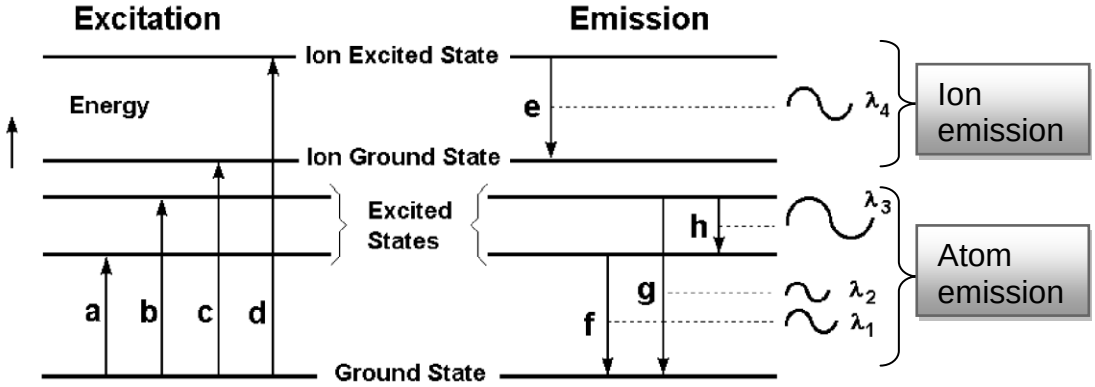

Figure 3-3: Energy transitions illustrated in energy level diagrams, with a and b representing excitation, c ionization, d ionization/excitation, e ion emission, and f, g and h atom emission [64]

According to the Planck's equation, the energy difference is proportional to the frequency:

$$\Delta E = h \times \nu \qquad 3\text{-}1$$

with ΔE as the energy difference [J], h the Planck's constant ($h = 6.626 \times 10^{-34}$ J s) and ν the frequency [Hz]. By inserting c / λ, whereby c is the speed of light ($c = 2.998 \times 10^{8}$ m s^{-1} in vacuum) and λ the wavelength [m], into the above equation in place of the frequency ν, the relationship between the energy difference and the wavelength is obtained:

$$\Delta E = \frac{h \times c}{\lambda} \qquad 3\text{-}2$$

In this equation, the wavelength is inversely proportional to the energy difference, i.e., an emission transition with a higher energy difference will result in a shorter wavelength.

In analytical chemistry, four techniques are based on the principles of atomic spectroscopy:

- Atomic absorption spectroscopy (AAS)
- Atomic fluorescence spectroscopy (AFS)
- Atomic Emission spectroscopy (AES)
- Atomic mass spectrometry / inductively coupled plasma mass spectrometry (ICP-MS)

Whereas the first three techniques (AAS, AFS and AES) measure the absorption, fluorescence or emission of light with the help of a monochromator or a polychromator that separate the electromagnetic radiation according to the wavelength, an ICP-MS utilizes a mass spectrometer, e.g. quadrupole, to separate ions according to their mass-to-charge ratio. In short, the former, which are the optical spectroscopic methods, measures the characteristic wavelength of atoms and ions and the latter the mass-to-charge ratio an ion. With these features, an element-specific analytical determination is ensured. ICP-MS, moreover, distinguishes itself from the other methods due to its excellent sensitivity, i.e. very low detection limit, which facilitates the assay of trace elements. The figures below (see Figure 3-4 to Figure 3-7) describe these techniques and illustrate their differences.

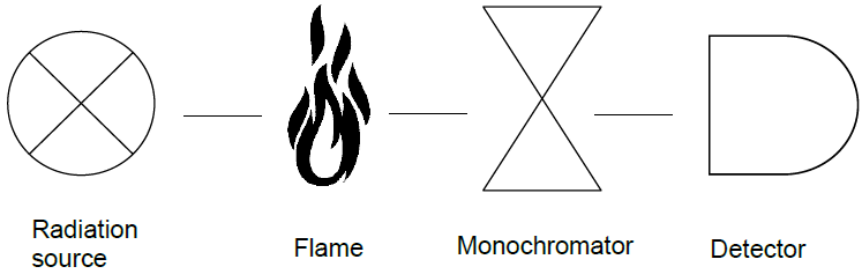

Figure 3-4: An atom absorption spectrometer with a radiation source (e.g. HCL or EDL) for the excitation of atoms, a flame (e.g. acetylene/air or acetylene/nitrous oxide) for the atomization, a monochromator (e.g. filter) to separate light according to wavelength and a detector (e.g. photomultiplier) to measure the amount of light absorbed [64]–[66]

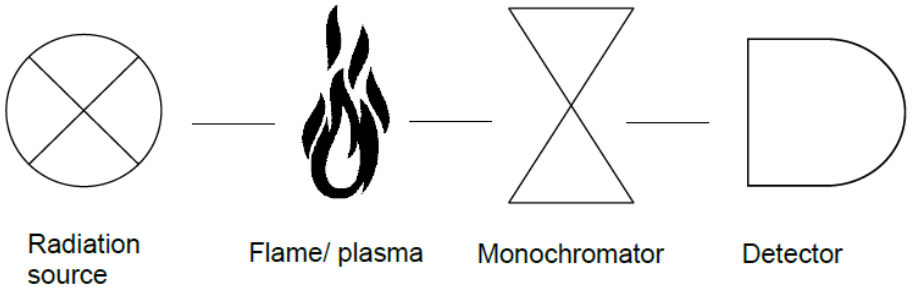

Figure 3-5: An atomic fluorescence spectrometer with a radiation source (e.g. lamp or Laser) for the excitation of atoms, flame or plasma for the atomization, a monochromator (e.g. diffraction grating) to separate light according to wavelength and a detector (e.g. photomultiplier) to measure the light emission [64]–[66]

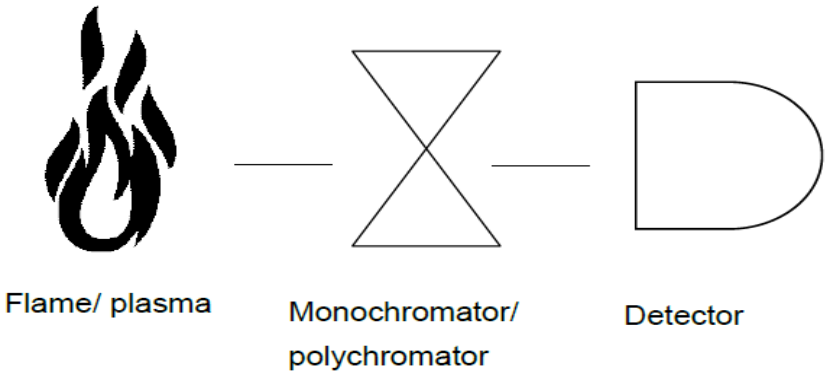

Figure 3-6: An atomic emission spectrometer with a flame (in the flame photometry) or plasma (in the ICP-OES) for the excitation as well as for the atomization and/or ionization, a monochromator (e.g. filter) or polychromator (e.g. echelle grating) to separate light according to wavelength and a detector (e.g. photomultiplier, array detector, such as CCD, CID) to measure the light emission [64]–[66]

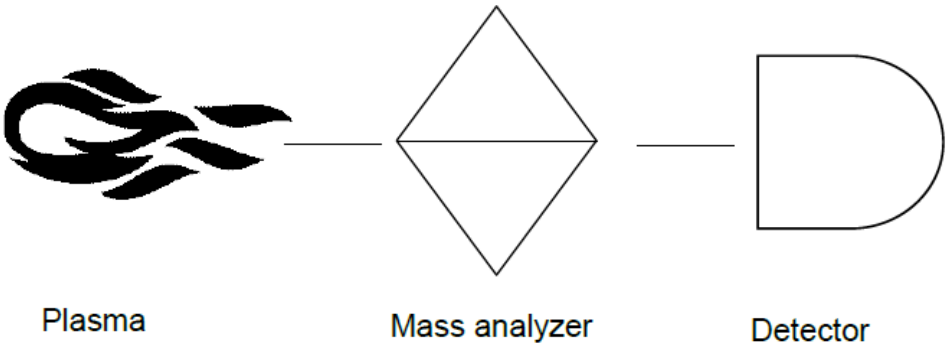

Figure 3-7: An ICP-MS which consist of an argon plasma as an ion source and for excitation, a mass analyzer (e.g. quadrupole) to separate the ions according to their mass-to-charge ratio and a detector (e.g. photomultiplier) to record the separated ions [64]–[66]

In the AAS and AFS, other atomization techniques like, graphite furnace and cold vapor are also used depending on the application. Moreover, a high-resolution continuum source (HR-CS), which uses a xenon lamp as light source, is gaining

much attention in the AAS due to its ability of simultaneous excitation. Although AFS is not widespread, its detection limit is better than that of the AAS due to its lower background noise [65], [66]. Unlike absorption spectra with fewer spectral lines and so less prone to spectral interference, emission spectra are complex since the electron of the excited atoms can collide with other atoms and so fall back to different energy levels [65], [66].

Flame photometry and OES are the analytical methods based on emission spectroscopy. The former, by which the atomization is carried out in the flame, is a technique suitable for the determination of the alkaline elements lithium, sodium and potassium and the earth alkaline metal calcium. Due to their low excitation energy, the valence electrons of these elements are easily excited with thermic energy in the flame [67]. The latter will be explained into details in chapter 3.2.1 since it is the method of choice in this work.

Application examples of the above mentioned methods can be found in the following citations [68]–[81].

3.2.1 Inductively coupled plasma optical emission spectroscopy (ICP-OES)

As stated in chapter 3.2, ICP-OES belong to the atomic spectroscopic techniques based on the detection of the spontaneous emission of light in the UV/visible range (160 - 800 nm) of the electromagnetic spectrum from excited atoms and ions in form of photons. ICP-OES is one of the most powerful multi-element methods for the simultaneous determination of up to 70 elements in both high concentrated ranges as well as in the trace ranges with lower susceptibility to matrix interferences and long-term stability due to its high and stable plasma temperature [64].
Although the ICP source was originally developed for OES, it is currently one of the highly sensitive and wide-spread techniques in modern trace analysis since its introduction into ICP-MS due to its ability to generate single-charged ions with the argon plasma and since the discovery of its axial configuration in the OES [64], [82]–[84].

The development of a plasma source originated from the difficulties associated with low flame temperatures (between 2000-3500 K e.g. acetylene/air flame about 2400-2700 K) used in flame photometry and AAS which are not able to compensate for interference effects caused by the depression of the other elements [65], [83]. A good example is the depression of calcium caused in the presence of phosphorus or aluminum by building complexes which are very difficult to dissociate in an air/ acetylene flame [83], [85]. This could be overcome by increasing the flame temperature through the addition of oxygen in this flame or using flames with higher temperature, such as oxy-cyanogen or hydrogen-fluorine, which are rather hazardous in routine analysis [83], [86]. However, lanthanum or strontium could be added to overcome the effect of phosphorus. After several approaches, the excellent solution to this issue was the introduction of plasma source in the mid-1960s [83], [84], [87].
A plasma is an electrically-conducting and very hot gaseous mixture that contains particles, such as free ions, electrons, neutral atoms, radicals and molecules and in all been neutrally charge as well as been able to be affected by a magnetic field [65], [66]. Three types of plasma sources are currently used in emission spectrometry, argon-assisted inductively coupled plasma (ICP), direct current plasma (DCP) and microwave induced plasma (MIP), whereby the former is state-of-the-art [64].

The argon-plasma in an ICP spectrometer is generated in a so called plasma torch, which consists of three concentric quartz tubes through which the argon gas flows. In Figure 3-10 is a picture of an ICP torch connected to a chamber which sprays the sample aerosol into the plasma. The two entrances beside the torch are for the cooling gas (second hose connection from the bottom), which flows in the outer chamber of the torch and the auxiliary gas (first hose connection from the bottom), which flows between the outer and the inner chamber of the torch.

The light emission from the plasma can be observed in two different configurations, radial or side-on viewing and axial or end-on viewing. In the radial view, which was the first commercial ICP, the torch configuration is vertical and so the emission from the normal analytical zone is observed laterally in a 90° angle, whereas the cooler tail plume (see Figure 3-11a), which is normally the cause of most chemical and ionization interference, is removed easily. This approach is therefore more robust, less prone to matrix interference and suitable for concentrated samples. However, it is less applied for trace analysis due to its lower sensitivity compared to the axial configuration [64], [66], [82], [88], [89].
Due to this, the end-on viewing was introduced in the early 1990s. In this horizontal torch configuration, the emission from the normal analytical zone is detected from the end of the plasma (see Figure 3-11b). The outer zone having high background noise is, therefore, not observed. Thus, the signal-to-noise ratio and consequently the sensitivity are increased, which improves the limit of detection (LOD), approximately 5- to 10-folds better than the side-on view. Due to this, axial ICP is gaining much importance in trace analysis [64], [66], [82], [88], [89].
A combination of the axial and radial plasma observation, called dual view, which extends the linear dynamic range, has been introduced for the determination of, usually, complex samples. However, since the torch configuration is horizontal, not all the advantages of the radial technique can be achieved [64], [82], [90].

An ICP-OES instrument consists basically of the individual components illustrated in the following figures (see Figure 3-8 to Figure 3-13). The components in the figures are in descending order according to their arrangement in the spectrometer, beginning with the parts outside. Apart from Figure 3-11b, all the figures below

illustrate the individual parts of the ICP spectrometer (“SPECTRO ARCOS SOP” from SPECTRO Analytical Instruments GmbH in Kleve - Germany) used in this work.

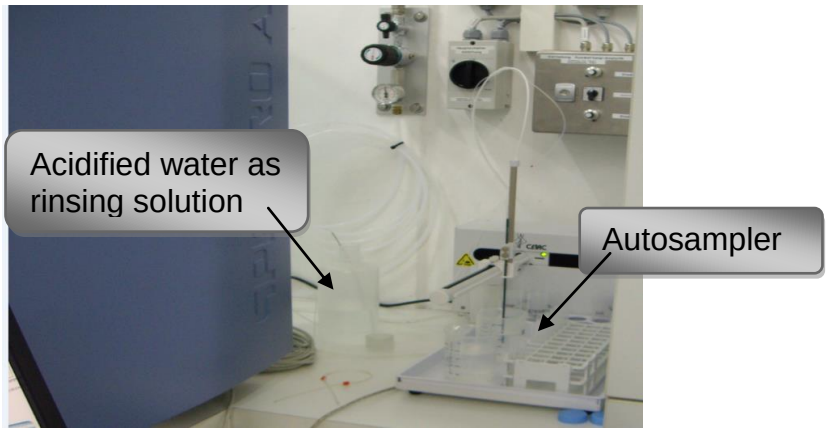

Figure 3-8: An autosampler which automatically supplies the spectrometer with the sample solution and an acidified water as rinsing solution, to avoid sample deposition and sample carryover

Figure 3-9: A peristaltic pump beside the spectrometer that pumps the sample and the rinsing solutions into it and waste solutions out of the device with the help of a hose system [91]

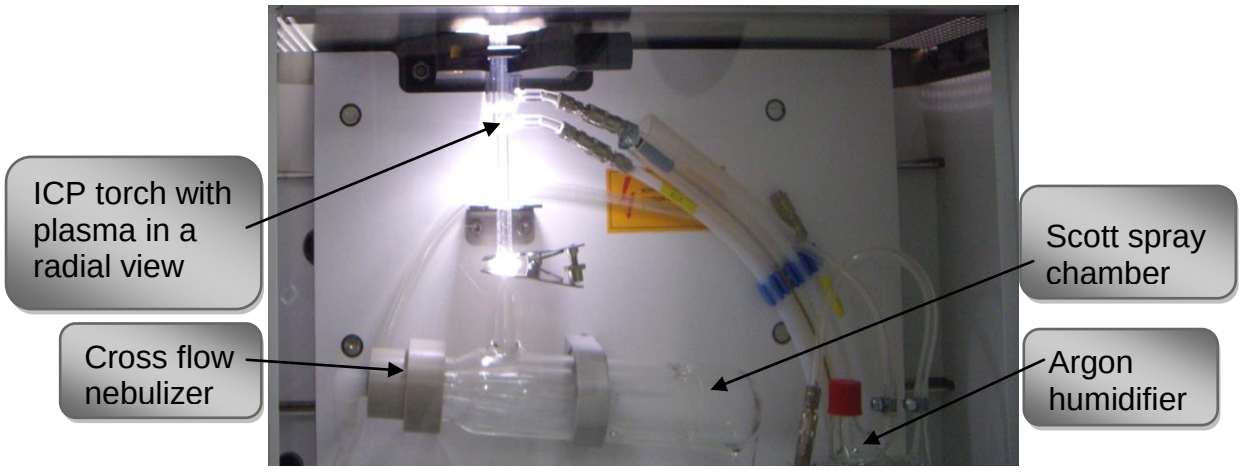

Figure 3-10: A sample introduction system consisting of a cross flow nebulizer that converts the sample into an aerosol and a scott spray chamber that spray the aerosol into the plasma and lastly an argon humidifier usually for samples with high matrix to prevent salt deposit

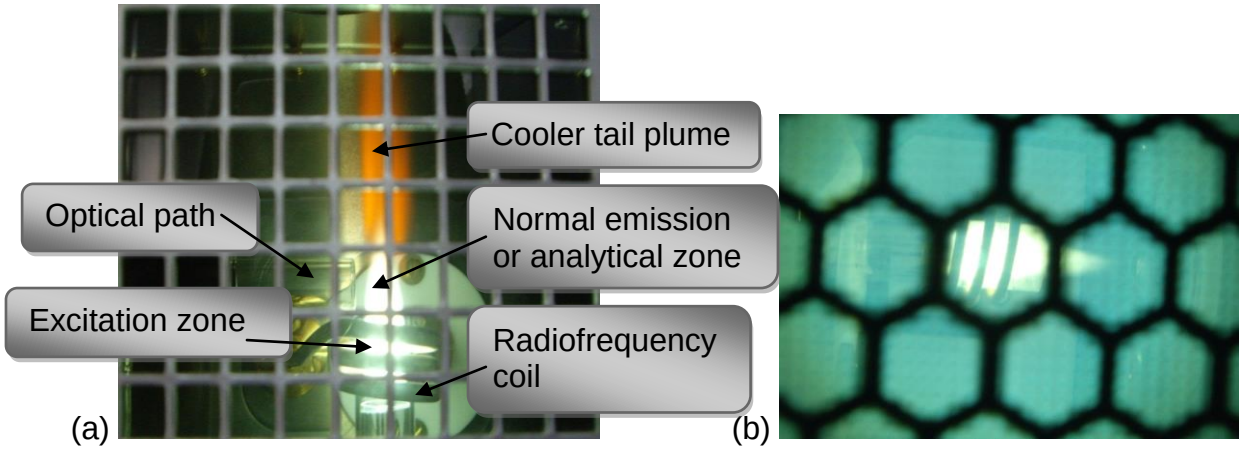

Figure 3-11: A plasma with radial view showing the different zones of an ICP (a) and a plasma with an axial view from a different ICP spectrometer (b).

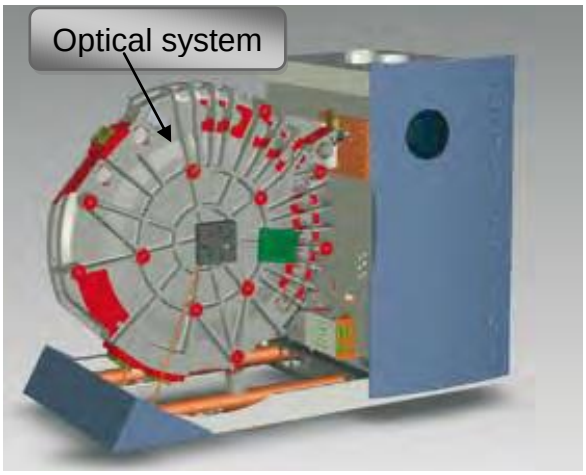

Figure 3-12:The optical system of an ICP-OES consisting of a 32 linearly arranged CCD-detectors which covers the total wavelength region of 130 – 770 nm with about 3648 pixels per line and a dynamic range of 8 decades [92]

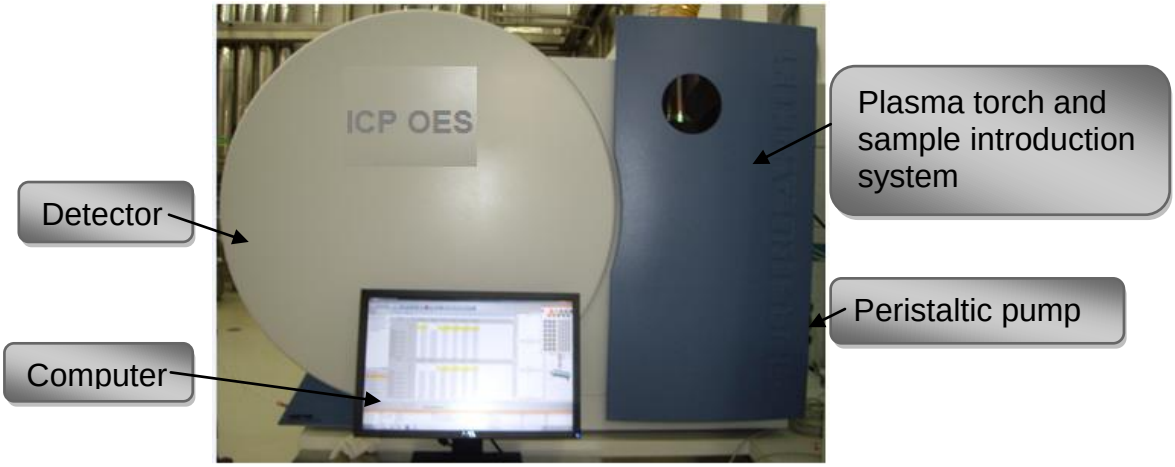

Figure 3-13: An ICP-OES “Spectro Arcos” consisting of a peristaltic pump, a sample introduction system and a plasma torch on the right, and on the left a detector, as well as a computer to control the spectrometer, collect, manipulate and report analytical data

As illustrated in Figure 3-14, different processes take place when a sample is introduced into an ICP spectrometer. Liquid or gas samples are converted into finely dispersed aerosol droplets with the help of a nebulizer before they are sprayed into the inductively coupled argon-plasma with a temperature of about 6.000 – 10.000 K. Solid samples, however, have to be pretreated first before their introduction into the instrument [82], [93]. In the plasma, solvent molecules are removed in the process of desolvation to generate aerosols of fine salt particles. The vaporization of these solid particles produces gas molecules which are then dissociated into free atoms. These atoms are excited to higher energy levels as a result of additional collisional excitation with energetic electrons within the plasma which transfers more energy to the atoms. Due to the high plasma temperature, the free atoms are mostly ionized and the generated ions are excited afterwards [64], [66], [82]. After some few seconds, the excited atoms and ions fall back to a lower energy level by emitting photon proportional to their characteristic wavelength (see Figure 3-3).

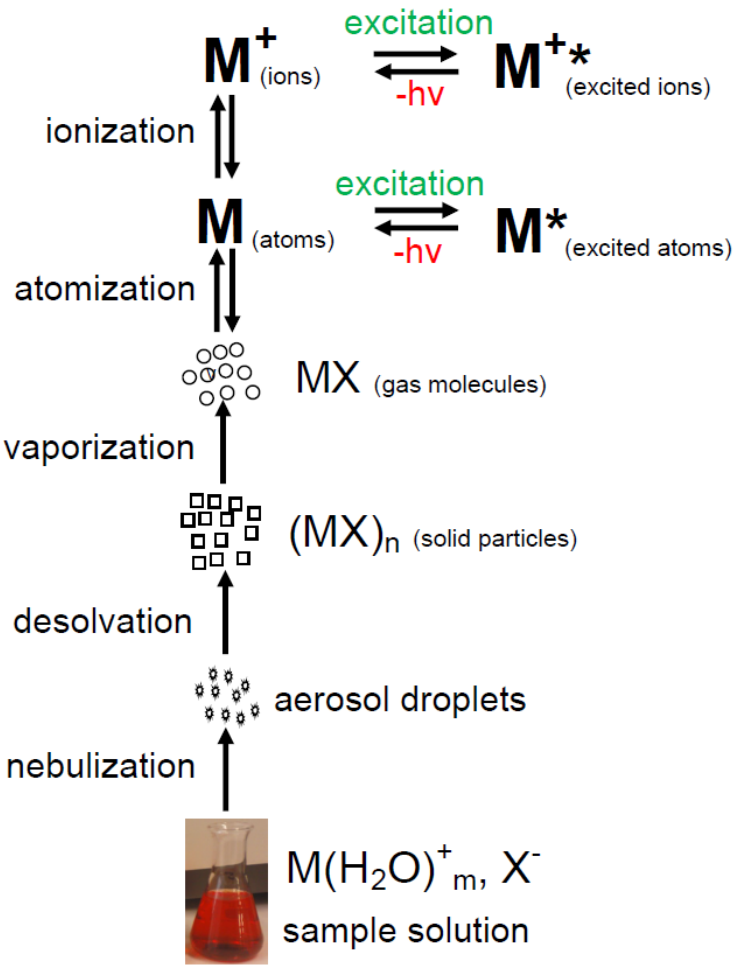

Figure 3-14: The processes that take place in an inductively coupled argon-plasma after the introduction of a sample [64], [66]

Unlike AAS und flame photometry, ICP-OES is less prone to chemical interference due to the high plasma temperature. However, spectral interferences arise as a result of the simultaneous emission of different elements which leads to an increase in wavelengths too close to be separated easily [64].

Some examples of possible applications of ICP-OES as well as some difficulties which users normally face can be read in the following citations [68], [69], [87]–[90], [93]–[117].

4. Materials and Methods

4.1 Materials

4.1.1 Instruments

Instrument	Company
ICP-OES (SPECTRO ARCOS SOP) and an auto sampler	Spectro
ProcessLab with tiamo 2.3 and Processlab Manager 2.6	Metrohm
Analytical balance XS	Mettler Toledo

4.1.2 Chemicals

Chemicals	Company
1000 ppm Lithium ICP standard	Merck
1000 ppm Barium ICP standard	Merck
1000 ppm Sodium ICP standard	Merck
10000 ppm Sodium ICP standard	Merck
1000 ppm Calcium ICP standard	Merck
10000 ppm Calcium ICP standard	Merck
1000 ppm Magnesium ICP standard	Merck
10000 ppm Potassium ICP standard	Merck
1000 ppm Potassium ICP standard	Merck
10000 ppm Potassium ICP standard	Merck
1000 ppm Multi-element standard with 23 elements	Merck
65 % Nitric acid (HNO_3) suprapur	Merck
0.1 mol L^{-1} Hydrochloric acid (HCl) titripur	Merck
Multi-element standard (Spectro Genesis ICAL-solution)	Bernd Kraft

4.1.3 Reagents and samples

Water for injection and a 65 % nitric acid (suprapur) is used for the preparation of all solutions and standards. In all the standards and solutions, 1 % of the nitric acid is present. For the preparation of all calibration standards, 1000 ppm or 10000 ppm ICP-single element stock standard solutions are used.

The samples used for the determination of matrix effect are prepared from stock solutions of the metal salts containing chloride ions (NaCl, KCl, $CaCl_2$ and $MgCl_2$). Stock solutions of sodium lactate and sodium hydrogen carbonate and of glucose are also prepared. The raw materials used to prepare these stock solutions are obtained from the production of the dialysis solution and are therefore of high pharmaceutical grade (about 99 % purity). Due to the non-disclosure agreement, the names of the suppliers of these raw materials cannot be declared.

Ready-to-use dialysis solutions are used as samples for the long term stability tests and for the examination of the sample preparation unit as well as for the determination in the on-line analysis. These samples are mostly obtained from production tanks and are therefore not sterilized. The composition and concentration of the solutions utilized for long-term stability test are summarized in Table 4-1 and their dilution factors are in Table 4-2.

Table 4-1: Composition and concentration of the solutions for the long-term stability test

Concentration [mmol L^{-1}]					
Components	**CAPD3**	**CAPD17**	**Balance A 4.25 / 1.75**	**Bicavera A 1.5/1.75**	**Multibic A 4K**
Sodium	132.00	132.00	191.10	196.00	-
Calcium	1.75	1.25	3.50	3.50	30.00
Magnesium	0.50	0.50	1.00	1.00	10.00
Glucose	242.54	85.75	471.75	166.50	111.00
Lactate	35.00	35.00	-	-	-
Potassium	-	-	-	-	80.00
Chloride	101.50	101.00	201.00	207.00	110.00

Table 4-2: Dilution factor of the solutions analyzed in the long-term stability test

Solutions	**Dilution factor**
CAPD3 and CAPD17	20
Balance A 4.25/1.75 and Bicavera A 1.5/1.25	20
Multibic A 4K	10
NaCl solution	50

4.2 Methods

4.2.1 Operation conditions of the ICP-OES and detected emission lines

The ICP-OES is operated with the software Smart Analyzer Vision 4.0 from Spectro. All measurements are carried out under the same operating conditions (see Table 4-3). However, different methods are created and used in measuring the samples due to the different concentrations of the individual ions and so to their different dilutions. The wavelengths at which the elements are detected are summarized in Table 4-4.

Table 4-3: Operating conditions of the ICP-OES

Parameter	Value
Plasma power	1475 W
Pump speed	30 Upm
Coolant gas flow rate	14 L min^{-1}
Auxilary gas flow rate	0.90 L min^{-1}
Nebulizer gas flow rate	0.85 L min^{-1}
Additional gas flow rate	0.00 L min^{-1}
Oxygen	0.00 L min^{-1}
Pre-flush time	80 s
Number of replicates	3
Integration time	30 s

Table 4-4: Emission lines (wavelengths (λ)) used for the detection of the elements

Atomic lines (I) and ionic lines (II) of the earth alkaline metals	λ [nm]	Atomic lines (I) of the alkaline metals	λ [nm]
Mg II	279.553	Li I	670.780
Mg II	280.270	Na I	588.995
Mg I	285.213	Na I	589.592
Ca II	183.801	K I	766.491
Ca II	315.887	-	-
Ca II	317.933	-	-
Ca II	396.847	-	-
Ba II	230.424	-	-
Ba II	233.527	-	-
Ba II	455.404	-	-

4.2.2 ICALization, calibration and determination of the ratio of the intensity of analyte to that of the internal standard

a. ICALization

ICALization is a method of standardizing the optical system. The standard solution used here is prepared from a multi-element standard (10 folds concentrate). This is to match the wavelengths to the pixels of the CCD detector and so avoid large shifts of the emission lines which lead to erroneous analytical results. Therefore, ICALization has to be performed regularly, latest before setting up a new method and after maintenance. The standard is diluted 1:10 with water and mixed with 20 ml L^{-1} HCl and 20 ml L^{-1} HNO_3 to achieve a solution with the composition in Table 4-5.

Table 4-5: Concentration of elements required for the ICALization

Element	**concentration [mg L^{-1}]**
Ca	1.0
Be; Li	2.0
Sr	2.1
Sc	4.9
Mn; Mo; Na	5.0
K; Ni; Zr	9.8
P	9.9
Ce; Fe; In; Cu; Si; Ti; Y	10.0
Eu; V	10.1
S	49.8

b. Calibration

A three point calibration is performed daily with three aqueous reference solutions prepared from single element standards. In order to cover the necessary measuring range of the methods, create smaller calibration ranges and thus improve the quality of the calibration. The calibration is not accepted if a minimum correlation coefficient of 0.996 is not achieved. After this criterion is fulfilled, the second calibration standard is measured to check the accurateness of the calibration. The recovery rate of this standard, also known as continuing calibration verification (CCV), should vary between the ranges of 100 ± 10 %. The concentration of an element in a sample can be calculated with the help of this calibration as shown in Figure 4-1.

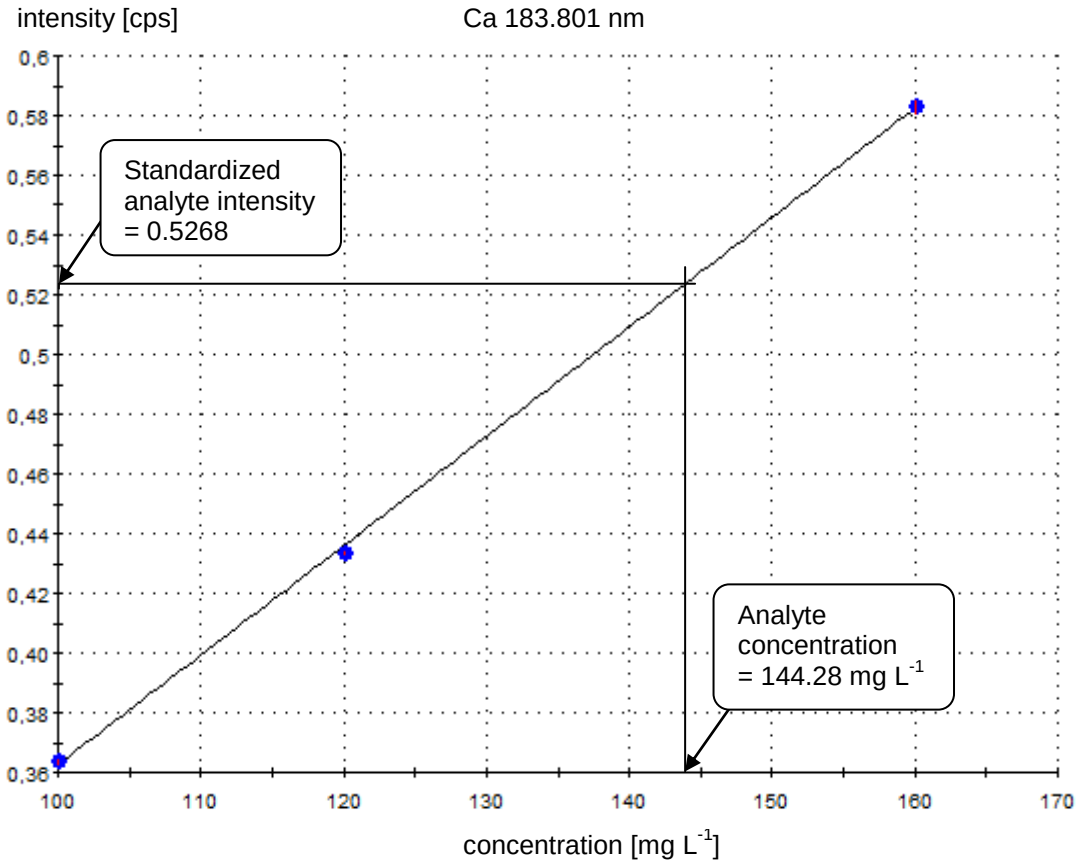

Figure 4-1: An example of a standardized calibration curve for the determination of 144.28 mg L^{-1} Ca with Ba as internal standard

The standardized analyte intensity can be calculated with the following equation:

$$\begin{aligned}&\text{Standardized analyte intensity}\\ &= \frac{\text{Analyte intensity } (\text{Ca}183.801\ \text{nm})}{\text{Intensity of internal standard } (\text{Ba}233.527\ \text{nm})}\\ &= \frac{585633\ \text{cps}}{1111630\ \text{cps}}\\ &= 0.5268\end{aligned} \qquad 4\text{-}1$$

c. <u>Determination of the ratio of the intensity of analyte to that of the internal standard</u>

A blank solution and four standard solutions are used in this method (see Table 4-6). Standard one to three are prepared from a 1000 ppm multi element standard with 23 elements (Ag, Al, B, Ba, Bi, Ca, Cd, Co, Cr, Cu, Fe, Ga, In, K, Li, Mg, Mn, Na, Ni, Pb, Sr, Tl, Zn) and standard four is prepared from 1000 ppm single element standards.

Table 4-6: Concentration of standard and blank solution for screening

Standard and blank solutions	c (ion) [ppm]
blank	0
1	1
2	10
3	20
4	50

4.2.3 Method for the determination of matrix interference effect

To cover the validation ranges, the total concentrations of the substances to be examined (see Table 2-2) are extended to ± 20 %, according to the ICH guideline Q2(R1) [118]. Due to the wider concentration ranges of sodium and glucose, values close to their average values are calculated to generate smaller ranges. The concentration ranges of all the substances are summarized in Table 4-7.
The determination of matrix effect on the lowest sodium concentration marked with (*) could not be determined due to the limited time and resources.

Table 4-7: Concentration ranges of the samples for the determination of matrix effect (concentrations (see Table 2-2) are extended to include the validation requirements of ± 20 % of target value)

Total concentration range ± 20 % (values [mmol L^{-1}])			
substances	**min values**	**average values**	**max values**
sodium	55*	140	235
calcium	0.8	-	36
magnesium	0.4	-	24
potassium	0.8	-	96
L-lactate	28	-	84
glucose	4.4 (0.8 g L^{-1})	277.5 (50 g L^{-1})	566.2 (102 g L^{-1})

4.2.4 The process of sample preparation and gravimetric determination

The sample preparation unit is built like a cupboard integrated with dosing units, pumps, vessels, loops, selector valve, water connection and hose systems connecting the individual parts (see Figure 4-2). This unit is called ProcessLab and is controlled by the software tiamo, meaning titration and more. Tiamo operates all the methods for the sample preparation. However, the communication interface between the sample preparation unit and the analytical instrument (ICP-OES) is controlled by

the master software ProcessLab Manager. The measurement results are also stored in the ProcessLab Manager database. Figure 4-3 and Figure 4-4 displays the order of how a method for calibration as well as for the determination of the sample and the quality control (QC) standard, which is used to correct the vaues of the sample, are controlled by ProcessLab Manager.

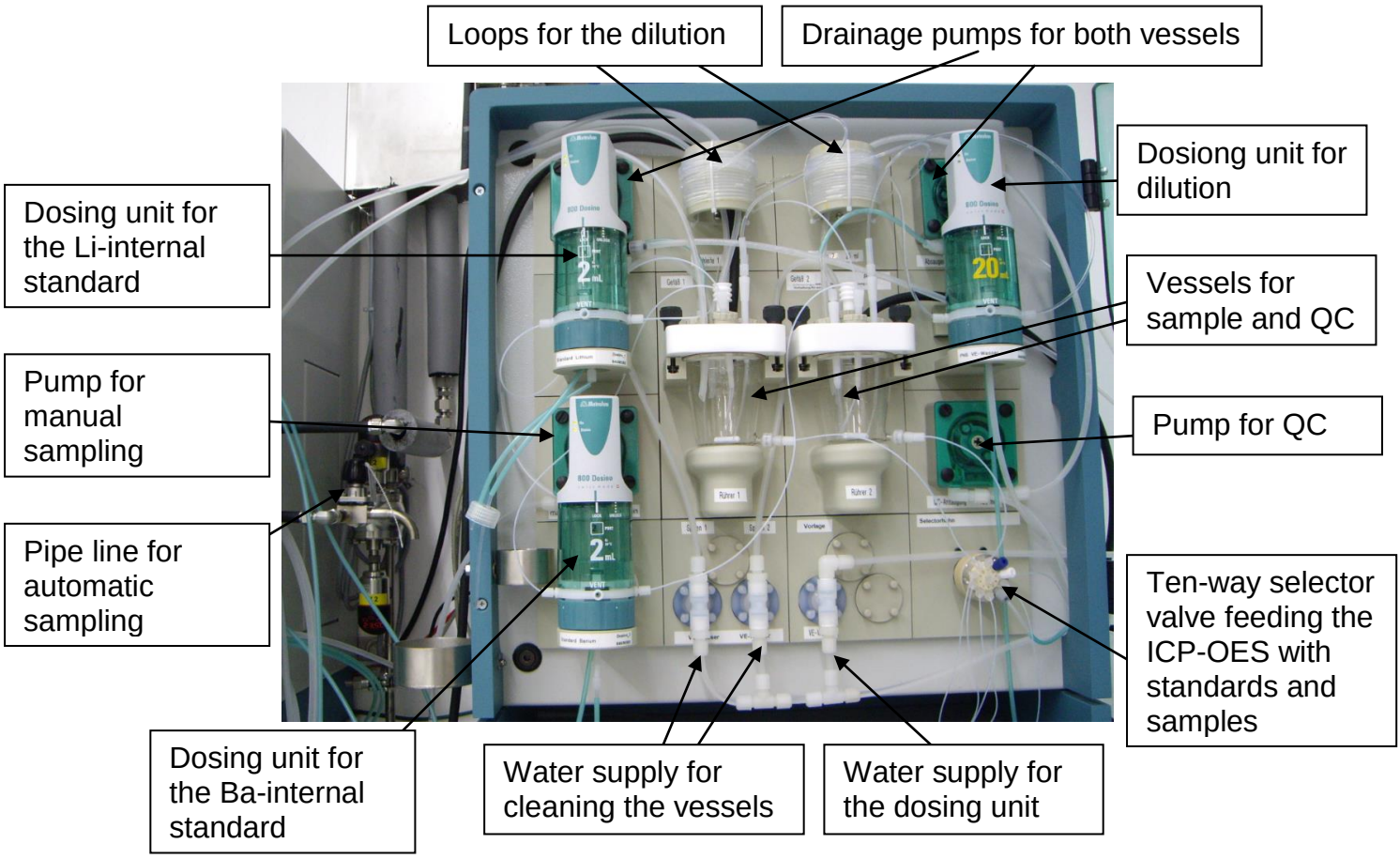

Figure 4-2: The sample preparation unit

Programmeditor - ICP_ICAL_Kalibration_CCV.xmthd

Datenbank | Bedingung
LIMS-Export | Bedingung
Fehlerverhalten: Programmabbruch | betr. Arbeitsplatz nicht mehr verwenden

Programm IDs

ID	Feldart	Standardwert
ID02	nicht verfügbar	
ID03	nicht verfügbar	
ID04	nicht verfügbar	
ID05	nicht verfügbar	
ID06	nicht verfügbar	
ID07	nicht verfügbar	

Typ	Methodenname	Zyklen	Basismethode	Parallel
Tiamo	Ventil auf 8	1	Ventil_Port08	
Smart Analyzer Vision	iCal	1	FMC KP3	
Tiamo	Ventil auf 3	1	Ventil_Port03	
Modul	warte lange	1		
Smart Analyzer Vision	Kalib 1	1	FMC KP3	
Tiamo	Ventil auf 4	1	Ventil_Port04	
Modul	Warte 30	1		
Smart Analyzer Vision	Kalib 2	1	FMC KP3	
Tiamo	Ventil auf 5	1	Ventil_Port05	
Modul	Warte 31	1		
Smart Analyzer Vision	Kalib 3	1	FMC KP3	
Smart Analyzer Vision	Regression	1	FMC KP3	
Tiamo	Ventil auf 4 für CCV = Std 2	1	Ventil_Port04	
Modul	Warte 32	1		
Smart Analyzer Vision	CCV	1	FMC KP3	
Tiamo	Ventil auf 6	1	Ventil_Port06	

Figure 4-3: Calibration method controlled by ProcessLab Manager

Programmeditor - ICP_QC_Probe_Kolben_KP3.xmthd

Datenbank: ProcessLab Manager | Bedingung
LIMS-Export | Bedingung
Fehlerverhalten: Programmabbruch | betr. Arbeitsplatz nicht mehr verwenden

Programm IDs

ID	Feldart	Standardwert
ID02	nicht verfügbar	
ID03	nicht verfügbar	
ID04	nicht verfügbar	
ID05	nicht verfügbar	
ID06	nicht verfügbar	
ID07	nicht verfügbar	

Typ	Methodenname	Zyklen	Basismethode	Parallel
Tiamo	Ventil auf Probe ohne IS_1	1	Ventil_Port06	
Input	Eingabe Kontrollprobenwerte	1		
Tiamo	Start mit QC	1	QC_KP3_1	
Tiamo	QC+Probe Vorb.	1	Kolben_QC_Probe_KP3	
Tiamo	QC Vorb 2	1	QC_KP3_2	☑
Modul	warte	1		
Smart Analyzer Vision	Probe messen	1	FMC KP3	
Tiamo	Ventil auf Probe ohne IS_2	1	Ventil_Port06	
Tiamo	Sync QC	1	Sync QC	
Tiamo	Ventil auf QC	1	Ventil_Port01	
Modul	warte1	1		
Smart Analyzer Vision	Kontrollprobe	1	FMC KP3	
Tiamo	Ventil auf Probe ohne IS_3	1	Ventil_Port06	
Calc	QC prüfen	1		
Tiamo	QC 2. mal bedingt	1	QC_KP3_1	
Smart Analyzer Vision	Kontrollprobe1 bedingt	1	FMC KP3	
Calc	QC 2 umrechnen	1		
Tiamo	Ventil auf Probe ohne IS_4	1	Ventil_Port06	
Calc	Berechnung	1		
Calc	Berechnung1	1		
Calc	Kontrolle merken	1		

Figure 4-4: Method for measuring the sample and QC-standard controlled by ProcessLab Manager

4.2.4.1 The process of sample preparation

In Figure 4-2 are the left vessel and the left loop for the dilution of the sample and the ones on the right are for dilution of the QC-standard since the latter is used to standardize the measured values of the sample and should therefore be treated equally as the sample. The idea of the automatic preparation of the QC is to avoid the manual preparation which is on one hand, different from the automatic preparation of the sample and on the other hand carries the error of the preparation of different people which can influence the intermediate precision negatively. To save time, the dilution of the sample and that of the quality control standard are carried out almost simultaneously. While the measurement of the QC-standard is taking place and that vessel is busy, the preparation of the sample will be carried out.

The 20 mL dosing unit and the two loops, which are linked to it, are filled with water for the dilution. At the beginning of every dilution method, the vessels are emptied, cleansed with water and then emptied again while the three dosing units are prepared. This means the standards and water in these dosing units are pumped out and fresh once are pumped into it again to free them from air bubbles, which can affect the process negatively by resulting in erroneous measurement values.

To begin with the preparation of sample or QC, some amount of water is released from the 20 mL dosing unit to create space. After that, 0.1 mL air is sucked into the loop with the help of the 20 mL dosing unit and then the concentrated sample or the quality control standard is pumped into their vessels. An exact amount of the solution is then drawn into the loop and the vessel is then emptied. 0.1 mL air is drawn again into the loop so that the loop will have areas containing (in the order of their arrangement) water, air, solution and finally air. Afterwards, the vessel is cleansed again with water and then emptied so that the solution and an exact amount of water for the dilution can be released from the loop into the vessel. The total amount of air (0.2 mL) in the loop is considered during the release of the solution and the water from the loop. Finally, the exact amount of internal standard is added to the diluted solution in the vessel and then stirred to achieve a homogenous solution. With the help of the ten-way selector valve, the prepared sample or QC-standard is transferred into the ICP-OES for its determination.

4.2.4.2 The process of gravimetric determination

As shown in Figure 4-5, the gravimetric determination is carried out in three steps: First, an empty bottle covered with a lid is weighed. After that, the sample is diluted and collected into the bottle to avoid its release into the vessel. Finally, the bottle is closed and weighed again. By the determination of the amount of its content, the weight of the bottle with content is subtracted from that of the empty bottle. This is repeated for about ten times for each loop (see Figure 4-2) and afterwards their RSD is calculated and compared. Since the solutions collected in the vessels are diluted with two different loops, these two loops are examined individually to find out whether their results are comparable.With this method, factors influencing the presicion of the preparation process, such as the dilution, addition of internal standard and the densities of the solutions, as well as the difference between the preparation of the sample and the QC-standard, are evaluated.

a) Weighing an empty bottle

b) Collecting diluted solution into the bottle

c) Weighing the diluted solution in the bottle

Figure 4-5: Procedure for the gravimetric determination

5. Results and discussion

By the production of analytical instruments, most manufacturers tend to focus on the clinical analysis since it offers a large market, and relatively similar types of material to be analyzed [119]. Consequently, the analysis of pharmaceuticals faces greater challenges due to the higher quality demands and the different types of analysis required in this field. To guard their high product quality and patient safety perspectives, pharmaceutical industries are, moreover, subjected to regulations like Ph. Eur., GMP Guideline, ICH Guideline, Medicinal Devices Act etc. which set restrictions in every step of the manufacturing process [68].
Several analytical techniques are available for the determination of the elements Na, K, Ca and Mg (see Table 5-2). However, the different requirements in the individual fields, pharmaceutical, chemical, clinical environmental agricultural and other areas, can influence the choice of assay.

By the quality control of dialysis solutions, the type of method and the specification limits for the determination of these elements (Na, K, Ca and Mg) are prescribed in the European Pharmacopoeia (see Table 5-1). This, as stated above, limits the choice of method for the determination of these ions in this field.

Table 5-1: Analytical requirements for the determination of Na, K, Ca and Mg in dialysis solutions according to Ph. Eur. [120]–[122]

Element	Method of analysis	Wavelength [nm]	Specification [%]
Na	AES	589.0 or 589.6	97.5 - 102.5
Mg	F-AAS	285.2	95.0 - 105.0
K	F-AAS	766.5	95.0 - 105.0
Ca	F-AAS	422.7	95.0 - 105.0

Table 5-2: Some methods for the determination of Na, K, Ca and Mg and their references

Methods	Sodium	Potassium	Magnesium	Calcium
AAS	[70], [72], [123]–[125]	[70], [72], [123], [125]	[6], [70], [72], [125]–[127]	[6], [70], [72], [125], [126]
Flame photometer	[6], [71], [128]	[71], [128]	-	[6], [71], [127]
Potentiometry with ISE	[6], [129]–[134]	[129]–[132], [134], [135]	[136]	[129], [136]–[138]
Titration	[139], [140]	[141]	[6], [142], [143]	[6], [138], [142], [143]
Photometry	-	-	[144], [145]	[144], [145]
ICP-OES / ICP-MS	[146]	[146]	[146]	[146], [147]
FIA- / SIA-Photometry	-	-	[148]	[148]
FIA- / SIA-potentiometry	-	-	[149], [150]	[149], [151], [152]
FIA- / SIA-AAS	[153]	[153]	[153]–[156]	[153]–[157]
FIA- / SIA-Flame photometer	[153], [158]	[153], [158]	[153]	[153]
HPLC	[159]	[159]	[159], [160]	[159], [160]
Capillary electrophoresis	[135]	[135]	[135]	[135]
Ion chromatography	-	[135]	[135]	[135]
Stopped-flow	-	-	[161]	[161]

Irrespective of the requirements of the Ph. Eur. in terms of assay, some common methods for the determination of the ions - Na, K, Ca and Mg - were tested at the beginning of this work, in order to select the appropriate method for the simultaneous determination of these ions in dialysis solutions, which also fulfills their analytical demands. With a simultaneous technique, the time-consuming determination of the four ions with two different methods (AAS and flame photometry) as described in the

Ph. Eur. is improved. In Table 2-3 and in chapter 5.1 is a summary of the methods which were examined beside ICP-OES before the later was selected as the suitable technique.

As the state of the art for the determination of trace elements beside ICP-MS, ICP-OES has become famous in various fields due to its stability, suitability for the determination of highly concentrated sample matrices, less susceptibility to interference and its ability to detect up to 70 elements simultaneously. Unlike ICP-OES instruments from other companies which were also examined, the ICP-OES instrument from Spectro used in this work is equipped with an automation client for software connection, which facilitates its integration into an on-line process.
Based on these advantages, this ICP-OES is chosen as the best method and the best instrument for the on-line determination of the analytes of interest in this work (Na, K, Ca and Mg).
Since this analytical instrument cannot stand alone in the on-line analysis system, an automatic sample preparation unit, which is responsible for sampling, sample preparation and sample transfer into the analytical instrument, is attached with the help of a communication interface. Figure 5-1 displays the three main parts of the on-line process analysis system and their individual areas which can influence the whole system in different ways.
Since interferences from the communication interface usually cannot be termed as analytical errors, the main focus of this work is on the examination of the analytical method (ICP-OES) and the automatic sample preparation unit which can influence the analytical requirements of the on-line system. The chapters 5.2, 5.3 and 5.4 deal with the analytical instrument (ICP-OES), chapter 5.5 with the automatic sample preparation unit and chapter 5.6 with the on-line process analysis system as a whole.

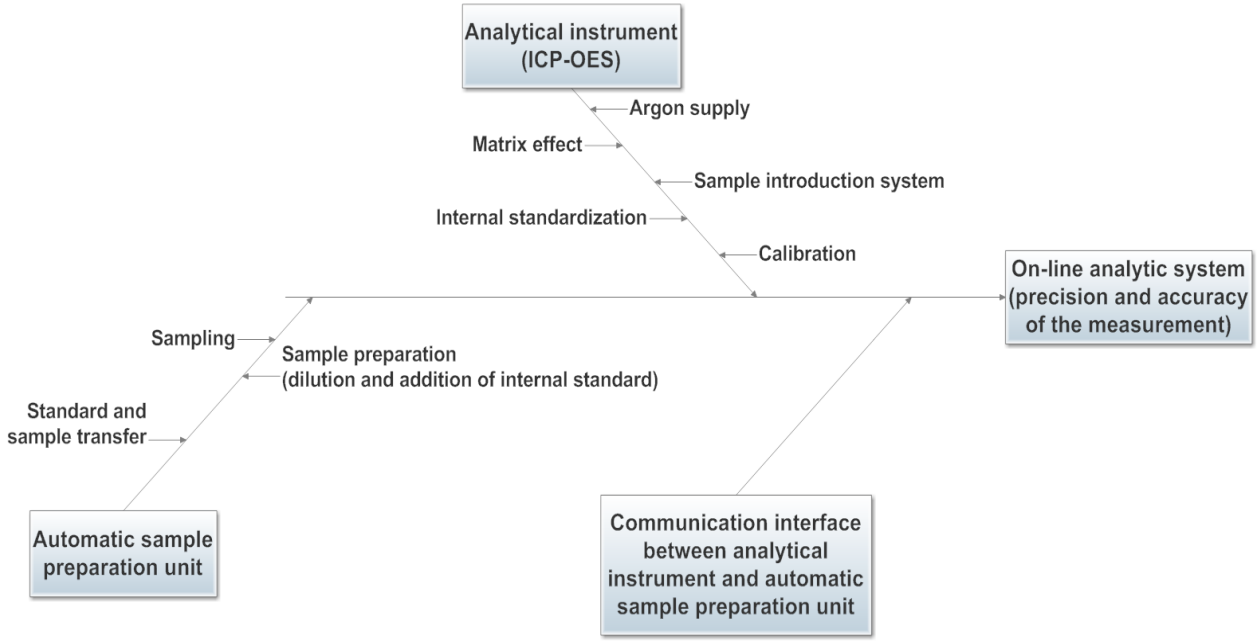

Figure 5-1: An Ishikawa fishbone model displaying the three parts of the on-line process analysis system and their sources of error

5.1 Examined methods for the selection of the suitable on-line technique

As stated in Table 2-3, all the methods examined could not fulfill the requirements apart from ICP-OES, which is, therefore, applied in this work.
The examinations carried out for the determination of Ca and Mg by titration as well as most of the determination of Na by ISE can be found in my diploma thesis [6].
Apart from FIA, by which the analysis was carried out externally by Medizin- und Labortechnik Engineering GmbH in Dresden, all the other methods were examined internally.
The following paragraphs summarize the reasons for which the methods stated in Table 2-3 could not fulfill the requirements of this work.

a. Determination of Na with ISE

The ISE could easily be integrated into the process. Due to the unreliability of the electrodes, however, this method could not fulfill the requirements of this work.
Since the electrodes stay in solution throughout, an earlier bleeding of the membrane, i.e. a leakage of the ionophore and the plasticizer onto the membrane surface is caused [162], which makes the ISE instable and so results in drifting values. Though this behavior could be avoided by regular calibration of the electrode and offset correction, it extends the measuring time and makes a long-term determination a bit complex. In Figure 5-2 is a typical behavior of the Na-ISE during calibration.

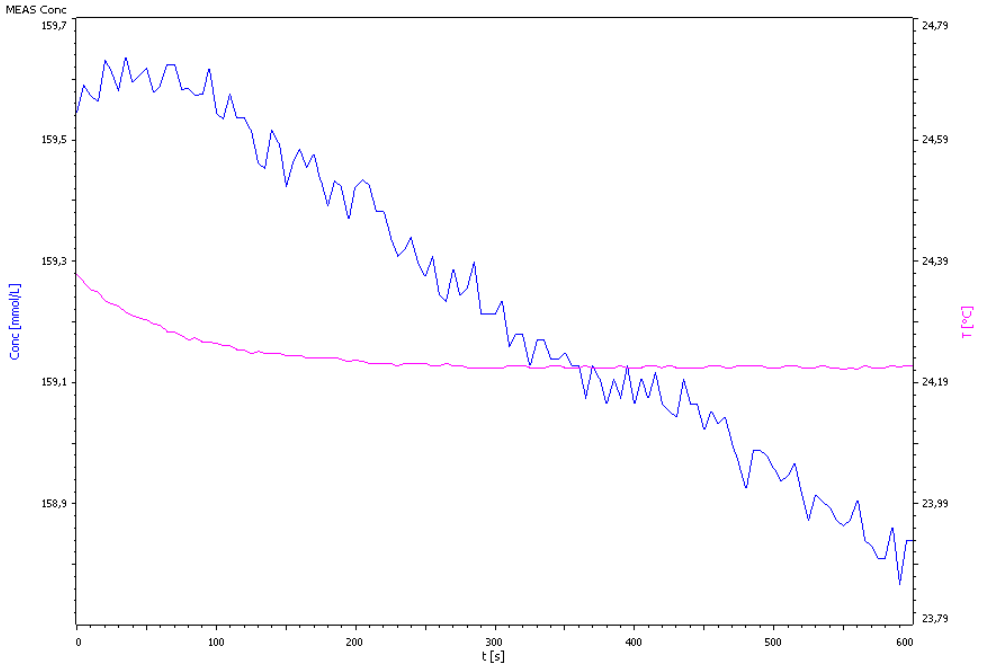

Figure 5-2: A typical behavior of the Na-ISE during calibration (after 600 s measureing time)

Moreover, the electrodes of different batches mostly behave differently. This can cause great deviations in the values after an electrode has been changed since these electrodes can be used for maximum 6 months, depending on their application. Interferences from other ions (K, Ca or Mg) were negligible since the electrode is selective for sodium and the concentration of the other ions in the samples are mostly very low. Although the influence of glucose and lactate was not examined, it could, however, be assumed that these species can accelerate the bleeding of the membrane and so increase the instability of the electrode. Moreover, their matrix influence cannot be neglected.

Therefore, the application of ISE in an on-line process cannot be warranted. Moreover, the other ions K, Ca and Mg would require individual measurements with individual electrodes, which cannot enable simultaneous determinations. Furthermore, influences disturbing these ions (K, Ca and Mg) and the instability of the electrode discussed above could be of a greater problem than that of Na since they are mostly present in low concentrations compared to Na.

b. Complexometric titration of Ca and Mg

The complexometric titration of Ca and Mg was carried out with EDTA as complexing agent and the end point was indicated potentiometrically with a Ca-ISE. This method was easily integrated into the process.

With this method, the total amount of Ca and Mg could be detected successfully although the difference between the stability constant of Ca^{2+}-EDTA ($logK_B$ = 10.7) and that of Mg^{2+}-EDTA ($logK_B$ = 8.7) is not great [163]. Acetylacteone (AcAc) in Tris-buffer was, therefore, added to help separate the peaks from each other (see Figure 5-3) and so help obtain acceptable values for the individual ions. The first equivalence point (EP) corresponds to the amount of Ca and the difference between the first and second EP to that of Mg. Although the amount of AcAc in Tris-buffer was varied, the separation of Ca and Mg from each other was not successful. In most cases, higher Ca values were obtained which then resulted in lower Mg values. In Figure 5-3 are diagrams displaying the influence of AcAc in Tris-buffer on the measurement.

The determination of Ca alone with EGTA was also tested but this lead to no satisfactory results since the influence of Mg on Ca could not be avoided. Although the stability constant ($logK_B$) of Mg^{2+}-EGTA ($logK_B$ = 5.2) is far less than that of Ca^{2+}-EGTA ($logK_B$ = 11.0) [163], some amount of Mg was detected together with Ca which lead to higher results.

Due to these arguments and the fact that the method cannot be used to determine all the analytes of interest simultaneously in order to save time and minimize the analytical error, it is not suitable for the on-line system required here.

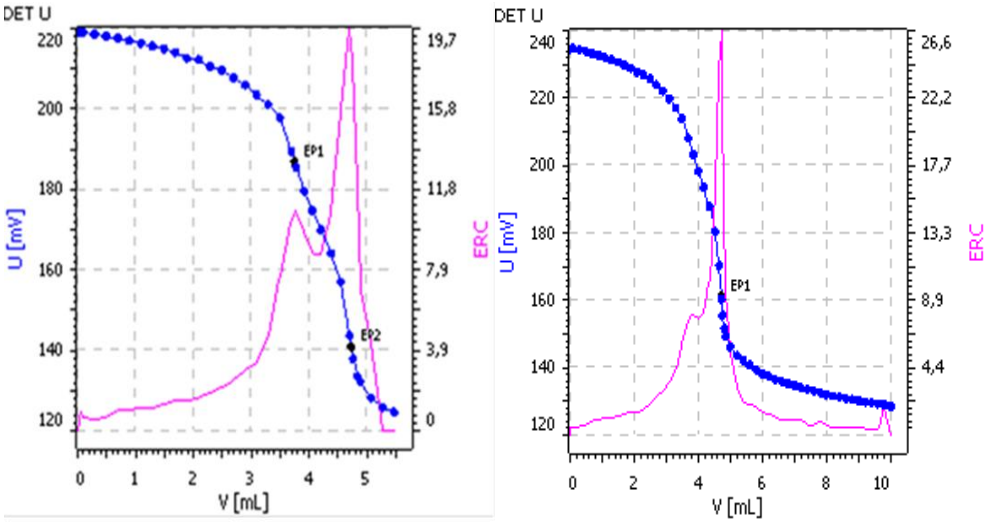

(a) (b)

Figure 5-3: Graphs displaying the simultaneous titration of a CAPD2 solution by the addition of (a) 12 mL and (b) 2.5 mL of AcAc in Tris-buffer,

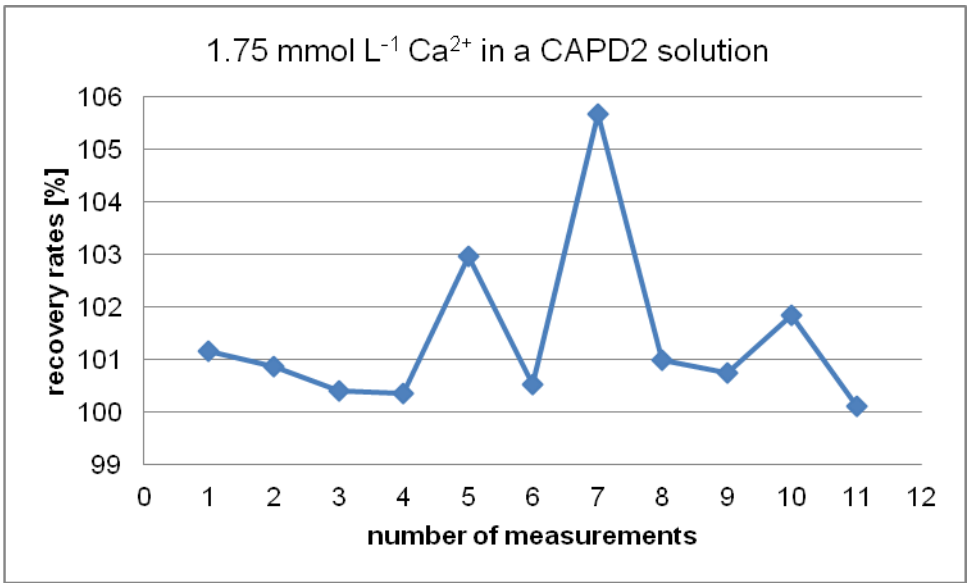

Figure 5-4: Results obtained after the determination of Ca in a CAPD2 solution by complexometric titration with EDTA

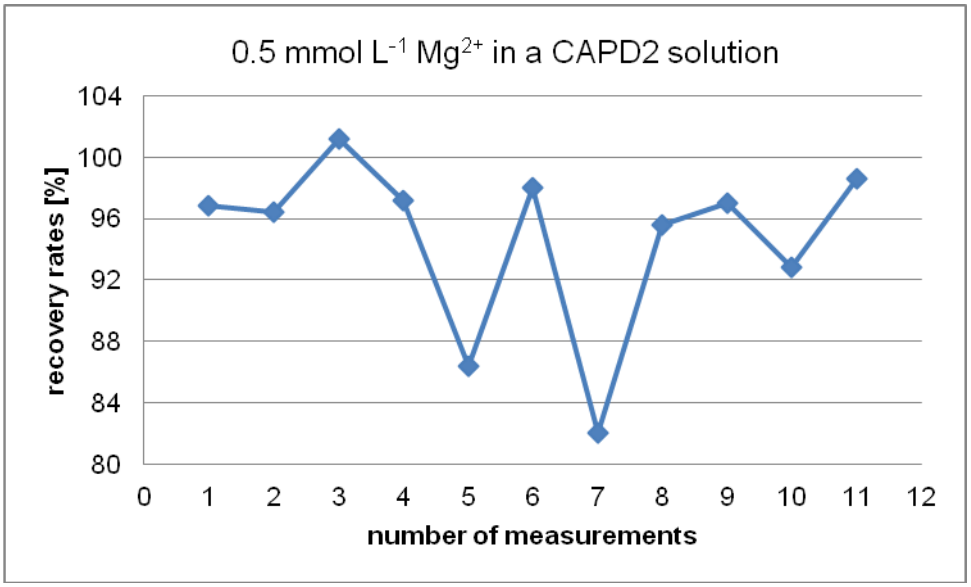

Figure 5-5: Results obtained after the determination of Mg in a CAPD2 solution by complexometric titration with EDTA

c. Flow injection analysis (FIA) with photometric detection for the determination of Ca and Mg

As mentioned already, this method was tested externally by Medizin- und Labortechnik Engineering GmbH in Dresden an off-line process.

Ca and Mg are determined sequentially with the help of colorant complexing agents which enables their photometric detection.

The determination of Ca is carried out with o-cresolphthalein-complexone as a colorant complexing agent, with which Ca is detected at a wavelength of 560 nm. To avoid the interference of Mg, 8-hydroxyquinoline is added as a sequestrant.

Mg, on the other hand, is detected at a wavelength of 510 nm after building a complex with the o,o-dihydroxy azo dye, xylidine blue 1. Ca is hereby masked with EGTA to avoid its influence on this assay. Since Mg can also build a complex with EGTA, which can reduce its detectable concentration, Ba is added in excess.

Apart from the different chemicals which are applied and can produce toxic waste, such as barium chloride, this method has no software connection for its integration into the process. Moreover, the analysis time could be longer since a simultaneous assay is not possible. The results obtained in this test also show that a lot of optimizations have to be carried out since the analytical requirements were not fulfilled (see Table 5-3).

Table 5-3: Results obtained after the determination of Ca and Mg in different sample solutions by FIA (values in red are above the upper specification limit (USL))

Samples	Detected ions	RSD [%]	Recovery rates [%]
Balance 2.3/1.75	Ca	1.8	116.113
	Mg	2.2	107.248
CAPD2	Ca	1.8	98.683
	Mg	1.6	104.318
Multibic 4K	Ca	1.7	102.197
	Mg	1.4	104.871

d. Flame photometry for the determination of Na, K and Ca

A flame photometer from MIT Projekt GmbH & Co. KG in Norderstadt which is equipped with a software connection was integrated into the process as an on-line system. Since this method has to be tested alone, the measurements were carried out in an off-line process and also without dilutor and autosampler since they were not available.

The three ions (Na, K, and Ca) are determined simultaneously with the help of an eight-point characteristic curve which is generated as a calibration curve to develop a method. This characteristic curve is created once and adjusted at the beginning of every measurement with two standard solutions, standard low and standard high.

Although all the calibrations were successful, both the precision and the recovery rate could not lead to acceptable results. Therefore, different optimizations were carried out to improve the performance of the method.

- The application of lithium as internal standard:
    - This is to improve the precision and also compensate for ionization effects on Na and K due to the use of the acetylene-air-flame with a higher temperature than propane which is normally used for the determination of these ions because of its favorable conditions. Acetylene was used since Ca has to be determined with the same method.
    - The results obtained for both the measurements with internal standard and the once without internal standard showed no difference.

- The application of ethanol to improve the accuracy and sensitivity:
    - Ethanol is used here as solvent instead of water in other to achieve a better separation of the alkaline metals (Na, K), which are mostly present in higher concentrations, from the earth-alkaline metal (Ca) to improve the emission of the earth-alkaline metal and so improve the accuracy and sensitivity [164]. As with the internal standard, no difference was indentified between the measurements with water and that with ethanol.

- The application of matrix-matched calibration:
    - The calibration was first carried out with aqueous standards but when it was realized that the method was prone to matrix interference a matrix-matched calibration was also carried out which unfortunately could not improve the poor recovery rates obtained with aqueous standards.

Some of these optimizations were also carried out by the manufacturer of the instrument who confirmed the results obtained. Moreover, the nebulizer was quickly blocked by samples with higher glucose concentration. Regular rinsing could not help when measurements were carried out after some few hours. In this case, the nebulizer had to be cleaned manually, i.e. maintenance work had to be carried out after some few hours which could have a negative effect on the on-line system.
It was found that further internal oiptimizations had to be carried out by the manufacturer before the instrument can be applied since it is not reliable and also shows no robustness. The results achieved could, therefore, not be used since the instrument proved to be in its early manufacturing state and, therfore requires a lot of internal optimizations.

e. Flame-AAS for the determination of Na, K, Ca and Mg

To determine these elements simultaneously in the sample solutions a high-resolution continuous source (HR-CS) AAS (ContrAA 300) from Analytik Jena AG in Jena was used in an off-line process.
Unlike Mg and K, the results of Na and Ca are mostly either below the lower specification limit (LSL) or above the upper specification limt (USL) of the IPC. Moreover, the precision sometimes exceeded the limit of less than 1 %. The poor

precision could have been improved with the help of an internal standard and the recovery rates with matrix-matched calibration since in this test the calibration was carried out with aqueous standards. Since it was known from the beginning, that neither this instrument nor that of other companies could be integrated into the process due to the absence of a software connection, no further optimizations to fulfill the analytical reqirements of this work were carried out.

Table 5-4: Results obtained after the determination of Na, K, Ca and Mg in different sample solutions by AAS (values in red values are above the USL and in blue below the LSL)

Samples	Detected ions	Desired values [mmol·L^{-1}]	Measured values [mmol·L^{-1}]	RSD [%]	Recovery rates [%]
CAPD3	Na	132	126.783	0.5	96.048
	Ca	1.75	1.938	1.4	110.743
	Mg	0.5	0.502	0.4	100.400
CAPD10	Na	132	129.522	0.2	98.123
	Ca	1	1.092	1.0	109.200
	Mg	0.5	0.499	1.4	99.800
Balance 1.5/1.25	Na	191.1	185.	0.7	96.899
	Ca	2.5	2.665	0.7	106.600
	Mg	1	0.9755	1.6	97.550
Balance 4.25/1.75	Na	191.1	182.261	0.2	95.375
	Ca	3.5	3.793	0.9	108.371
	Mg	1	0.992	0.2	99.200
Multibic 4K	K	80	80.797	0.7	100.996
	Ca	30	31.389	0.5	104.630
	Mg	10	9.899	1.0	98.990
Bicavera B	Na	69.3	67.261	0.8	97.058

5.2 Determination of the ratio of the intensity of analyte to that of the internal standard

Beside matrix matching and standard addition, internal standardization is one of the techniques used in the ICP-OES to overcome or minimize matrix effects and other unexpected interferences, such as fluctuations in the plasma, in order to improve accuracy and precision [80], [88], [99], [165].

To meet the high analytical requirements in this thesis, this method is applied in this work. Two internal standard elements (lithium and barium) are selected for the two groups of metals of interest. Lithium is chosen mostly for the alkaline metals (sodium and potassium) and barium for the alkaline-earth metals (calcium and magnesium). These elements are chosen because of their similar behavior to the analytes to which they are linked. Moreover, they are not present in the sample and are therefore not of analytical interest. Furthermore, the combinations of internal standard ionic lines with analyte ionic lines as well as internal standard atomic lines with analyte atomic lines are considered to avoid erroneous results [64], [82], [88], [165]. In some few cases, however, cross combinations, i.e. IS ionic line linked to analyte atomic line and vice versa, are applied to examine the response of these elements.

Beside these features considered for the selection of the suitable IS, the concentration of the internal standards is also calculated theoretically in a so called screening method to achieve a good ratio of the intensity of the analyte to that of the internal standard.

The IF-function of Microsoft Excel is used in this screening method to calculate the theoretical intensities of the analyte and the internal standard. Equation 5-1 is a general equation, whereas 5-2 and 5-3 are the equations used to calculate the theoretical intensity of the analyte and that of the IS. The results in Table 5-6 and Table 5-7 are selected examples calculated with the help of these equations. In these tables, the analytes and IS linked to each other are marked with the same colour. The figures beside the element symbols in these tables represent the wavelength at which the elemente are detected.

With the help of Table 5-5 and equation 5-4 the calculation of the theoretical intensities are displayed using Na 589.592 as an example.

Intensity of analyte or IS $=$
If $\left(\text{logical test};\ \text{value if true};\ \text{value if false}\right)$ 5-1

Intensity of analyte $=$
if $(\text{c}\left(\text{analyte}\right);$ analyte intensity of blank $+$ analyte intensity of the average of standard 1 and standard $4 \times \text{c}\left(\text{analyte}\right) \div$ dilution factor; 0) 5-2

Intensity of IS $=$
if $(\text{c}\left(\text{IS}\right);$ IS-intensity of blank solution of $+$ IS intensity of the average of standard 1 and standard $4 \times \text{c}\left(\text{IS}\right);$ 0) 5-3

Table 5-5: Values used to calculate the theoretical intensity of Na 589.592 (see equation 5-4) in Table 5-6 (as an example of how the intensities in Table 5-6 and Table 5-7 are calculated)

Standard	**Na 589.592**	
Blank	79220.4	Values obtained after measuring the standards
Std 1	145106	
Std 2	734968	
Std 3	1358600	
Std 4	3129070	
c (Std 1) [ppm]	1	
c (Std 4) [ppm]	50	
intensity per c(Std 1)	(Intensity (Std 1) - Intensity (blank)) / c(Std 1)	65885.6
intensity per c(Std 4)	(Intensity (Std 4) - Intensity (blank)) / c(Std 4)	60997.0
mean		63441.3

Intensity of Na 589.592 $=$
if (3034.654 ppm; 79220.4 cps + 63441.3 cps/ppm $\times$ 3034.654 ppm $\div$ 20; 0) 5-4
$=$ 9,705,340 cps

Table 5-6: Theoretical calculation of the intensity ratio analyte to IS for the simultaneous determination of Na, Mg, and Ca (wavelength [nm] and intensity [cps])

Ion	**values [mg L^{-1}]**	Ca 183.801	Ca 315.887	Ca 317.933	Ca 396.847	Ca 422.673
Ca	70.137	23,440	279,218	505,866	14,652,499	416,786
K	-					
Mg	12.153	Mg 202.647	Mg 279.079	Mg 279.553	Mg 280.270	Mg 285.213
Na	3034.654	41,219	9,080	1,168,871	675,316	65,018
dilution factor	20	K 766.491			Na 588.995	Na 589.592
		-			19,867,998	9,705,340
IS	**c (IS) [mg L^{-1}]**					
Ba	15	Ba 230.424	Ba 233.527	Ba 455.404		Li 670.780
Li	40	1,834,605	2,284,710	19,121,856		7,508,544

Table 5-7: Theoretical calculation of the intensity ratio analyte to IS for the simultaneous determination of Mg, Ca and K (wavelength [nm] and intensity [cps])

Ion	**values [mg L^{-1}]**	Ca 183.801	Ca 315.887	Ca 317.933	Ca 396.847	Ca 422.673
Ca	1442.808	919,326	10,427,869	19,754,064	598,360,310	13,886,058
K	3753.437					
Mg	583.32	Mg 202.647	Mg 279.079	Mg 279.553	Mg 280.270	Mg 285.213
Na	-	3,756,386	339,281	110,212,938	63,471,636	5,595,300
dilution factor	10	K 766.491			Na 588.995	Na 589.592
		1,878,574			-	-
IS	**c (IS) [mg L^{-1}]**					
Ba	10	Ba 230.424	Ba 233.527	Ba 455.404		Li 670.780
Li	10	1,225,224	1,525,306	12,763,545		1,907,083

5.3 Determination of the long-term stability of the ICP-OES

Long-term stability is a test normally required in different stages in developing pharmaceutical products to investigate their out-of-specification before the new product can be approved [166], [167]. Stability of a pharmaceutical product may be defined as the capability of a particular formulation in a specific container/closure system to remain within its physical, chemical, microbiological, therapeutic, toxicological, protective, and informational specifications [168].

In this work, long-term stability can be defined as the ability of an analytical method to carry out an analysis over a long period of time under constant conditions, accurately and precisely. This method has been utilized in a gas chromatograph/ mass spectrometry system to supervise a test program for evaluating the potential of a natural gas storage plant [169]. Since the ICP-OES has to operate continuously in the on-line process, its stability over a long period is therefore one of the basic prerequisites for a reliable quality control of the dialysis solutions.

Due to this, samples containing the ions of interest in different concentrations are measured over a period of time. These measurements are assessed according to the analytical requirements (precision and accuracy) and the behavior of the graphs. In order to evaluate the behavior of the ICP-OES very well, no additional QC-standardization, i.e. correction with a quality control standard, is performed. This would have, moreover, improved the accuracy of the results and so compensate for other deviations, which would have been very useful for this evaluation.

The composition of the solutions used here can be found in Table 4-1 and their dilutions factors are in Table 4-2.

Two red lines are drawn in the graphs indicating the upper and lower specification limits of the ions of interest in the measured samples. These are the specification limits to be complied with in the in-process control (IPC). In case of the NaCl solution, which is just a test solution and so has no defined tolerance limit; the specification for sodium according to Ph. Eur. is presented. The solutions are measured within different periods of time.

5.3.1 The study of the long-term stability of the determination of sodium by ICP-OES

By the determination of sodium, the analyte emission lines Na 588.995 nm and/or Na 589.592 nm are linked to the internal standard emission line Li 670.780 nm and in case of NaCl additionally to Ba 455.404 nm. The solutions used here are CAPD3, Bicavera A 1.5/1.75 and Balance A 4.25/1.75. The composition of these solutions can be found in Table 4-1. A sodium chloride solution with a sodium concentration of 235 mmol L^{-1} is also measured. All dilution factors used for these measurements are in Table 4-2.

The results obtained here show that ICP-OES can determine sodium precisely and accurately over a long period of time, irrespective of the sample matrix and the sodium concentration.

The downward trends at the beginning of the measurements in Figure 5-6 to Figure 5-9, in which the sodium in these samples is surrounded by other matrices, could have probably result from an unstable plasma temperature. Since this does not occur with the NaCl sample (see Figure 5-10 and Figure 5-11), the matrices surrounding the sodium ions in the other samples seem to cause a decrease in the plasma temperature by their introduction into the plasma. It would, therefore, be necessary to stabilize the plasma with the sample for at least 40 min before the measurements takes place.

The abnormal behavior of sodium in the samples CAPD17 in Figure 5-7 and in Bicavera A 1.5/1.75 in Figure 5-9 could have probably resulted from plasma fluctuations or external influences on that day since the other elements in this solution, calcium and magnesium, are affected equally. Even though the calibration was carried out with aqueous standards, matrix interference can be excluded since the samples CAPD3 in Figure 5-6 and Balance A 4.25/1.75 in Figure 5-8 contain similar matrix components. A repetition of the calibration or a recalibration would have probably be necessary to improve this measurement or to help achieve possible reason for this behavior.

Although the results in Figure 5-7 and Figure 5-9 are out of the tolerance limit of the IPC in terms of accuracy, the precision is very good with RSD less than the required

limit of 1 %. Moreover, all of the results in the figures below are within the specification limit of Ph. Eur. which is ± 2.5 %, apart from that of Figure 5-7.

Furthermore, the results obtained in Figure 5-10 and Figure 5-11 confirm the reproducibility of this method.

Both sodium emission lines proved to be suitable for the determination of sodium. Moreover, the corrections carried out with both internal standards proved very effective since they were able to compensate for most effects (see intensities in chapter 9). They are, therefore, essential for the long-term stability of such measurements.

Although the barium line used in Figure 5-10 and Figure 5-11 is an ionic line which was linked to the sodium atomic lines, the results obtained with it are similar to those with lithium. In this case, linking an atomic line with an ionic line did not lead to erroneous results as it is known in the literature [165].

If a QC-standardization, correction with a QC-standard, is carried out in addition to the internal standization, the recovery rates achieved here would greatly be improved.

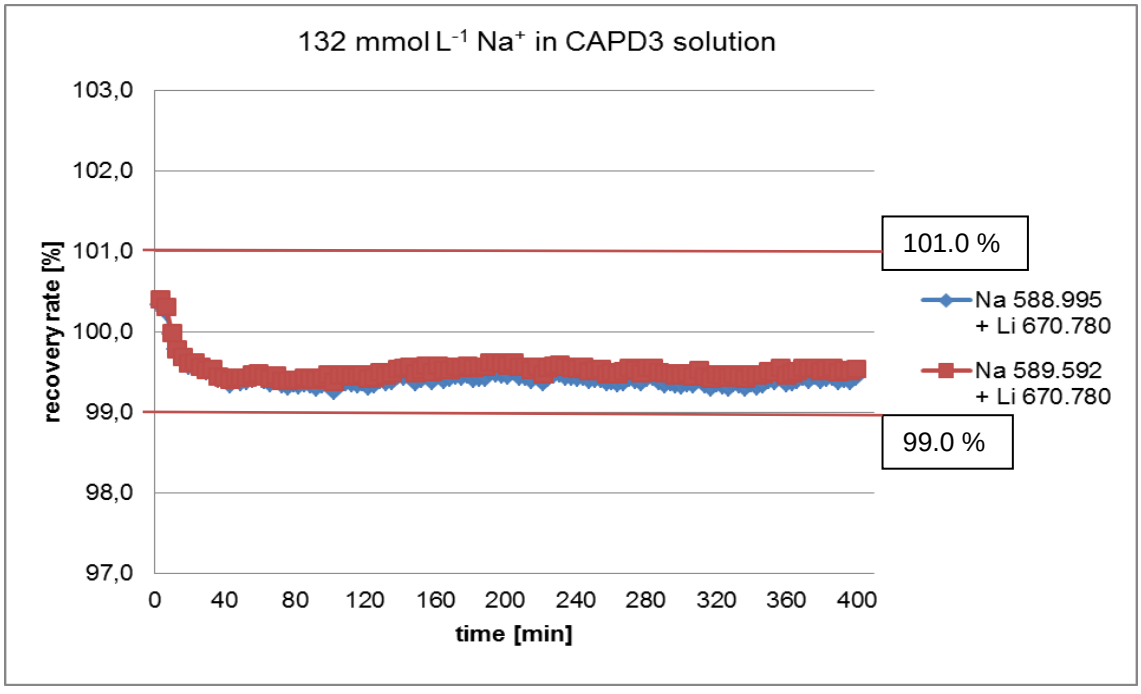

Figure 5-6: Determination of 132.0 mmol L^{-1} Na^{+} in a CAPD3 solution within a period of about 393 min. The two additional red lines drawn in the graph show the specification limit for Na in this sample in the IPC.

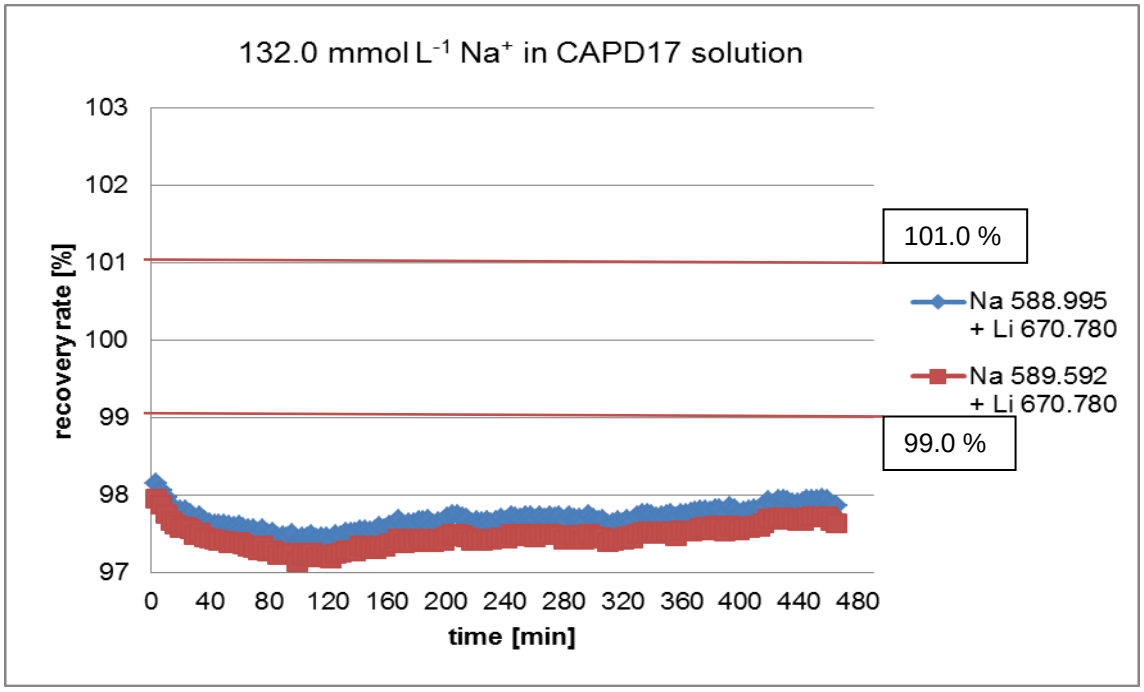

Figure 5-7: Determination of 132.0 mmol L^{-1} Na^+ in a CAPD17 solution within a period of about 465 min. The two additional red lines drawn in the graph show the specification limit for Na in this sample in the IPC.

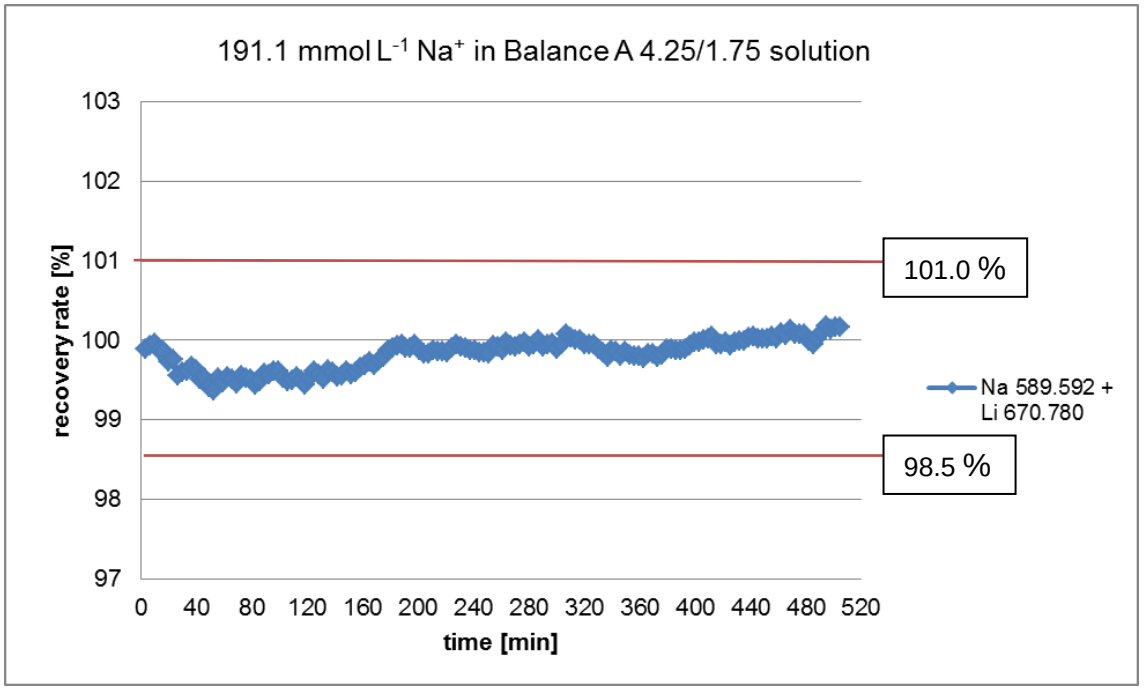

Figure 5-8: Determination of 191.1 mmol L^{-1} Na^+ in a Balance A 4.25/1.75 solution within a period of about 505 min. The two additional red lines drawn in the graph show the specification limit for Na in this sample in the IPC.

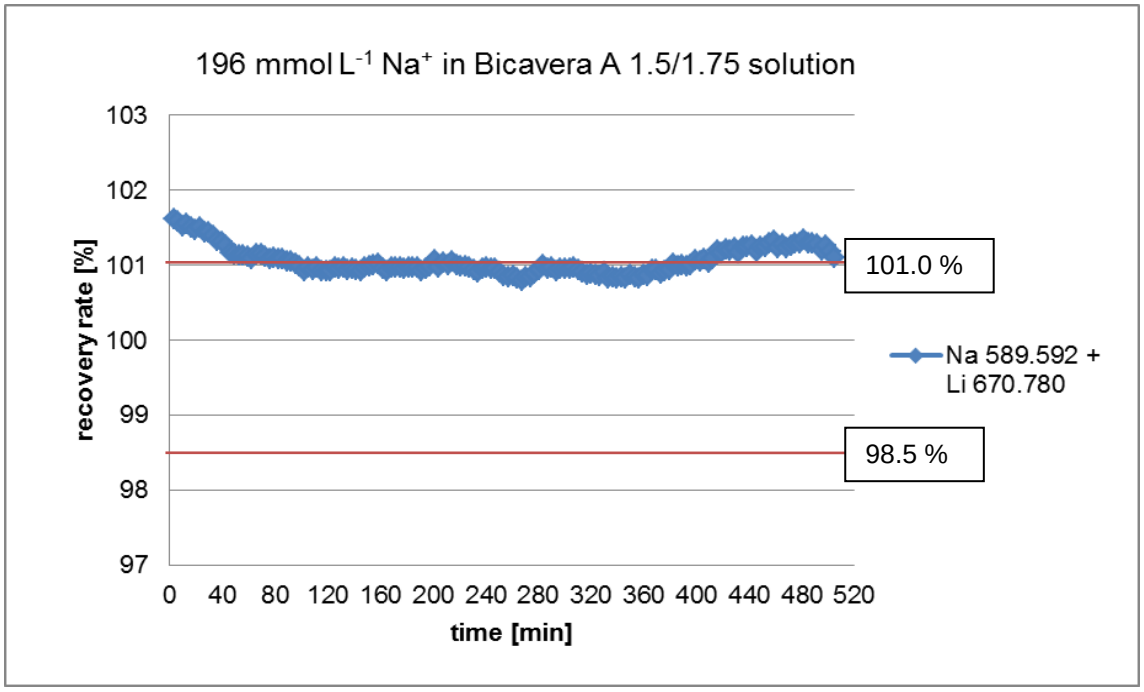

Figure 5-9: Determination of 196.0 mmol L^{-1} Na^{+} in a Bicavera A 1.5/1.75 solution within a period of about 505 min. The two additional red lines drawn in the graph show the specification limit for sodium in this sample, in the IPC.

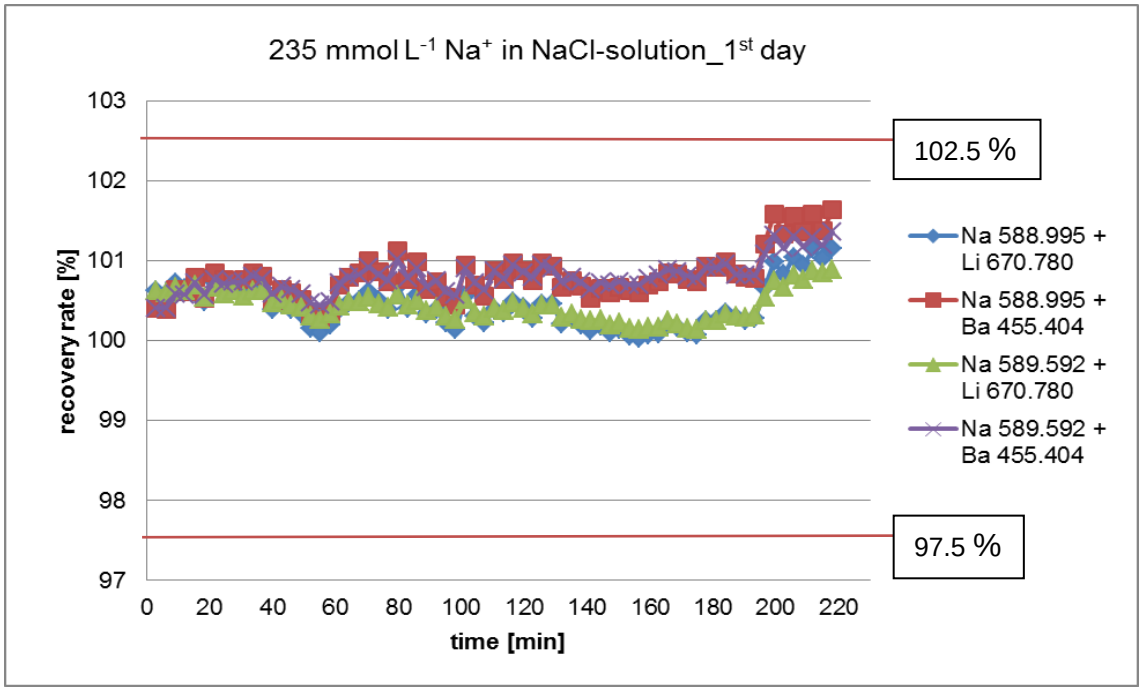

Figure 5-10: Determination of 235.0 mmol L^{-1} Na^{+} in an NaCl solution within a period of about 218 min (1^{st} day). The two additional red lines drawn in the graph show the specification limit for sodium according to Ph. Eur. (see Table 5-1)

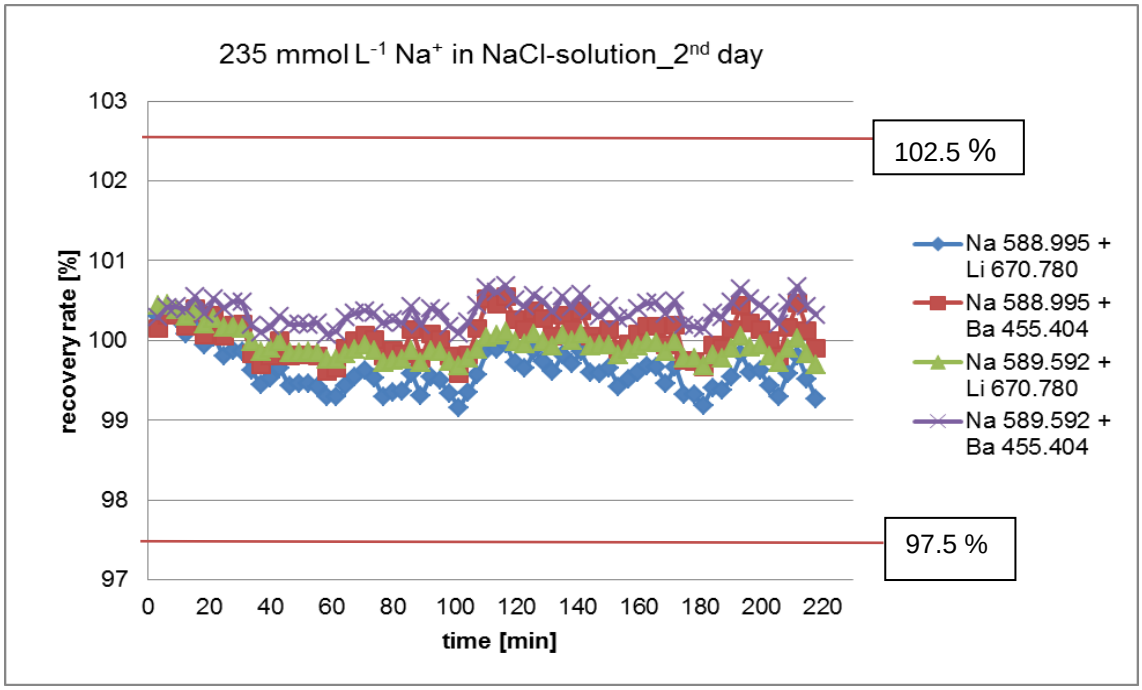

Figure 5-11: Determination of 235.0 mmol L^{-1} Na^+ in an NaCl solution within a period of about 218 min (2nd day). The two additional red lines drawn in the graph show the average specification limit for sodium according to Ph. Eur. (see Table 5-1)

5.3.2 The study of the long-term stability of the determination of calcium by ICP-OES

By the determination of calcium, the analyte emission lines Ca 315.887 nm, Ca 317.933 nm and Ca 396.847 nm are linked to one or two of the internal standards emission lines of barium (Ba 230.424 nm, Ba 233.527 nm and Ba 455.404 nm). The solutions used here are CAPD3, CAPD17, Bicavera A 1.5/1.75 and Balance A 4.25/1.75. The composition of these solutions can be found in Table 4-1.The dilution factors used for these measurements are in Table 4-2.

As already mentioned and explained in chapter 5.3.1, the detected calcium concentration in the CAPD17 solution (see Figure 5-13) is lower compared to that of the other solutions although the precision is acceptable.

All the three calcium emission lines linked with their individual IS gave satisfactory results with Ca 396.847 nm and Ba 455.404 nm been the best combination, irrespective of the Ca concentration and the sample matrix. Although the values in Figure 5-14 and Figure 5-15 show an upward trend, the increase in the recovery rate is less than 1 % within the measuring time of more than 8 h which is not that bad.

This trend could have resulted from the fact that barium lines used here are not very suitable and should, therefore, be replaced or a different internal standard, such as strontium, scandium or yttrium, should be used instead. Different dilution factors for Ca and Mg can also be applied in order to achieve a better intensity ratio between the individual analytes and the internal standard.

The internal standardization is very effective and also necessary in view of the results and the raw intensities in the appendix. All the results obtained here are within the tolerance limit of the IPC and so within the specification limit of Ph. Eur. which is ± 5 %.

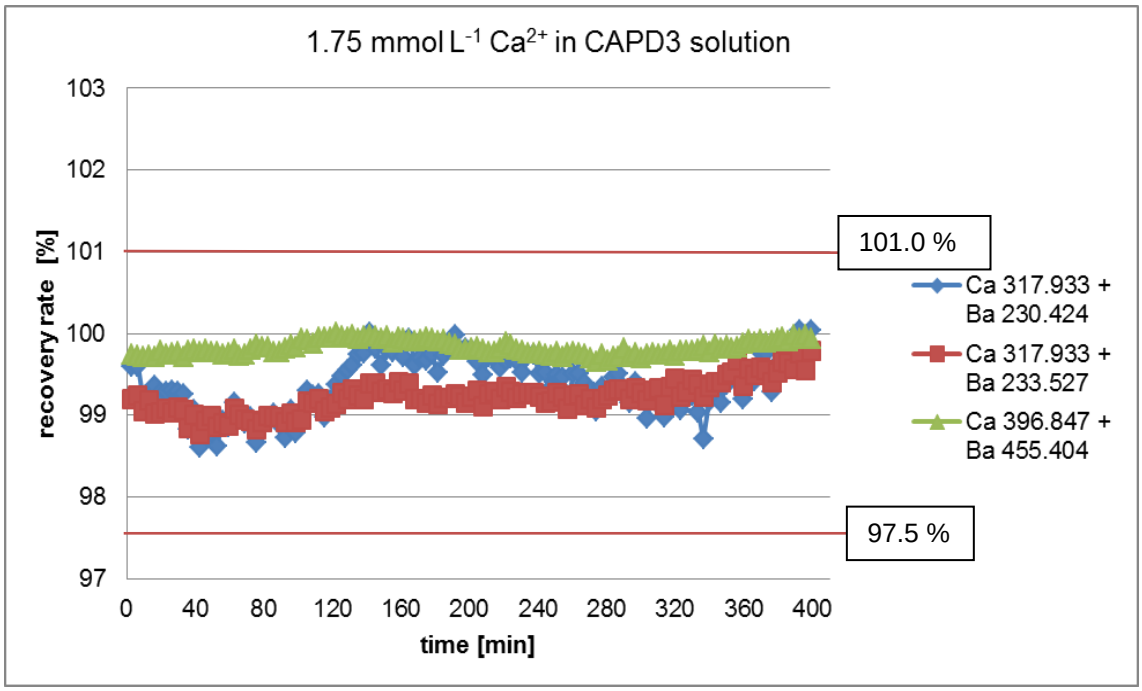

Figure 5-12: Determination of 1.75 mmol L^{-1} Ca^{2+} in a CAPD3 solution within a period of about 393 min. The two additional red lines drawn in the graph show the specification limit for calcium in this sample, in the IPC

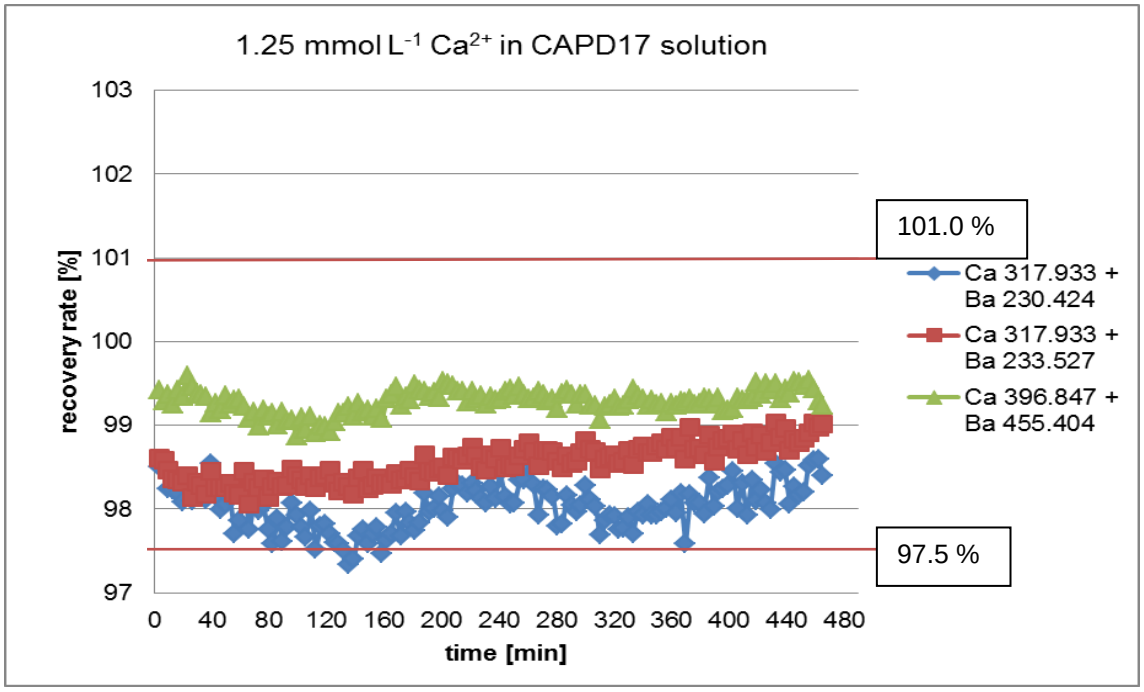

Figure 5-13: Determination of 1.25 mmol L^{-1} Ca^{2+} in a CAPD17 solution within a period of about 465 min. The two additional red lines drawn in the graph show the specification limit for calcium in this sample, in the IPC

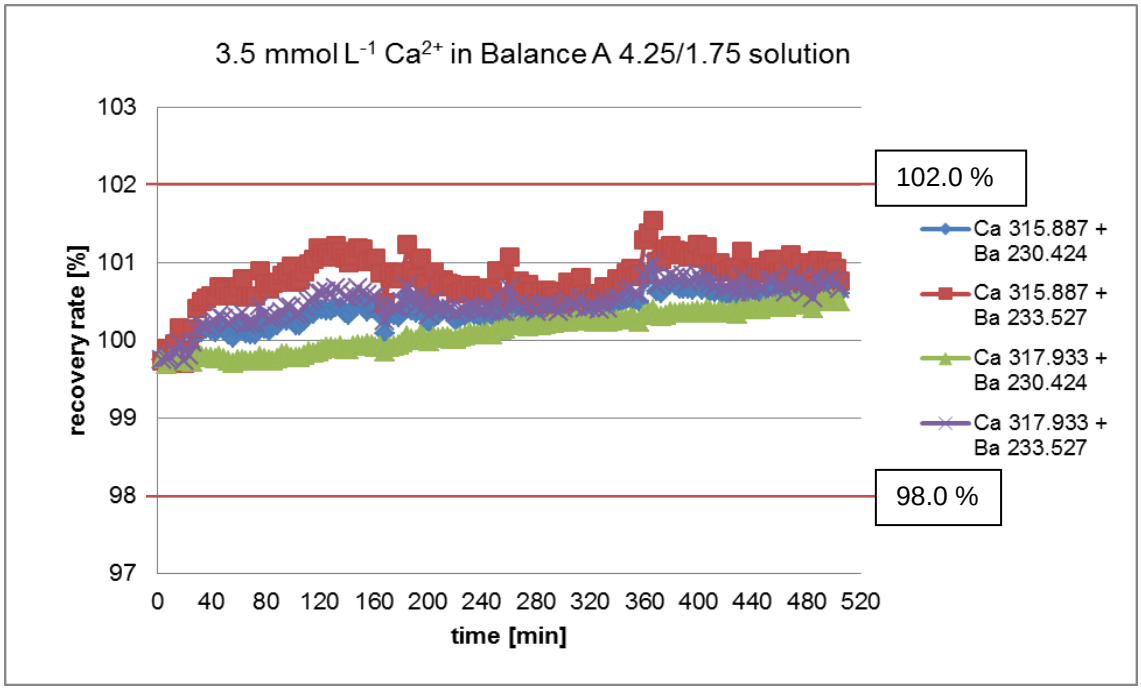

Figure 5-14: Determination of 3.5 mmol L^{-1} Ca^{2+} in a Balance A 4.25/1.75 solution within a period of about 505 min. The two additional red lines drawn in the graph show the specification limit for calcium in this sample, in the IPC

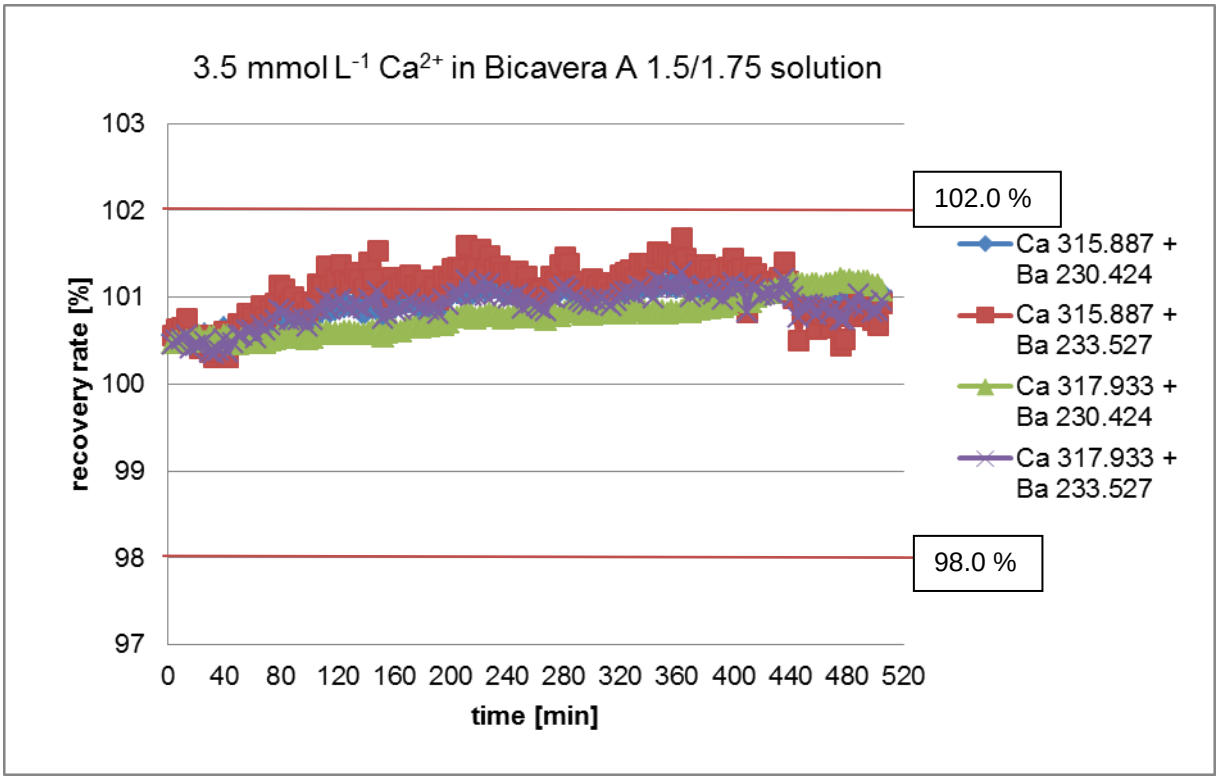

Figure 5-15: Determination of 3.5 mmol L^{-1} Ca^{2+} in a Bicavera A 1.5/1.75 solution within a period of about 505 min. The two additional red lines drawn in the graph show the specification limit for calcium in this sample, in the IPC

5.3.3 The study of the long-term stability of the determination of magnesium by ICP-OES

By the determination of magnesium, the analyte emission lines Mg 279.553 nm and Mg 280.270 nm are linked to the two internal standards emission lines of barium (Ba 230.424 nm and Ba 233.527 nm). The solutions used here are CAPD3, CAPD17, Bicavera A 1.5/1.75 and Balance A 4.25/1.75. The composition of these solutions can be found in Table 4-1. The dilution factors used for these measurements are in Table 4-2.

Both the precision and the accuracy of all the measurements are tolerable since almost all the values of the individual emission lines fulfill the requirements. All the results are within the specification limit of Ph. Eur. which is ± 5 % although some of the values are out of the tolerance range of the IPC (see Figure 5-16 and Figure 5-17). Some possible causes of the low magnesium values in the CAPD17 solution (see Figure 5-17) have been mentioned and explained already in chapter 5.3.1.

The application of an internal standard in this measurement has also proven very efficient and is therefore required for such long-term measurements. However, the results obtained with the magnesium emission line Mg 280.270 nm is better than that of Mg 279.553 nm, irrespective of the barium emission line they are linked to.

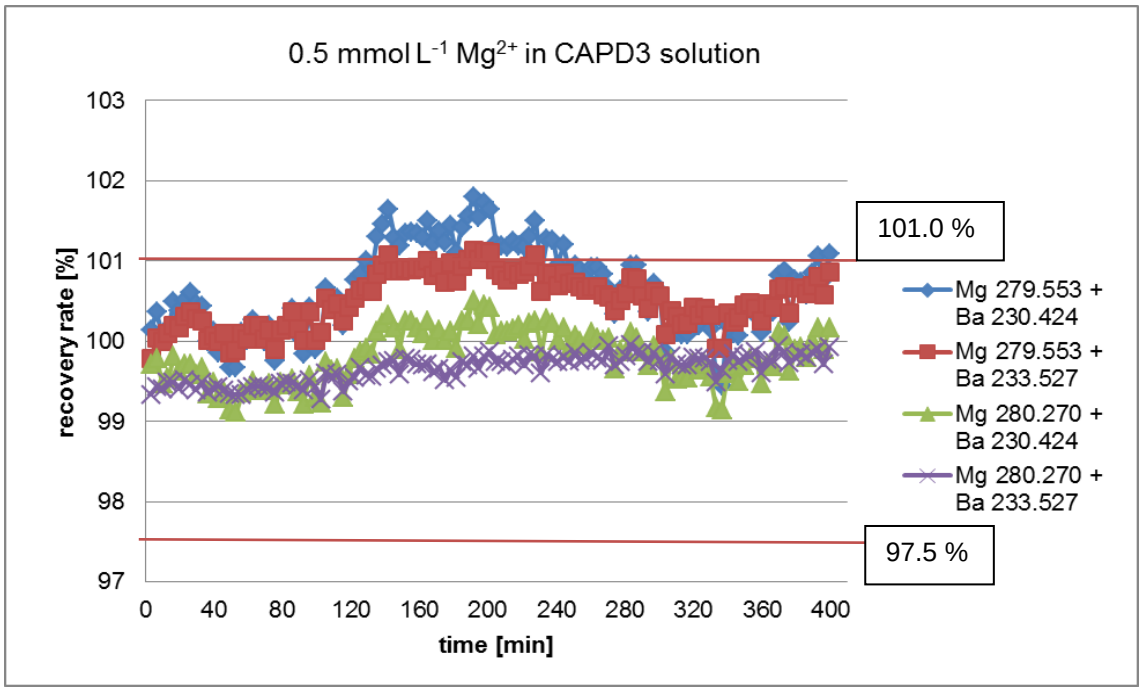

Figure 5-16: Determination of 0.5 mmol L^{-1} Mg^{2+} in a CAPD3 solution within a period of about 393 min. The two additional red lines drawn in the graph show the specification limit for magnesium in this sample, in the IPC

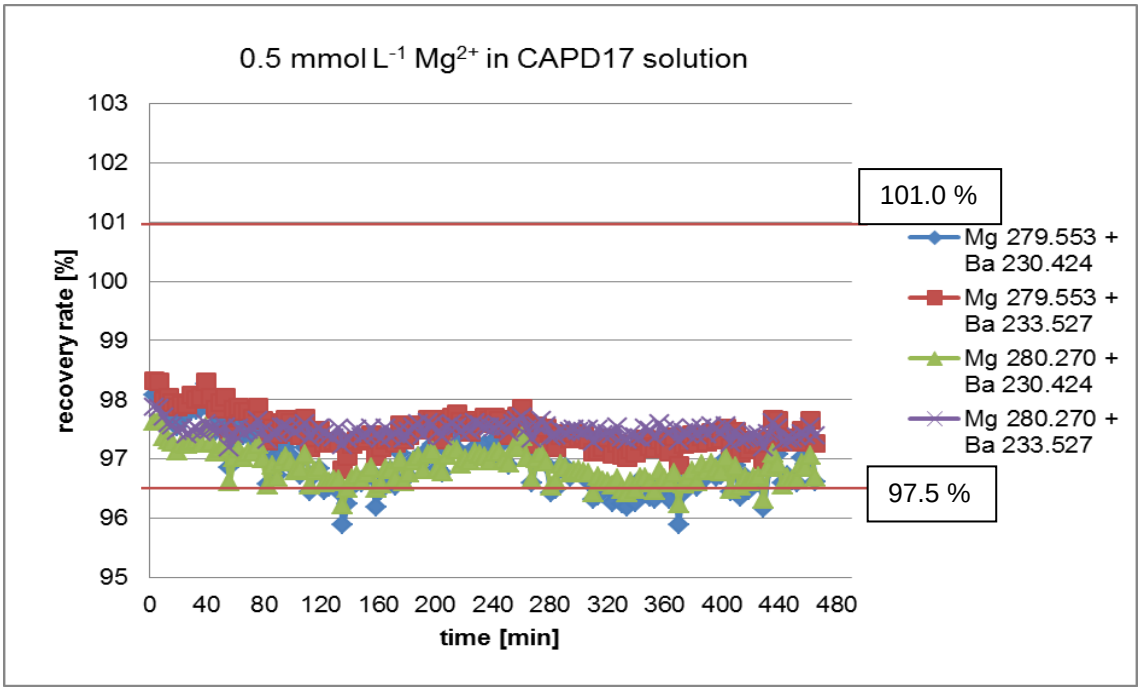

Figure 5-17: Determination of 0.5 mmol L^{-1} Mg^{2+} in a CAPD17 solution within a period of about 465 min. The two additional red lines drawn in the graph show the specification limit for magnesium in this sample, in the IPC

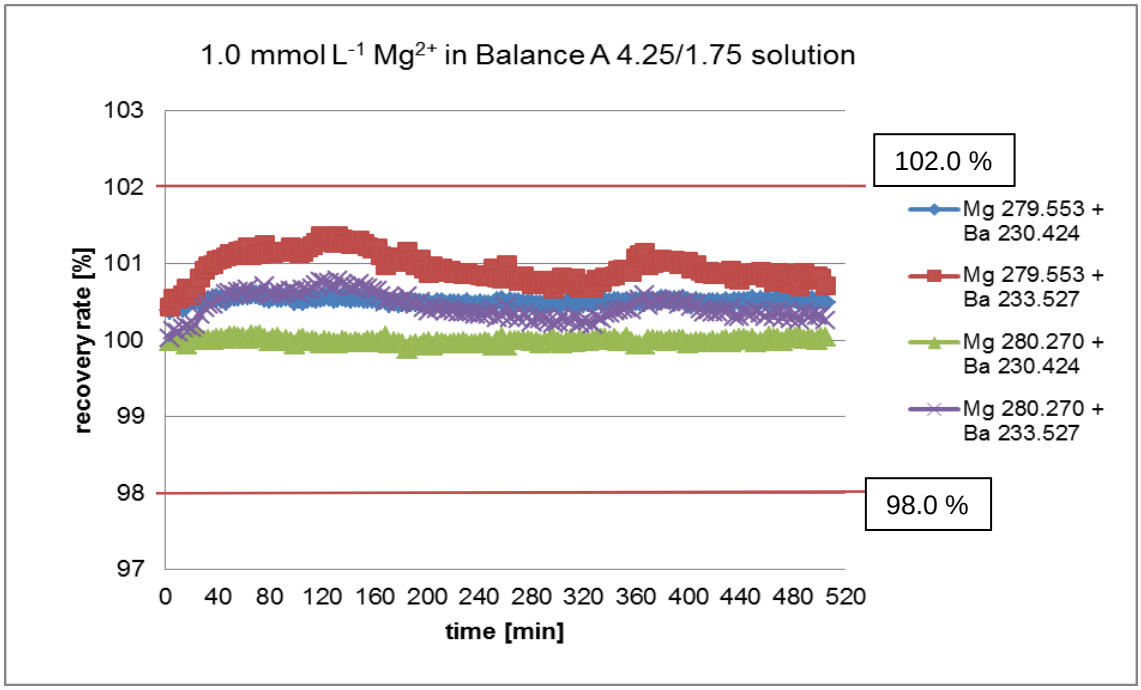

Figure 5-18: Determination of 1.0 mmol L^{-1} Mg^{2+} in a Balance A 4.25/1.75 solution within a period of about 505 min. The two additional red lines drawn in the graph show the specification limit for magnesium in this sample, in the IPC

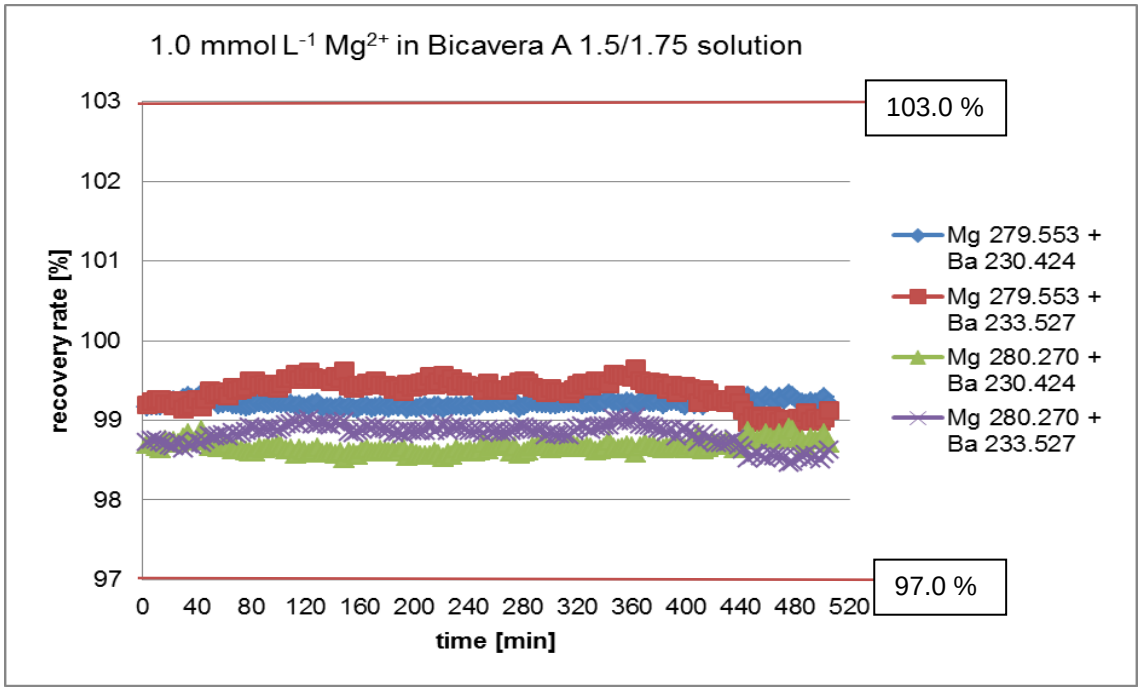

Figure 5-19: Determination of 1.0 mmol L^{-1} Mg^{2+} in a Bicavera A 1.5/1.75 solution within a period of about 505 min. The two additional red lines drawn in the graph show the specification limit for magnesium in this sample, in the IPC

5.3.4 The study of the long-term stability of the determination of potassium by ICP-OES

By the determination of potassium, the analyte emission line K 766.491 nm is linked to the internal standards emission line of lithium Li 670.780 nm. The solution used here is Multibic A 4K. The composition of this solution can be found in Table 4-1 and the dilution factor in Table 4-2.

Although the values in Figure 5-20 show some slight upward trend, the recovery rate increases less than 1 % within the measuring period of more than 4 h. Since the values are within the tolerance range of the IPC, they are also within the ± 5 % specification range of Ph. Eur.

The use of internal standard is also necessary for the long-term determination of potassium due to the high precision required in this study.

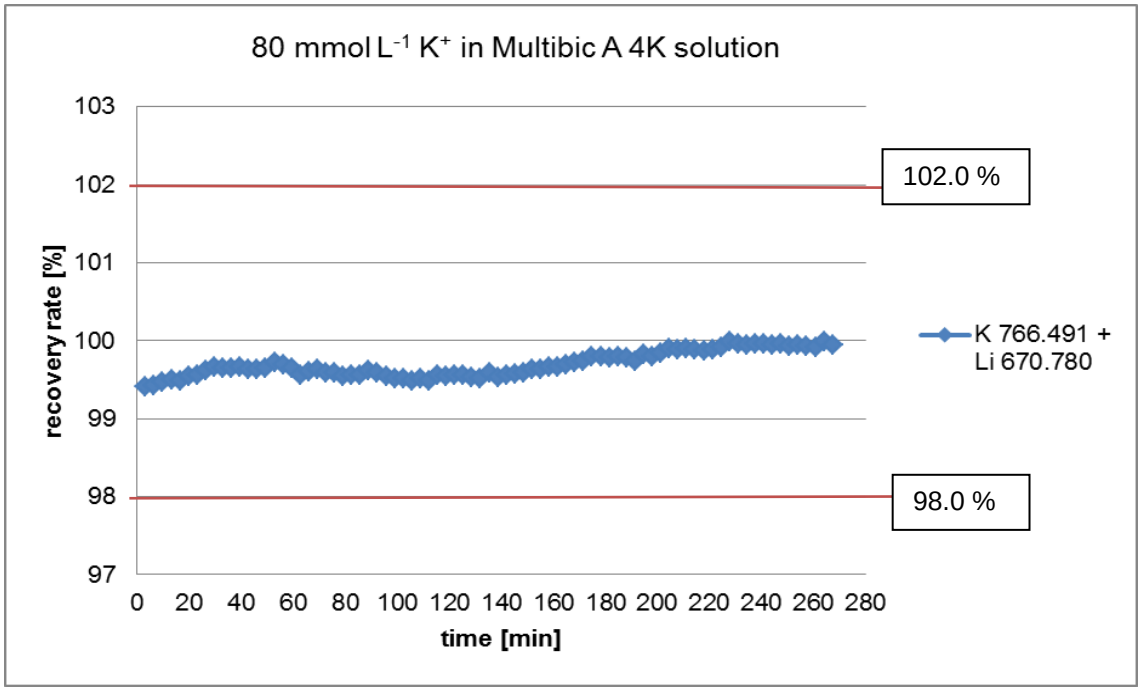

Figure 5-20: Determination of 80.0 mmol L^{-1} K^{+} in a Multibic A 4K solution within a period of about 267 min. The two additional red lines drawn in the graph show the specification limit for potassium in this sample, in the IPC

5.4 Examination of interference effects on the determination of Na, Ca, Mg and K by ICP-OES

Since no analytical technique is free from matrix effect, this term has become one of the key words in analytical chemistry. The IUPAC, in their nomenclature for automated and mechanical analysis define matrix effect as “the combined effect of all components of the sample other than the analyte on the measurement of the quantity. If a specific component can be identified as causing an effect then this is referred to as interference. In this context, matrix is defined as “the components of the sample other than the analyte” [170].
Unlike AAS and flame photometry, ICP-OES is less susceptible to interferences caused as a result of inter-element effects or by organic substances due to the high plasma temperature used for atomization and ionization [64], [82]. However, analyte signals can be influenced if the necessary steps are not taking in the presence of complex sample matrices.

In ICP-OES, organic compounds are well known as a type of matrix which influences analytes in many ways. Organic acids and solvents, in particular, mostly cause a change in the chemical and physical properties of the plasma which result in plasma destabilization and a change in plasma excitation conditions. They are observed to cause a decrease in the excitation temperature [100]–[103], [106], [107], [171].
Thus, the organic substances, glucose und lactate, in the dialysis solutions are assumed to be responsible for most of the interferences that occur in the determination of the metal ions Na, K, Ca and Mg by ICP-OES. The main focus of this work is therefore on the study and evaluation of the effect of glucose and lactate.
The following points are considered by the determination of the matrix effect in this work:

- Do glucose and lactate have influence on the measurements and how?
- Which analyte or IS emission line is the best?
- Which IS-analyte-emission line-combination is the best?
- How efficient is the internal standardization in terms of accuracy and precision?

Most of the graphs representing the results obtained can be found in the appendix. The results of the samples measured on the same day are summarized in the same graph since they are measured under the same calibration conditions. The names of the curves are indicated in the legend beside the graphs. The descending order of the names in the legend indicates the measuring order of the samples on each day.

5.4.1 The effect of glucose and lactate on the determination of magnesium by ICP-OES

The emission lines of Mg and that of the internal standard barium to which they are linked are summarized in Table 5-8. By the determination of the lowest concentration of Mg, only ionic lines are linked to each other. In case of the determination of the highest Mg concentration, ionic lines of the IS are linked to the atomic line of the analyte.

Table 5-8: IS-analyte emission line-combination used for the determination of the matrix effect on magnesium (atomic lines (I) and ionic lines (II))

0.4 mmol L^{-1} Mg^{2+}		24 mmol L^{-1} Mg^{2+}	
Analyte emission line [nm]	IS emission line [nm]	Analyte emission line [nm]	IS emission line [nm]
Mg II 279.553	Ba II 230.424	Mg I 285.213	Ba II 230.424
Mg II 279.553	Ba II 233.527	Mg I 285.213	Ba II 233.527
Mg II 280.270	Ba II 230.424	-	-
Mg II 280.270	Ba II 233.527	-	-

5.4.1.1 Matrix effects on the determination of the lowest magnesium concentration (0.4 mmol L^{-1})

In the presence of either glucose or lactate the recovery rates obtained after the internal standardization are almost equal. Contrary to this, the results obtained after the internal standardization in the presence both glucose and lactate vary on both days. This difference in the values is even stronger when the Mg line 279.553 nm is linked to the Ba line 230.424 nm. The best IS-analyte emission line-combination with which higher precision and higher accuracy are achieved in all sample matrices is Mg 280.270 nm with Ba 233.527 nm. The lower recovery rates obtained for the samples containing both glucose and lactate could be as a result of interference in the plasma supply on the day the measurements were carried out.

Apart from the decrease in signal intensities of both the analyte and the IS from the first day to the second day which may have resulted from the different calibrations on both days, no significant effects are detected.

The results obtained before and after the internal standardization are summarized in Table 5-9 to Table 5-11.

Table 5-9: RSD of analyte and internal standard emission lines before internal standardization by the determination of 0.4 mmol L^{-1} Mg (n = 42)

RSD before internal standardization [%]	**Mg II 279.553**	**Mg II 280.270**	**Ba II 230.424**	**Ba II 233.527**
$MgCl_2$-samples	0.19 - 0.47	0.21 - 0.35	0.31 - 0.49	0.20 - 0.49
$MgCl_2$+glucose-samples	0.18 - 0.41	0.15 - 0.22	0.22 - 0.52	0.15 - 0.43
$MgCl_2$+Na-lactate-samples	0.17 - 0.37	0.13 - 0.31	0.17 - 0.28	0.11 - 0.24
$MgCl_2$+glucose+Na-lactate-samples	0.14 - 0.92	0.13 - 0.60	0.21 - 0.70	0.21 - 0.60

Table 5-10: RSD of analyte and internal standard emission lines after internal standardization by the determination of 0.4 mmol L^{-1} Mg

RSD after internal standardization [%]	**Mg II 279.553 + Ba II 230.424**	**Mg II 279.553 + Ba II 233.527**	**Mg II 280.270 + Ba II 230.424**	**Mg II 280.270 + Ba II 233.527**
$MgCl_2$-samples	0.29 - 0.34	0.18 - 0.22	0.24 - 0.25	0.15 - 0.19
$MgCl_2$+glucose-samples	0.28 - 0.57	0.19 - 0.43	0.23 - 0.43	0.16 - 0.30
$MgCl_2$+Na-lactate-samples	0.27 - 0.38	0.18 - 0.23	0.22 - 0.29	0.15 - 0.18
$MgCl_2$+glucose+Na-lactate-samples	0.27 - 0.91	0.18 - 0.53	0.19 - 0.59	0.13 - 0.29

Table 5-11: Recovery rates of analyte and internal standard emission lines after internal standardization by the determination of 0.4 mmol L^{-1} Mg

Recovery rate after internal standardization [%]	**Mg II 279.553 + Ba II 230.424**	**Mg II 279.553 + Ba II 233.527**	**Mg II 280.270 + Ba II 230.424**	**Mg II 280.270 + Ba II 233.527**
$MgCl_2$-samples	98.59 - 99.93	98.67 - 99.36	98.92 - 99.86	99.01 - 99.25
$MgCl_2$+glucose-samples	98.45 - 99.10	98.58 - 99.08	98.59 - 99.34	98.79 - 99.41
$MgCl_2$+Na-lactate-samples	97.67 - 98.06	97.89 - 98.37	98.10 - 98.71	98.33 - 99.04
$MgCl_2$+glucose+Na-lactate-samples	93.26 - 99.09	94.92 - 97.96	94.96 - 98.46	96.67 - 97.37

5.4.1.2 Matrix effects on the determination of the highest magnesium concentration (24 mmol L^{-1})

In view of the results obtained here, the Mg line Mg 285.213 nm mostly has a better precision than both internal standard emission lines. However, the results obtained after the internal standardization is very good. The recovery rate varies between the ranges of about 2 % in most cases. The results obtained before and after the internal standardization are summarized in Table 5-12 to Table 5-14.

The graphs obtained after measuring the samples containing both glucose and lactate show a decrease in the signal intensity of both the analyte and the IS from the first day to the second day. In spite of this, the internal standardization resulted in very good recovery rates. The values obtained for both days after the correction are therefore comparable.

Table 5-12: RSD of analyte and internal standard emission lines before internal standardization by the determination of 24 mmol L^{-1} Mg (red values displays RSD > 1 %) (n = 42)

RSD before internal standardization [%]	Mg I 285.213	Ba II 230.424	Ba II 233.527
$MgCl_2$-samples	0.29 - 0.57	0.39 - 0.54	0.42 - 0.53
$MgCl_2$+glucose-samples	0.16 - 0.53	0.34 - 0.64	0.27 - 0.87
$MgCl_2$+Na-lactate-samples	0.24 - 0.56	0.30 - 0.71	0.36 - 0.89
$MgCl_2$+glucose+Na-lactate-samples	0.12 - 0.52	0.17 - 0.55	0.14 - 1.11

Table 5-13: RSD of analyte and internal standard emission lines after internal standardization by the determination of 24 mmol L^{-1} Mg

RSD after internal standardization [%]	Mg I 285.213 + Ba II 230.424	Mg I 285.213 + Ba II 233.527
$MgCl_2$-samples	0.18 - 0.36	0.07 - 0.20
$MgCl_2$+glucose-samples	0.20 - 0.46	0.19 - 0.42
$MgCl_2$+Na-lactate-samples	0.27 - 0.39	0.14 - 0.36
$MgCl_2$+glucose+Na-lactate-samples	0.18 - 0.41	0.07 - 0.61

Table 5-14: Recovery rates of analyte and internal standard emission lines after internal standardization by the determination of 24 mmol L^{-1} Mg

Recovery rate after internal standardization [%]	**Mg I 285.213 + Ba II 230.424**	**Mg I 285.213 + Ba II 233.527**
$MgCl_2$-samples	98.66 - 98.68	97.59 - 98.18
$MgCl_2$+glucose-samples	97.71 - 99.22	98.84 - 100.88
$MgCl_2$+Na-lactate-samples	98.35 - 99.07	98.77 - 101.20
$MgCl_2$+glucose+Na-lactate-samples	97.23 - 99.59	97.83 - 99.73

5.4.1.3 Conclusion on the effect of glucose and lactate on the determination of magnesium

Irrespective of the type of emission line used for Mg or its concentration, the RSD of the raw intensities in the different samples is mostly better than that of the internal standard. However, the required precision of less than 1 % is achieved for both the IS and the analyte in all the different matrices, except for the sample "$MgCl_2$ + 277.5 mM glucose + 84 mM lactate" with a Mg concentration of 20 mmol L^{-1}. The RSD of the raw intensities of the IS emission line Ba 233.527 nm after measuring this sample on the first day is greater than 1 %, as highlighted in red in Table 5-12, due to the decreasing values within the first 50 min. This shows the unreliability of Ba points out the fact that an alternative internal standard, such as scandium of yttrium, should be taken into consideration.

The internal standardization for the determination of magnesium is therefore not necessarily needed in terms of precision because the corrections carried out to improve the RSD of the measurements are not always effective. In case of the IS-analyte emission line-combination (Mg II 279.553 + Ba II 230.424), the corrections mostly lead to poorer results.

The argon signal intensity of the matrices with the highest glucose concentration (566 mmol L^{-1} glucose) is mostly lower compared to that of the other matrices. It could be assumed that glucose has a depressive effect on argon when it is present in a very high concentration.

5.4.2 The effect of glucose and lactate on the determination of calcium by ICP-OES

All the calcium emission lines used in this work are ionic lines which are mostly linked to the ionic line of the internal standard barium. By the determination of the highest calcium concentration, lithium is also chosen as an internal standard. In this case, a calcium ionic line is linked to an atomic line of lithium. The internal standard-analyte-combinations used for the determination of calcium can be found in Table 5-15.

Table 5-15: IS-analyte-combinations used for the determination of the matrix effect on calcium (atomic lines (I) and ionic lines (II))

0.8 mmol L^{-1} Ca^{2+}		36 mmol L^{-1} Ca^{2+}	
Analyte emission line [nm]	IS emission line [nm]	Analyte emission line [nm]	IS emission line [nm]
Ca II 317.933	Ba II 230.424	Ca II 183.801	Ba II 230.424
Ca II 317.933	Ba II 233.527	Ca II 183.801	Ba II 233.527
Ca II 396.847	Ba II 455.404	Ca II 183.801	Li I 670.780

5.4.2.1 Matrix effects on the determination of the lowest calcium concentration (0.8 mmol L^{-1})

With the exception of the matrices, 0.8 mmol L^{-1} $CaCl_2$ + 277.5 mmol L^{-1} glucose + 84 mmol L^{-1} Na-lactate, 0.8 mmol L^{-1} $CaCl_2$ + 566.2 mmol L^{-1} glucose + 28 mmol L^{-1} Na-lactate and 0.8 mmol L^{-1} $CaCl_2$ + 566.2 mmol L^{-1} glucose + 84 mmol L^{-1} Na-lactate, by which a repeatability greater than 1 % is obtained due to some fluctuations which occurred during the measurement on the first day, the precision of the measurements in all the different matrices is extraordinarily good. The RSD obtained even before the internal standardization is within the required limit of less than 1 %. The internal standardization improved these values and the results achieved after the correction are remarkably great, especially with the IS-analyte emission line-combination Ca 396.847 nm + Ba 455.404 nm which proved as the best in this study. As displayed in Figure 5-21, a sudden decrease in the argon signal intensity occurred just before the last measurement of the sample 0.8 mmol L^{-1} $CaCl_2$ + 277.5 mmol L^{-1} glucose + 84 mmol L^{-1} Na-lactate. The argon intensities of the samples that are measured afterwards are therefore lower. On the other hand, the signal intensities of the analyte and the IS are higher. This caused strong fluctuations

in the measurements. The poor precision achieved as a result is high-lighter in red in Table 5-16 and Table 5-17.

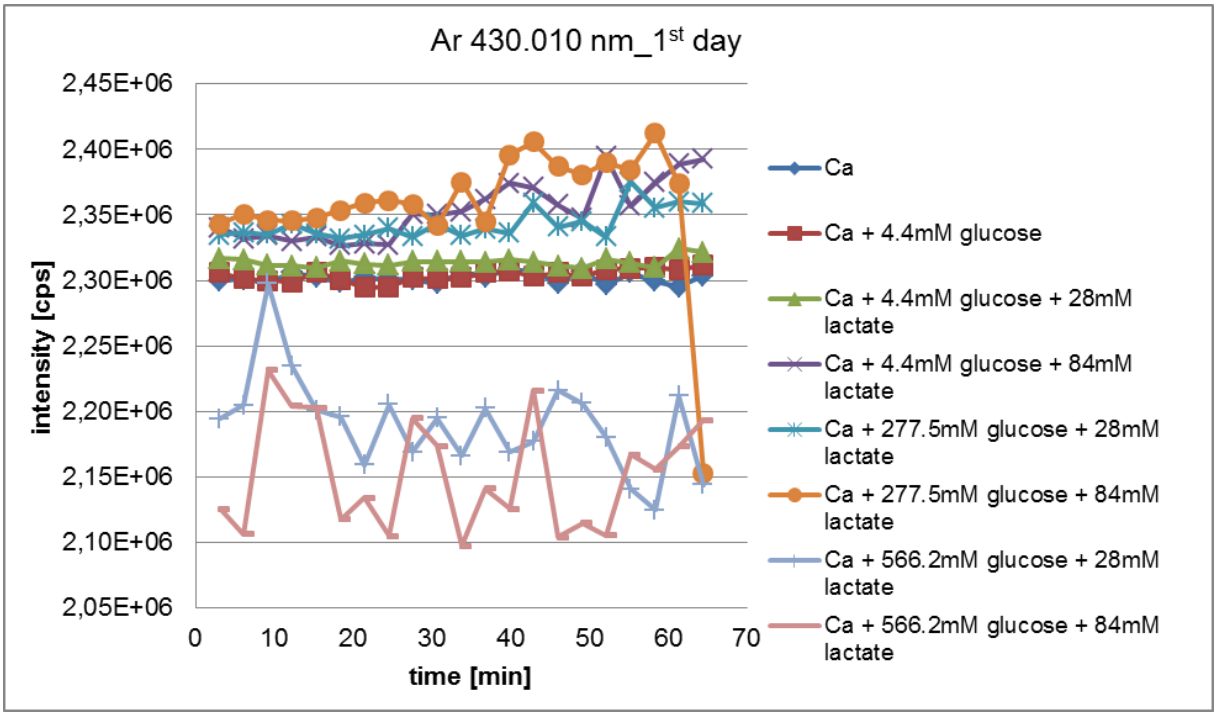

Figure 5-21: Intensity of argon by the determination of 0.8 mmol L^{-1} Ca in different sample matrices

According to the graphs display in the appendix, all the samples containing both glucose and lactate are measured on the same day together with the sample containing only $CaCl_2$. The Ar-intensities of these measurements are greater compared to that of the samples containing $CaCl_2$+glucose and $CaCl_2$+lactate. Due to this, the intensities of the IS and that of the analyte are less, which consequently result in very low recovery rates.

On account of the results obtained here, glucose and lactate have no significant effect on the lowest Ca concentration of 0.8 mmol L^{-1}.

The results obtained before and after the internal standardization are summarized in Table 5-16 to Table 5-18.

Table 5-16: RSD of analyte and internal standard emission lines before internal standardization by the determination of 0.8 mmol L^{-1} Ca (red values displays RSD > 1 %) (n = 42)

RSD before internal standardization [%]	Ca II 317.933	Ca II 396.847	Ba II 230.424	Ba II 233.527	Ba II 455.404
$CaCl_2$-samples	0.41 - 0.67	0.52 - 0.64	0.52 - 0.68	0.40 - 0.72	0.56 - 0.57
$CaCl_2$+glucose-samples	0.28 - 0.50	0.30 - 0.68	0.31 - 0.55	0.21 - 0.42	0.29 - 0.66
$CaCl_2$+Na-lactate-samples	0.16 - 0.51	0.21 - 0.45	0.36 - 0.52	0.21 - 0.53	0.20 - 0.50
$CaCl_2$+glucose+Na-lactate-samples	0.18 - 2.91	0.28 - 5.72	0.29 - 3.96	0.22 - 3.94	0.26 - 5.64

Table 5-17: RSD of analyte and internal standard emission lines after internal standardization by the determination of 0.8 mmol L^{-1} Ca (red values displays RSD > 1 %)

RSD after internal standardization [%]	Ca II 317.933 + Ba II 230.424	Ca II 317.933 + Ba II 233.527	Ca II 396.847 + Ba II 455.404
$CaCl_2$-samples	0.23 - 0.47	0.20 - 0.29	0.08 - 0.12
$CaCl_2$+glucose-samples	0.29 - 0.55	0.23 - 0.30	0.09 - 0.24
$CaCl_2$+Na-lactate-samples	0.32 - 0.49	0.19 - 0.27	0.09 - 0.18
$CaCl_2$+glucose+Na-lactate-samples	0.34 - 1.35	0.15 - 1.31	0.04 - 0.12

Table 5-18: Recovery rate of analyte and internal standard emission lines after internal standardization by the determination of 0.8 mmol L^{-1} Ca

Recovery rate after internal standardization [%]	Ca II 317.933 + Ba II 230.424	Ca II 317.933 + Ba II 233.527	Ca II 396.847 + Ba II 455.404
$CaCl_2$-samples	96.84 - 97.4	95.91 - 96.24	94.78 - 95.01
$CaCl_2$+glucose-samples	96.90 - 103.33	96.47 - 102.16	94.90 - 100.36
$CaCl_2$+Na-lactate-samples	100.63 - 101.62	101.27 - 101.77	98.01 - 99.19
$CaCl_2$+glucose+Na-lactate-samples	94.70 - 99.49	94.11 - 99.02	94.95 - 96.50

5.4.2.2 Matrix effects on the determination of the highest calcium concentration (36 mmol L^{-1})

The RSD achieved before the internal standardization is within the specified limit of less than 1 %. The corrections carried out with this standardization improved the values greatly, in particular, with the IS emission line Ba 233.527 nm linked to the analyte emission line Ca 183.801 nm.

Although the results obtained with the combination, analyte-ionic line Ca 183.801 nm with the IS-atomic line Li 670.780 nm are not that poor, this combination could be used alternatively but shouldn't be preferred since ionic lines and atomic lines behave differently and so linking such lines would not always produce reliable results. Moreover, lithium is an alkaline metal and calcium an earth alkaline metal so their different chemical and physical properties could also affect the measurements negatively. Furthermore, the calcium line Ca II 183.801 nm is in the UV region whereas Li I 670.780 nm is in the visible region therefore background effects on these lines could possibly be different. Furthermore, linking an ionic line to an atomic line can result in higher analyte concentrations. In some cases, the combination Ca II 183.801 nm + Li I 670.780 nm resulted in higher analyte concentrations as reported in the literature [165].

All the results obtained in this study are summarized in Table 5-19 to Table 5-21.

Table 5-19: RSD of analyte and internal standard emission lines before internal standardization by the determination of 36 mmol L^{-1} Ca (n = 42)

RSD before internal standardization [%]	Ca II 183.801	Ba II 230.424	Ba II 233.527	Li I 670.780
$CaCl_2$-samples	0.57 - 0.62	0.20 - 0.38	0.37 - 0.44	0.16 - 0.41
$CaCl_2$+glucose-samples	0.36 - 0.94	0.34 - 0.71	0.34 - 0.89	0.16 - 0.96
$CaCl_2$+Na-lactate-samples	0.21 - 0.52	0.22 - 0.51	0.16 - 0.48	0.14 - 0.58
$CaCl_2$+glucose+Na-lactate-samples	0.25 - 0.90	0.16 - 0.62	0.21 - 0.75	0.14 - 0.72

Table 5-20: RSD of analyte and internal standard emission lines after internal standardization by the determination of 36 mmol L^{-1} Ca

RSD after internal standardization [%]	Ca II 183.801 + Ba II 230.424	Ca II 183.801 + Ba II 233.527	Ca II 183.801 + Li I 670.780
$CaCl_2$-samples	0.34 - 0.58	0.19 - 0.26	0.38 - 0.53
$CaCl_2$+glucose-samples	0.44 - 0.57	0.16 - 0.36	0.18 - 0.73
$CaCl_2$+Na-lactate-samples	0.34 - 0.86	0.13 - 0.36	0.14 - 0.53
$CaCl_2$+glucose+Na-lactate-samples	0.32 - 0.50	0.13 - 0.23	0.18 - 0.46

Table 5-21: Recovery rate of analyte and internal standard emission lines after internal standardization by the determination of 36 mmol L^{-1} Ca

Recovery rate after internal standardization [%]	Ca II 183.801 + Ba II 230.424	Ca II 183.801 + Ba II 233.527	Ca II 183.801 + Li I 670.780
$CaCl_2$-samples	99.27 - 99.68	99.22 - 99.34	101.57 - 101.63
$CaCl_2$+glucose-samples	97.75 - 101.39	99.01 - 100.45	100.00 - 102.93
$CaCl_2$+Na-lactate-samples	98.95 - 103.70	99.81 - 102.12	99.70 - 103.80
$CaCl_2$+glucose+Na-lactate-samples	98.19 - 100.33	99.09 - 100.38	98.54 - 101.93

5.4.2.3 Conclusion on the effect of glucose and lactate on the determination of calcium

As with the Mg-samples in chapter 5.4.1, all the $CaCl_2$-samples containing the highest glucose concentration (566 mmol L^{-1} glucose) lead to a decrease in the argon signal intensity. This behavior of glucose is similar to that of some mineral acids which decrease the excitation temperature of the plasma [108].

In view of the results obtained here, the internal standardization has proven very effective in terms of precision for both concentrations.

The RSD is mostly within the required limit of less than 1 % even before the internal standardization which then improves it. This shows that ICP-OES is a suitable method for the determination of calcium. Moreover, no significant matrix effect is detected in the presence of glucose or lactate or in the presence of both substances.

5.4.3 Comparing the effect of lactate and some other α-hydroxy-carboxylates on the determination of calcium by ICP OES

Two α-hydroxy-carboxylates (glycolate and 2-hydroxy-butyrate) are chosen to examine their effect on the determination of calcium compared to that of lactate. According to organic chemistry, the main α-hydroxy-carboxylates are lactate and 2-hydroxy-butyrate, since they have one or more methyl rest(s) attached to the carbon atom with the OH rest. Glycolate, however, has two hydrogen rests attaching the carbon atom with the OH rest, which, chemically, gives it some different properties. The methods and emission lines used here are similar to that of the calcium determinations in chapter 5.4.2. The IS-analyte emission line combinations are also the same depending on the concentration of calcium (see Table 5-15).

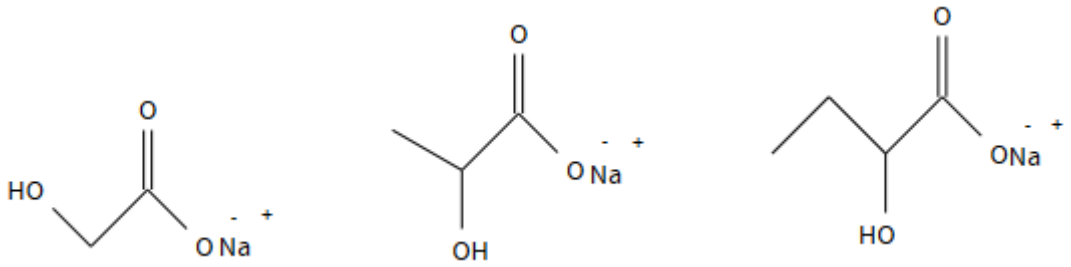

Sodium glycolate Sodium L-lactate Sodium 2-hydroxybutyrate

Figure 5-22: Chemical structures of the three α-hydroxy-carboxylates compared in this work

5.4.3.1 The effect of α-hydroxy-carboxylates on the determination of the lowest calcium concentration (0.8 mmol L^{-1})

At low calcium concentrations, the precision of all the samples both before and after the internal standardization are within the required limit of less than 1 %. However, the results obtained after the internal standardization with the IS-analyte emission line-combination Ca 317.933 nm + Ba 230.424 nm are poorer compared to the results obtained before the standardization of this analyte emission line Ca 317.933 nm. With the combination Ca 396.847 nm + Ba 455.404 nm, which has been found as the best IS-analyte emission line-combination for this concentration range, the precision is greatly improved. This confirms the results achieved in chapter 5.4.2.1.

In the presence of glycolate, the intensities of both analyte emission lines are greater compared to that of the samples with the other matrix components. Since the analyte

emission lines and that of the internal standards behave differently in this case, the recovery rates of the samples with glycolate are also higher whereas the results of the samples with the other matrices and that with only $CaCl_2$ are very similar. The different behavior of glycolate could result from the fact that its properties are a bit different from that of the real α-hydroxy-carboxylates, lactate and 2-hydroxy-butyrate, which, compared to glycolate, have one or more methyl rest(s) (see Figure 5-22). This makes them chemically more similar and glycolat.

The RSD and recovery rates can be found in Table 5-22 to Table 5-24.

Table 5-22: RSD of analyte and internal standard emission lines before internal standardization by the determination of the effect of α-hydroxy-carboxylates on 0.8 mmol L^{-1} Ca (n = 42)

RSD before internal standardization [%]	**Ca II 317.933**	**Ca II 396.847**	**Ba II 230.424**	**Ba II 233.527**	**Ba II 455.404**
$CaCl_2$-samples	0.20 - 0.53	0.20 - 0.40	0.31 - 0.30	0.26 - 0.37	0.30 - 0.43
$CaCl_2$+Na-lactate-samples	0.26 - 0.27	0.20 - 0.24	0.28 - 0.28	0.22 - 0.23	0.19 - 0.22
$CaCl_2$+Na-glycolate-samples	0.22 - 0.35	0.28 - 0.32	0.20 - 0.36	0.20 - 0.29	0.22 - 0.26
$CaCl_2$+Na-2-OH-butyrate-samples	0.28 - 0.36	0.27 - 0.39	0.26 - 0.45	0.25 - 0.43	0.23 - 0.36

Table 5-23: RSD of analyte and internal standard emission lines after internal standardization by the determination of the effect of α-hydroxy-carboxylates on 0.8 mmol L^{-1} Ca

RSD after internal standardization [%]	**Ca II 317.933 + Ba II 230.424**	**Ca II 317.933 + Ba II 233.527**	**Ca II 396.847 + Ba II 455.404**
$CaCl_2$-samples	0.38 - 0.60	0.21 - 0.30	0.07 - 0.17
$CaCl_2$+Na-lactate-samples	0.32 - 0.40	0.13 - 0.22	0.03 - 0.05
$CaCl_2$+Na-glycolate-samples	0.35 - 0.45	0.15 - 0.19	0.06 - 0.07
$CaCl_2$+Na-2-OH-butyrate-samples	0.31 - 0.49	0.18 - 0.20	0.05 - 0.06

Table 5-24: Recovery rate of analyte and internal standard emission lines after internal standardization by the determination of the effect of α-hydroxy-carboxylates on 0.8 mmol L^{-1} Ca

Recovery rate after internal standardization [%]	**Ca II 317.933 + Ba II 230.424**	**Ca II 317.933 + Ba II 233.527**	**Ca II 396.847 + Ba II 455.404**
$CaCl_2$-samples	101.04 - 101.60	100.97 - 101.16	100.04 - 100.13
$CaCl_2$+Na-lactate-samples	100.63 - 100.81	100.96 - 101.20	99.88 - 100.08
$CaCl_2$+Na-glycolate-samples	102.24 - 103.18	102.57 - 102.84	101.49 - 101.79
$CaCl_2$+Na-2-OH-butyrate-samples	100.76 - 101.20	101.38 - 101.45	100.20 - 100.36

5.4.3.2 The effect of α-hydroxy-carboxylates on the determination of the highest calcium concentration (36 mmol L^{-1})

The RSD of the analyte emission line Ca 183.801 nm before the internal standardization is sometimes poor for the samples with matrices since values greater than 1 % are achieved.

With the best IS-analyte emission line-combination Ca 183.801 nm + Ba 233.527 nm, the precision of all the samples are improved and so all the values achieved are within the limit of less than 1 %, whereas the results of the other IS-analyte emission line-combinations are not very satisfactory. The recovery rates achieved here are also within the acceptable range of ± 2 % with the best IS-analyte emission line-combination Ca 183.801 nm + Ba 233.527 nm, as found already in chapter 5.4.2.2.

The argon intensities of the samples with glucose are also very low compared to that of the other samples due to the, probably, suppressive effect of glucose. This also confirms the results obtained in chapters 5.4.1 and 5.4.2.

The summarized results can be found in Table 5-25 to Table 5-27.

Table 5-25: RSD of analyte and internal standard emission lines before internal standardization by the determination of the effect of α-hydroxy-carboxylates on 36 mmol L^{-1} Ca (red values displays RSD > 1 %) (n = 42)

RSD before internal standardization [%]	**Ca II 183.801**	**Ba II 230.424**	**Ba II 233.527**	**Li I 670.780**
$CaCl_2$-samples	0.23 - 0.62	0.26 - 0.44	0.29 - 0.36	0.25 - 0.49
$CaCl_2$+glucose-samples	0.38 - 1.21	0.23 - 0.49	0.23 - 0.94	0.25 - 0.44
$CaCl_2$+Na-lactate-samples	0.66 - 1.67	0.22 - 0.34	0.37 - 0.99	0.12 - 0.28
$CaCl_2$+Na-glycolate-samples	0.41 - 1.09	0.26 - 0.41	0.28 - 0.78	0.13 - 0.33
$CaCl_2$+Na-2-OH-butyrate-samples	0.66 - 1.26	0.32 - 0.58	0.51 - 0.85	0.16 - 0.43

Table 5-26: RSD of analyte and internal standard emission lines after internal standardization by the determination of the effect of α-hydroxy-carboxylates on 36 mmol L^{-1} Ca (red values displays RSD > 1 %)

RSD after internal standardization [%]	**Ca II 183.801 + Ba II 230.424**	**Ca II 183.801 + Ba II 233.527**	**Ca II 183.801 + Li I 670.780**
$CaCl_2$-samples	0.41 - 0.62	0.21 - 0.36	0.42 - 0.81
$CaCl_2$+glucose-samples	0.48 - 0.84	0.18 - 0.28	0.42 - 0.91
$CaCl_2$+Na-lactate-samples	0.70 - 1.59	0.33 - 0.69	0.63 - 1.89
$CaCl_2$+Na-glycolate-samples	0.38 - 0.72	0.17 - 0.32	0.38 - 0.78
$CaCl_2$+Na-2-OH-butyrate-samples	0.61 - 1.03	0.20 - 0.42	0.55 - 1.33

Table 5-27: Recovery rate of analyte and internal standard emission lines after internal standardization by the determination of the effect of α-hydroxy-carboxylates on 36 mmol L^{-1} Ca

Recovery rate after internal standardization [%]	**Ca II 183.801 + Ba II 230.424**	**Ca II 183.801 + Ba II 233.527**	**Ca II 183.801 + Li I 670.780**
$CaCl_2$-samples	100.60 - 101.62	100.69 - 100.98	102.61 - 102.99
$CaCl_2$+glucose-samples	96.51 - 100.16	99.21 - 100.72	98.09 - 102.32
$CaCl_2$+Na-lactate-samples	99.78 - 99.84	100.36 - 100.41	99.93 - 100.65
$CaCl_2$+Na-glycolate-samples	98.32 - 103.11	99.93 - 101.99	98.78 - 104.04
$CaCl_2$+Na-2-OH-butyrate-samples	96.12 - 97.97	98.93 - 99.71	96.19 - 98.32

5.4.3.3 Conclusion on the comparison of the effect of lactate and some other α-hydroxy-carboxylates on the determination of calcium

In view of the results obtained, there is no great difference between lactate and the other “α-hydroxy-carboxylates” since their impact on calcium is mostly similar to that of lactate. This could result from the similar dissoziation constants (K) of the Ca-salt of these α-hydroxy-carboxylates, with K(glycolate) = 0.026, K(lactate) = 0.034 [172]. Although glycolate is chemically a bit different, its results are not much different from the other. According to this literature, α-hydroxy acid salts are similary weak, however, their five-membered chelat ring gives them a stable intermediate ion. Although the dissoziation constant of the Ca-salt of α-hydroxybutyrate is not stated, the results obtained for lactate and α-hydroxybutyrate in this work confirm their much similar behavior compared to that of glycolat. The β-hydroxybutyrate, however, has a much higher dissoziation contant (K = 0.15) [172]. This substance was not tested in this work but it could have probably behaved much differently than even glycolate since its properties are chemically more different.

Moreover, the results obtained with these matrices confirm those achieved with the normal matrix in the dialysis solutions. The best internal standard-analyte emission line combinations obtained in chapter 5.4.2 are also achieved here (see Table 5-42).

Furthermore, these results also prove that all these matrix components have negligible influence on calcium by its determination with ICP-OES.

These results also confirm the less susceptibility of ICP-OES to chemical interferences compared to other atomic spectroscopic techniques, such as flame photometry and AAS [64], [65], [82].

5.4.4 The effect of glucose and lactate on the determination of potassium by ICP-OES

By the determination of potassium only one analyte emission line is used. This is linked with an emission line of the internal standard lithium. The wavelengths of both alkaline elements are atomic lines and can be found in Table 5-28.

Table 5-28: IS-analyte-combinations used for the determination of the matrix effect on potassium (atomic lines (I))

0.8 mmol L^{-1} K^+		96 mmol L^{-1} K^+	
Analyte emission line [nm]	IS emission line [nm]	Analyte emission line [nm]	IS emission line [nm]
K I 766.490	Li I 670.780	K I 766.490	Li I 670.780

5.4.4.1 Matrix effects on the determination of the lowest potassium concentration (0.8 mmol L^{-1})

At this low potassium concentration, the precision of the internal standard Li 670.780 nm is better than that of the analyte in all the samples examined although the RSD of the analyte obtained before the standardization is less than 1 %. With the internal standardization, the precision of the analyte is improved to a higher degree, so that the values achieved afterwards are between the ranges of 0.05 – 0.36 %. The analyte intensity of the samples containing only KCl and that containing KCl+glucose and KCl+lactate are lower compared to that of the samples with both matrices, KCl+glucose+lactate. However, the intensities of the internal standard are comparable in all the samples. Due to this slight difference between the IS and the analyte, the recovery rates of the samples containing both matrices (glucose and lactate) are higher than that of the other samples. The values of the RSD and that of the recovery rates are summarized in Table 5-29 to Table 5-31.

Table 5-29: RSD of analyte and internal standard emission lines before internal standardization by the determination of 0.8 mmol L^{-1} K (n = 42)

RSD before internal standardization [%]	K I 766.491	Li I 670.780
KCl-samples	0.41 - 0.44	0.11 - 0.18
KCl+glucose-samples	0.23 - 0.98	0.20 - 0.44
KCl+lactate-samples	0.32 - 0.60	0.17 - 0.36
KCl+glucose+lactate-samples	0.18 - 0.53	0.13 - 0.41

Table 5-30: RSD of analyte and internal standard emission lines after internal standardization by the determination of 0.8 mmol L^{-1} K

RSD after internal standardization [%]	K I 766.491 + Li I 670.780
KCl-samples	0.07 - 0.10
KCl+glucose-samples	0.05 - 0.20
KCl+lactate-samples	0.11 - 0.16
KCl+glucose+lactate-samples	0.12 - 0.36

Table 5-31: Recovery rate of analyte and internal standard emission lines after internal standardization by the determination of 0.8 mmol L^{-1} K

Recovery rate after internal standardization [%]	K I 766.491 + Li I 670.780
KCl-samples	97.87 - 98.16
KCl+glucose-samples	97.17 - 97.89
KCl+lactate-samples	98.02 - 98.39
KCl+glucose+lactate-samples	101.33 - 105.72

5.4.4.2 Matrix effects on the determination of the highest potassium concentration (96 mmol L^{-1})

Although the precision of all the measurements here are less than 1 % which is within the required range, almost all the RSD of the internal standard Li 670.780 nm are a bit poorer than that of the analyte K 766.491 nm. Regardless of this, the precision obtained after the internal standardization is far below that of the internal standard and of the analyte with values between 0.06 – 0.59 %.

Unfortunately, the recovery rates of the samples containing both matrix components (KCl+glucose+lactate) are very low. The values obtained are between 94.5 - 96.5 %. The results of the other samples (KCl, KCl+glucose and KCl+lactate), however, are

better (between 96.5 - 98.5 %). Although these recovery rates are a bit lower, they vary within a range of about 2 %. An additional correction with the quality control (QC) standard could help eliminate other factors disturbing the measurement and improve the recovery rate. Consequently, the determination of potassium at this high concentration can produce acceptable results. The RSD and recovery rates can be found in Table 5-32 to Table 5-34.

Table 5-32: RSD of analyte and internal standard emission lines before internal standardization by the determination of 96 mmol L^{-1} K (n = 42)

RSD before internal standardization [%]	**K I 766.491**	**Li I 670.780**
KCl-samples	0.69 - 0.74	0.71 - 0.75
KCl+glucose-samples	0.28 - 0.67	0.27 - 0.71
KCl+lactate-samples	0.39 - 0.77	0.43 - 0.83
KCl+glucose+lactate-samples	0.16 - 0.55	0.14 - 0.70

Table 5-33: RSD of analyte and internal standard emission lines after internal standardization by the determination of 96 mmol L^{-1} K

RSD after internal standardization [%]	**K I 766.491 + Li I 670.780**
KCl-samples	0.39 - 0.59
KCl+glucose-samples	0.34 - 0.10
KCl+lactate-samples	0.23 - 0.40
KCl+glucose+lactate-samples	0.06 - 0.24

Table 5-34: Recovery rate of analyte and internal standard emission lines before internal standardization by the determination of 96 mmol L^{-1} K

Recovery rate after internal standardization [%]	**K I 766.491 + Li I 670.780**
KCl-samples	98.65 - 99.76
KCl+glucose-samples	97.38 - 98.95
KCl+lactate-samples	100.61 - 103.90
KCl+glucose+lactate-samples	94.71 - 95.67

5.4.4.3 Conclusion on the effect of glucose and lactate on the determination of potassium

Since only one potassium emission line and one lithium emission line are used in the study of both concentrations, no better analyte-IS emission line combination could be figured out. However, the correction with lithium proved very effective in both concentrations.

It has been confirmed that internal standardization alone cannot compensate for negative impacts on the accuracy [88]. Therefore other approaches, such as standardization with a quality control standard, should be carried out by the determination of potassium.

5.4.5 The effect of glucose and lactate on the determination of sodium by ICP-OES

The emission lines of the analyte and that of the IS, to which they are linked, are summarized in Table 5-35 for the examined concentration ranges. The emission lines of both alkaline metals (sodium and lithium) are atomic lines, whereas that of the alkaline earth metal (barium) is an ionic line. Beside sodium chloride, other sodium sources, such as sodium lactate and sodium hydrogen carbonate, which normally serve as buffering substances in the dialysis solutions, are also present. By the determination of interferences on sodium, the differences between these three sodium sources, sodium chloride, sodium lactate and sodium hydrogen carbonate, with regard to their matrix effects, are also studied.

Table 5-35: IS-analyte-combinations used for the determination of the matrix effect on sodium (atomic lines (I) and ionic lines (II))

140 mmol L^{-1} Na^+		235 mmol L^{-1} Na^+	
Analyte emission line [nm]	IS emission line [nm]	Analyte emission line [nm]	IS emission line [nm]
Na I 589.592	Li I 670.780	Na I 589.592	Li I 670.780
Na I 588.995	Li I 670.780	Na I 588.995	Li I 670.780
-	-	Na I 589.592	Ba II 455.404
-	-	Na I 588.995	Ba II 455.404

5.4.5.1 Matrix effects on the determination of the average sodium concentration (140 mmol L^{-1})

The results obtained in this work confirm the similarity of the pair of sodium emission lines resulting in its yellow flame, Na 588.995 nm and Na 589.592 nm. In all the measurements performed, influences that occurred affected these lines equally. The similar behavior of these lines is clearly illustrated in the diagrams in the appendix. In most cases, the emission line of the internal standard lithium behaviors similar to that the analyte. Therefore, the internal standard is able to compensate for effects on both sodium emission lines. As a result, the precision of the results obtained after the internal standardization is remarkably good with values far less than the required RSD of less than 1 %. The precision of the results before the internal standardization is also within this acceptable range.

The samples containing glucose as matrix influence the sodium intensity, irrespective of the sodium source in that sample. With increasing glucose concentration (from 4.4 mmol L^{-1} to 566.2 mmol L^{-1}), the intensity of the analyte and that of the internal standard decreases. Since this effect influence both the emission lines of the analyte and that of the IS, the internal standardization could compensate for it so that the recovery rates give satisfactory results.

However, the recovery rates of the samples containing sodium lactate are mostly higher although no direct influence on the intensities of the analyte nor on that of the internal standard are detected in the presence of lactate. This is clearer with the samples containing both sodium lactate and sodium hydrogen carbonate. In this case, the recovery rates of both sodium emission lines display a formation of two groups, irrespective of the glucose concentration. The recovery rates of the samples containing higher Na-lactate concentration and lower $NaHCO_3$ concentration are higher than those with lower Na-lactate and higher $NaHCO_3$. A summary of the RSD and the recovery rates can be found in Table 5-36 to Table 5-38.

Table 5-36: RSD of analyte and internal standard emission lines before internal standardization by the determination of 140 mmol L^{-1} Na (n = 42)

RSD before internal standardization [%]	**Na I 588.995**	**Na I 589.592**	**Li I 670.780**
NaCl-samples	0.27 - 0.55	0.25. - 0.54	0.21 - 0.50
$NaHCO_3$-samples	0.15 - 0.35	0.14 - 0.25	0.18 - 0.25
Na-lactate-samples	0.15 - 0.68	0.15 - 0.65	0.16 - 0.64
NaCl+$NaHCO_3$-samples	0.16 - 0.31	0.81 - 0.30	0.20 - 0.33
NaCl+Na-lactate-samples	0.22 - 0.33	0.23 - 0.31	0.22 - 0.34
NaCl+glucose-samples	0.16 - 0.39	0.15 - 0.35	0.16 - 0.35
NaCl+glucose+Na-lactate-samples	0.18 - 0.50	0.16 - 0.54	0.20 - 0.53
$NaHCO_3$+glucose-samples	0.14 - 0.23	0.13 - 0.24	0.15 - 0.35
$NaHCO_3$+Na-lactate-samples	0.15 - 0.35	0.15 - 0.30	0.19 - 0.28
$NaHCO_3$+glucose+Na-lactate-samples	0.10 - 0.36	0.12 - 0.33	0.13 - 0.42
Na-lactate+glucose-samples	0.14 - 0.35	0.14 - 0.32	0.16 - 0.24

Table 5-37: RSD of analyte and internal standard emission lines after internal standardization by the determination of 140 mmol L^{-1} Na

RSD after internal standardization [%]	Na I 588.995 + Li I 670.780	Na I 589.592 + Li I 670.780
NaCl-samples	0.12 - 0.24	0.10 - 0.22
$NaHCO_3$-samples	0.07 - 0.18	0.07 - 0.15
Na-lactate-samples	0.07 - 0.17	0.05 - 0.14
NaCl+$NaHCO_3$-samples	0.09 - 0.15	0.07 - 0.12
NaCl+Na-lactate-samples	0.08 - 0.19	0.06 - 0.15
NaCl+glucose-samples	0.07 - 0.16	0.05 - 0.17
NaCl+glucose+Na-lactate-samples	0.09 - 0.19	0.07 - 0.21
$NaHCO_3$+glucose-samples	0.06 - 0.17	0.06 - 0.14
$NaHCO_3$+Na-lactate-samples	0.13 - 0.17	0.10 - 0.13
$NaHCO_3$+glucose+Na-lactate-samples	0.05 - 0.16	0.06 - 0.13
Na-lactate+glucose-samples	0.06 - 0.39	0.06 - 0.37

Table 5-38: Recovery rate of analyte and internal standard emission lines after internal standardization by the determination of 140 mmol L^{-1} Na

Recovery rate after internal standardization [%]	Na I 588.995 + Li I 670.780	Na I 589.592 + Li I 670.780
NaCl-samples	100.28 - 100.54	100.41 - 100.74
$NaHCO_3$-samples	99.65 - 100.73	99.85 - 100.92
Na-lactate-samples	100.63 - 101.52	100.84 - 101.70
NaCl+$NaHCO_3$-samples	99.79 - 100.39	100.00 - 100.59
NaCl+Na-lactate-samples	100.41 - 101.35	100.52 - 101.57
NaCl+glucose-samples	99.77 - 100.62	99.95 - 100.78
NaCl+glucose+Na-lactate-samples	101.52 - 102.32	101.72 - 102.50
$NaHCO_3$+glucose-samples	99.65 - 100.28	99.86 - 100.47
$NaHCO_3$+Na-lactate-samples	100.56 - 101.18	100.75 - 101.38
$NaHCO_3$+glucose+Na-lactate-samples	100.58 - 102.35	100.80 - 102.61
Na-lactate+glucose-samples	100.57 - 101.64	100.76 - 101.81

5.4.5.2 Matrix effects on the determination of the highest sodium concentration (235 mmol L^{-1})

The suppressive effect of glucose on the intensities of the analyte and that of the IS depending on its concentration is also detected at this sodium concentration. The similarities of both sodium emission lines and that of the internal standard to the analyte lines which lead to a better effect compensation is also seen here. This better compensation, probably results from the similar behavior of the analyte and the internal standard.

At this concentration, barium is selected additionally to lithium as an alternative internal standard. Although the barium line is ionic, its results after the standardization are tolerable. Both internal standards (lithium and barium) are able to compensate for all fluctuations that occur since both sodium emission lines and that of the internal standards are influenced equally. The RSD obtained for both sodium lines linked to both internal standards are very good. The recovery rates are also acceptable. The corresponding results are in Table 5-39 to Table 5-41.

Table 5-39: RSD of analyte and internal standard emission lines before internal standardization by the determination of 235 mmol L^{-1} Na (red values displays RSD > 1 %) (n = 42)

RSD before internal standardization [%]	Na I 588.995	Na I 589.592	Li I 670.780	Ba II 455.404
NaCl-samples	0.25 - 0.43	0.18 - 0.39	0.17 - 0.38	0.19 - 0.38
$NaHCO_3$-samples	0.19 - 0.42	0.20 - 0.42	0.19 - 0.41	0.21 - 0.54
Na-lactate-samples	0.15 - 0.18	0.14 - 0.16	0.17 - 0.19	0.18 - 0.19
NaCl+$NaHCO_3$-samples	0.20 - 0.40	0.18 - 0.41	0.20 - 0.42	0.21 - 0.49
NaCl+Na-lactate-samples	0.14 - 0.25	0.13 - 0.22	0.13 - 0.20	0.15 - 0.26
NaCl+glucose-samples	0.14 - 0.28	0.12 - 0.28	0.14 - 0.27	0.14 - 0.31
NaCl+glucose+Na-lactate-samples	0.14 - 1.00	0.13 - 0.96	0.11 - 0.89	0.14 - 1.04
NaCl+$NaHCO_3$+Na-lactate-samples	0.18 - 0.30	0.14 - 0.22	0.16 - 0.19	0.13 - 0.23

Table 5-40: RSD of analyte and internal standard emission lines after internal standardization by the determination of 235 mmol L^{-1} Na

RSD after internal standardization [%]	Na I 588.995 + Li I 670.780	Na I 589.592 + Li I 670.780	Na I 589.592 + Ba II 455.404	Na I 588.995 + Ba II 455.404
NaCl-samples	0.11 - 0.20	0.03 - 0.11	0.05 - 0.08	0.09 - 0.15
$NaHCO_3$-samples	0.08 - 0.12	0.04 - 0.05	0.08 - 0.15	0.09 - 0.22
Na-lactate-samples	0.08 - 0.21	0.04 - 0.12	0.06 - 0.11	0.09 - 0.17
NaCl+$NaHCO_3$-samples	0.09 - 0.18	0.04 - 0.12	0.06 - 0.11	0.09 - 0.17
NaCl+Na-lactate-samples	0.09 - 0.14	0.05 - 0.08	0.05 - 0.09	0.06 - 0.14
NaCl+glucose-samples	0.09 - 0.14	0.03 - 0.10	0.04 - 0.10	0.07 - 0.16
NaCl+glucose+Na-lactate-samples	0.14 - 0.41	0.07 - 0.25	0.10 - 0.33	0.13 - 0.51
NaCl+$NaHCO_3$+Na-lactate-samples	0.11 - 0.20	0.06 - 0.13	0.05 - 0.16	0.10 - 0.26

Table 5-41: Recovery rate of analyte and internal standard emission lines after internal standardization by the determination of 235 mmol L^{-1} Na

Recovery rate after internal standardization [%]	Na I 588.995 + Li I 670.780	Na I 589.592 + Li I 670.780	Na I 589.592 + Ba II 455.404	Na I 588.995 + Ba II 455.404
NaCl-samples	100.10 - 100.60	100.36 - 100.70	99.59 - 100.96	99.33 - 100.87
$NaHCO_3$-samples	100.23 - 100.53	100.52 - 100.68	99.47 - 100.36	99.30 - 100.21
Na-lactate-samples	99.98 - 100.39	100.34 - 100.51	100.18 - 100.45	99.81 - 100.30
NaCl+$NaHCO_3$-samples	100.30 - 100.79	100.60 - 100.90	99.79 - 99.95	99.49 - 99.74
NaCl+Na-lactate-samples	99.79 - 100.71	100.25 - 100.80	100.29 - 100.71	99.81 - 100.65
NaCl+glucose-samples	99.99 - 101.31	100.30 - 101.44	99.45 - 99.92	99.16 - 99.85
NaCl+glucose+Na-lactate-samples	98.70 - 100.70	99.32 - 100.92	100.23 - 102.75	100.19 - 102.58
NaCl+$NaHCO_3$+Na-lactate-samples	99.39 - 101.36	100.0 - 101.30	100.28 - 100.88	99.66 - 101.05

5.4.5.3 Conclusion on the effect of glucose and lactate on the determination of sodium

In the entire results obtained in chapter 5.4.5, the similarity of the pair of sodium emission lines (Na 588.995 nm and Na 589.592 nm) resulting in its yellow flame, is confirmed since both lines behave similarly and they are, moreover, mostly influenced equally.

On account of the results obtained, the internal standardization with lithium has proven very effective. Although the barium line used here is an ionic line linked to the atomic lines of the analyte (Na), the results with this IS are within the acceptable range. This means that at higher sodium concentrations, the barium emission line Ba 455.404 nm can be used alternatively to compensate for effects on both sodium lines. However, the results obtained with lithium at both analyte concentrations make it the most suitable internal standard for these sodium lines within this wide concentration range. At the analyte concentration 140 mmol L^{-1}, barium could not be added as an IS because the intensity difference between the barium lines and the sodium lines is very high.

Although both sodium emission lines show many similarities, the best line obtained, in view of the results obtained here is Na 589.592 nm. With the IS-analyte emission line-combination Na 589.592 nm + Li 670.780 nm, the best RSD and recovery rates are achieved.

Apart from the decrease in the argon intensity that occurs in the presence of NaCl and sometimes the higher recovery rates obtained mostly in the presence of Na-lactate, the behavior of the three sodium sources (sodium chloride, sodium lactate and sodium hydrogen carbonate) is comparable. Both internal standards, Li and Ba, are able to compensate for interferences and so improve the precision of Na, irrespective of its source.

The depressive effect of the samples with a higher glucose concentration could not be detected when NaCl is present as a sodium source since it obviously has a greater effect on decreasing the argon temperature than glucose. However, this does not directly affect the analyte as in the case of glucose.

Furthermore, it is been detected at both analyte concentrations (140 mmol L^{-1} and 235 mmol L^{-1}) that an increase in the glucose concentration lead to a decrease in the intensity of both the analyte and the IS, irrespective of the sodium source.

5.4.6 Conclusion on the examination of interference effects on the determination of Na, Ca, Mg and K by ICP-OES

In view of the results obtained in this study, the internal standardization performed by the determination of the ions (Na, K, Ca and Mg) with ICP-OES is very effective in terms of precision. As a result, the required RSD of less than 1 % is achieved in almost all the examinations carried out. With the best internal standard-analyte emission line-combinations (see Table 5-42), fluctuations that occurred during the measurements are better compensated for to improve the precision. In terms of the accuracy, however, the internal standardization could not always compensate for all signal enhancements and suppressions. This confirms the fact that, the compensation for lack of accuracy with the internal standardization is more complex [88].

To compensate for effects on the accuracy, a quality control (QC) standard which has the same composition as the sample could be very useful. With this standardization, the accuracy could be improved.

Table 5-42: Best internal standard - analyte emission line-combination

Ion	Concentration [mmol L^{-1}]	Best internal standard - analyte emission line-combination [nm]
Mg	0.4	Mg II 280.270 + Ba II 233.527
	24.0	Mg I 285.213 + Ba II 230.424 and Mg I 285.213 + Ba II 233.527
Ca	0.8	Ca II 396.847 + Ba II 455.404
	36.0	Ca II 183.801 + Ba II 233.527
K	0.8	K I 766.490 + Li I 670.780
	96.0	K I 766.490 + Li I 670.780
Na	140.0	Na I 589.592 + Li I 670.780
	235.0	Na I 589.592 + Li I 670.780

The depressive effect of high concentrated glucose samples on the argon intensity is detected in almost all the measurements in the absence of NaCl.

NaCl seems to have a stronger suppressive effect on the Ar-intensity than glucose. According to literature, mineral acids and some organic acids display similar effect on

the excitation temperature of the plasma [106], [108]. Since the cause of this effect could not be figured out in this work, the optimization of some instrumental parameters, like plasma power, gas flow rates, etc. could be helpful. Nevertheless, a direct effect on the analyte line intensities as it happens in the presence of organic substances and mineral acids could not be detected in this study [106], [108], [171].

Linking an atomic emission line to an ionic emission line does not always lead to erroneously higher concentration as perhaps realized in other studies [165]. The internal standardizations performed by linking ionic to atomic lines occasionally gave acceptable results as it is detected by the combination of sodium (Na 588.995 nm or Na 589.592 nm) and barium line (Ba 455.404 nm). Although the results obtained with this combination is not better than that obtained with the lithium atomic line, barium, however, can be chosen as an alternative internal standard for sodium at higher concentrations. Due to the fact that sodium is an alkaline metal and barium an earth alkaline metal and so mostly behavior differently, it should be kept in mind that such combinations may not always be reliable. This also applies to the combination of the calcium ionic line Ca 183.801 nm with the lithium atomic line Li 670.780 nm.

Unlike Ba, the application of Li as IS proved very effective for both alkaline metals (Na & K). It was able to improve the precision of these ions in almost all cases. Although Rb could have also been a better IS due to its less interference with salt solutions, it could not be tested due to the limited time and resources. An alternative for barium, however, would be much reasonable since its performace was sometimes poor. Yttrium, as a well known internal standard ion, could be very good since its emission lines, such as Y II 324.228 nm, Y II 360.073 nm, Y II 371.030 nm and Y II 377.433 nm, are mostly ionic lines like that of Mg and Ca. However, it would be advisable to dilute Mg and Ca differently in order to achieve a better ratio of the intensity of the analyte to that of the internal standard. This could improve the effectiveness of the internal standard on the individual analyte.
Mg, however, could be determined without IS at lower concentrations.

According to these examinations, glucose and lactate have less influence on the determination of these ions under internal standardization. Unlike the other ions (Mg, Ca and K), the recovery rates of Na are extraordinarily good.

The less matrix influence detected so far makes ICP-OES, under the conditions carried out here, a suitable method for the determination of Na, K, Ca, and Mg in dialysis solutions. The results obtained in this study confirm the less susceptibility of ICP-OES to chemical interferences, compared to techniques like AAS and flame photometer, due to its high and stable plasma temperature [64], [65], [82]. Although the examination of spectral interferences was not part of this study, the results obtained here show that such interferences could equally be negligible as the chemical interferences examined so far.

Under the conditions carried out here, the elements of interest in this work (Na, K, Ca, and Mg) can be determined by the ICP-OES with satisfactory analytical results. Thus this technique is suitable for simultaneous determinations as preferred for the on-line analysis of these ions.

5.5 The automatic sample preparation unit

Although not all analytical methods need sample preparation, nevertheless, it is as important as the determination of the sample, when analytical chemistry is concerned. ICP-OES is a technique which is mostly associated with a sample preparation depending on its application. As shown in the Ishikawa fishbone model in Figure 5-1, the automatic sample preparation system has three main parts which can individually influence the whole system in different ways:

- Sampling:
    - Function: Taking sample directly from the production line
    - Influence: It has very little or no influence since the sample is homogeneous and its source is mostly well known due to its direct integration into the production process in a form of ring system which is cleansed with distilled water before the production of every solution and regularly sterilized with steam.

- Sample preparation:
    - Function: Accurate and precise dilution of sample and exact addition of required standards, in this case, internal standards
    - Influence: Inaccurate and imprecise dilution or addition of internal standard which can lead to errorenous results.

- Sample transfer:
    - Function: Transfer of calibration standards and prepared samples into analytical instrument
    - Influence: Apart from leakages that can occur, the influence from this part is very low

In analytical chemistry, sample preparation plays a very important role. Different sample preparation methods are carried out depending on the type of sample and the analytical method involved. Whereas liquid samples are mostly easily prepared, solid samples, however, are associated with complex preparation methods [173]–[176]. Unlike biological samples, the preparation method in this work is one of the

comparatively simple techniques [177]. However, its accurateness is very crucial since it can affect the analysis equally in many ways as biological samples.
In view of the above mentioned arguments, the sample preparation is assumed to be one of the main sources of error that can influence the analysis greatly in terms of precision and accuracy. Thus, the sample preparation is studied carefully to evaluate its effect on the measurement in terms of the analytical requirements.

To examine the precision of the dosing units which are responsible for the sample preparation, the following factors are considered and evaluated in the chapters 5.5.1 and 5.5.2:

- the different densities of the solutions
- The different dilution factors and the addition of the internal standards (lithium and barium)
- Differences in the dilution of the sample and the QC-standard with the help of the two hose systems or loops connected to the dosing units (see Figure 4-2)

The precision of the dilution system is determined gravimetrically as described in chapter 4.2.4. Each solution is diluted 10 times with both the left and the right loop connected to the 20 mL dosing unit (Figure 4-2).
The results are displayed in individual value plots or individual control charts and the repeatability of each dilution are expressed as relative standard deviation (RSD) which is also showed in the diagramms.

5.5.1 Gravimetric determination of the influence of the density of the solutions on the precision of the dilution systems

The two solutions Bicavera B and Bicavera A 4.25/1.75 are applied to examine the effect of the different densities of the solutions on the precision of the dilution.
Bicavera B has the lowest density among the dialysis solutions (1.0025 g cm^{-3}) since it contains only $NaHCO_3$ and Bicavera A 4.25/1.75 has the highest density (1.039 g cm^{-3}) due to its high glucose concentration (see Table 4-1). These two samples, therefore, cover the density range of all the dialysis solutions (from 1.0025 to 1.039 g cm^{-3}).

The results in Figure 5-23 show that the densities of the different solutions resulting from their individual matrices do not have any negative impact on the precision of the dilution since the difference in the density is not that high. Therefore, the dilution of all the dialysis solutions should be equally good.

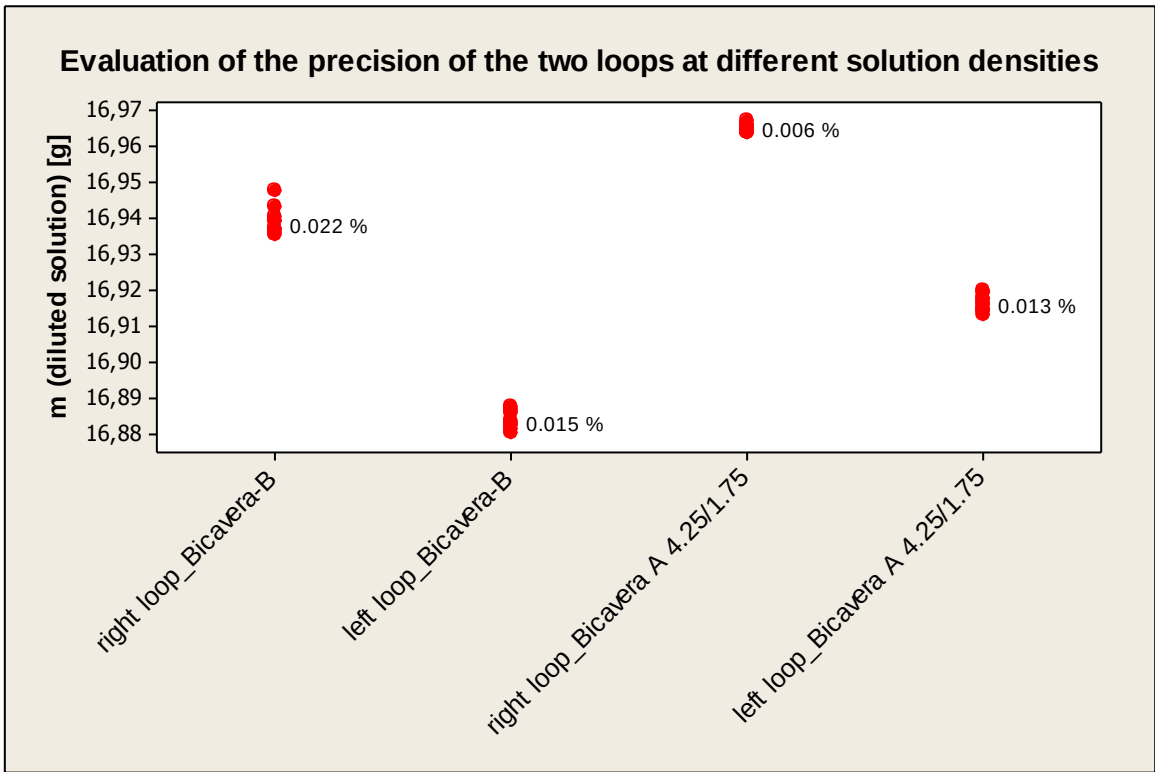

Figure 5-23: An individual value plot illustrating the precision of the dilution of two solutions with different densities at a dilution factor of 20.

5.5.2 Gravimetric evaluation of the precision of the dilution and the addition of internal standard

In this study, a 1:10, 1:20 and 1:50 dilution of a CAPD3 solution (see Table 4-1 for its composition) is carried out to evaluate the precision of the different dilutions. Furthermore, the addition of the internal standards (lithium and barium) for a concentration of 40 mg L^{-1} Li and a 15 mg L^{-1} Ba in a 1:20 diluted sample is also performed. Each dilution is carried out on two different days to evaluate the intermediate precision in addition to the repeatability.

In Figure 5-24 to Figure 5-29, the results obtained in this examination is illustration in individual value plots. The RSD of the individual dilutions are also displayed in the plots. The results show that both the repeatability and the intermediate precision are surprisingly good. Moreover, there is not any substantial difference between the different dilutions and the addition of the internal standards in terms of precision.
However, there is a significant difference between the mass of the solutions diluted on the first day and that on the second day although the same solution is used on both days. In this case, a systematic error occurred since the accuracy of the measured values is affected. Unfortunately, the cause of this difference could not be identified since all conditions are equal on both days including the room temperature because it is air-conditioned and the flask, in which the solution is kept, is tightly closed. The temperature difference of this air-conditioned room is max ± 3°C which is unlikely to cause such an obvious difference.

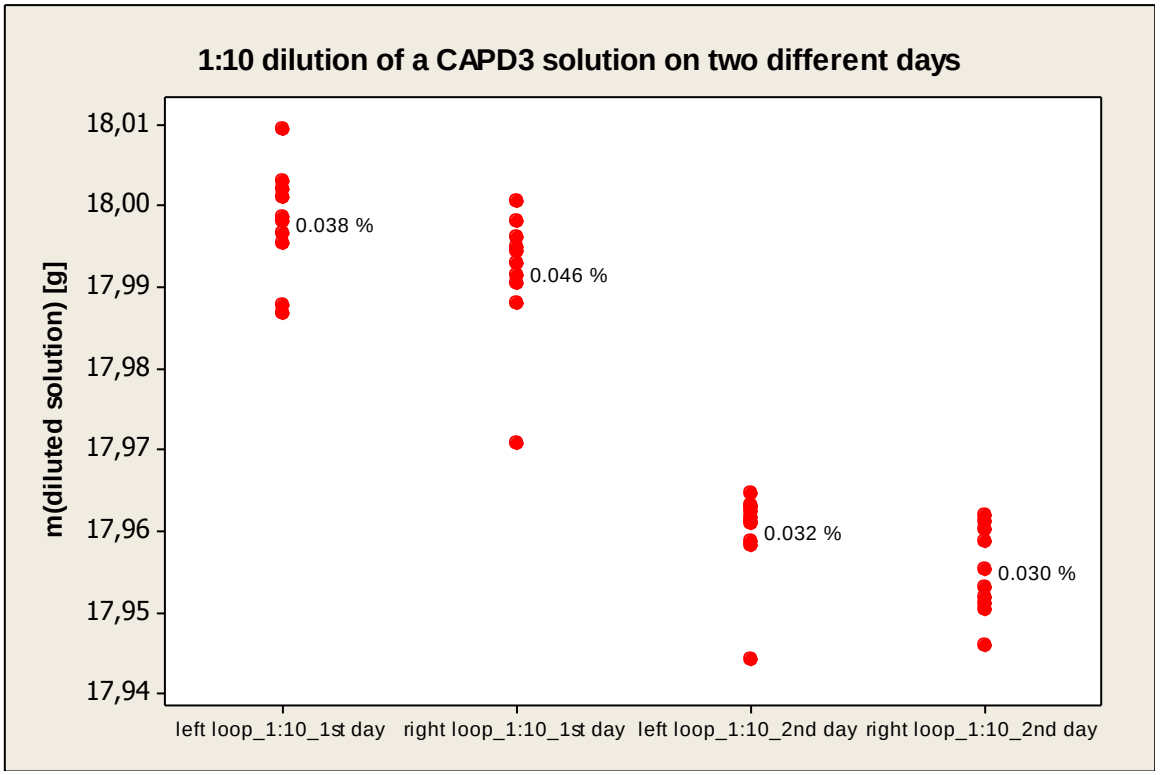

Figure 5-24: An individual value plot illustrating the precision of a 1:10 dilution of a CAPD3 solution carried out on two different days.

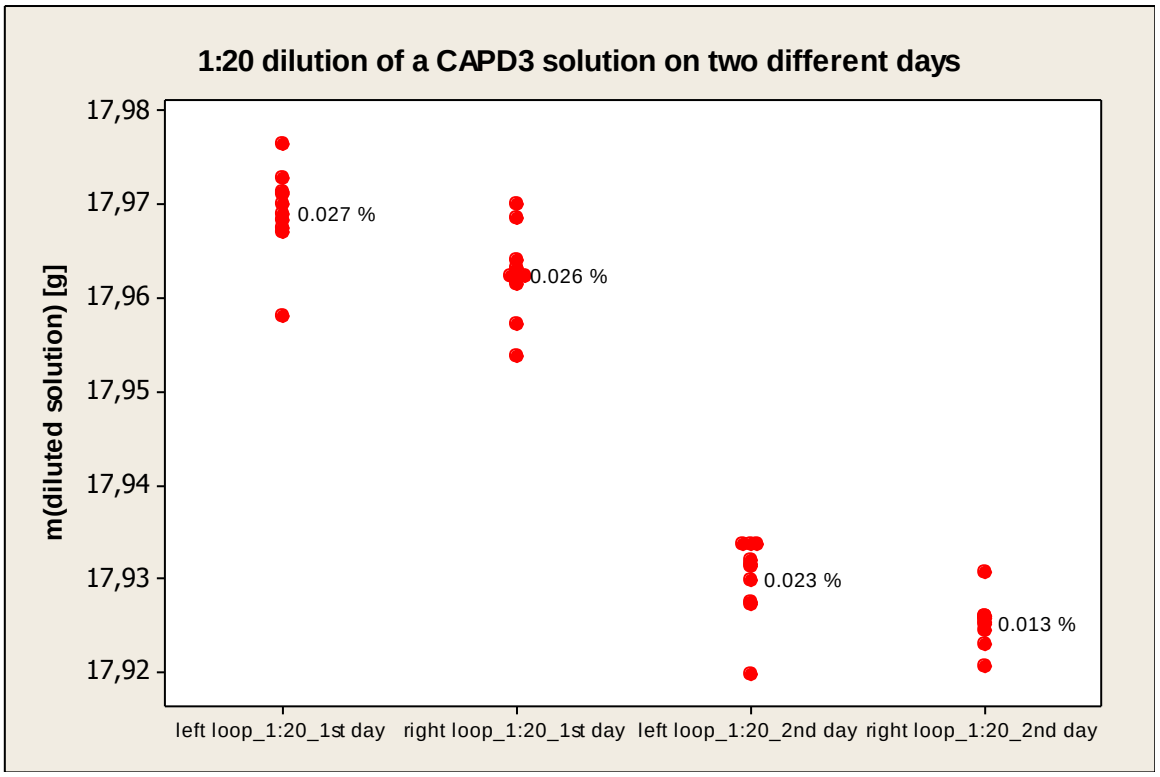

Figure 5-25: An individual value plot illustrating the precision of a 1:20 dilution of a CAPD3 solution carried out on two different days.

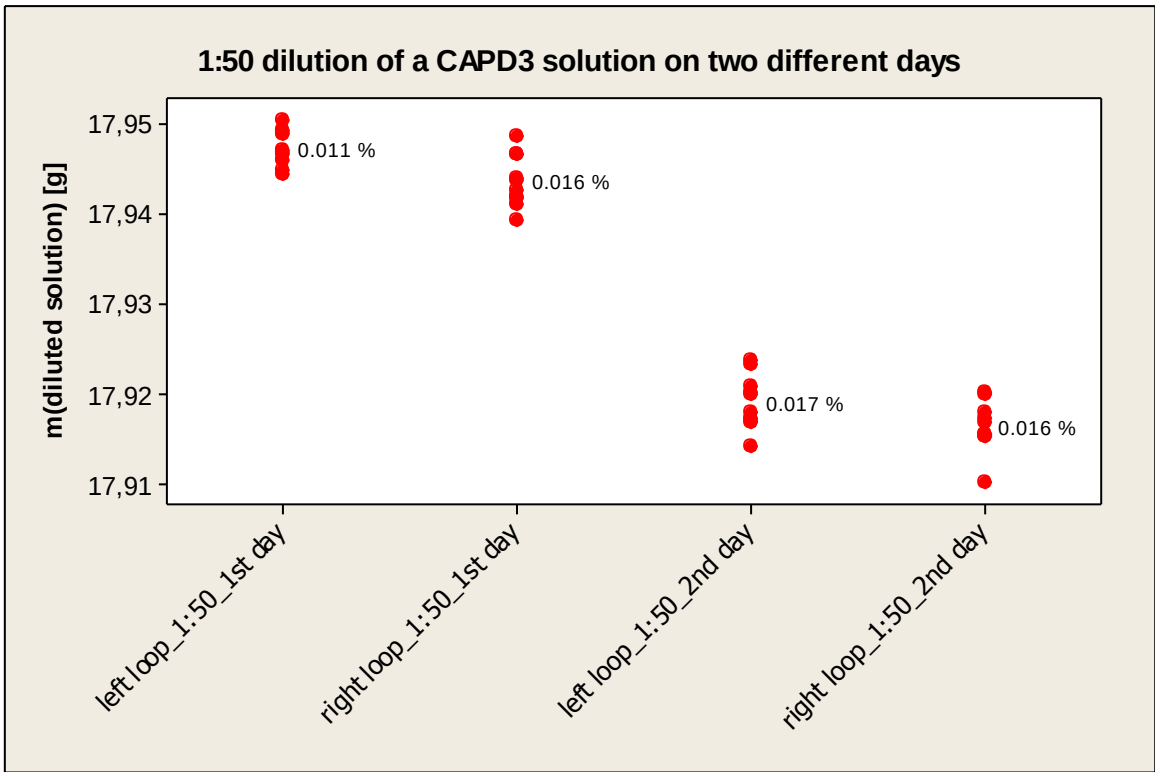

Figure 5-26: An individual value plot illustrating the precision of a 1:50 dilution of a CAPD3 solution carried out on two different days.

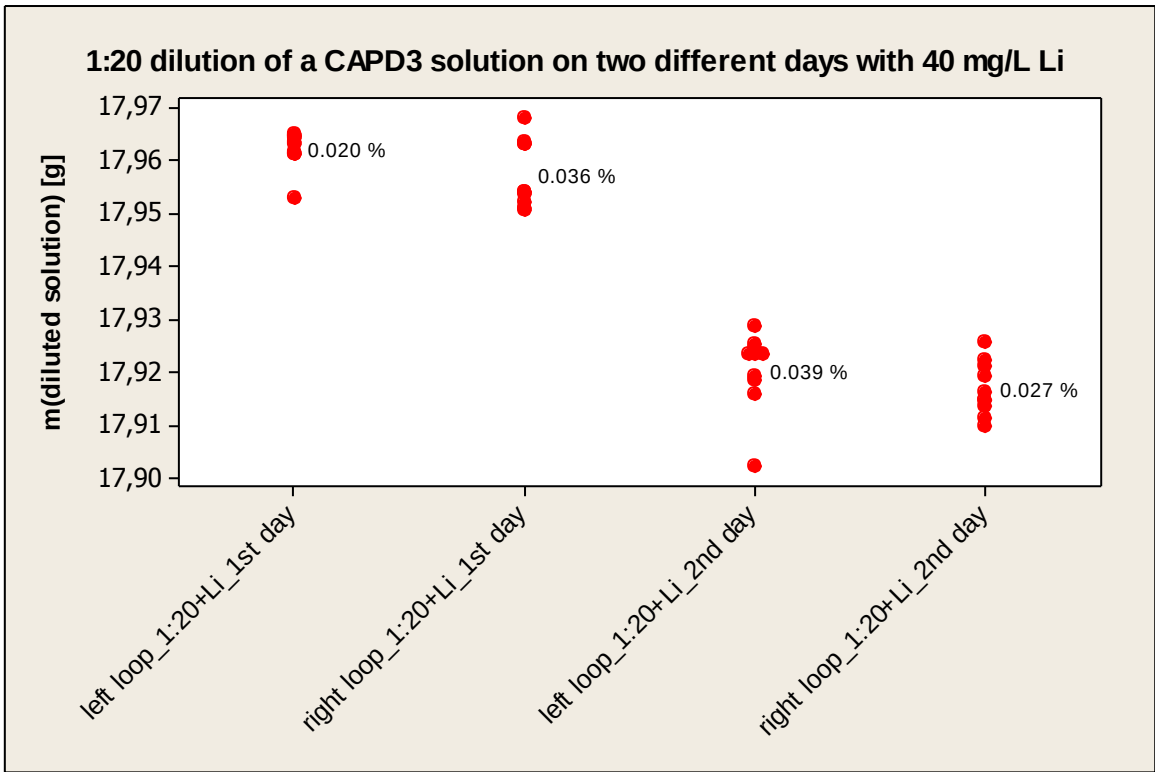

Figure 5-27: An individual value plot illustrating the precision of the addition of lithium as IS to a 1:20 dilution of a CAPD3 solution carried out on two different days.

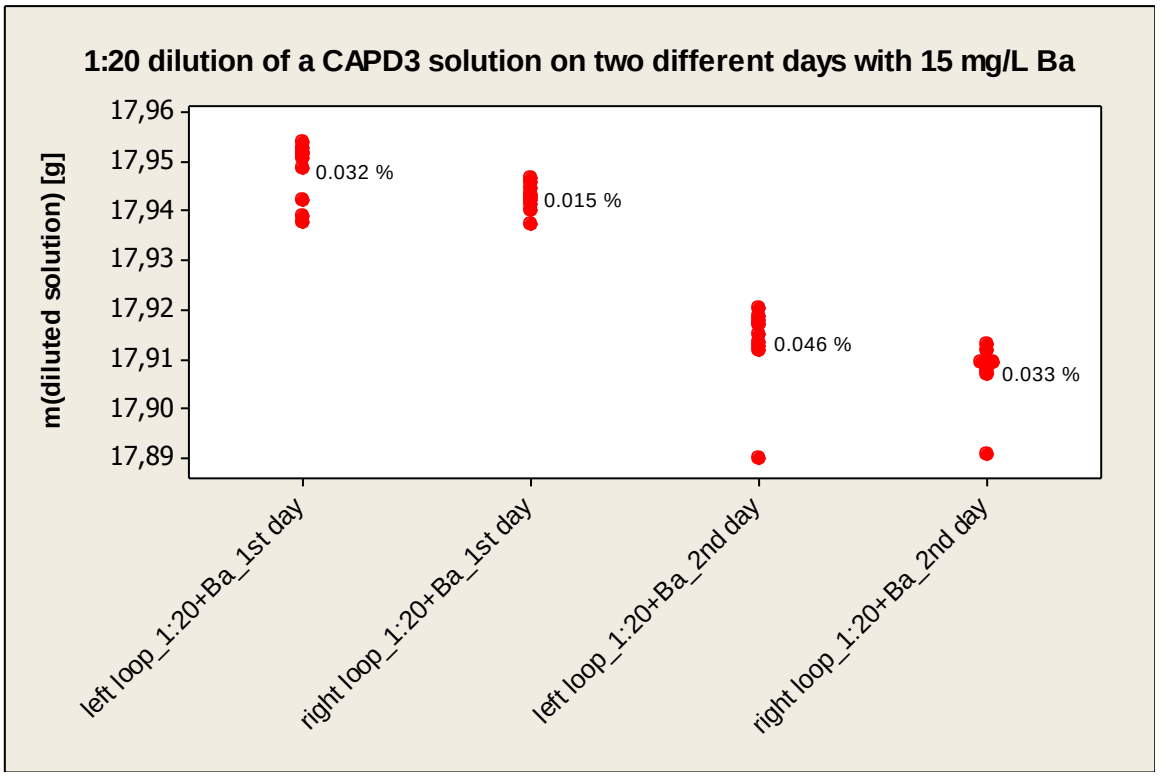

Figure 5-28: An individual value plot illustrating the precision of the addition of barium as IS to a 1:20 dilution of a CAPD3 solution carried out on two different days.

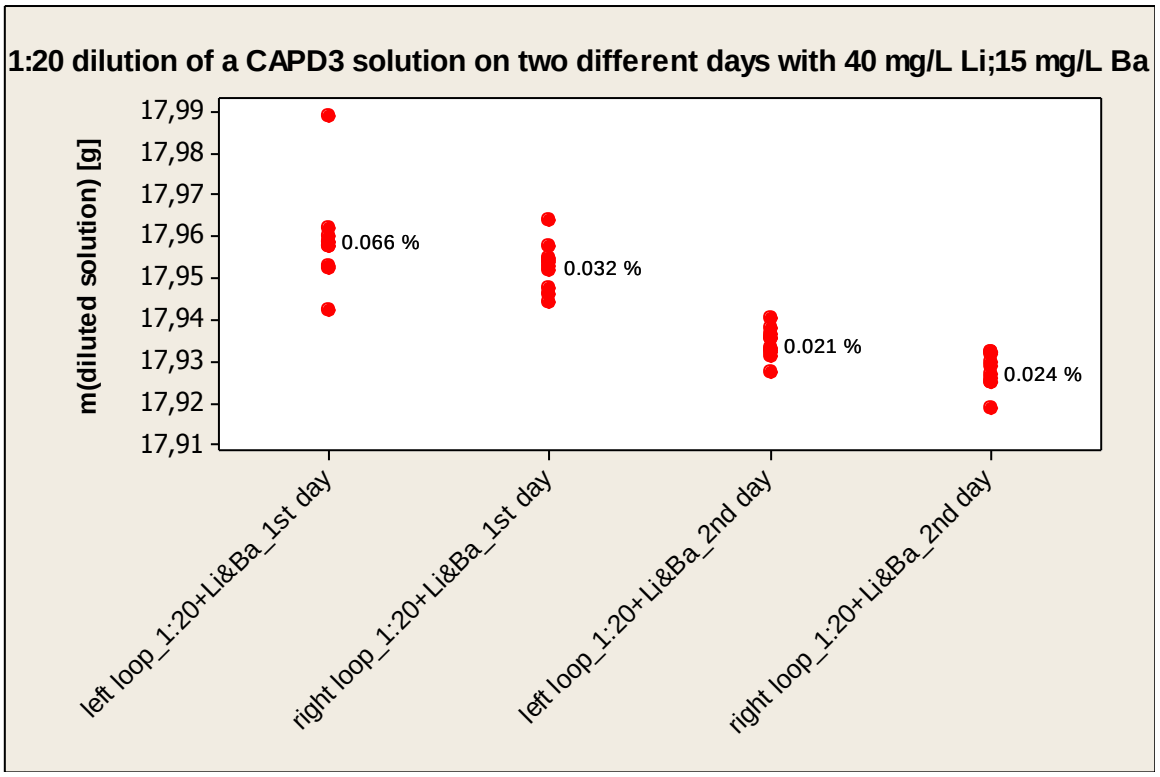

Figure 5-29: An individual value plot illustrating the precision of the addition of lithium and barium as IS to a 1:20 dilution of a CAPD3 solution carried out on two different days.

5.5.3 Evaluation of the similarity or difference between the preparation of the sample and the QC-standard

As stated in chapter 4.2.4.1, the dilution of the sample and the QC-standard are carried out with the same dosing unit which is connected to two different loop systems (see Figure 4-2). The one on the left is for the sample and on the right for the QC-standard.

Since the value of the sample is corrected with that of the QC-standard in the standardization process, these two (sample and QC) have to be prepared equally to avoid erroneous results. Due to this, an evaluation of the preparation processes (dilution process and the addition of internal standard) of both the sample and the QC is carried out individually to identify their similarity or difference, respectively.

With the help of the one-way analysis of variance (ANOVA), with which the hypothesis is determined that the mean of different populations are the same, the equality of the average values between the preparation process of the sample and that of QC are verified [178]. Moreover, the p-value (probability value) obtained in this

analysis is used to evaluate their differences. The average values are significantly different when a p-value of ≤ 0.05 is obtained.

The results of the two preparation processes are presented in a box plot and their average values, which display their difference, are connected to each other. The lines in each box represent the median. Outliers are marked with an asterisk (*) beyond the outgoing lines from the box which represent the upper and lower 25 % of the data, also known as whisker.

Out of twelve different measurements carried out in this evaluation, a p-value of ≤ 0.05 is obtained in six different measurements, i.e. there is a significant difference between the preparation process of the sample and QC in half of the studies. The other six, however, show no significant difference. The results of this study are summarized in Table 5-43.

Although this analysis shows that the preparation processes of the sample and the QC are not as similar as required for a precise and accurate analysis, however, a final conclusion can only be drawn with the results of the on-line analysis in chapter 5.6.

Table 5-43: Results of the ANOVA to evaluate the difference between the preparation process of the sample and QC (see Figure 4-2); p-values ≤ 0.05 are highlighted in red and p-values > 0.05 are highlighted in green

			left loop (sample)		right loop (QC)	
	day	**p-value**	**mean**	**std. dev.**	**mean**	**std. dev.**
1:10	1	0.088	17.9979	0.0068	17.9918	0.0082
	2	0.069	17.9599	0.0058	17.9551	0.0053
1:20	1	0.006	17.9692	0.0048	17.9626	0.0047
	2	0.008	17.9301	0.0043	17.9254	0.0025
1:50	1	0.004	17.9474	0.0020	17.9437	0.0029
	2	0.052	17.9192	0.0030	17.9164	0.0029
1:20 + Li	1	0.046	17.9623	0.0035	17.9573	0.0064
	2	0.213	17.9205	0.0074	17.9169	0.0051
1:20 + Ba	1	0.020	17.9480	0.0061	17.9427	0.0028
	2	0.098	17.9134	0.0086	17.9075	0.0062
1:20 + Ba + Li	1	0.151	17.9590	0.0119	17.9527	0.0058
	2	0.002	17.9342	0.0037	17.9276	0.0043

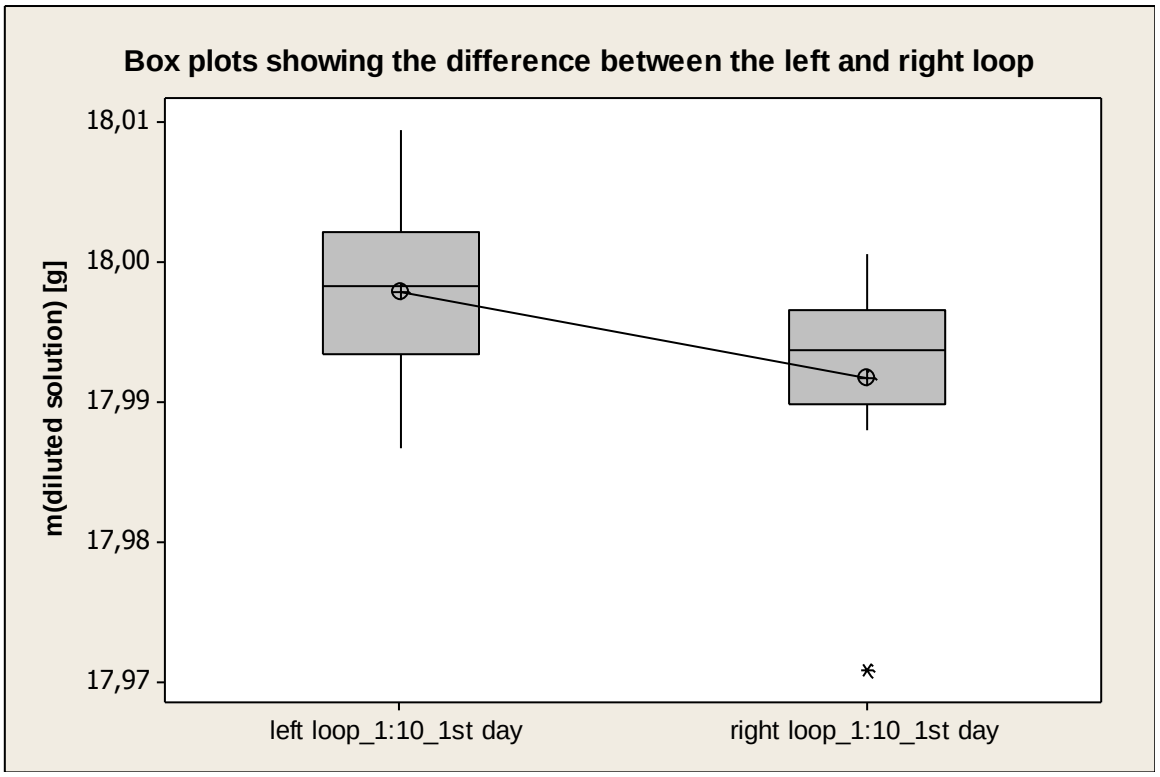

Figure 5-30: Evaluating the difference of the preparation process of the sample and QC with the help of box plots in a 1:10 solution dilution (first day)

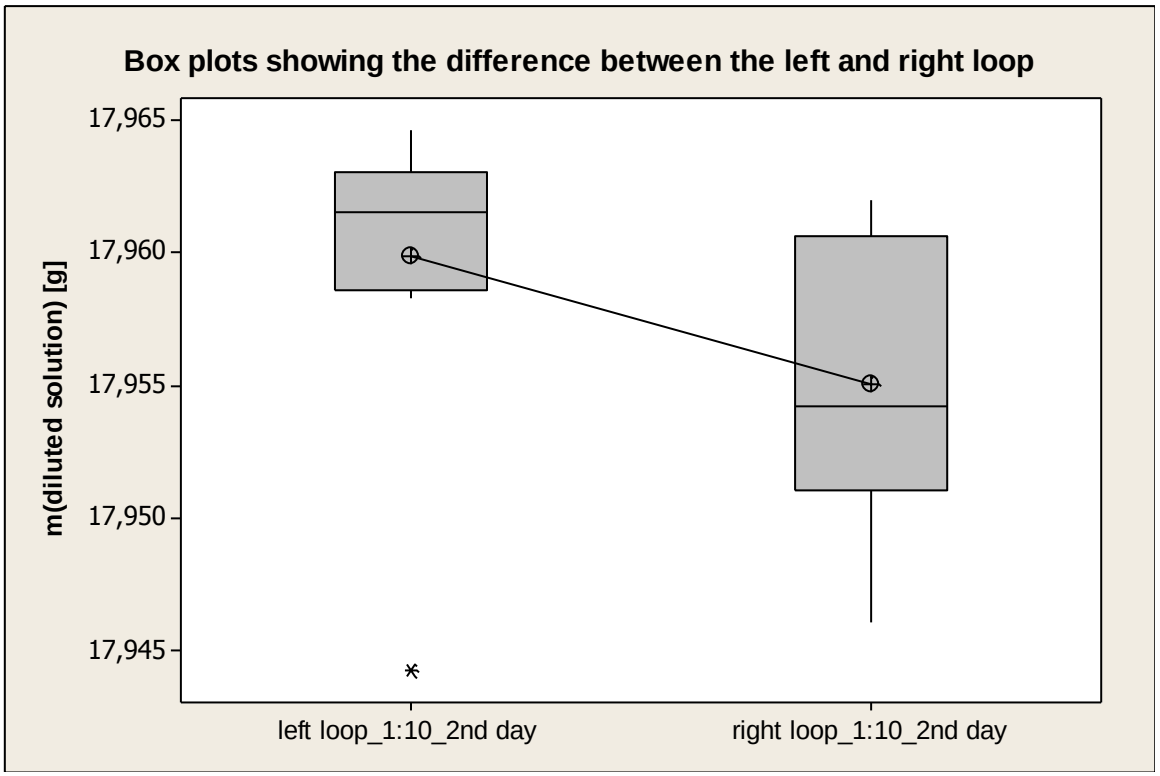

Figure 5-31: Evaluating the difference of the preparation process of the sample and QC with the help of box plots in a 1:10 solution dilution (second day)

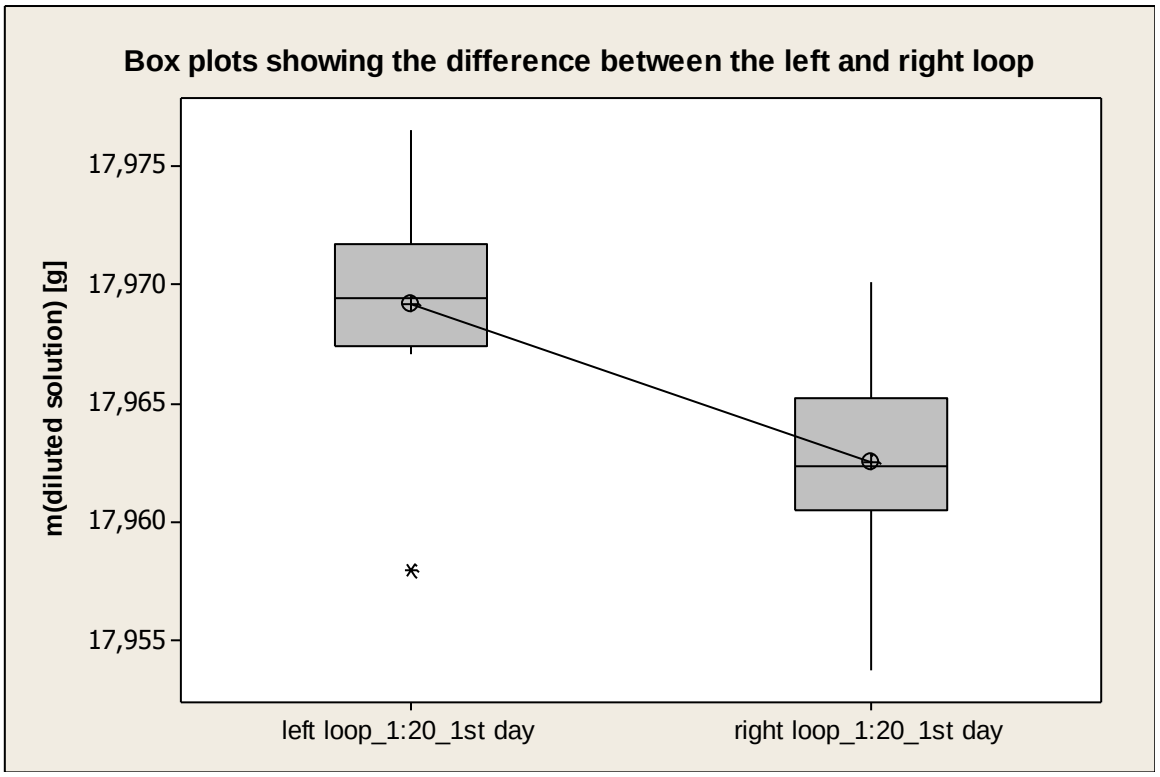

Figure 5-32: Evaluating the difference of the preparation process of the sample and QC with the help of box plots in a 1:20 solution dilution (first day)

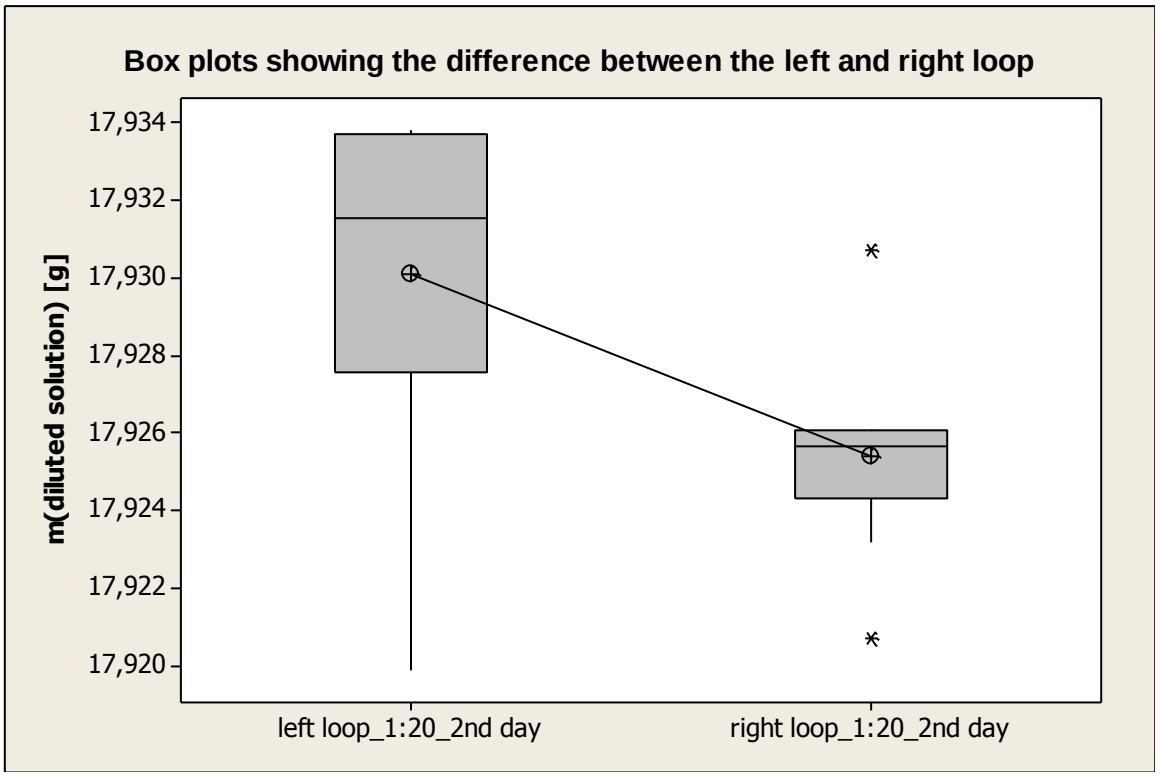

Figure 5-33: Evaluating the difference of the preparation process of the sample and QC with the help of box plots in a 1:20 solution dilution (second day)

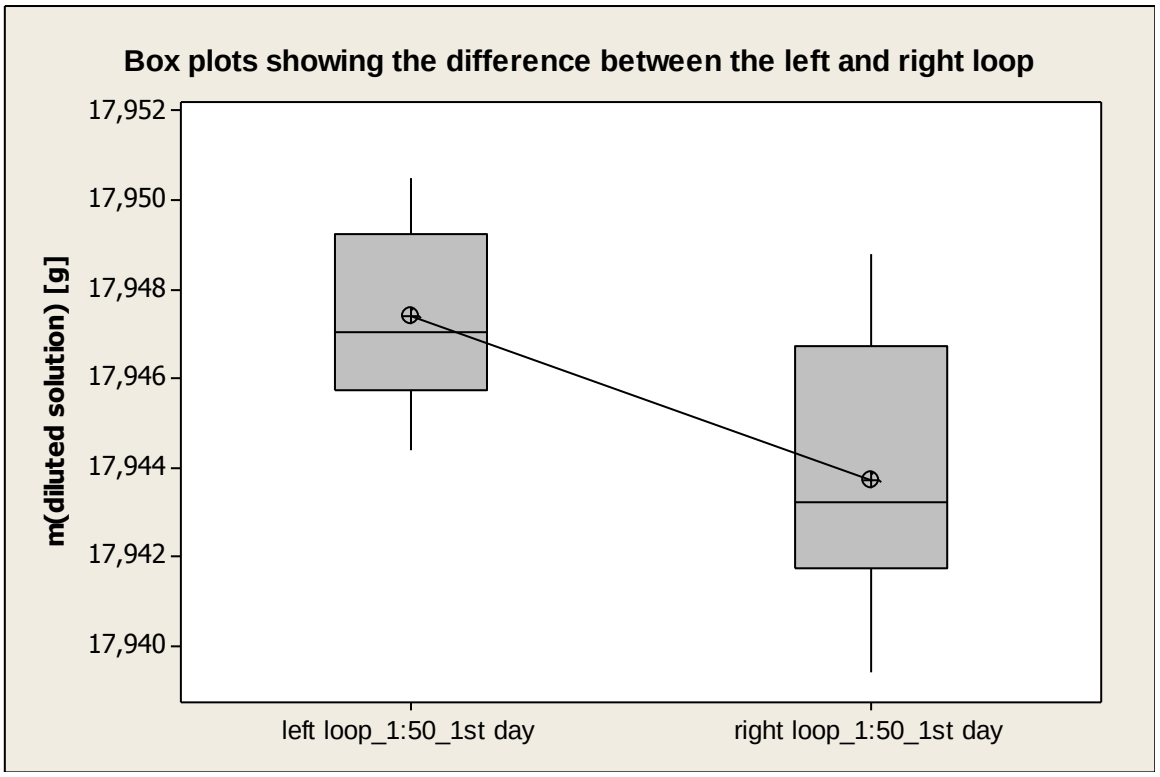

Figure 5-34: Evaluating the difference of the preparation process of the sample and QC with the help of box plots in a 1:50 solution dilution (first day)

Figure 5-35: Evaluating the difference of the preparation process of the sample and QC with the help of box plots in a 1:50 solution dilution (second day)

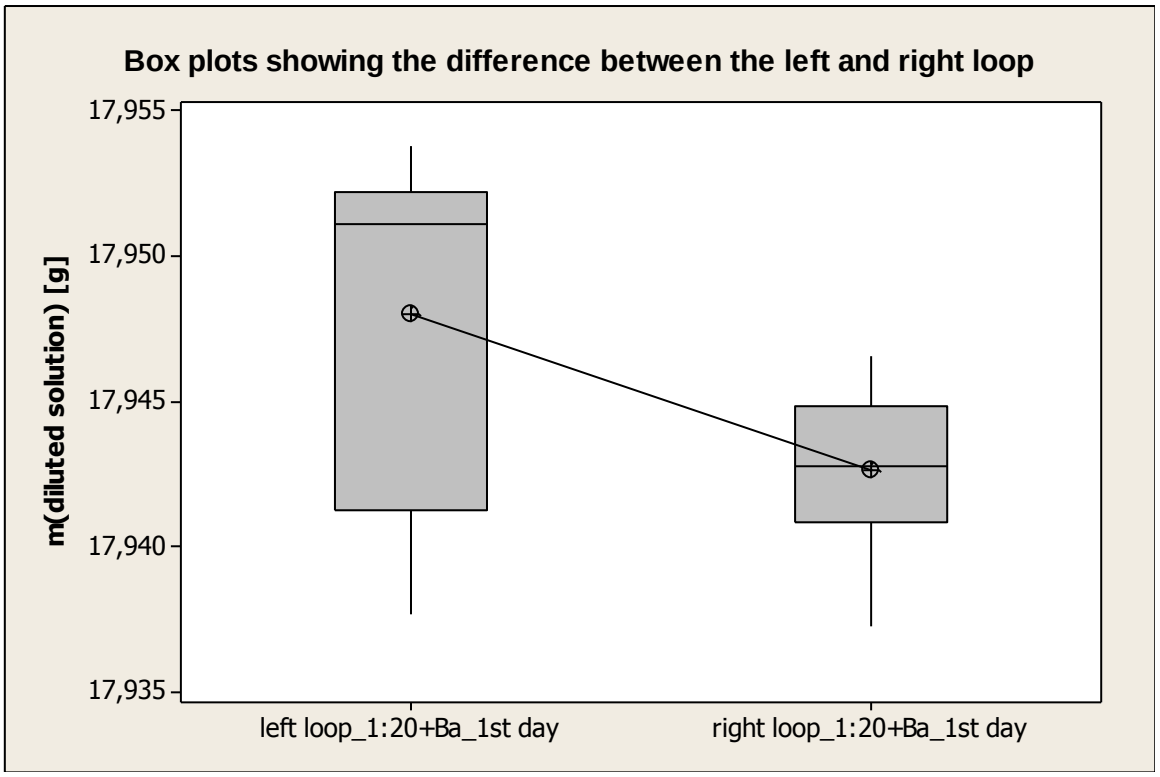

Figure 5-36: Evaluating the difference of the preparation process of the sample and QC with the help of box plots, in a 1:20 solution dilution and the addition of Ba as internal standard (first day)

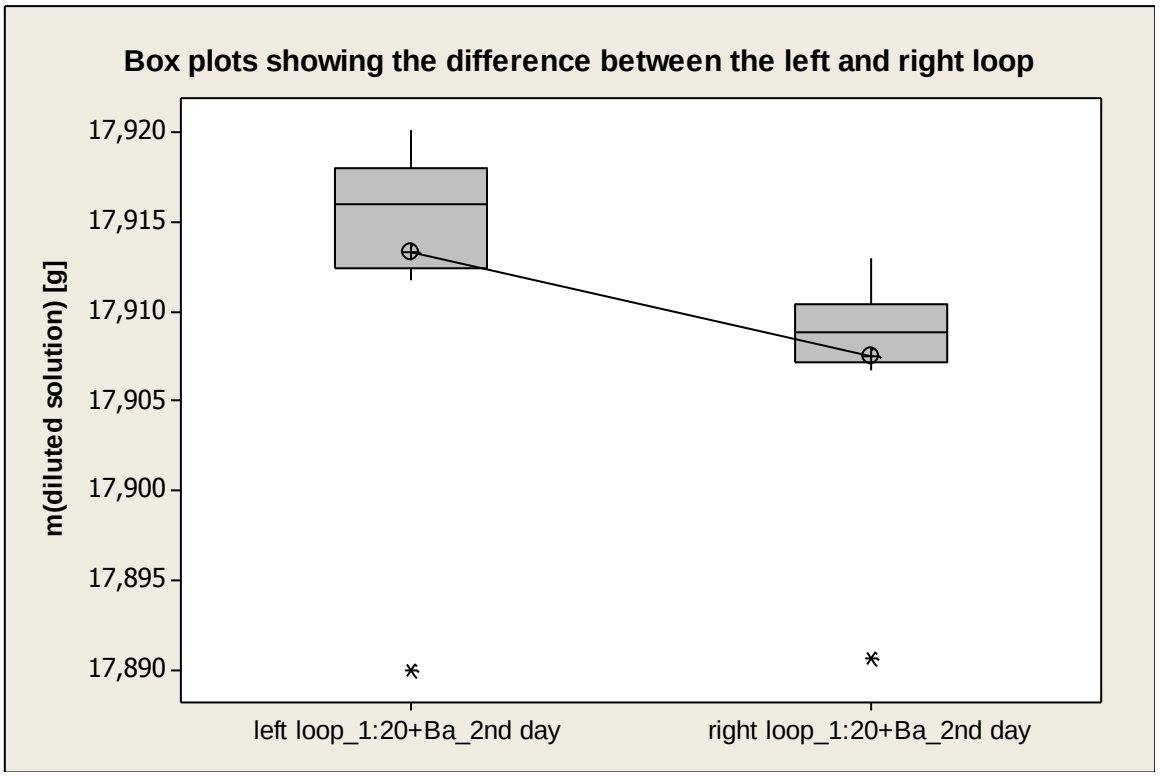

Figure 5-37: Evaluating the difference of the preparation process of the sample and QC with the help of box plots, in a 1:20 solution dilution and the addition of Ba as internal standard (second day)

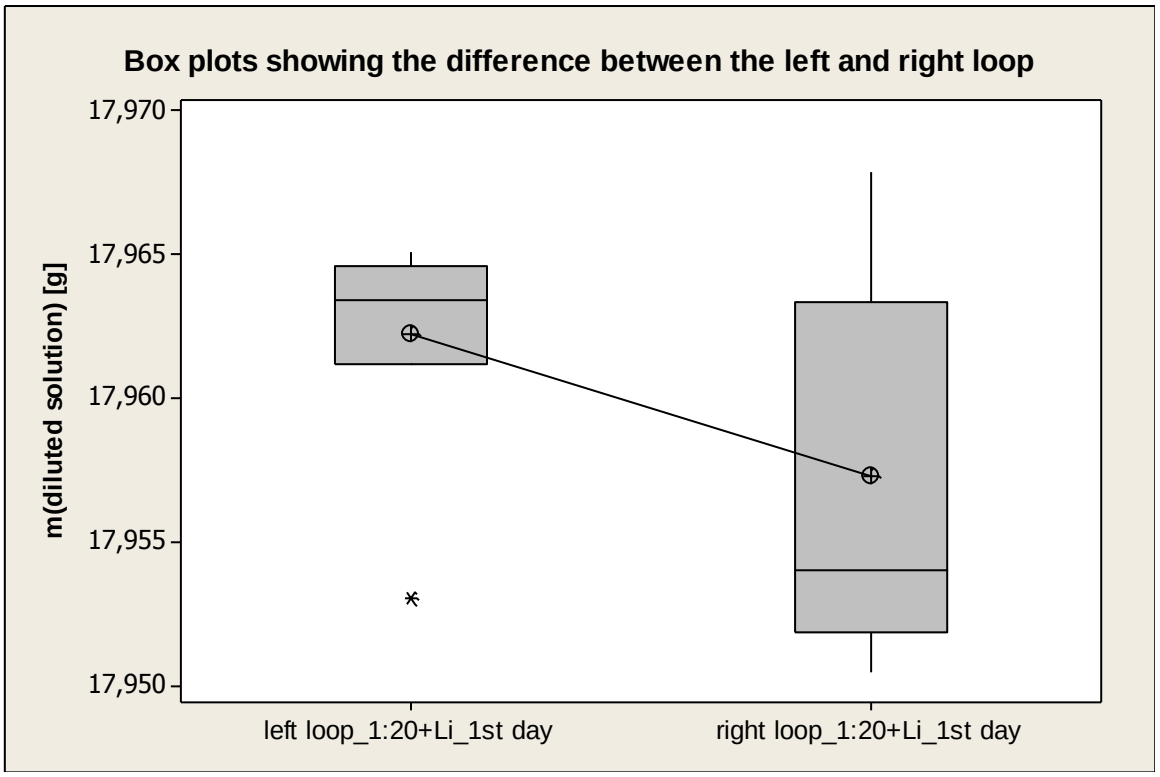

Figure 5-38: Evaluating the difference of the preparation process of the sample and QC with the help of box plots, in a 1:20 solution dilution and the addition of Li as internal standard (first day)

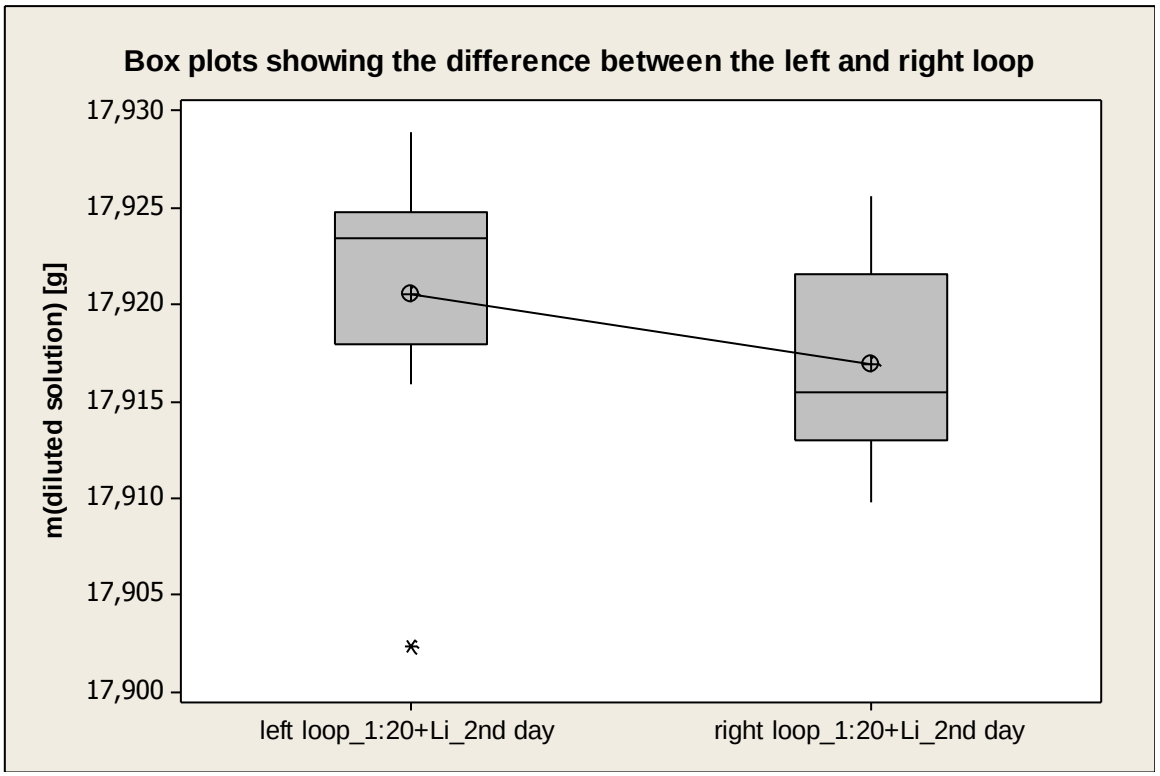

Figure 5-39: Evaluating the difference of the preparation process of the sample and QC with the help of box plots, in a 1:20 solution dilution and the addition of Li as internal standard (second day)

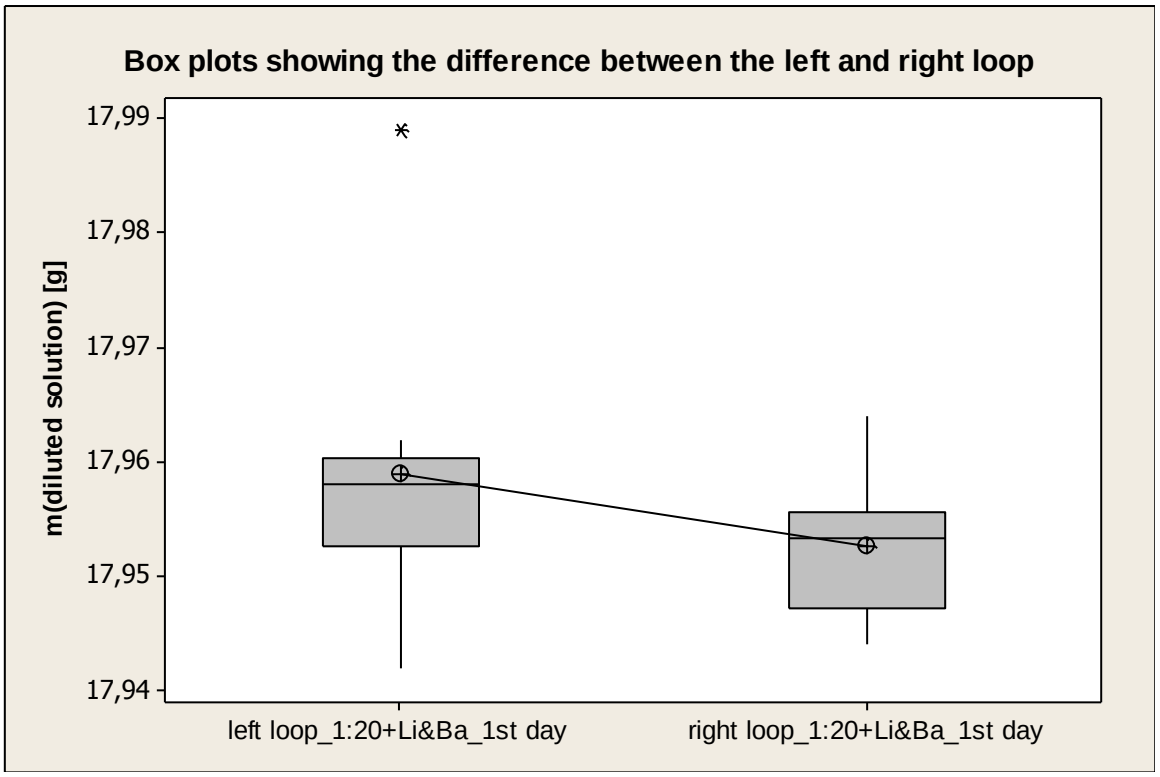

Figure 5-40: Evaluating the difference of the preparation process of the sample and QC with the help of box plots, in a 1:20 solution dilution and the addition of Ba and Li as internal standards (first day)

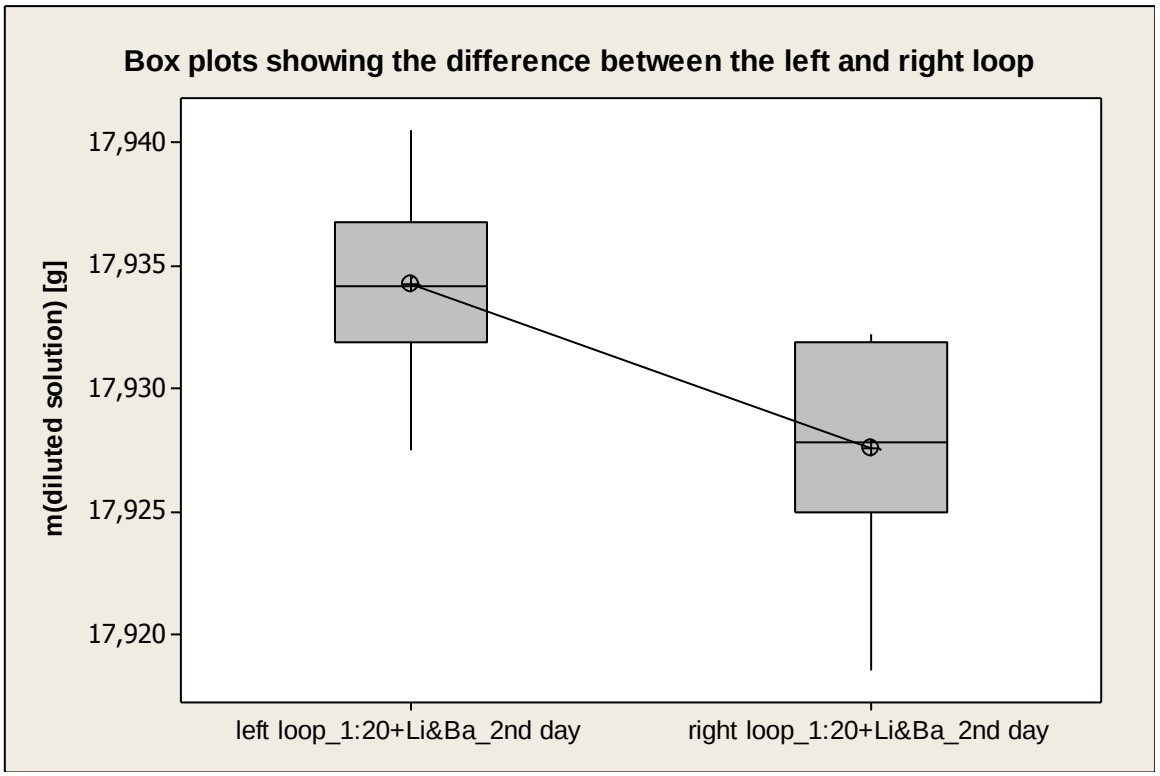

Figure 5-41: Evaluating the difference of the preparation process of the sample and QC with the help of box plots, in a 1:20 solution dilution and the addition of Ba and Li as internal standards (second day)

5.5.4 Conclusion on the determination of the precision of the sample preparation

According to Figure 5-42 and Figure 5-43, the precision of the sample preparation is surprisingly good with a mean value around 0.027 % after considering the examined factors that can influence this process. In view of the results in chapter 5.5.1 and 5.5.2, neither the density differences of the solutions nor the dilution factor nor the addition of internal standard has a significant impact on the sample preparation that can increase the total error of the on-line process analysis system greatly.
Since the gravimetric determination is carried out through manual collection of the diluted sample as well as weighing of the sample (see Figure 4-5), the precision of 0.027 % can be much better if the manual influence causing an increase in the standard deviation and outliers is avoided (see Figure 5-42). With this, however, the required precision of less than 1 % can be achieved in the on-line process analysis system. The inspection and certification values according to the manufacturer of the dosing unit, Metrohm, can be found in Table 5-44 and Table 5-45. The values in Table 5-45 confirm the precision of 0.027 % which is achieved in this work.

Table 5-44: Typical measurement deviation of Metrohm dosing unit [179]

Cylinder volume [mL]	Max. systematic deviation [µL]
2	± 6
5	± 15
10	± 20
20	± 30
50	± 50

Table 5-45: Permissible limit values as per ISO/EN/DIN 8655-3 [179]

Cylinder volume	Max. systematic Measurement deviation		Max. permissible Measurement deviation	
[mL]	[%]	[µL]	[%]	[µL]
2	0.5	10	0.1	2
5	0.3	15	0.1	5
10	0.2	20	0.07	7
20	0.2	40	0.07	14
50	0.2	100	0.05	25

Differences between the preparation processes of the sample and QC could adversely affect the results of the sample and, therefore, cause strong deviations in its measured values. However, the results in chapter 5.6 will show the consequence of this difference on the on-line analysis.

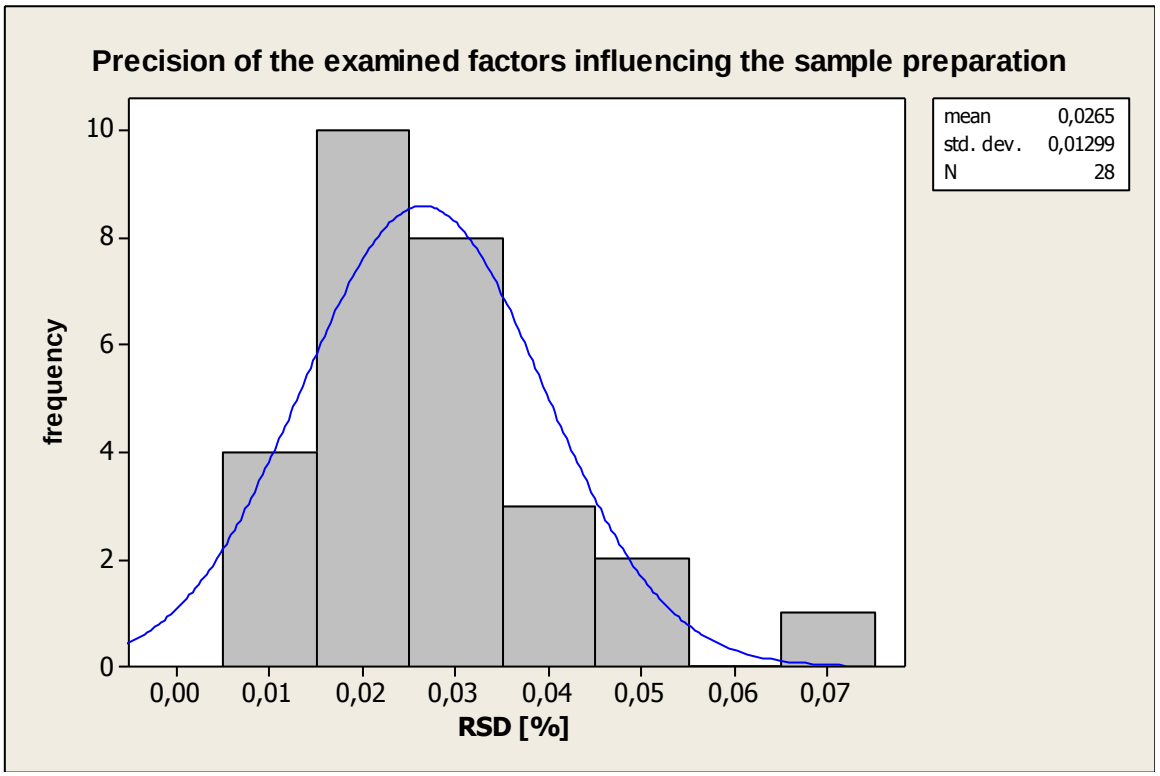

Figure 5-42: A bar chart illustrating the precision of the sample preparation (Summary of the RSD of the examined factors influencing this process, with N been the number of measurements)

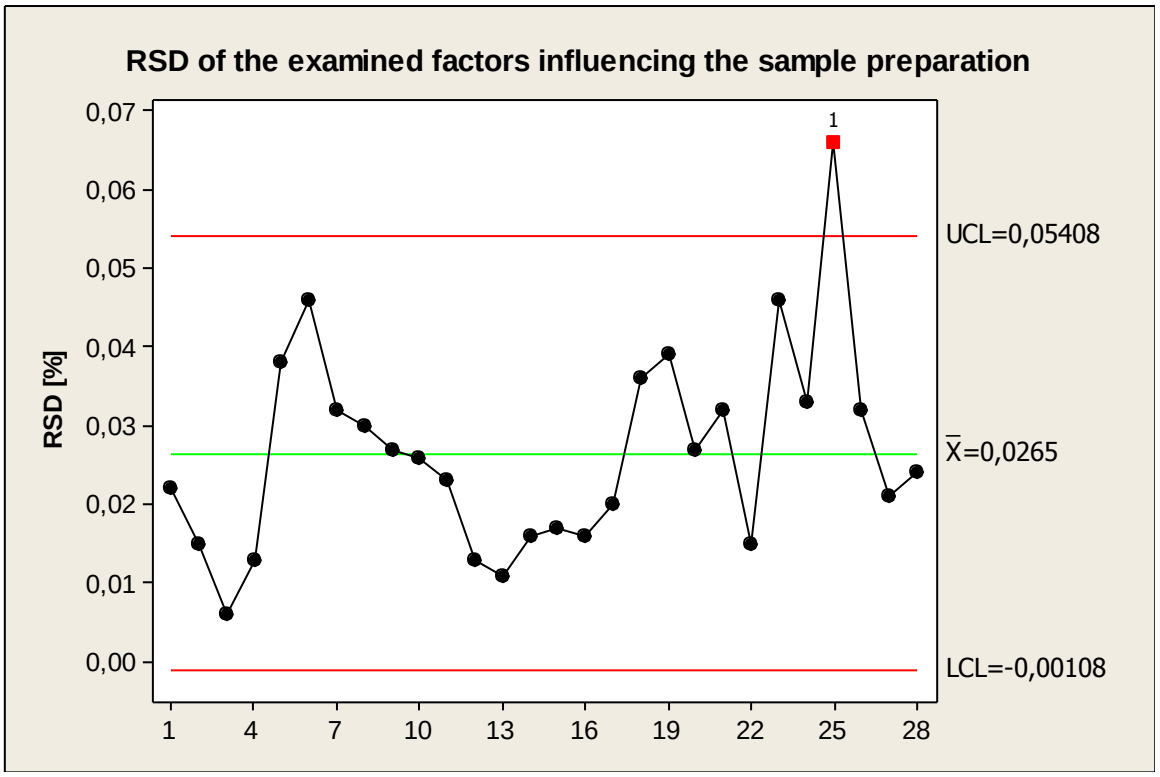

Figure 5-43: An individual control chart illustrating the precision of the examined factors influencing the sample preparation process (The RSD of all the factors are within the upper control limit (UCP) with the exception of the value marked in red)

5.6 Results of the on-line process analysis system

The following results are obtained from measurements carried out with the on-line system (see Figure 2-3). A CAPD2 solution is used for the measurement both as sample and as QC in order to compare the results of both preparations with each other. Apart from the glucose concentration of 15.45 g L^{-1} in CAPD2, this solution has the same composition as the CAPD3 solution in Table 4-1. Measurements carried out in two different days are compared to examine not only the repeatability and accuracy but also the intermediate precision.
Figure 5-44 to Figure 5-49 are the results obtained before the standardization, i. e. before the values of the sample are corrected with that of the QC. Therefore, the results obtained for the sample and that for the QC are compared individually on each day. The results obtained after the standardization, i.e. after the correction with the QC-standard, are summarized in Figure 5-50 and Figure 5-51. In these figures, not all the analyte emission lines used in this analysis are presented; only one emission line is selected for each ion in the on-line analysis.

The strong fluctuations in the Ca and Mg values (see Figure 5-44, Figure 5-45, Figure 5-47 and Figure 5-48) are caused by an effect on barium which is used as internal standard for these ions. However, the increase in the values at the beginning of the measurements is caused by a colder plasma temperature at the beginning which can be avoided by a longer condition time, i.e. leaving the plasma temperature to stabilize longer before the starting the measurement.

The differences between the average values of the sample and that of QC in Figure 5-46 and Figure 5-49 show that the differences in the values of Ca and Mg with about 2 mmol L^{-1} is higher than that of Na with about 1 mmol L^{-1}. This could result from a stronger difference in the addition of Ba than in that of Li since the addition of the internal standard is the only source of influence that can distinguish the results of these ions in this way. However, the difference in the preparation processes of the sample and the QC as found in chapter 5.5.3 could also contribute to these variations. It is, moreover, obvious that the results of all the ions are higher. This could have resulted from an inaccurate preparation of both the sample and the QC.

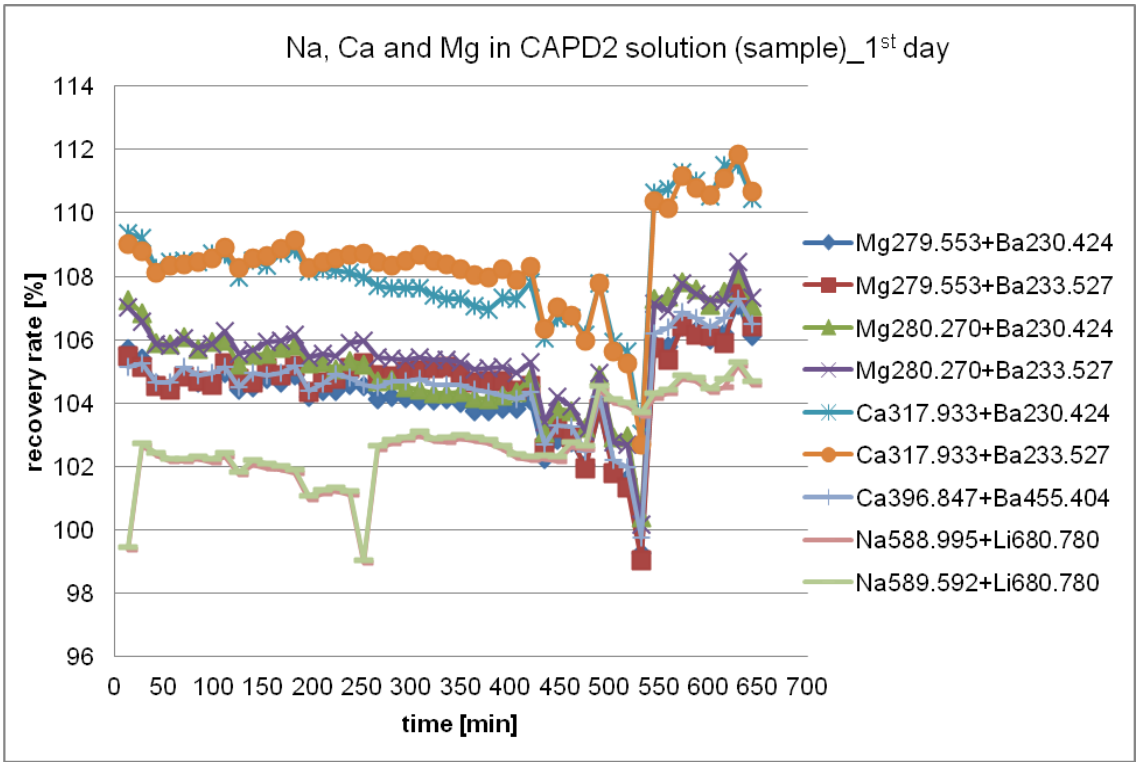

Figure 5-44: Determination of Na, Ca and Mg in CAPD2 solution, as sample, prepared with the left loop and in the left vessel (see Figure 4-2) and measured on the first day

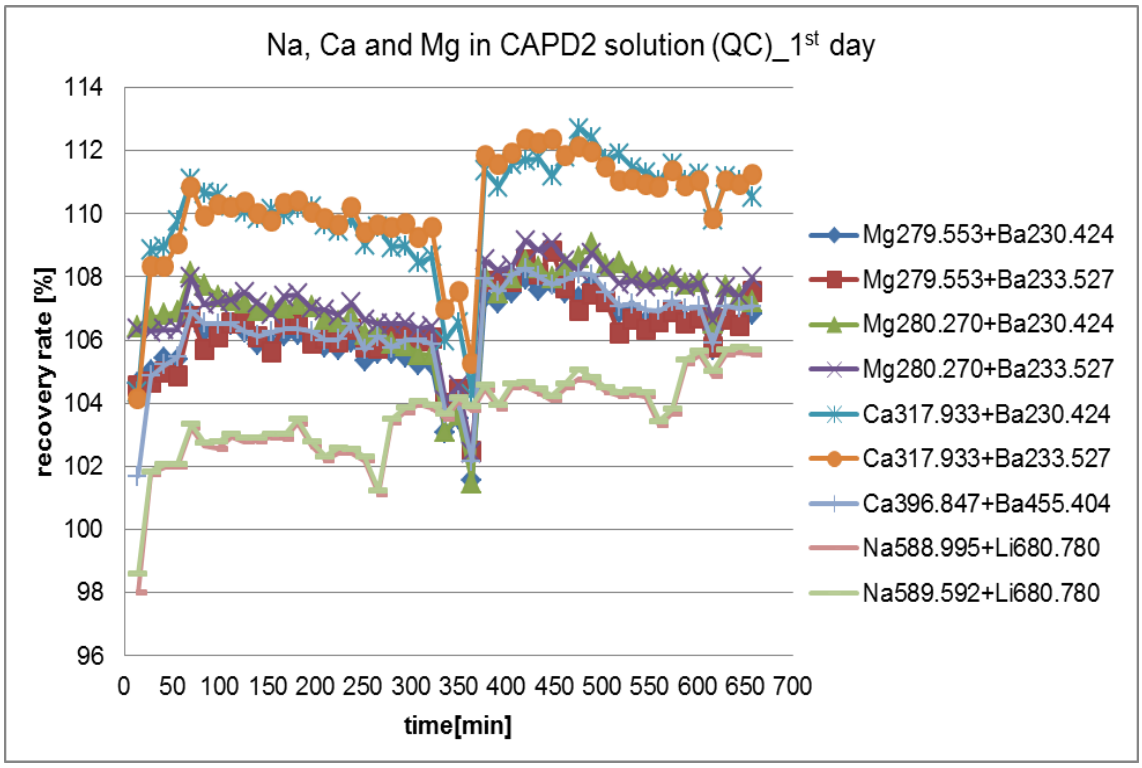

Figure 5-45: Determination of Na, Ca and Mg in CAPD2 solution, as QC, prepared with the right loop and in the right vessel (see Figure 4-2) and measured on the first day

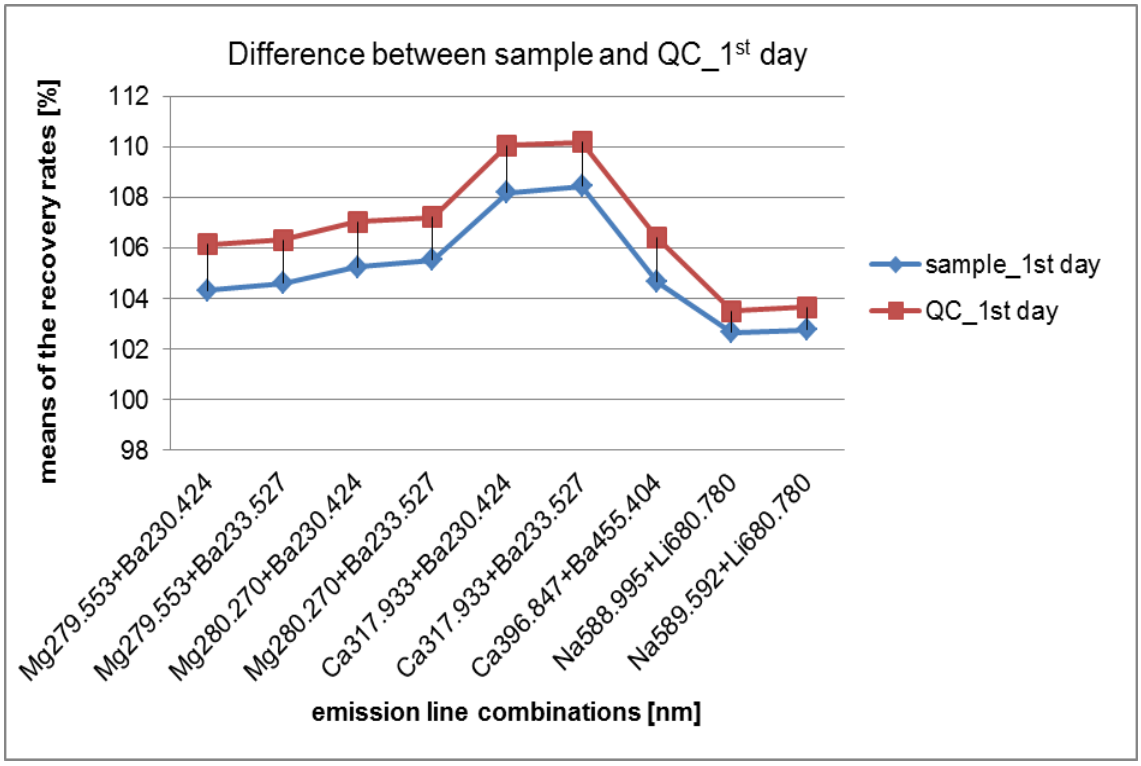

Figure 5-46: The difference between the mean values of the sample and that of QC for each IS-analyte emission line-combination obtained on the first day

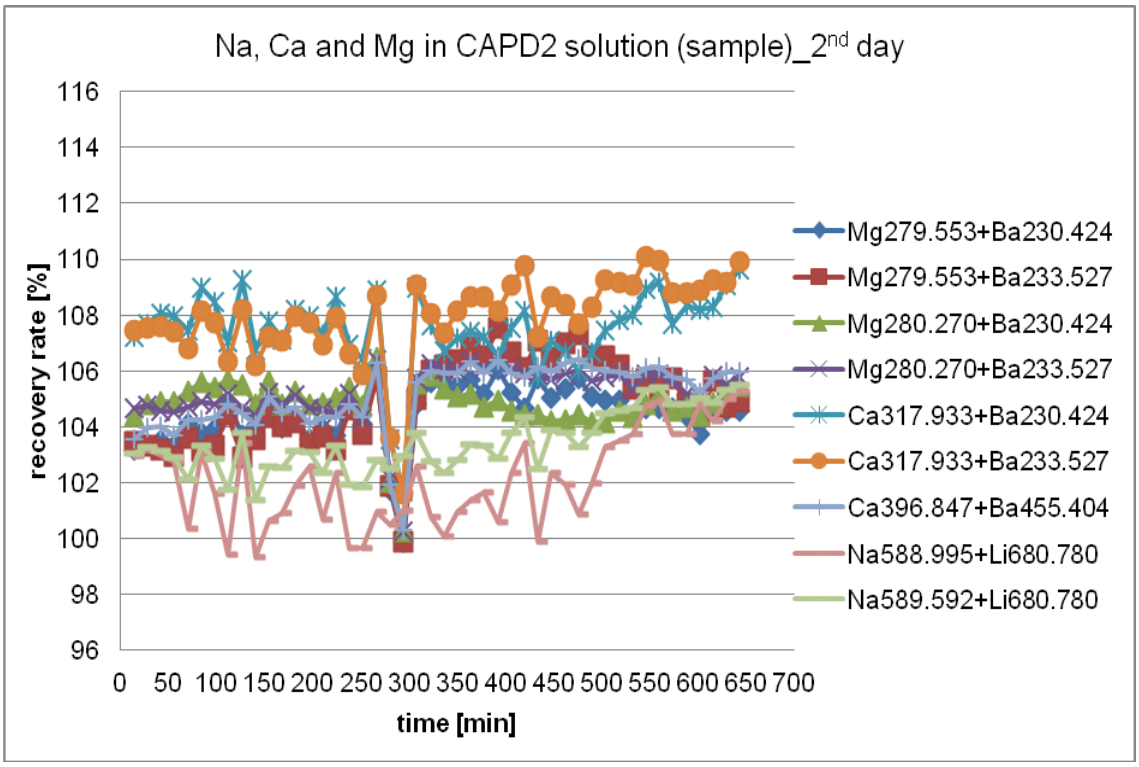

Figure 5-47: Determination of Na, Ca and Mg in CAPD2 solution, as sample, prepared with the left loop and in the left vessel (see Figure 4-2) and measured on the second day

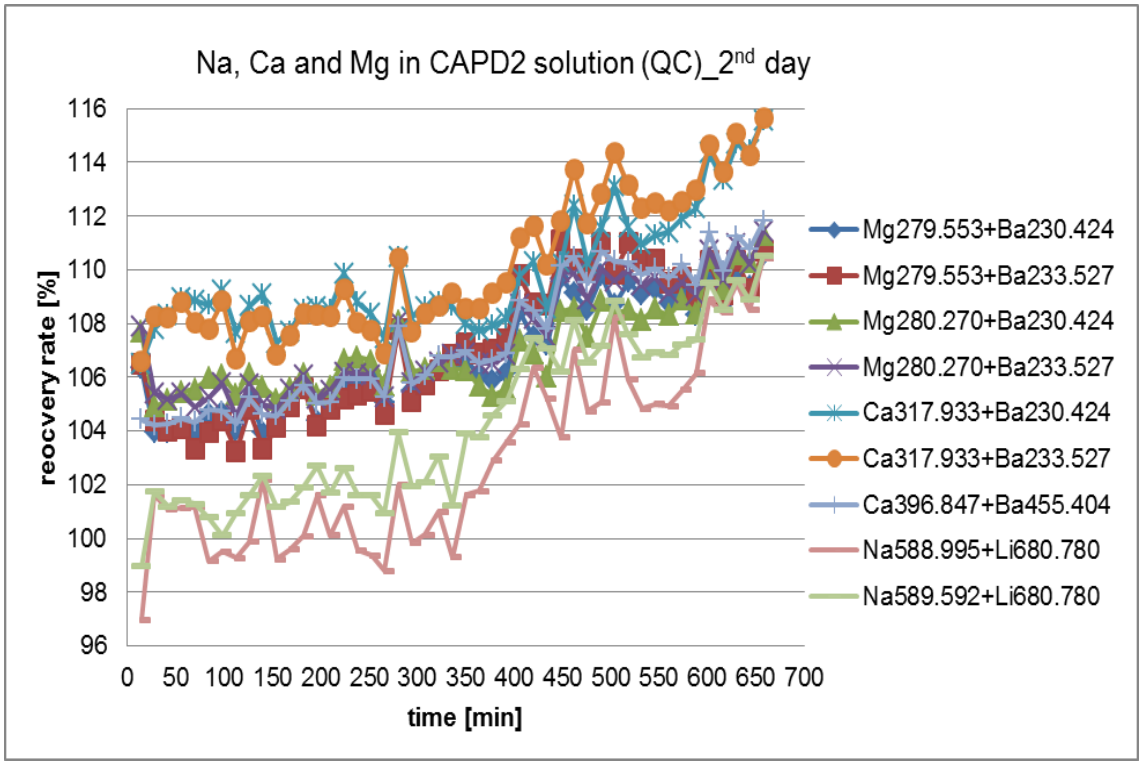

Figure 5-48: Determination of Na, Ca and Mg in CAPD2 solution, as QC, prepared with the right loop and in the right vessel (see Figure 4-2) and measured on the second day

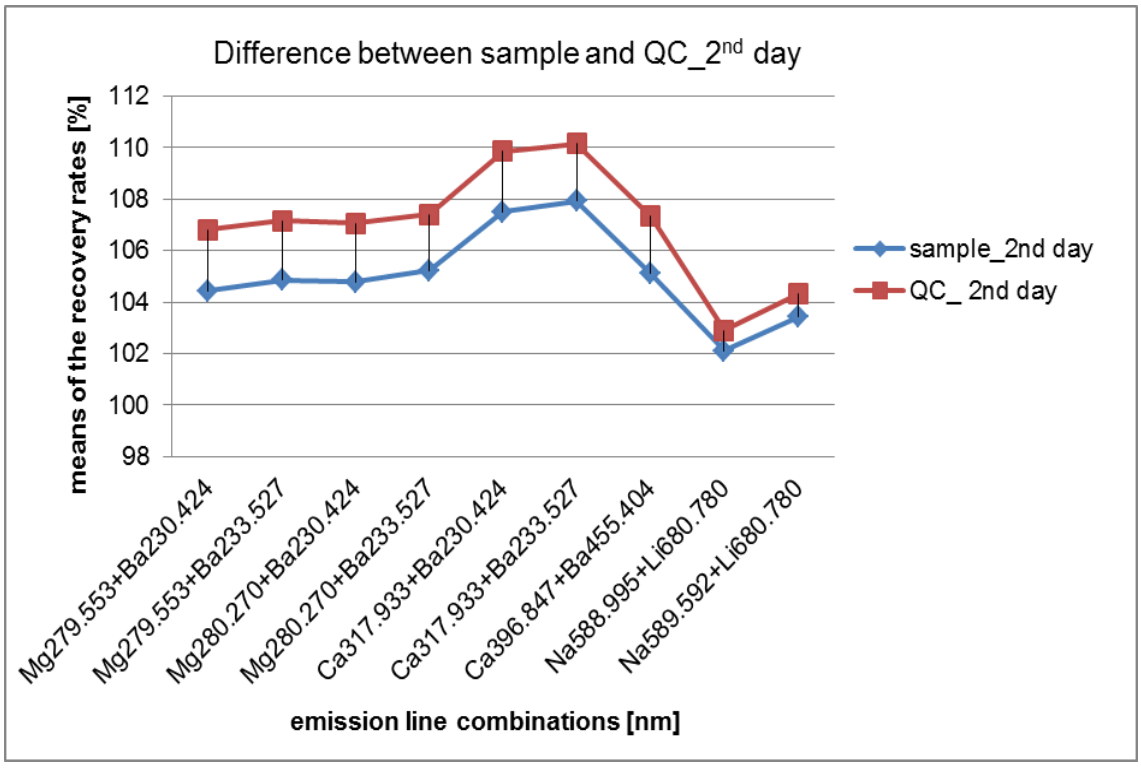

Figure 5-49: The difference between the mean values of the sample and that of QC for each IS-analyte emission line-combination obtained on the second day

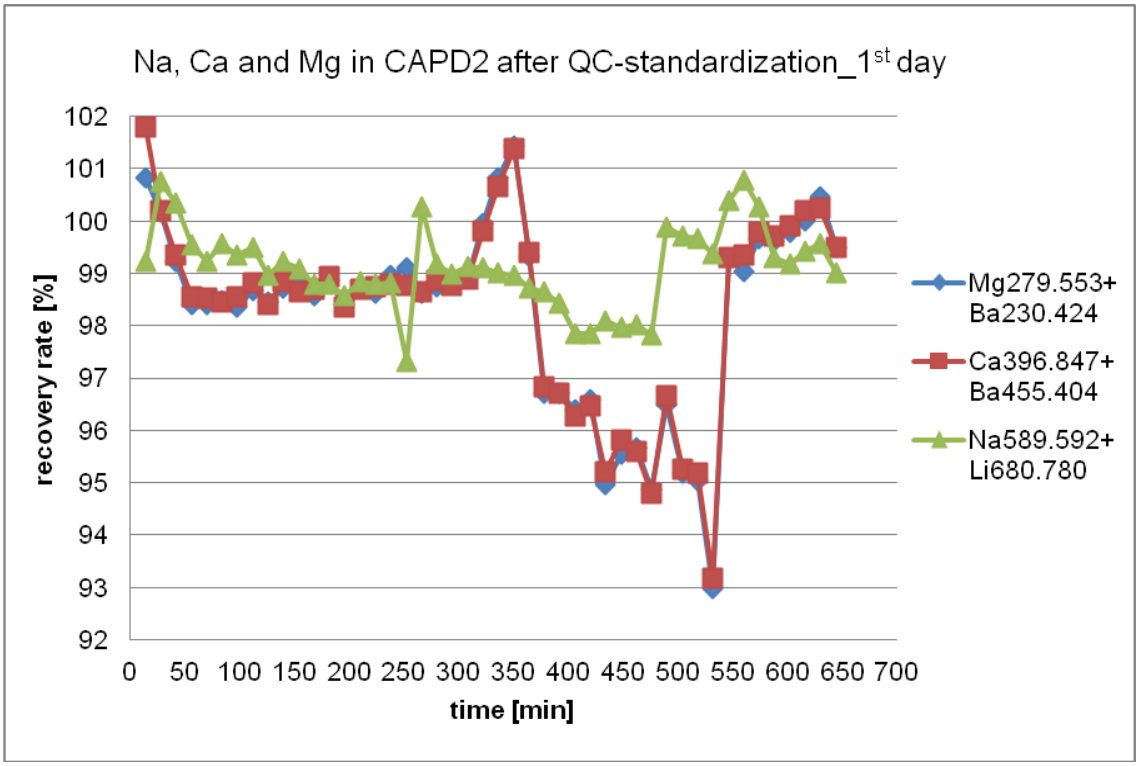

Figure 5-50: Results obtained from the determination of Na, Ca and Mg in CAPD2 after standardization with QC (measurements on the first day within about 10 h)

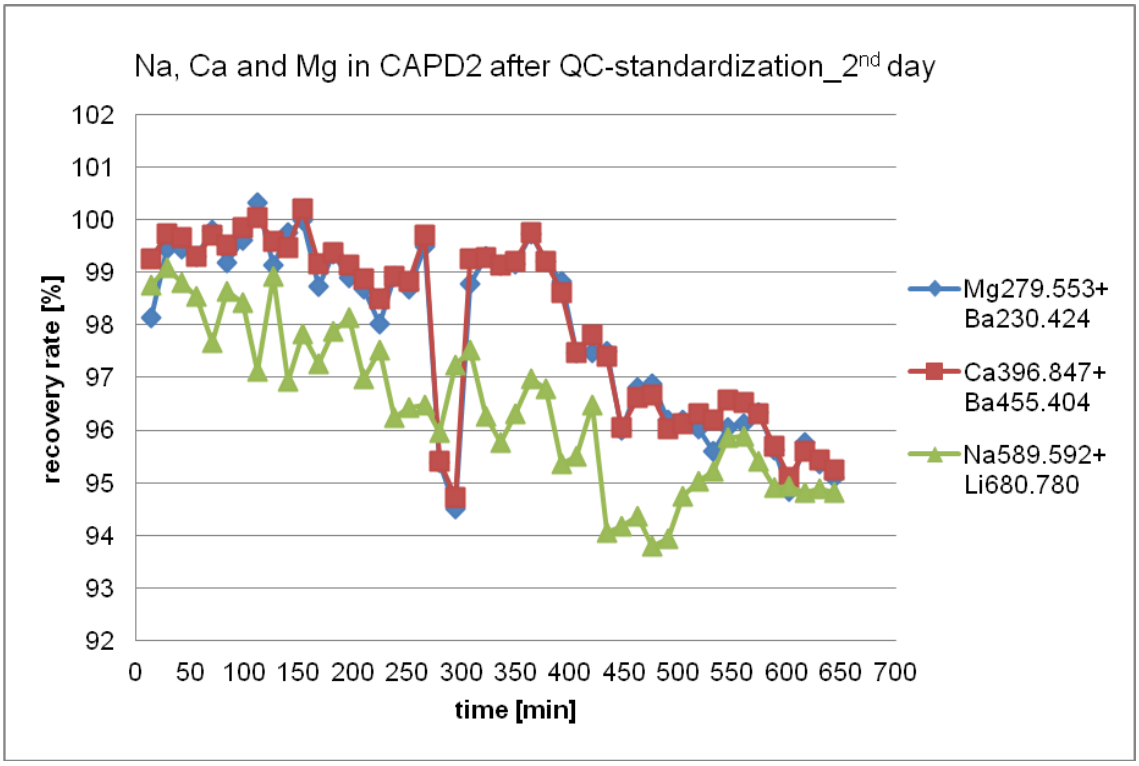

Figure 5-51: Results obtained from the determination of Na, Ca and Mg in CAPD2 after standardization with QC (measurements on the second day within about 10 h)

Figure 5-50 and Figure 5-51 show the effectiveness of the QC standardization as it is mentioned in chapters 5.3 and 5.4. The strong fluctuations in both the Mg and the Ca values can be attributed to the poor addition of the IS, barium. However, the results for Mg could be improved if the best IS-analyte emission line combination (Table 5-42) is used instead.

Although the QC-standardization has proven much effective, further optimizations are necessary to improve the accuracy and the repeatability (see Figure 5-51) of the sample preparation in order to fulfill all required specifications since the results obtained before the QC-standardization are mostly higher than expected.

6. Conclusion

On-line techniques play an important role in the process analytical chemistry (PAC), most especially in the pharmaceutical field, due to their ability to analyze a process automatically without getting into contact with the sample and so not affecting its sterile condition and not destroying its integrity, unlike in-line methods. Moreover, many laboratory instruments can be applied in an on-line system; however, it must be ensured that process requirements are higher due to their full-time application. Thus, any time efficient, robust, precise and stable method can be integrated into this system.

The examinations carried out on the two main parts of the on-line process analysis sytem, ICP-OES and sample preparation unit, in this work, have given satisfactory results with regard to both the precision of less than 1 % and the accuracy (specification limit of both the IPC and Ph. Eur.).

The results obtained with the ICP-OES correspond to some of the properties of this method [64], [82]. Unlike the mostly used techniques (AAS, flame photometer, ISE and titration (see Table 5-2)) for the determination of the analytes of interest (Na, K, Ca and Mg), the ICP-OES used in this work has proven to be very precise, accurate and less susceptive to matrix interference. It's stability in the sence of long-term determinations could also be confirmed in this study.
The two main matrix substances studied in this work seems to have no strong effect on any of the analytes. This could have probably resulted from the fact that the analytes of interest are mostly present in high concentrations and so sensitivity is not a great issue, unlike in the case of trace analysis [93], [180]. Moreover, the use of the plasma with a radial view could have also contributed to the great performance of this method and so to the remarkable results obtained since it is the ideal approach for salty and highly concentrated samples [88], [89]. The effectiveness of the internal standardization on the precision could also be confirmed in this work although lithium was extraordinarily better than barium [88], [99], [112]. Moreover, the QC-standardization in chapter 5.6 proved to be very effective and therefore, inevitable to achieve the goal of this work.

In view of these results, ICP-OES has confirmed to be the best technique among all the investigated methods of analysis (see Table 2-3), and is the most suitable on-line process analytical method for the determination of Na, K, Ca and Mg in dialysis solutions.

The sample preparation in this work, which involves the dilution and the addition of internal standard, proved to be very precise with the RSD of about 0.027 %. Neither the density differences of the dialysis solutions, the sample matrix, the different dilution factors nor the addition of internal standards could influence the precision negatively. However, the results achieved before the QC-standardization in the determination with the on-line process analysis system in chapter 5.6 indicates that the accuracy of the sample preparation unit requires further optimizations since the variation in the values achieved were higher. The investigations could not be carried out fully due to the limited time and resources.

7. Outlook

According to the results achieved in this work and that of my diploma thesis, the on-line determination of chloride, hydrogen carbonate and the metal ions (Na, K, Ca and Mg) in dialysis solutions can be carried out successfully with the methods tested in these theses. On-line methods and determinations for glucose, lactate, phosphate, pH and density need to be studied.

In case of the on-line determination of pH, several on-line and in-line sensors from different companies, such as Wissenschaftlich-Technische Werkstätten (WTW) GmbH, Metrohm, Hach, Endress+Hauser, etc., are available and also applied in different fileds, such as in the biotechnology [181].
Analyzers for the on-line or in-line determination of density are also available in companies, like Anton Paar, Bopp & Reuther, SensoTech, etc. A practical example can be found in an on-line density and crystallinity measurement during the melt spinning of the polymer, polyethylene terephthalate (PET) [182].
Some few tests have been carried out for the on-line determination of glucose and lactate with near-infrared spectroscopy (NIRS), with which phospate can probably be determined too. As mentioned in the introduction, NIRS is one of the most popular on-line and in-line methods used in the PAC due to the sensor involved in its application.
In this test, the measurements were carried out off-line (see Figure 7-1). Calibration models, which are created with matrix-matched solutions, were created and used to predict the concentration of the analytes in a sample. The results in Figure 7-2 and Figure 7-3 show that NIRS has the potential of fulfilling the requirements of this work and, therefore, needs further studies and optimizations.

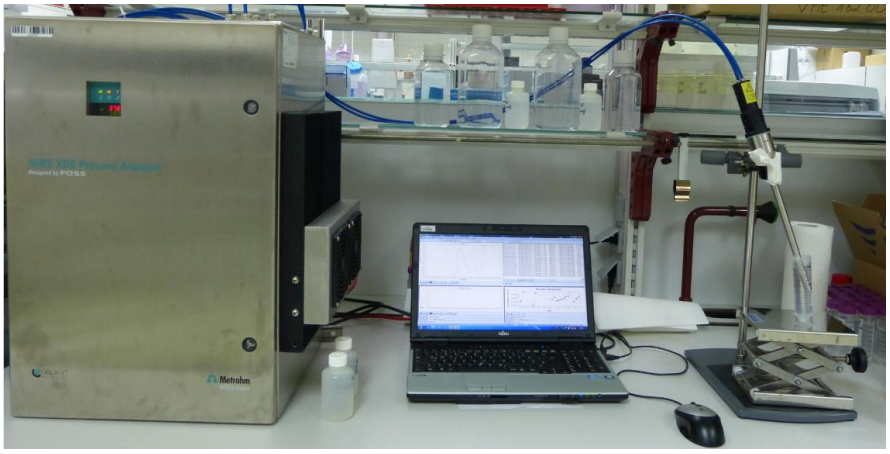

Figure 7-1: A near-infrared analyzer from Metrohm in an off-line operation

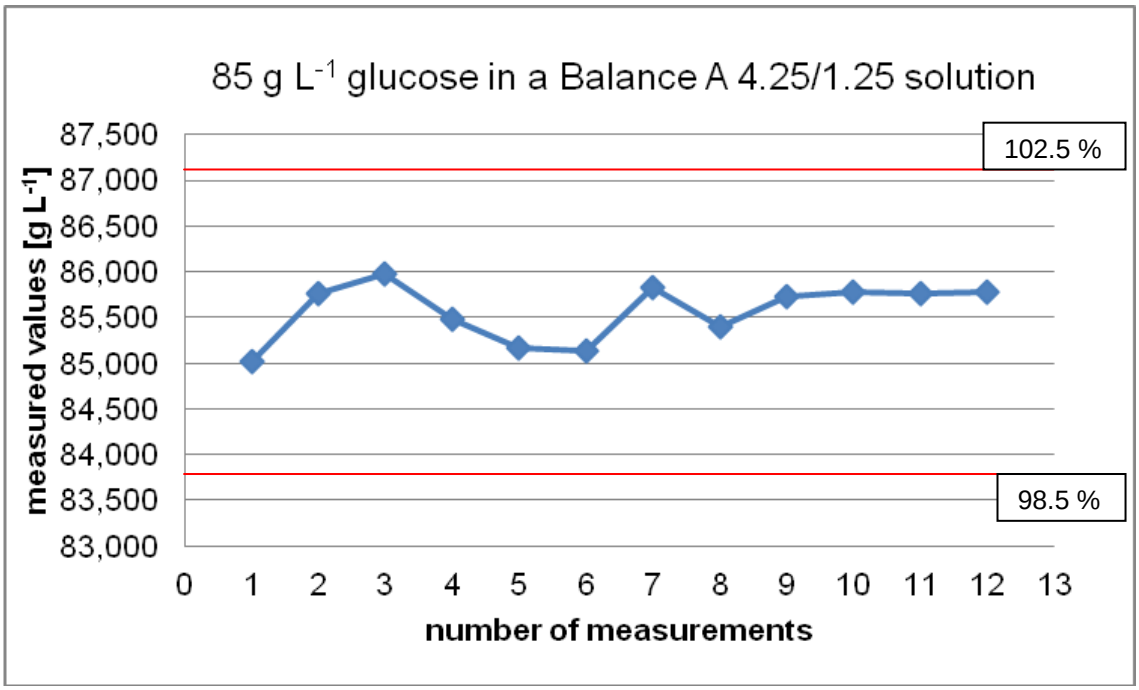

Figure 7-2: Determination of 85 g L^{-1} glucose in a Balance A 4.25/1.25 solution by NIRS. The two additional red lines drawn in the graph show the specification limit for glucose in this sample, in the IPC.

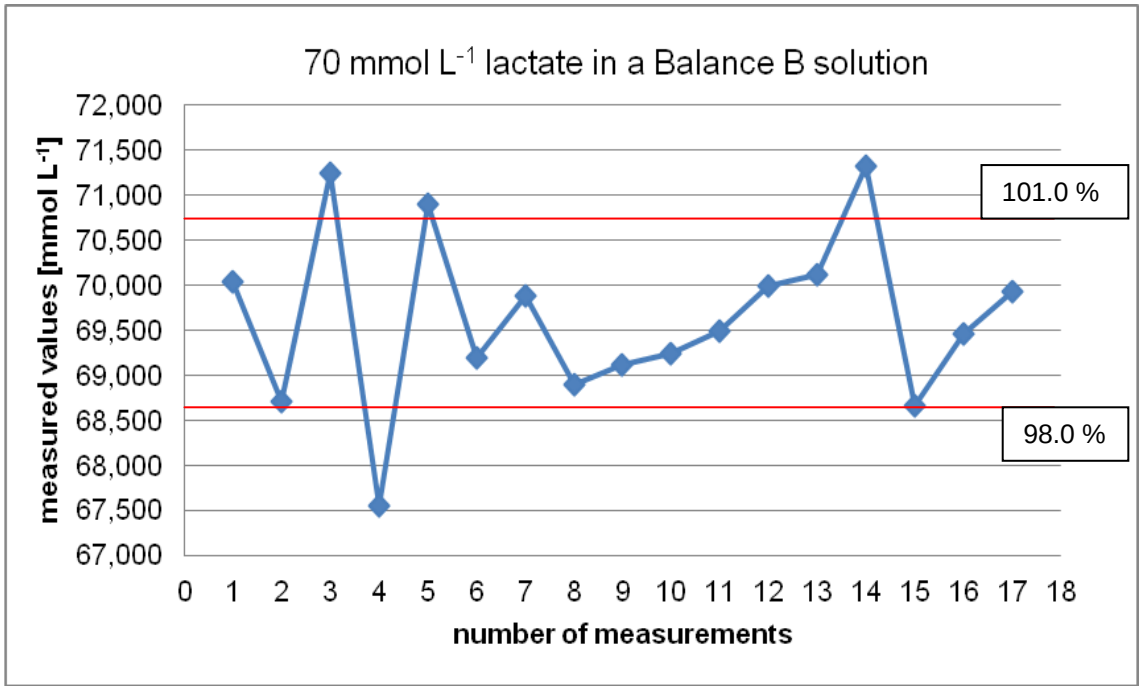

Figure 7-3: Determination of 70 mmol L^{-1} lactate in a Balance B solution by NIRS. The two additional red lines drawn in the graph show the specification limit for lactate in this sample, in the IPC.

8. References

[1] M. Haider and S. Kueppers, “Process analytical chemistry – future trends in industry,” *Anal. Bioanal. Chem.*, vol. 376, pp. 313–315, 2003.

[2] J. A. DiMasi, R. W. WHansen, and H. G. Grabowski, “The Price of Innovation: New Estimates of Drug Develpomlent Costs,” *J. Health Econ.*, vol. 22, pp. 151–185, 2003.

[3] K. A. Bakeev, *Process Analytical Technology: Spectroscopic Tools and Implementation Strategies for the Chemical and Pharmaceutical Industries: Second Edition*. John Wiley and Sons, 2010.

[4] J. P. Hughes, S. S. Rees, S. B. Kalindjian, and K. L. Philpott, “Principles of early drug discovery,” *British Journal of Pharmacology*, vol. 162, no. 6. pp. 1239–1249, 2011.

[5] Food and Drug Administration (FDA), *Guidance for Industry Industry PAT — A Framework for Innovative Pharmaceutical Development, Manufacturing, and Quality Assurance*. 2004.

[6] A. Serwah, “Untersuchung prozessanalytischer Methoden in der Pharmafertigung bei der Herstellung flüssiger steriler Arzneiformen,” Universität des Saarlandes, 2012.

[7] M. T. Riebe and D. J. Eustace, “Process Analytical Chemistry AN INDUSTRIAL PERSPECTIVE,” *Anal. Chem.*, vol. 62, no. 2, p. 65A–71A, 2001.

[8] process analytic work group of GDCh, *Arbeitsrichtlinie des Arbeitskreises Prozessanalytik der GDCh*. 2008, pp. 1–2.

[9] L. Olsson, U. Schulze, and J. Nielsen, “On-line bioprocess monitoring - An academic discipline or an industrial tool?,” *TrAC - Trends Anal. Chem.*, vol. 17, no. 2, pp. 88–95, 1998.

[10] J. B. Callls, D. L. Illman, and B. R. Kowalski, “Process analytical chemistry,” *Anal. Chem.*, vol. 59, no. 9, pp. 624–637, 1987.

[11] A. S. Rathore, R. Bhambure, and V. Ghare, “Process analytical technology (PAT) for biopharmaceutical products,” *Anal. Bioanal. Chem.*, 2010.

[12] R. W. Kessler, *Prozessanalytik: Strategien und Fallbeispiele aus der industriellen Praxis*. Wiley-VCH, 2006.

[13] J. Workman, M. Koch, and D. J. Veltkamp, “Process Analytical Chemistry,” *Anal. Chem.*, vol. 79, no. 12, pp. 4345–4363, 2007.

[14] J. J. Workman, M. Koch, and D. J. Veltkamp, “Process Analytical Chemistry,” *Anal. Chem.*, vol. 75, no. 12, pp. 2859–2876, 2003.

[15] M. V. Koch, “Optimizing the impact of developments in micro-instrumentation on process analytical technology: A consortium approach,” *Anal. Bioanal. Chem.*, vol. 384, no. 5, pp. 1049–1053, 2006.

[16] K. R. Beebe, W. W. Blaser, R. A. Bredeweg, J. P. Chauvel, R. S. Harrier, M. LaPack, A. Leugers, D. P. Martin, L. G. Wright, and E. D. Yalvac, “Process Analytical Chemistry,” *Anal. Chem.*, vol. 65, no. 12, pp. 199–216, 1993.

[17] H. Freund and K. Sundmacher, “Towards a methodology for the systematic analysis and design of efficient chemical processes. Part 1. From unit operations to elementary process functions,” *Chem. Eng. Process. Process Intensif.*, vol. 47, pp. 2051–2060, 2008.

[18] H. Huang, H. Yu, H. Xu, and Y. Ying, “Near infrared spectroscopy for on/in-line monitoring of quality in foods and beverages: A review,” *J. Food Eng.*, vol. 87, pp. 303–313, 2008.

[19] J. Workman, K. E. Creasy, S. Doherty, L. Bond, M. Koch, A. Ullman, and D. J. Veltkamp, “Process Analytical Chemistry,” *Anal. Chem.*, vol. 73, no. 12, pp. 2705–2718, 2001.

[20] T. Layloff, “An overview of process analytical technology in the pharmaceutical industry,” *Am. Pharm. Rev.*, vol. 7, pp. 30–34, 2004.

[21] S. Banerjee and N. Bhatwadekar, “Process Analytical Technology (PAT) : Boon to Pharmaceutical Industry,” *Pharm. Inf.*, vol. 6, no. 6, pp. 238–247, 2008.

[22] J. Munson, C. F. Stanfield, and B. Gujral, “A review of Process Analytical Technology (PAT) in the U.S. Pharmaceutical Industry,” *Curr. Pharm. Anal.*, vol. 2, no. 4, pp. 405–414, 2006.

[23] B. Scott and A. Wilcock, “Process analytical technology in the pharmaceutical industry: a toolkit for continuous improvement,” *PDA J Pharm Sci Technol.*, vol. 60, no. 1, pp. 17–53, 2006.

[24] B. Scott and A. Wilcock, “Process analytical technology in the pharmaceutical industry: a toolkit for continuous improvement.,” *PDA J. Pharm. Sci. Technol.*, vol. 60, no. 1, pp. 17–53, 2006.

[25] V. Saravana Kumar and P. Shanmugasundaram, “Process analytical technology implementation progression for a pharmaceutical industry,” *Int. J. Pharma Bio Sci.*, vol. 5, no. 2, 2014.

[26] W. Kasten, “Neue Entwicklungen auf dem Gebiet der Inline-Prozessanalysentechnik,” *ATP edition*, pp. 58–68, 2008.

[27] H. Wu and M. Khan, “THz spectroscopy: An emerging technology for pharmaceutical development and pharmaceutical Process Analytical Technology (PAT) applications,” *Journal of Molecular Structure*, vol. 1020. pp. 112–120, 2012.

[28] J. Märk, M. Andre, M. Karner, and C. W. Huck, “Prospects for multivariate classification of a pharmaceutical intermediate with near-infrared spectroscopy as a process analytical technology (PAT) production control supplement,” *Eur. J. Pharm. Biopharm.*, vol. 76, no. 2, pp. 320–327, 2010.

[29] S. P. Mulvaney and C. D. Keating, “Raman spectroscopy.,” *Anal. Chem.*, vol. 72, no. 12, p. 145R–157R, 2000.

[30] T. R. M. De Beer, W. R. G. Baeyens, J. Ouyang, C. Vervaet, and J. P. Remon, “Raman spectroscopy as a process analytical technology tool for the understanding and the quantitative in-line monitoring of the homogenization process of a pharmaceutical suspension.,” *Analyst*, vol. 131, no. 10, pp. 1137–1144, 2006.

[31] T. R. M. De Beer, W. R. G. Baeyens, a. Vermeire, D. Broes, J. P. Remon, and C. Vervaet, “Raman spectroscopic method for the determination of medroxyprogesterone acetate in a pharmaceutical suspension: validation of quantifying abilities, uncertainty assessment and comparison with the high performance liquid chromatography reference method,” *Anal. Chim. Acta*, vol. 589, no. 2, pp. 192–199, 2007.

[32] T. R. M. De Beer, C. Bodson, B. Dejaegher, B. Walczak, P. Vercruysse, A. Burggraeve, A. Lemos, L. Delattre, Y. Vander Heyden, J. P. Remon, C. Vervaet, and W. R. G. Baeyens, “Raman spectroscopy as a process analytical technology (PAT) tool for the in-line monitoring and understanding of a powder blending process,” *J. Pharm. Biomed. Anal.*, vol. 48, no. 3, pp. 772–779, 2008.

[33] T. R. M. DE BEER, P. VERCRUYSSE, A. BURGGRAEVE, T. QUINTEN, J. OUYANG, X. ZHANG, C. VERVAET, J. P. REMON, and W. R. G. BAEYENS, “In-Line and Real-Time Process Monitoring of a Freeze Drying Process Using Raman and NIR Spectroscopy as Complementary Process Analytical Technology (PAT) Tools,” *J. Pharm. Sci.*, vol. 98, no. 9, pp. 3430–3446, 2009.

[34] A. S. El-Hagrasy, M. Delgado-Lopez, and J. K. Drennen, “A process analytical technology approach to near-infrared process control of pharmaceutical powder blending: Part II: Qualitative near-infrared models for prediction of blend homogeneity,” *J. Pharm. Sci.*, vol. 95, no. 2, pp. 407–421, 2006.

[35] A. S. El-Hagrasy, F. D'Amico, and J. K. Drennen, "A process analytical technology approach to near-infrared process control of pharmaceutical powder blending. Part I: D-optimal design for characterization of powder mixing and preliminary spectral data evaluation," *J. Pharm. Sci.*, vol. 95, no. 2, pp. 392–406, 2006.

[36] A. S. El-Hagrasy and J. K. Drennen, "A process analytical technology approach to near-infrared process control of pharmaceutical powder blending. Part III: Quantitative near-infrared calibration for prediction of blend homogeneity and characterization of powder mixing kinetics," *J. Pharm. Sci.*, vol. 95, no. 2, pp. 422–434, 2006.

[37] A. S. El Hagrasy, S. Y. Chang, D. Desal, and S. Kiang, "Raman spectroscopy for the determination of coating uniformity of tablets: Assessment of product quality and coating pan mixing efficiency during scale-up," *J. Pharm. Innov.*, vol. 1, no. 1, pp. 37–42, 2006.

[38] G. Fini, "Applications of Raman spectroscopy to gemology," *J. RAMAN Spectrosc.*, vol. 35, pp. 335–337, 2004.

[39] T. Vankeirsbilck, a. Vercauteren, W. Baeyens, G. Van der Weken, F. Verpoort, G. Vergote, and J. P. Remon, "Applications of Raman spectroscopy in pharmaceutical analysis," *TrAC - Trends Anal. Chem.*, vol. 21, no. 12, pp. 869–877, 2002.

[40] G. J. Vergote, T. R. M. De Beer, C. Vervaet, J. P. Remon, W. R. G. Baeyens, N. Diericx, and F. Verpoort, "In-line monitoring of a pharmaceutical blending process using FT-Raman spectroscopy," *Eur. J. Pharm. Sci.*, vol. 21, no. 4, pp. 479–485, 2004.

[41] G. M. Walker, S. E. J. Bell, K. Greene, D. S. Jones, and G. P. Andrews, "Characterisation of fluidised bed granulation processes using in-situ Raman spectroscopy," *Chem. Eng. Sci.*, vol. 64, no. 1, pp. 91–98, 2009.

[42] P. L. D. Wildfong, A. S. Samy, J. Corfa, G. E. Peck, and K. R. Morris, “Accelerated fluid bed drying using NIR monitoring and phenomenological modeling: Method assessment and formulation suitability,” *J. Pharm. Sci.*, vol. 91, no. 3, pp. 631–639, 2002.

[43] D. S. Hausman, R. T. Cambron, and A. Sakr, “Application of Raman spectroscopy for on-line monitoring of low dose blend uniformity,” *Int. J. Pharm.*, vol. 298, no. 1, pp. 80–90, 2005.

[44] R. L. Green, G. Thurau, N. C. Pixley, A. Mateos, R. a. Reed, and J. P. Higgins, “In-line monitoring of moisture content in fluid bed dryers using near-IR spectroscopy with consideration of sampling effects on method accuracy,” *Anal. Chem.*, vol. 77, no. 14, pp. 4515–4522, 2005.

[45] J. Rantanen, H. Wikström, R. Turner, and L. S. Taylor, “Use of in-line near-infrared spectroscopy in combination with chemometrics for improved understanding of pharmaceutical processes,” *Anal. Chem.*, vol. 77, no. 2, pp. 556–563, 2005.

[46] J. Rantanen, “Process analytical applications of Raman spectroscopy.,” *J. Pharm. Pharmacol.*, vol. 59, no. 2, pp. 171–177, 2007.

[47] J. Rantanen, O. Antikainen, J. P. Mannermaa, and J. Yliruusi, “Use of the near-infrared reflectance method for measurement of moisture content during granulation.,” *Pharm. Dev. Technol.*, vol. 5, no. 2, pp. 209–217, 2000.

[48] J. Rantanen, S. Lehtola, P. Rämet, J.-P. Mannermaa, and J. Yliruusi, “On-line monitoring of moisture content in an instrumented fluidized bed granulator with a multi-channel NIR moisture sensor,” *Powder Technol.*, vol. 99, pp. 163–170, 1998.

[49] J. Rantanen, E. Räsänen, J. Tenhunen, M. Känsäkoski, J. P. Mannermaa, and J. Yliruusi, “In-line moisture measurement during granulation with a four-wavelength near infrared sensor: An evaluation of particle size and binder effects,” *Eur. J. Pharm. Biopharm.*, vol. 50, no. 2, pp. 271–276, 2000.

[50] A. C. Olivieri, N. M. Faber, J. Ferré, and R. Boqué…, “Uncertainty estimation and figures of merit for multivariate calibration (IUPAC Technical Report),” *Pure Appl. …*, 2006.

[51] A. C. Olivieri, N. K. M. Faber, J. Ferre, R. Boque, J. H. Kalivas, and H. Mark, “Uncertainty estimation and figures of merit for multivariate calibration,” *Pure Appl. Chem.*, vol. 78, no. 3, pp. 633–661, 2006.

[52] S. J. Doherty and A. J. Lange, “Avoiding pitfalls with chemometrics and PAT in the pharmaceutical and biotech industries,” *TrAC - Trends Anal. Chem.*, vol. 25, no. 11, pp. 1097–1102, 2006.

[53] S. Wold, J. Cheney, N. Kettaneh, and C. McCready, “The chemometric analysis of point and dynamic data in pharmaceutical and biotech production (PAT) - some objectives and approaches,” *Chemom. Intell. Lab. Syst.*, vol. 84, no. 1–2, pp. 159–163, 2006.

[54] P. Schulze, M. Ludwig, F. Kohler, and D. Belder, “Deep UV laser-induced fluorescence detection of unlabeled drugs and proteins in microchip electrophoresis,” *Anal. Chem.*, vol. 77, no. 5, pp. 1325–1329, 2005.

[55] J. Ruzicka, “The second coming of flow-injection analysis,” *Anal. Chim. Acta*, vol. 261, no. 1–2, pp. 3–10, 1992.

[56] J. Ruzicka and G. D. Marshall, “Sequential injection: a new concept for chemical sensors, process analysis and laboratory assays,” *Anal. Chim. Acta*, vol. 237, pp. 329–343, 1990.

[57] N. Piehl, M. Ludwig, and D. Belder, “Subsecond chiral separations on a microchip,” *Electrophoresis*, vol. 25, no. 21–22, pp. 3848–3852, 2004.

[58] D. Belder and M. Ludwig, “Surface modification in microchip electrophoresis,” *Electrophoresis*, vol. 24, no. 21, pp. 3595–3606, 2003.

[59] A. Nordon, C. A. McGill, and D. Littlejohn, “Process NMR spectrometry,” *Analyst*, vol. 126, no. 2, pp. 260–272, 2001.

[60] VDI/VDE-Gesellschaft Mess- und Automatisierungstechnik and Namur, “Prozess-Sensoren 2015+,” 2009.

[61] U. Panne, “Spectrochemical analysis with lasers,” *Anal. Bioanal. Chem.*, vol. 372, no. 1, pp. 23–24, 2002.

[62] H. Fink, U. Panne, and R. Niessner, “Process analysis of recycled thermoplasts from consumer electronics by laser-induced plasma spectroscopy,” *Anal. Chem.*, vol. 74, no. 17, pp. 4334–4342, 2002.

[63] K. Lahtonen, M. Lampimäki, P. Jussila, M. Hirsimäki, and M. Valden, “Instrumentation and analytical methods of an x-ray photoelectron spectroscopy-scanning tunneling microscopy surface analysis system for studying nanostructured materials,” *Rev. Sci. Instrum.*, vol. 77, no. 8, 2006.

[64] C. B. Boss and K. J. Fredeen, *Concepts, Instrumentation and Techniques in Inductively Coupled Plasma Optical Emission Spectrometry*, 2nd Editio. Perkin Elmer, 1997.

[65] D. C. Harris, *Lehrbuch der Quantitativen Analyse*, 8th ed. Springer Spektrum, 2014.

[66] D. A. Skoog, F. J. Holler, and S. R. Crouch, *Instrumentelle Analytik: Grundlagen - Geräte - Anwendungen*, 6th ed. Springer Spektrum, 2013.

[67] J. Hallbach, *Klinische Chemie und Hämatologie für den Einstieg*. Thieme Georg, 2006.

[68] N. Lewen, “The use of atomic spectroscopy in the pharmaceutical industry for the determination of trace elements in pharmaceuticals,” *J. Pharm. Biomed. Anal.*, vol. 55, pp. 653–661, 2011.

[69] M. Aceto, O. Abollino, and M. C. Bruzzoniti, “a review Determination of metals in wine with atomic spectroscopy (¯ ame-AAS , GF-AAS and ICP-AES); a review,” vol. 19, no. January 2014, pp. 37–41, 2010.

[70] M. Carl, C. Vastel, T. Guerin, and L. Noel, “Determination of sodium , potassium , calcium and magnesium content in milk products by flame atomic absorption spectrometry (FAAS): A joint ISO / IDF collaborative study,” *Int. Dairy J.*, vol. 18, pp. 899–904, 2008.

[71] G. N. Havre, “The flame photometric determination of sodium, potassium and calcium in plant extract with special reference to interference effects,” *Anal. Chim. Acta*, vol. 25, pp. 557–566, 1961.

[72] C. V. S. Ieggli, D. Bohrer, P. C. Nascimento, and L. M. De Carvalho, “Determination of sodium , potassium , calcium , magnesium , zinc and iron in emulsified chocolate samples by flame atomic absorption spectrometry,” *Food Chem.*, vol. 124, no. 3, pp. 1189–1193, 2011.

[73] T. Guo, J. Baasner, and S. McIntosh, “Determination of highly concentrated Na, K, Mg and Ca in dialysis solution with flow injection on-line dilution and flame atomic absorption spectrometry,” *Anal. Chim. Acta*, vol. 331, no. 3, pp. 263–270, 1996.

[74] J. R. Lakowicz, *Principles of fluorescence spectroscopy*. Boston, MA, 2006.

[75] J. D. WINEFORDNER and T. J. VICKERS, “Atomic Fluorescence Spectrometry as a Means of Chemical Analysis,” *Anal. Chem.*, vol. 36, no. 1, pp. 161–165, 1964.

[76] J. D. WINEFORDNER and R. C. ELSER, “Atomic fluorescence spectrometry.,” *Anal. Chem.*, vol. 43, no. 4, pp. 24–42, 1971.

[77] D. Beauchemin, “Inductively coupled plasma mass spectrometry,” *Anal. Chem.*, vol. 80, no. 12, pp. 4455–4486, 2008.

[78] G. Jenner, H. Longerich, S. Jackson, and B. Fryer, “ICP-MS — A powerful tool for high-precision trace-element analysis in Earth sciences: Evidence from analysis of selected U.S.G.S. reference samples,” *Chem. Geol.*, vol. 83, no. 1–2, pp. 133–148, 1990.

[79] F. Vanhaecke, H. Vanhoe, and R. Dams, “The use of internal stanards in ICP-MS,” *Talanta*, vol. 39, no. 7, pp. 737–742, 1992.

[80] H. P. Longerich, “Effect of Nitric Acid , Acetic Acid and Ethanol on Inductively Coupled Plasma Mass Spectrometric Ion Signals as a Function of Nebuliser Gas Flow , With Implications on Matrix Suppression and Enhancements,” *J. Anal. At. Spectrom.*, vol. 4, pp. 665–667, 1989.

[81] S. N. Willie, J. W. H. Lam, L. Yang, and G. Tao, “On-line removal of Ca, Na and Mg from iminodiacetate resin for the determination of trace elements in seawater and fish otoliths by flow injection ICP-MS,” *Anal. Chim. Acta*, vol. 447, no. 1–2, pp. 143–152, 2001.

[82] X. Hou and B. T. Jones, “Inductively Coupled Plasma / Optical Emission Spectrometry,” *Encyclopedia of Analytical Chemistry*. John Wiley & Sons Ltd., pp. 9468–9485, 2000.

[83] S. Greenfield, I. L. Jones, and C. T. Berry, “High-pressure plasmas as spectroscopic emission sources,” *Analyst*, vol. 89, no. 11, pp. 713–720, 1964.

[84] R. Wendt and V. Fassel, “Induction Coupled Plasma Spectrometric Excitation Source,” *Anal. Chem.*, vol. 37, no. 7, pp. 920–922, 1965.

[85] W. Schuhknecht and H. Schinkel, “Beitrag zur Deutung von Verdampfungs-, Zersetzungs- und Anregungsvorgängen in Flammen,” *Fresenius’ Zeitschrift für Anal. Chemie*, vol. 162, no. 4, pp. 266–279, 1958.

[86] H. F. Priest and A. V. Grosse, “Hydrogen-Fluorine Torch,” *Ind. Eng. Chem.*, vol. 39, no. 3, pp. 431–434, 1947.

[87] A. L. Gray, “The ICP as an ion source—origins, achievements and prospects,” *Spectrochim. Acta*, vol. 40, no. 10–12, pp. 1525–1537, 1985.

[88] C. Dubuisson, E. Poussel, and J. M. Mermet, “Comparison of ionic line-based internal standardization with axially and radially viewed inductively coupled plasma atomic emission spectrometry to compensate for sodium e ff ects on accuracy,” *J. Anal. At. Spectrom.*, vol. 13, pp. 1265–1269, 1998.

[89] M. Chausseau, E. Poussel, and J. M. Mermet, “Self-absorption effects in radially and axially viewed inductively coupled plasma-atomic emission spectrometry--the key role of the operating conditions.,” *Fresenius J. Anal. Chem.*, vol. 370, no. 4, pp. 341–347, 2001.

[90] J. C. J. Silva, N. Baccan, and J. a Nóbrega, “Article Analytical Performance of an Inductively Coupled Plasma Optical Emission Spectrometry with Dual View Configuration,” *J. Braz. Chem. Soc.*, vol. 14, no. 2, pp. 310–315, 2003.

[91] Spectro Analytical Instrument GmbH, “Spectro MS,” 2012.

[92] Spectro Analytical Instrument GmbH, “Spectro Arcos,” 2011.

[93] F. C. Bressy, G. B. Brito, I. S. Barbosa, L. S. G. Teixeira, M. Graças, and A. Korn, “Determination of trace element concentrations in tomato samples at different stages of maturation by ICP OES and ICP-MS following microwave-assisted digestion,” *Microchem. J.*, vol. 109, pp. 145–149, 2013.

[94] M. Krachler, S. Van Winckel, M. Cardinale, B. Lynch, and T. Murakami, “Method development for the determination of alkali metals in samples from pyrochemical reprocessing using ICP-OES and comparison with sector field ICP-MS,” *Microchem. J.*, vol. 105, pp. 9–14, 2012.

[95] D. J. Butcher, “Advances in Inductively Coupled Plasma Optical Emission Spectrometry for Environmental Analysis,” *Instrum. Sci. Technol.*, vol. 38, no. 6, pp. 458–469, 2010.

[96] M. F. Zaranyika, A. T. Chirenje, and C. Mahamadi, “Interference Effects from Easily Ionizable Elements in Flame AES and ICP-OES: A Proposed Simplified Rate Model Based on Collisional Charge Transfer Between Analyte and Interferent Species,” *Spectrosc. Lett.*, vol. 40, no. 6, pp. 835–850, 2007.

[97] K. O’Hanlon, L. Ebdon, and M. Foulkes, “Effect of easily ionizable elements on solutions and slurries in an axially viewed inductively coupled plasma,” *J. Anal. At. Spectrom.*, vol. 11, no. 6, pp. 427–436, 1996.

[98] I. D. Holclajtner-Antunovic and M. R. Tripkovic, “Study of the matrix effect of easily and non-easily ionizable elements in inductively coupled argon plasma. Part 2. Equilibrium plasma composition,” *J. Anal. At. Spectrom.*, vol. 8, no. 2, pp. 349–357, 1993.

[99] G. A. Zachariadis and P. C. Sarafidou, “Internal standardization with yttrium spectral lines using axial-viewing inductively coupled plasma atomic emission spectrometry for plant certified reference materials analysis,” *Microchim Acta*, vol. 166, pp. 77–81, 2009.

[100] G. Knapp, B. Maichin, and U. Baumgartner, “Interferences in ICP-OES by Organic Residue after microwave-assisted sample digestion,” *At. Spectrosc.*, vol. 19, no. 6, pp. 220–222, 1998.

[101] R. I. Mccrindle and C. J. Rademeyer, “Excitation temperature and analytical parameters for an ethanol-loaded Inductively Coupled Plasma Atomic Emission Spectrometer,” *J. Anal. At. Spectrom.*, vol. 10, pp. 399–404, 1995.

[102] C. Pan, G. Zhut, and R. F. Browner, “Comparison of Desolvation Effects With Aqueous and Organic (Carbon Tetrachloride) Sample Introduction for Inductively Coupled Plasma Atomic Emission Spectrometry,” *J. Anal. At. Spectrom.*, vol. 5, pp. 537–542, 1990.

[103] A. W. Boorn and R. F. Browner, “Effects of Organic Solvents in Inductively Coupled Plasma Atomic Emission Spectrometry,” *Anal. Chem.*, vol. 54, no. 8, pp. 1402–1410, 1982.

[104] G. Kreuning and F. J. M. J. Maessen, “Effects of the solvent plasma load of various solvents on the excitation conditions in medium power inductively coupled plasmas,” *Spectrochim. Acta Part B At. Spectrosc.*, vol. 44, no. 4, pp. 367–384, 1989.

[105] B. L. Caughlin and M. W. BLADE, “Excitation temperature and electron density in the inductively coupled vs organic solvent introduction coupled plasma optical emission spectrometry (ICP-OES) has been extensively applied to the analysis of trace elements in organic samples . These appli,” *Spectrochim. Acta*, vol. 4, no. 4, pp. 579–591, 1985.

[106] J. Xu, H. Kawaguchi, and A. Mizuike, “Effects of organic inductively-coupled acids and solvents in plasma emission spectrometry,” *Anal. Chim. Acta*, vol. 152, pp. 133–139, 1983.

[107] T. D. Hettipathirana, A. P. Wade, and M. W. Blades, “Effects of organic acids in low power inductively coupled argon plasma-optical emission spectroscopy,” *Spectrochim. Acta*, vol. 45, no. 3, pp. 271–280, 1990.

[108] E. Yoshimura, H. Suzuki, S. Yamazaki, and S. Toda, “Interference by Mineral Acids in Inductively Coupled Plasma Atomic Emission Spectrometry,” *Analyst*, vol. 115, pp. 167–171, 1990.

[109] R. H. Scott, V. a. Fassel, R. N. Kniseley, and D. E. Nixon, “Inductively coupled plasma-optical emission analytical spectrometry,” *Anal. Chem.*, vol. 46, no. 1, pp. 75–80, 1974.

[110] W. B. Barnett, “Theoretical principles of internal standardization in analytical emission spectroscopy *,” *Sectrochimica Acta*, vol. 23, pp. 643–664, 1968.

[111] W. B. Barnett, V. A. Fassel, and R. N. Kniseley, “An experimental study of internal standardization in analytical emission spectroscopy *,” *Spectrochim. Acta*, vol. 25, pp. 139–161, 1970.

[112] S. A. Myers and D. H. Tracy, “Improved performance using internal standardization in inductively- coupled plasma emission spectroscopy,” *Spectrochim. Acta*, vol. 38, no. 9, pp. 1227–1253, 1983.

[113] M. Thompson and M. H. Ramsey, “Matrix effects due to calcium in inductively coupled plasma atomic-emission spectrometry: their nature, source and remedy,” *Analyst*, vol. 110, no. 12, pp. 1413–1422, 1985.

[114] J. Farino, J. R. Miller, D. D. Smith, and R. F. Browner, “Influence of solution uptake rate on signals and interferences in inductively coupled plasma optical emission spectrometry,” *Anal. Chem.*, vol. 59, no. 18, pp. 2303–2309, 1987.

[115] J. C. Ivaldl and J. F. Tyson, “Performance evaluation of an axially viewed horizontal inductively coupled plasma for optical emission spectrometry,” *Spectrochim. Acta*, vol. 50, pp. 1207–1226, 1995.

[116] Y. Morishige and A. Kimura, “Ionization interference in inductively coupled plasma-optical emission spectroscopy,” *Ind. Mater.*, no. 66, pp. 106–111, 2008.

[117] A. Väisänen and A. Ilander, “Optimization of operating conditions of axially and radially viewed plasmas for the determination of trace element concentrations from ultrasound-assisted digests of soil samples contaminated by lead pellets,” *Anal. Chim. Acta*, vol. 570, no. 1, pp. 93–100, 2006.

[118] Food and Drug Administration (FDA), “Validation of a analytical Procedures : text and methodology Q2(R1),” *ICH Guidel.*, pp. 1–17, 2005.

[119] E. H. Hansen, “Flow injection analyses: Part I. A new concept of fast continuous flow analysis,” *Anal. Chim. Acta*, vol. 78, pp. 145–157, 1975.

[120] E. D. for the Q. of M. & H. (EDQM), “Haemodialysis, Solutions for Solutiones ad haemodialysem Concentrated solutions for haemodialysis,” in *European Pharmacopoeia*, 8.0 ed., 2013, pp. 2376–2378.

[121] E. D. for the Q. of M. & H. (EDQM), “Solutiones ad haemocolaturam haemodiacolaturamque,” in *European Pharmacopoeia*, 8.0 ed., 2013, pp. 2378–2381.

[122] E. D. for the Q. of M. & H. (EDQM), “Solutiones ad peritonealem dialysem,” in *European Pharmacopoeia*, 8.0 ed., 2013, pp. 2994–2996.

[123] G. M. Neumann, “AAS-Bestimmung von Natrium und Kalium in den hochschmelzenden Metallen Wolfram und Molybdän,” *Talanta*, vol. 18, no. 10, pp. 1047–1051, 1971.

[124] J. W. Robinson, “Determination of sodium by atomic absorption spectroscopy,” *Anal. Chim. Acta*, vol. 23, pp. 458–461, 1960.

[125] C. V. S. Ieggli, D. Bohrer, P. C. Nascimento, L. M. De Carvalho, and S. C. Garcia, “Determination of sodium , potassium , calcium , magnesium , zinc , and iron in emulsified egg samples by flame atomic absorption spectrometry,” *Talanta*, vol. 80, pp. 1282–1286, 2010.

[126] W. S. G. . Macphee and D. F. Ball, “Routine determination of calcium and magnesium in soil extracts by atomic absorption spectrophotometry,” *J. Sci. Food Agric.*, vol. 18, no. 8, pp. 376–380, 1967.

[127] I. Rubeska and B. Molden, “The mechanisms of interference effects and their elimination in the determination of alkaline earth metals by flame photometry,” *Anal. Chim. Acta*, vol. 37, pp. 421–428, 1967.

[128] M. G. Woldring, “Flame photometric determination of sodium and potassium in some biological fluids,” *Anal. Chim. Acta*, vol. 8, pp. 150–167, 1953.

[129] A. C. Schneider, “Potentiometrische Bestimmung von Einzelionenaktivitätskoeffizienten wässriger Elektrolyte mit Hilfe ionenselektiver Elektroden,” Universität Duisburg-Essen, 2005.

[130] P. Flevet, A. Truchaud, J. Hersant, and G. Glikmanas, “Response of Ion-Selective Sodium and Potassium Electrodes in the Beckman Astra 4 and Astra 8 Analyzers Parallel Evaluation of Astra 8 and Astra 4 Multichannel Analyzers in Two Hospital Laboratories,” *Clin. Chem.*, vol. 26, no. 1, pp. 138–139, 1980.

[131] R. A. Durst, “Automated analyzer for the determination of potassium and sodium in whole blood,” *Clin. Chim. Acta*, vol. 80, no. 1, pp. 225–234, 1977.

[132] J. a Lustgarten, R. E. Wenk, C. Byrd, and B. Hall, “Evaluation of an automated selective-ion electrolyte analyzer for measuring Na+, K+, and Cl- in serum.,” *Clin. Chem.*, vol. 20, no. 9, pp. 1217–1221, 1974.

[133] G. B. Levy, “Determination of Sodium with Ion-Selective Electrodes,” *Clin. Chem.*, vol. 27, no. 8, pp. 1435–1438, 1981.

[134] E. Rabe, “Zur Natrium- und Kaliumbestimmung mit ionensensitiven Elektroden,” *Leb. Untersuchung und -forsch.*, vol. 176, pp. 270–274, 1983.

[135] F. Gilmer, “Der Nährstofftransport im Fernleitungssystem des Xylem und dessen Beeinflussung durch Transpiration bei Ricinus und Pappel Ruprecht-Karls-Universität Heidelberg,” Ruprecht-Karls-Universität Heidelberg, 2004.

[136] J. Saurina, E. López-aviles, A. Le Moal, and S. Hernández-cassou, “Determination of calcium and total hardness in natural waters using a potentiometric sensor array,” *Anal. Chim. Acta*, vol. 464, no. 1, pp. 89–98, 2002.

[137] G. N. Bowers, C. Brassard, and S. F. Sena, “Measurement of Ionized Calcium in Serum with Ion-Selective Electrodes : A Mature Technology That Can Meet the Daily Service Needs,” *Clin. Chem.*, vol. 32, no. 8, pp. 1437–1447, 1986.

[138] Metrohm, “Potentiometrische Titration von Calcium (Magnesium) in Milchprodukten,” *Appl. Bull.*, vol. 125/2 d, no. 235, pp. 1–4.

[139] Metrohm, “Thermometric titration of sodium , aluminum and fluorine,” *Metrohm information*, pp. 23–25, 2008.

[140] Metrohm, “Determination of sodium in margarine manufacture,” *Titration Application Note H–124*. .

[141] L. Stäudel and A. S. H. Wöhrmann, “Thermometrische Titrationen von Alkalimetall- und Ammoniumionen mit Natriumtetraphenylborat (Kalignost),” *GIT Fachz. Lab.*, vol. 23, pp. 291–293, 1979.

[142] Metrohm, “Simultaneous determination of calcium and magnesium in water samples and beverages and the different types of water hardness by complexometric titration with potentiometric indication,” *Appl. Bull.*, no. 125/2 e, pp. 1–5.

[143] C. M. Pereira, C. A. Neiverth, S. Maeda, M. Em, and E. D. E. Solo, “Complexometric titration with potenciometric indicator to determination of calcium and magnesium in soil extracts,” vol. 35, pp. 1331–1336, 2011.

[144] F. Ingman and A. Ringbom, “Spectrophotometric Determination of Small Amounts of Magnesium and Calcium Employing Calmagite,” *Microchem. J.*, vol. 10, pp. 545–553, 1966.

[145] E. Gomez, J. M. Estela, and V. Cerda, “Simultaneous spectrophotometric determination of calcium and magnesium in water,” *Anal. Chim. Acta*, vol. 249, pp. 513–518, 1991.

[146] J. A. C. Broekaert, “Einsatz der ICP_Atomspektroskopie in der Wasseranalytik.pdf,” *Technisches Messen*, vol. 59, no. 4, pp. 147–153, 1992.

[147] L. A. Simpson, R. Hearn, S. Merson, and T. Catterick, “A comparison of double-focusing sector field ICP-MS , ICP-OES and octopole collision cell ICP-MS for the high-accuracy determination of calcium in human serum,” *Talanta*, vol. 65, pp. 900–906, 2005.

[148] A. R. A. Nogueira, S. M. B. Brienza, E. A. G. Zagatto, L. F. C. Lima, and A. N. Arau, “Flow Injection System with Multisite Detection for Spectrophotometric Determination of Calcium and Magnesium in Soil Extracts and Natural Waters,” *J. Agric. Food Chem.*, vol. 44, no. 1, pp. 165–169, 1996.

[149] Z. Chen and M. A. Adams, “A metallic cobalt electrode for the indirect potentiometric determination of calcium and magnesium in natural waters using flow injection analysis,” *Talanta*, vol. 47, no. 3, pp. 779–786, 1998.

[150] N. A. Chaniotakis, J. K. Tsagatakis, E. A. Moschou, S. J. West, and X. Wen, “Magnesium ion-selective electrode : optimization and ¯ ow injection analysis application,” *Anal. Chim. Acta*, vol. 356, no. 1, pp. 105–111, 1997.

[151] H. Wada, T. Ozawa, G. Nakagawa, and Y. Asano, “Preparation and examination of calcium ion-selective electrodes for flow analysis,” *Anal. Chim. Acta*, vol. 211, pp. 213–221, 1988.

[152] E. H. HANSEN, J. RfizICKA, and A. K. GHOSE, “Flow injection analysis for calcium in serum, water and waste waters by spectrophotometry and by ion-selective electrode,” *Anal. Chim. Acta*, vol. 100, pp. 151–165, 1978.

[153] W. D. Basson and J. F. Van Staden, “Simultaneous Determination of Sodium, Potassium, Magnesium and Calcium in Surface, Ground and Domestic Water by Flow-Injection Analysis,” *Fresenius Z. Anal. Chem.*, vol. 374, pp. 370–374, 1980.

[154] Â. L. F. C. Lima, B. F. Reis, R. C. C. Costa, and A. N. Arau, “Sequential injection system in flame atomic absorption spectrometry for the determination of calcium and magnesium in mineral waters,” *Anal. Chim. Acta*, vol. 358, pp. 111–119, 1998.

[155] Z. Arslan and J. F. Tyson, “Determination of calcium , magnesium and strontium in soils by flow injection flame atomic absorption spectrometry,” *Talanta*, vol. 50, pp. 929–937, 1999.

[156] P. Vinas, N. Campillo, I. L. Garcia, and M. H. Cordoba, “Flow-injection flame atomic absorption spectrometry for slurry atomization . Determination of calcium , magnesium , iron , zinc and manganese in vegetables,” *Anal. Chim. Acta*, vol. 283, pp. 393–400, 1993.

[157] J. Nyman and A. Ivaska, “Spectrophotometric determination of calcium in paper machine white water by sequential injection analysis,” *Anal. Chim. Acta*, vol. 308, pp. 286–292, 1995.

[158] J. Junsomboon and J. Jakmunee, “Determination of Potassium, Sodium and Total Alkalies in Portland Cement, Fly Ash, Admixtures , and Water of Concrete by a Simple Flow Injection Flame Photometric System,” *J. Autom. Methods Manag. Chem.*, vol. 2011, pp. 1–9, 2011.

[159] Z. Spacil, J. Folbrova, N. Megoulas, P. Solich, and M. Koupparis, “Simultaneous liquid chromatographic determination of metals and organic compounds in pharmaceutical and food-supplement formulations using evaporative light scattering detection,” *Anal. Chim. Acta*, vol. 583, pp. 239–245, 2007.

[160] B. Paull, M. Macka, and P. R. Haddad, “Determination of calcium and magnesium in water samples by high-performance liquid chromatography on a graphitic stationary phase with a mobile phase containing o -cresolphthalein complexone,” *J. Chromatogr.*, vol. 789, pp. 329–337, 1997.

[161] M. A. Koupparis, E. P. Diamandis, and H. V Malmstadt, “Total Calcium and Magnesium Determined in Serum with an Automated Stopped-Flow Analyzer,” *Clin. Chem.*, vol. 28, no. 10, pp. 2149–2152, 1982.

[162] K. Cammann and H. Galste, *Das Arbeiten mit ionenselektiven Elektroden: Eine Einführung für Praktiker*, 3rd editio. Springer-Verlag Berlin Heidelberg, 1996.

[163] A. Ringbom, *Complexation in Analytical chemistry*. John Wiley & Sons Inc, 1963.

[164] A. Fink, “Die Verwendung alkoholischer Lösungen bei der flammenphotometrischen Analyse,” *Microchim. Acta*, vol. 43, no. 2, pp. 314–328, 1955.

[165] Glass expansion, “Internal standardization for ICP OES and ICP MS,” *Glass expansion newsletter*, pp. 1–7, 2006.

[166] I. Kuselman and I. Schumacher, “Long-term stability study of drug products and out-of-specification test results,” *Accred Qual Assur*, vol. 16, pp. 615–622, 2011.

[167] S. Bajaj, D. Singla, and N. Sakhuja, “Stability Testing of Pharmaceutical Products,” *J. Appl. Pharm. Sci.*, vol. 02, no. 03, pp. 129–138, 2012.

[168] B. Kommanaboyina and C. T. Rhodes, “Trends in Stability Testing , with Emphasis on Stability During Distribution and Storage,” *Drug Dev. Ind. Pharm.*, vol. 25, no. 7, pp. 857–868, 1999.

[169] H. Egsgaard and E. Larsen, “Long-term stability of a gas chromatography/mass spectrometry system in quantitative gas analysis,” *Anal. Chim. Acta*, vol. 199, pp. 265–270, 1987.

[170] G. G. Guilbault and M. Hjelm, “Nomenclature for automated and mechanised analysis,” *Pure Appl. Chem.*, vol. 61, no. 9, pp. 1657–1664, 1989.

[171] C. Dubuisson, E. Poussel, J. Mermet, and J. L. Todoli, “Comparison of the effect of acetic acid with axially and radially viewed inductively coupled plasma atomic emission spectrometry : influence of the operating conditions,” *J. Anal. At. Spectrom.*, vol. 13, pp. 63–67, 1998.

[172] B. C. W. Davies, “The Extent of Dissociation of Salts in Water. Part VI. Some Calcium Salts of Organic Acids.,” *J. Chem. Soc.*, pp. 277–281, 1938.

[173] M. Hoenig, “Preparation steps in environmental trace element analysis - Facts and traps,” *Talanta*, vol. 54, pp. 1021–1038, 2001.

[174] M. Hoenig and A. M. De Kersabiec, “Sample preparation steps for analysis by atomic spectroscopy methods: Present status,” *Spectrochim. Acta - Part B At. Spectrosc.*, vol. 51, pp. 1297–1307, 1996.

[175] B. E. Richter, B. a Jones, J. L. Ezzell, and N. L. Porter, “Accelerated Solvent Extraction : A Technique for Sample Preparation,” *Anal. Chem.*, vol. 68, no. 6, pp. 1033–1039, 1996.

[176] I. Kubrakova, “Microwave-assisted sample preparation and preconcentration for ETAAS,” *Spectrochim. Acta Part B At. Spectrosc.*, vol. 52, pp. 1469–1481, 1997.

[177] M. A. Innis, D. H. Gelfand, J. J. Sninsky, and T. J. White, *PCR protocols — A guide to methods and applications*. Academic Press, 1990.

[178] P. S. MANN, *INTRODUCTORY STATISTICS*, Seventh Ed. JOHN WILEY & SONS, INC., 2010.

[179] Metrohm, *807 Dosing Unit*. 2011.

[180] R. H. Scott, V. a. Fassel, R. N. Kniseley, and D. E. Nixon, “Inductively coupled plasma-optical emission analytical spectrometry,” *Anal. Chem.*, vol. 46, no. 1, pp. 75–80, 1974.

[181] K. M. Monzambe, H. P. Naveau, E. J. Nyns, N. Bogaert, and H. B. Hler, “Problematics and stability of on-line pH measurements in anaerobic environments: the jellied combined electrode,” *Biotechnol Bioeng*, vol. 31, no. 4, pp. 659–665, 1988.

[182] V. Bansal and R. L. Shambaugh, “On-line Density and Crystallinity of Polyethylene Terephthalate During Melt Spinning,” *Polym. Eng. Sci.*, vol. 38, no. 12, pp. 1959–1968, 1998.

9. Appendix

9.1 Attachments on the study of the long-term stability of the determination of sodium by ICP-OES

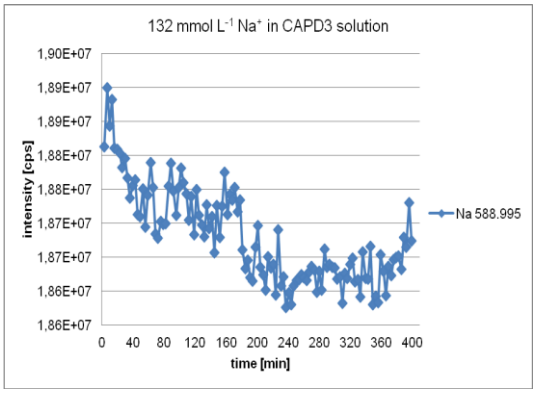

Figure 9-1: The intensity of Na 588.995 nm by the determination of 132.0 mmol L^{-1} Na^+ in a CAPD3 solution within a period of about 393 min.

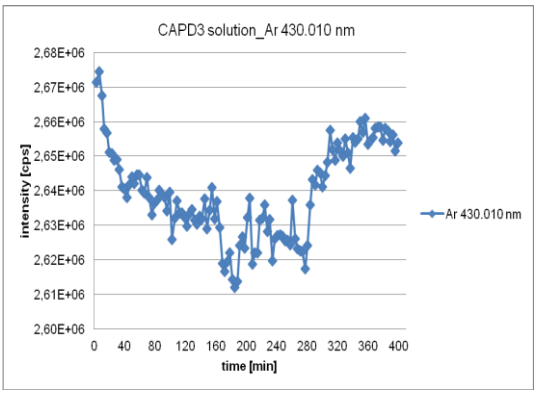

Figure 9-4: The intensity of Ar 430.010 nm by the determination of 132.0 mmol L^{-1} Na^+ in a CAPD3 solution within a period of about 393 min.

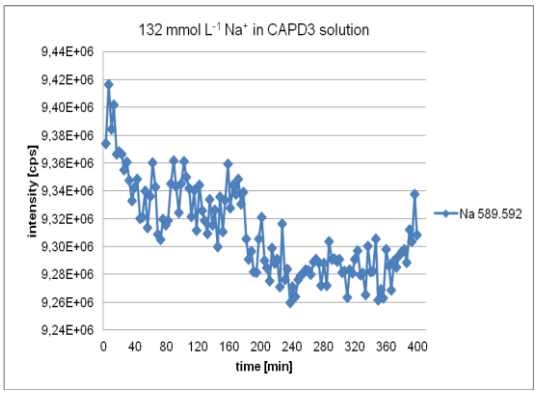

Figure 9-2: The intensity of Na 589.592 nm by the determination of 132.0 mmol L^{-1} Na^+ in a CAPD3 solution within a period of about 393 min.

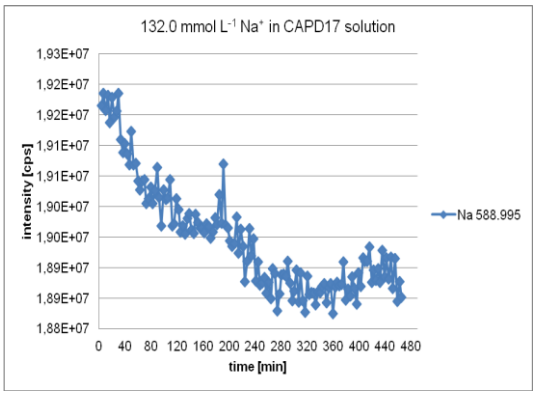

Figure 9-5: The intensity of Na 588.995 nm by the determination of 132.0 mmol L^{-1} Na^+ in a CAPD17 solution within a period of about 465 min.

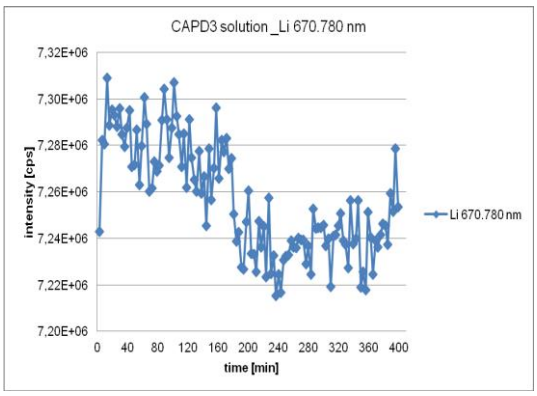

Figure 9-3: The intensity of Li 670.780 nm by the determination of 132.0 mmol L^{-1} Na^+ in a CAPD3 solution within a period of about 393 min.

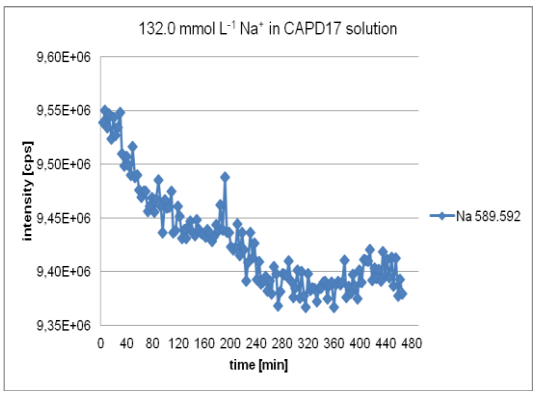

Figure 9-6: The intensity of Na 589.592 nm by the determination of 132.0 mmol L^{-1} Na^+ in a CAPD17 solution within a period of about 465 min

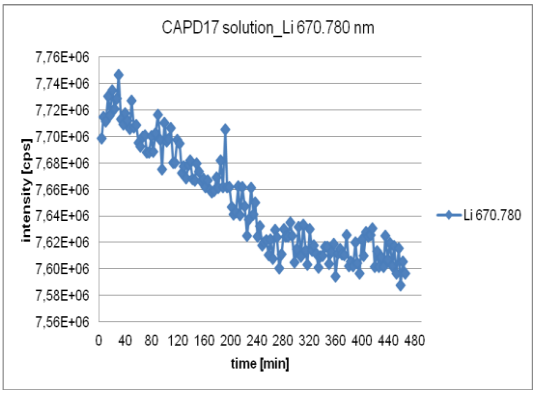

Figure 9-7: The intensity of Li 670.780 nm by the determination of 132.0 mmol L^{-1} Na^{+} in a CAPD17 solution within a period of about 465 min

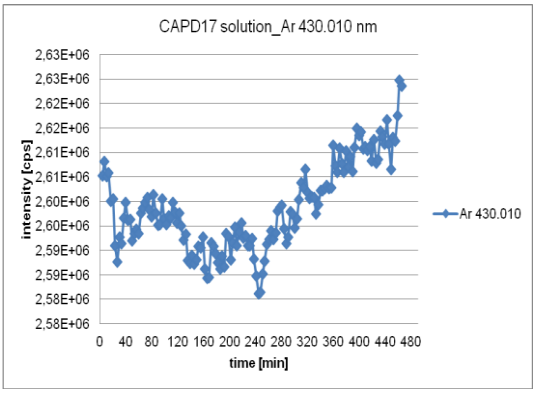

Figure 9-8: The intensity of Ar 430.010 nm by the determination of 132.0 mmol L^{-1} Na^{+} in a CAPD17 solution within a period of about 465 min

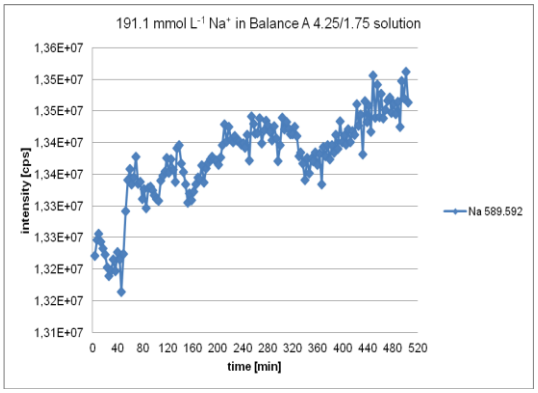

Figure 9-9: The intensity of Na 589.592 nm by the determination of 191.1 mmol L^{-1} Na^{+} in a Balance A 4.25/1.75 solution within a period of about 505 min

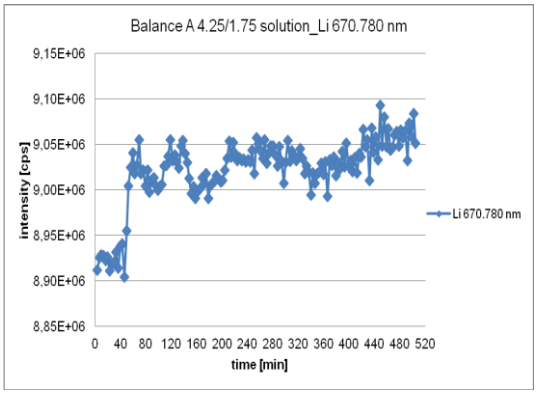

Figure 9-10: The intensity of Li 670.780 nm by the determination of 191.1 mmol L^{-1} Na^{+} in a Balance A 4.25/1.75 solution within a period of about 505 min

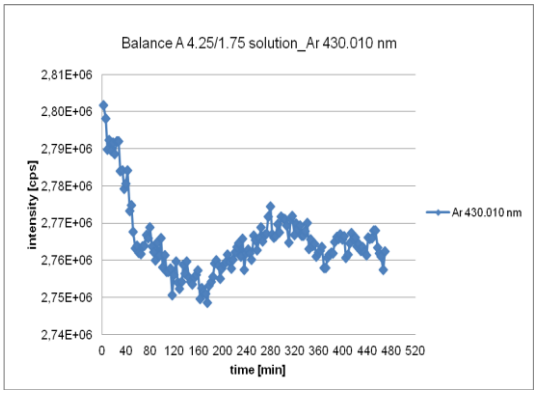

Figure 9-11: The intensity of Ar 430.010 nm by the determination of 191.1 mmol L^{-1} Na^{+} in a Balance A 4.25/1.75 solution within a period of about 505 min

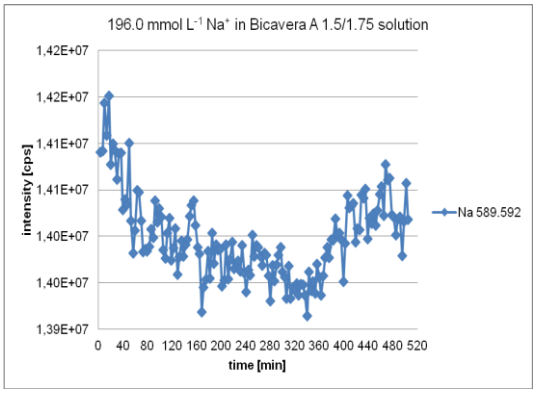

Figure 9-12: The intensity of Na 589.592 nm by the determination of 196.0 mmol L^{-1} Na^{+} in a Bicavera A 1.5/1.75 solution within a period of about 505 min

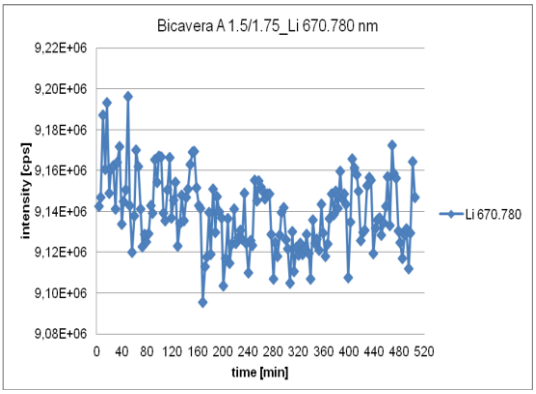

Figure 9-13: The intensity of Li 670.780 nm by the determination of 196.0 mmol L^{-1} Na^+ in a Bicavera A 1.5/1.75 solution within a period of about 505 min

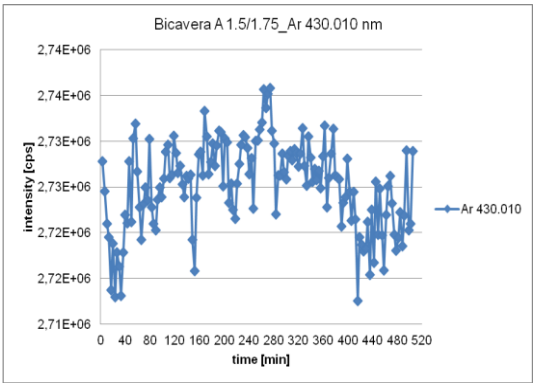

Figure 9-14: The intensity of Ar 430.010 nm by the determination of 196.0 mmol L^{-1} Na^+ in a Bicavera A 1.5/1.75 solution within a period of about 505 min

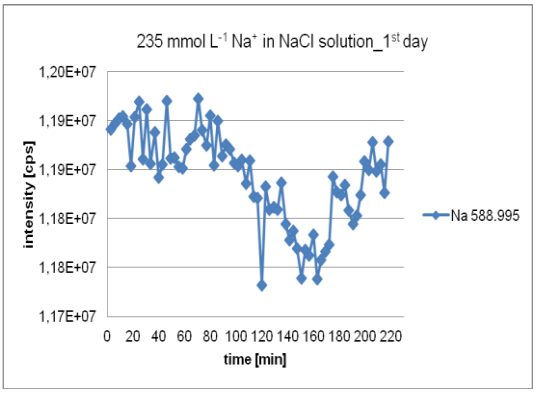

Figure 9-15: The intensity of Na 588.995 nm by the determination of 235.0 mmol L^{-1} Na^+ in a NaCl solution within a period of about 218 min (1^{st} day)

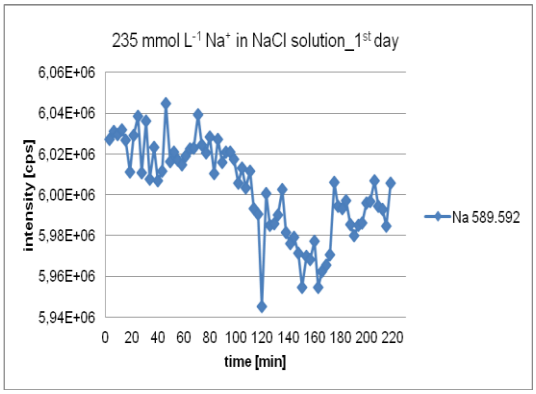

Figure 9-16: The intensity of Na 589.592 nm by the determination of 235.0 mmol L^{-1} Na^+ in a NaCl solution within a period of about 218 min (1^{st} day)

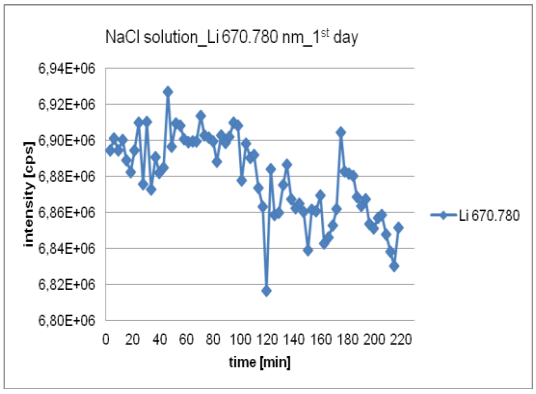

Figure 9-17: The intensity of Li 670.780 nm by the determination of 235.0 mmol L^{-1} Na^+ in a NaCl solution within a period of about 218 min (1^{st} day)

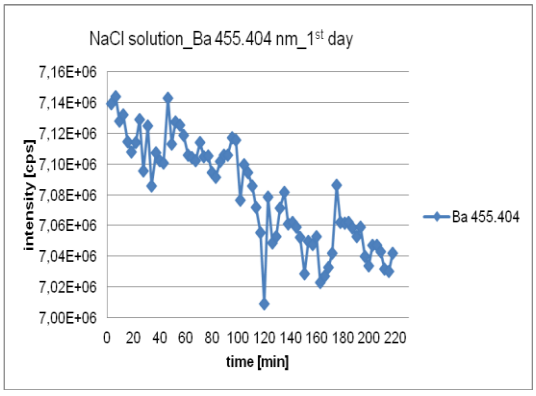

Figure 9-18: The intensity of Ba 455.404 nm by the determination of 235.0 mmol L^{-1} Na^+ in an NaCl solution within a period of about 218 min (1^{st} day)

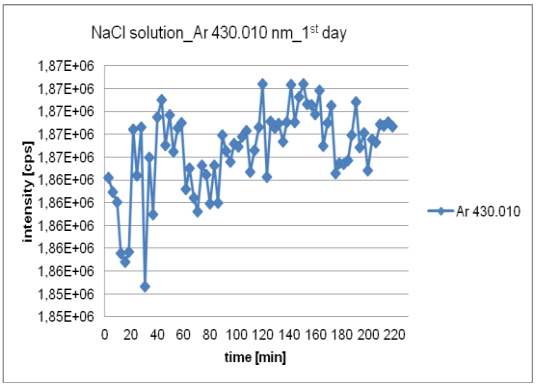

Figure 9-19: The intensity of Ar 430.010 nm by the determination of 235.0 mmol L^{-1} Na^+ in an NaCl solution within a period of about 218 min (1st day)

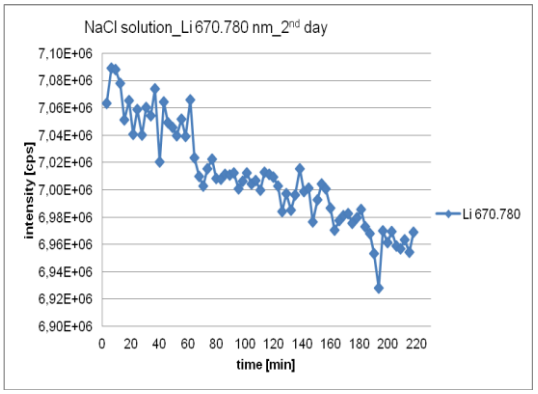

Figure 9-22: The intensity of Li 670.780 nm by the determination of 235.0 mmol L^{-1} Na^+ in an NaCl solution within a period of about 218 min (2nd day)

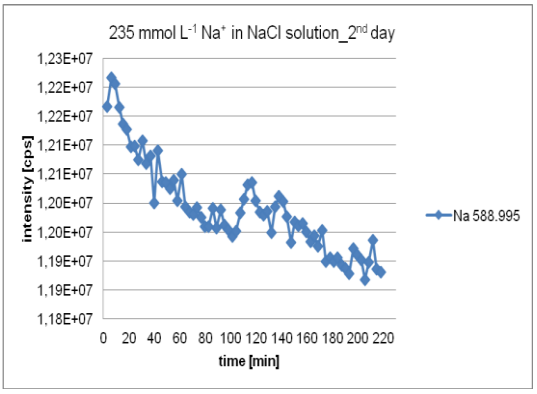

Figure 9-20: The intensity of Na 588.995 nm by the determination of 235.0 mmol L^{-1} Na^+ in an NaCl solution within a period of about 218 min (2nd day)

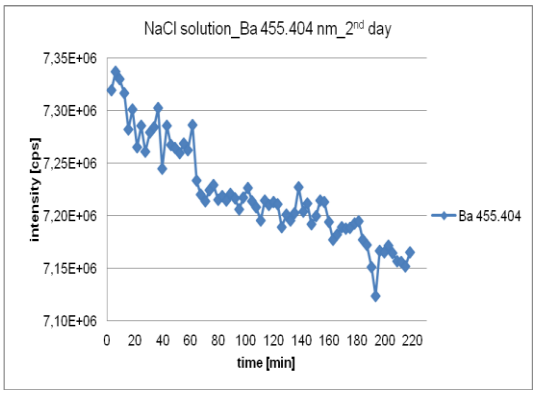

Figure 9-23: The intensity of Ba 455.404 nm by the determination of 235.0 mmol L^{-1} Na^+ in an NaCl solution within a period of about 218 min (2nd day)

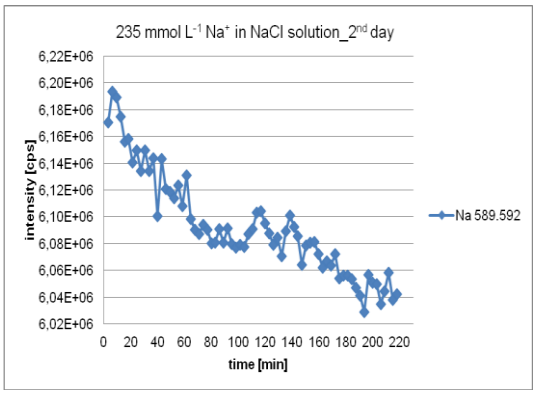

Figure 9-21: The intensity of Na 589.592 nm by the determination of 235.0 mmol L^{-1} Na^+ in an NaCl solution within a period of about 218 min (2nd day)

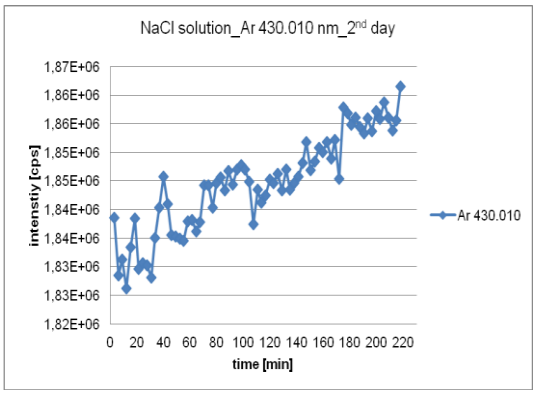

Figure 9-24: The intensity of Ar 430.010 nm by the determination of 235.0 mmol L^{-1} Na^+ in an NaCl solution within a period of about 218 min (2nd day)

9.2 Attachments on the study of the long-term stability of the determination of calcium by ICP-OES

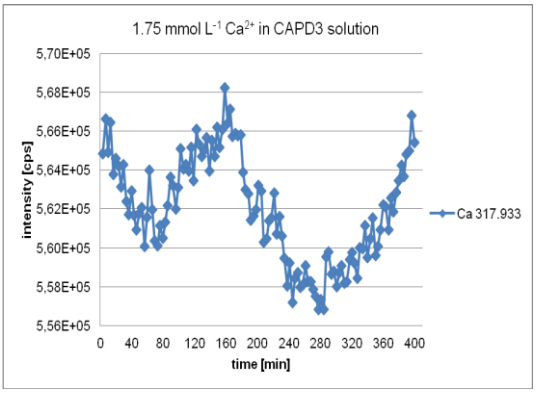

Figure 9-25: The intensity of Ca 317.933 nm by the determination of 1.75 mmol L^{-1} Ca^{2+} in a CAPD3 solution within a period of about 393 min.

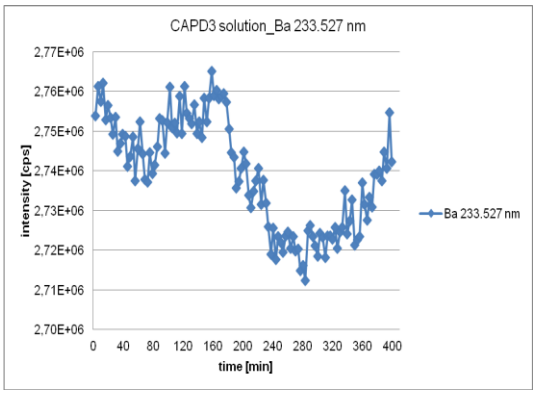

Figure 9-28: The intensity of Ba 233.527 nm by the determination of 1.75 mmol L^{-1} Ca^{2+} in a CAPD3 solution within a period of about 393 min.

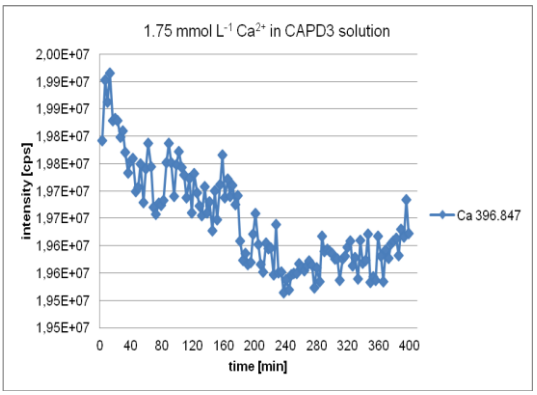

Figure 9-26: The intensity of Ca 396.847 nm by the determination of 1.75 mmol L^{-1} Ca^{2+} in a CAPD3 solution within a period of about 393 min.

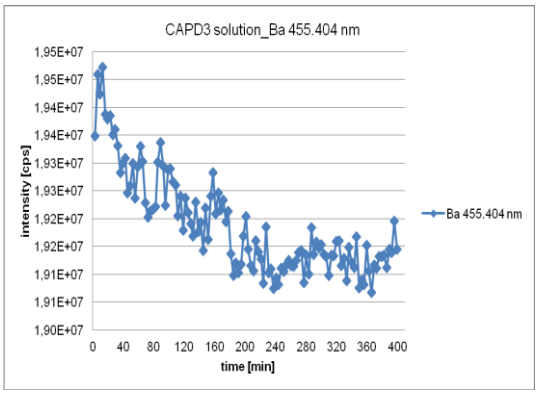

Figure 9-29: The intensity of Ba 455.404 nm by the determination of 1.75 mmol L^{-1} Ca^{2+} in a CAPD3 solution within a period of about 393 min.

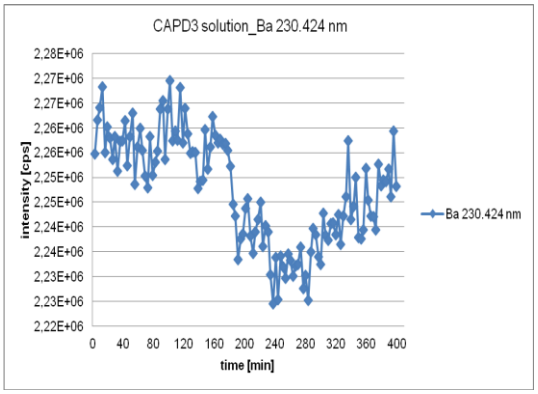

Figure 9-27: The intensity of Ba 230.424 nm by the determination of 1.75 mmol L^{-1} Ca^{2+} in a CAPD3 solution within a period of about 393 min.

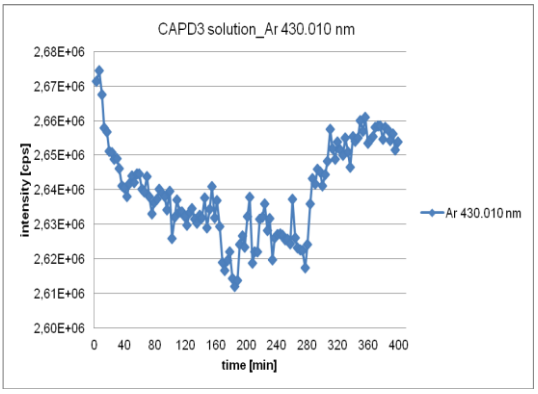

Figure 9-30: The intensity of Ar 430.010 nm by the determination of 1.75 mmol L^{-1} Ca^{2+} in a CAPD3 solution within a period of about 393 min.

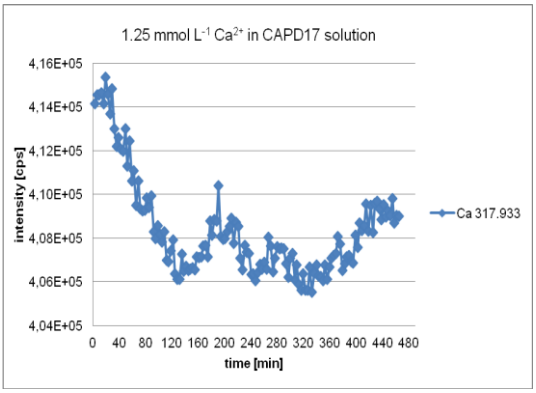

Figure 9-31: The intensity of Ca 317.933 nm by the determination of 1.25 mmol L^{-1} Ca^{2+} in a CAPD17 solution within a period of about 465 min.

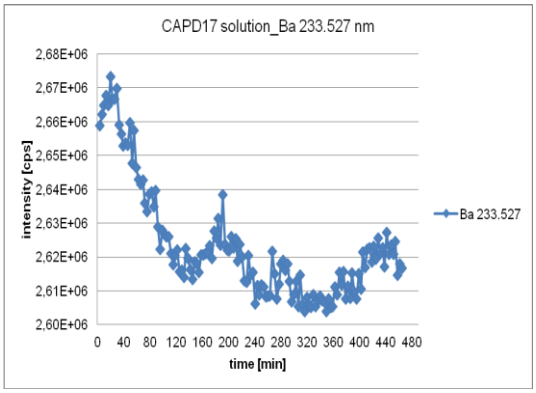

Figure 9-34: The intensity of Ba 233.527 nm by the determination of 1.25 mmol L^{-1} Ca^{2+} in a CAPD17 solution within a period of about 465 min.

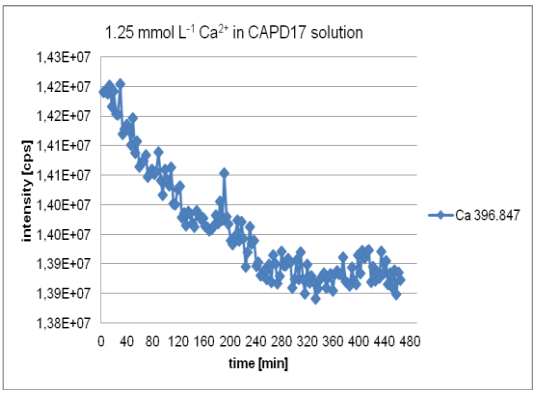

Figure 9-32: The intensity of Ca 396.847 nm by the determination of 1.25 mmol L^{-1} Ca^{2+} in a CAPD17 solution within a period of about 465 min.

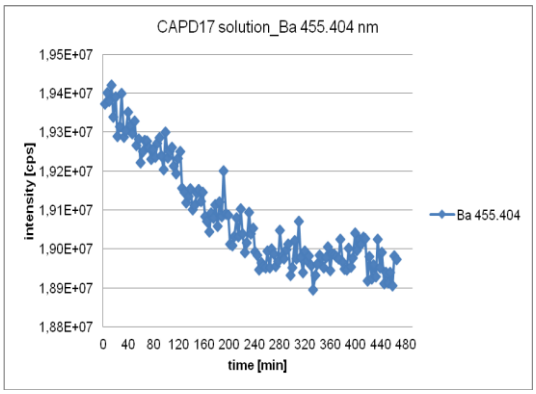

Figure 9-35: The intensity of Ba 455.404 nm by the determination of 1.25 mmol L^{-1} Ca^{2+} in a CAPD17 solution within a period of about 465 min

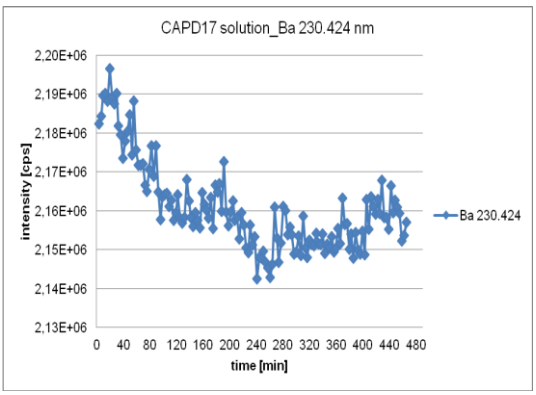

Figure 9-33: The intensity of Ba 230.424 nm by the determination of 1.25 mmol L^{-1} Ca^{2+} in a CAPD17 solution within a period of about 465 min.

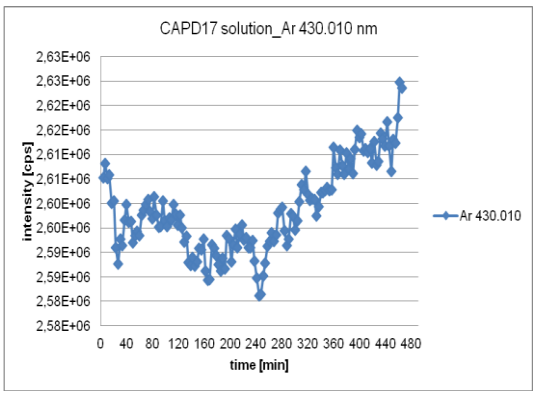

Figure 9-36: The intensity of Ar 430.010 nm by the determination of 1.25 mmol L^{-1} Ca^{2+} in a CAPD17 solution within a period of about 465 min

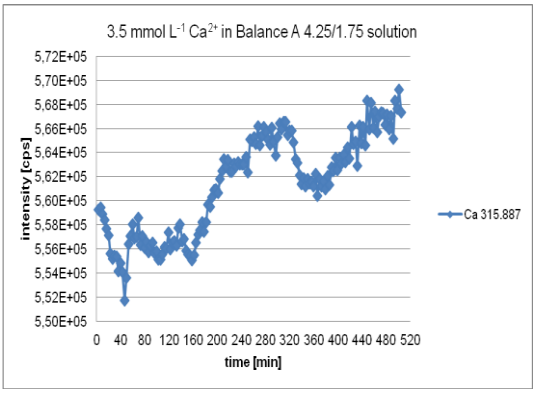

Figure 9-37: The intensity of Ca 315.887 nm by the determination of 3.5 mmol L^{-1} Ca^{2+} in a Balance A 4.25/1.75 solution within a period of about 505 min

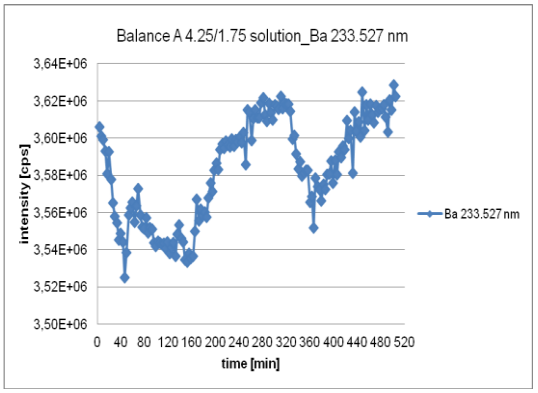

Figure 9-40: The intensity of Ba 233.527 nm by the determination of 3.5 mmol L^{-1} Ca^{2+} in a Balance A 4.25/1.75 solution within a period of about 505 min

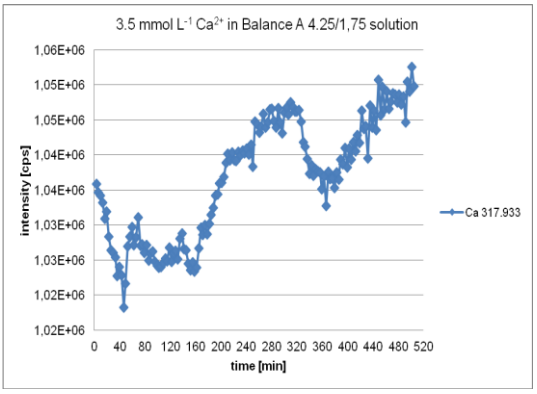

Figure 9-38: The intensity of Ca 317.933 nm by the determination of 3.5 mmol L^{-1} Ca^{2+} in a Balance A 4.25/1.75 solution within a period of about 505 min

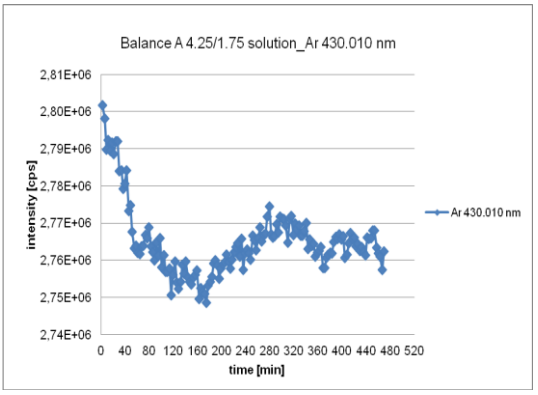

Figure 9-41: The intensity of Ar 430.010 nm by the determination of 3.5 mmol L^{-1} Ca^{2+} in a Balance A 4.25/1.75 solution within a period of about 505 min

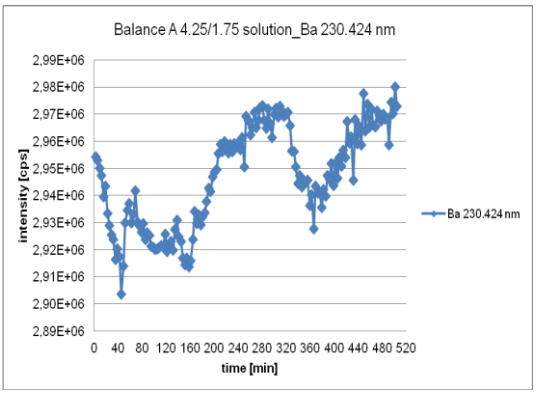

Figure 9-39: The intensity of Ba 230.424 nm by the determination of 3.5 mmol L^{-1} Ca^{2+} in a Balance A 4.25/1.75 solution within a period of about 505 min

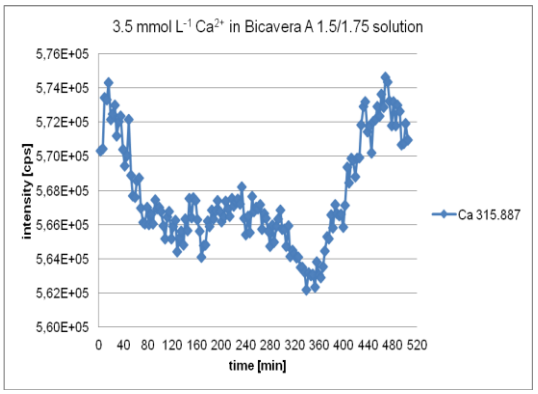

Figure 9-42: The intensity of Ca 315.887 nm by the determination of 3.5 mmol L^{-1} Ca^{2+} in a Bicavera A 1.5/1.75 solution within a period of about 505 min

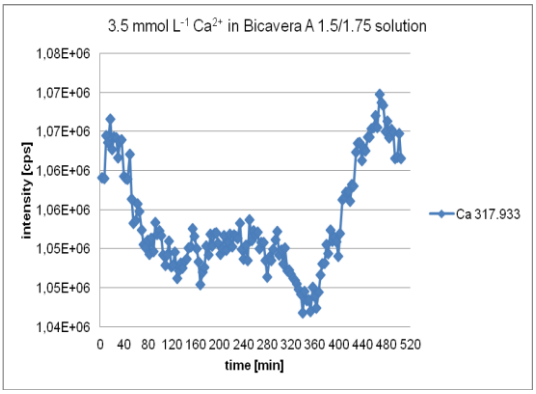

Figure 9-43: The intensity of Ca 317.933 nm by the determination of 3.5 mmol L^{-1} Ca^{2+} in a Bicavera A 1.5/1.75 solution within a period of about 505 min

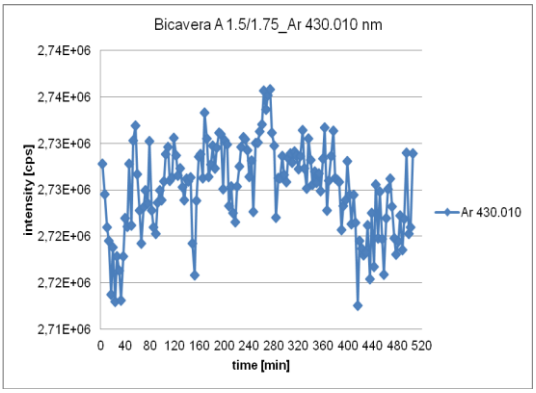

Figure 9-46: The intensity of Ar 430.010 nm by the determination of 3.5 mmol L^{-1} Ca^{2+} in a Bicavera A 1.5/1.75 solution within a period of about 505 min

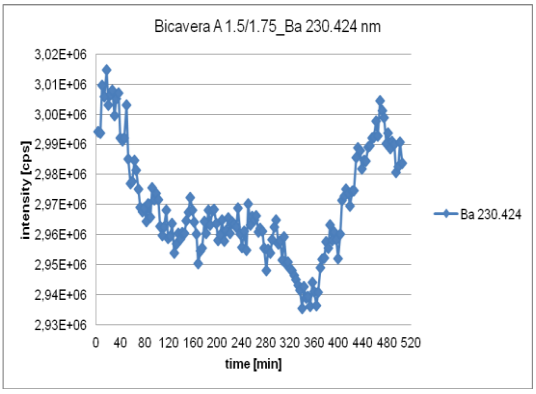

Figure 9-44: The intensity of Ba 230.404 nm by the determination of 3.5 mmol L^{-1} Ca^{2+} in a Bicavera A 1.5/1.75 solution within a period of about 505 min

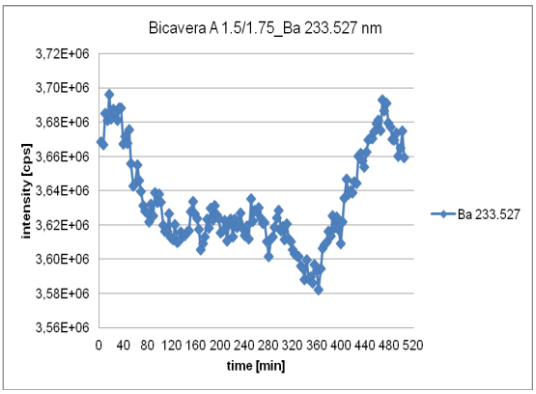

Figure 9-45: The intensity of Ba 233.527 nm by the determination of 3.5 mmol L^{-1} Ca^{2+} in a Bicavera A 1.5/1.75 solution within a period of about 505 min

9.3 Attachments on the study of the long-term stability of the determination of magnesium by ICP-OES

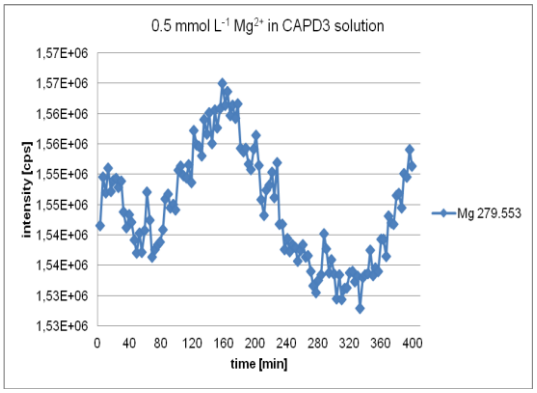

Figure 9-47: The intensity of Mg 279.553 nm by the determination of 0.5 mmol L^{-1} Mg^{2+} in a CAPD3 solution within a period of about 393 min

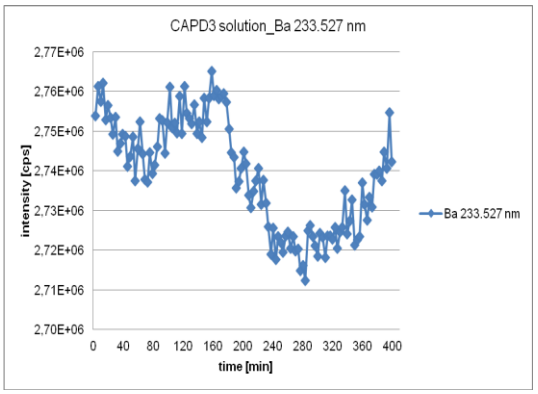

Figure 9-50: The intensity of Ba 233.527 nm by the determination of 0.5 mmol L^{-1} Mg^{2+} in a CAPD3 solution within a period of about 393 min

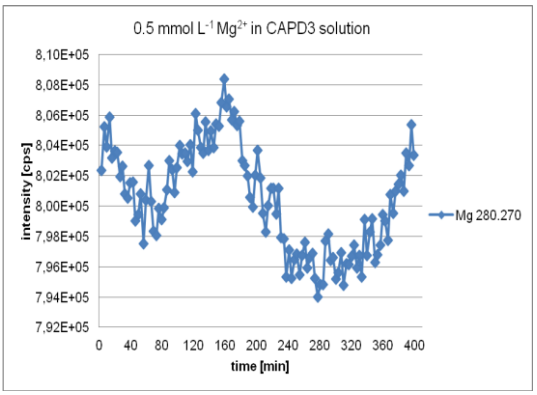

Figure 9-48: The intensity of Mg 280.270 nm by the determination of 0.5 mmol L^{-1} Mg^{2+} in a CAPD3 solution within a period of about 393 min

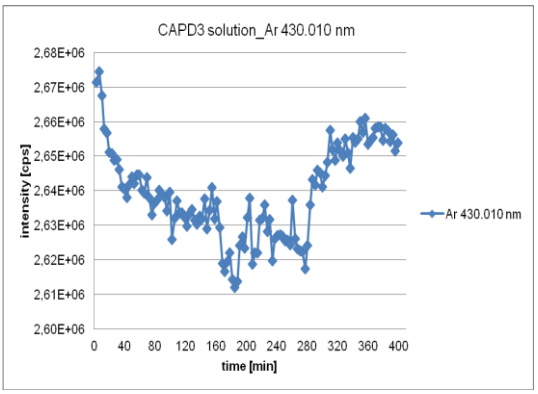

Figure 9-51: The intensity of Ar 430.010 nm by the determination of 0.5 mmol L^{-1} Mg^{2+} in a CAPD3 solution within a period of about 393 min

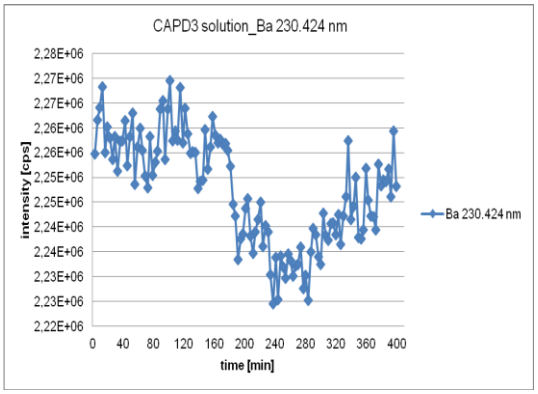

Figure 9-49: The intensity of Ba 230.424 nm by the determination of 0.5 mmol L^{-1} Mg^{2+} in a CAPD3 solution within a period of about 393 min

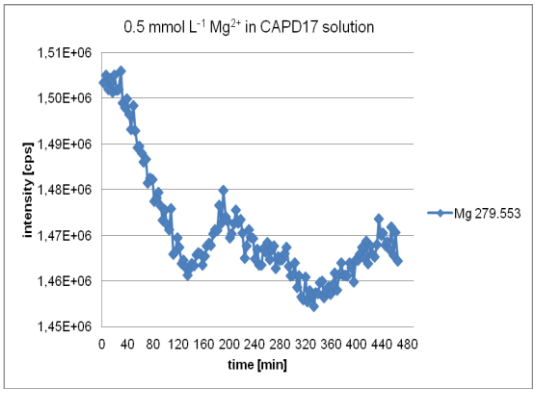

Figure 9-52: The intensity of Mg 279.553 nm by the determination of 0.5 mmol L^{-1} Mg^{2+} in a CAPD17 solution within a period of about 465 min

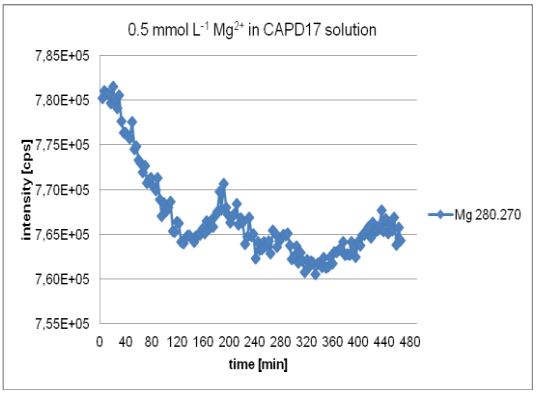

Figure 9-53: The intensity of Mg 280.270 nm by the determination of 0.5 mmol L^{-1} Mg^{2+} in a CAPD17 solution within a period of about 465 min

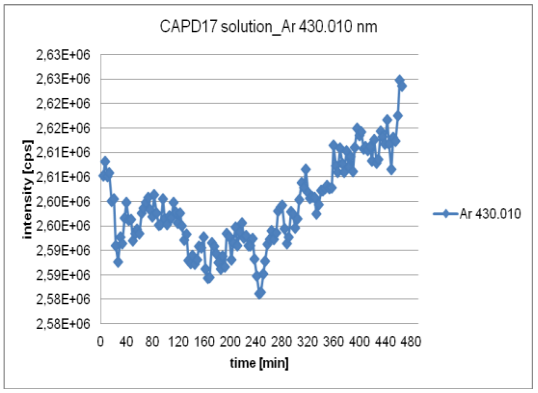

Figure 9-56: The intensity of Ar 430.010 nm by the determination of 0.5 mmol L^{-1} Mg^{2+} in a CAPD17 solution within a period of about 465 min

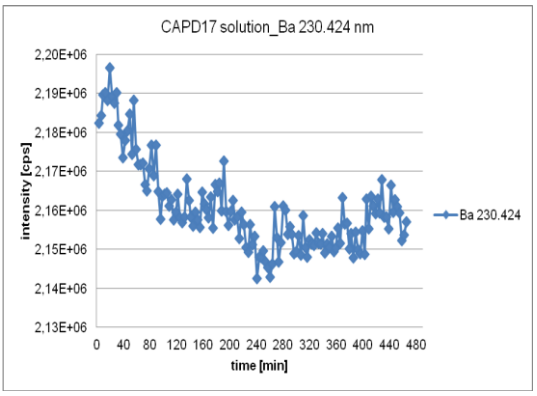

Figure 9-54: The intensity of Ba 230.424 nm by the determination of 0.5 mmol L^{-1} Mg^{2+} in a CAPD17 solution within a period of about 465 min

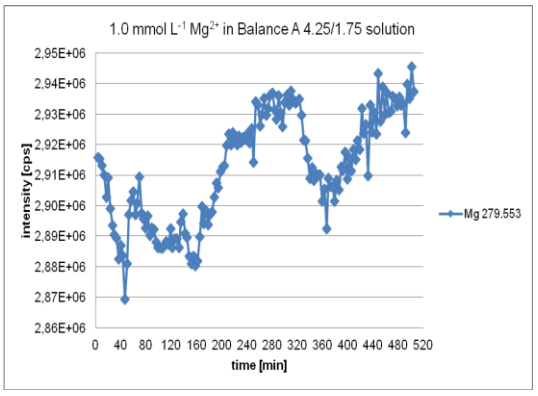

Figure 9-57: The intensity of Mg 279.553 nm by the determination of 1.0 mmol L^{-1} Mg^{2+} in a Balance A 4.25/1.75 solution within a period of about 505 min

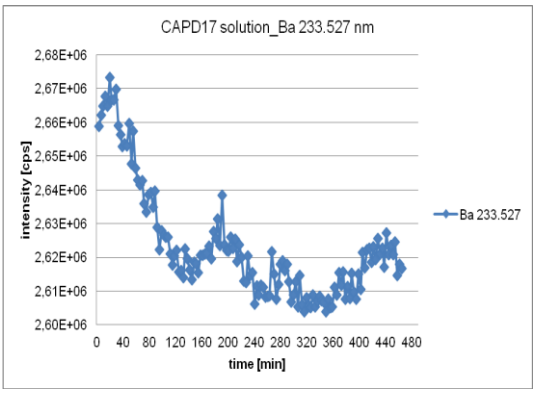

Figure 9-55: The intensity of Ba 233.527 nm by the determination of 0.5 mmol L^{-1} Mg^{2+} in a CAPD17 solution within a period of about 465 min

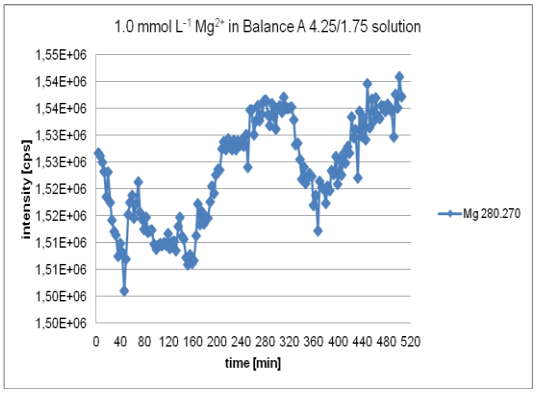

Figure 9-58: The intensity of Mg 280.270 nm by the determination of 1.0 mmol L^{-1} Mg^{2+} in a Balance A 4.25/1.75 solution within a period of about 505 min

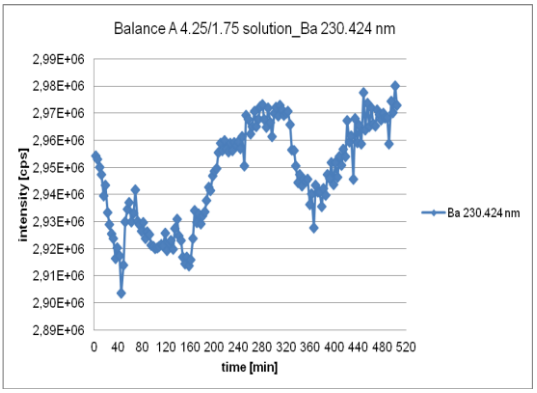

Figure 9-59: The intensity of Ba 230.424 nm by the determination of 1.0 mmol L^{-1} Mg^{2+} in a Balance A 4.25/1.75 solution within a period of about 505 min

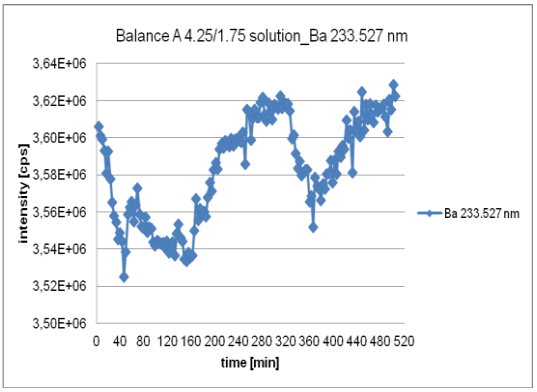

Figure 9-60: The intensity of Ba 233.527 nm by the determination of 1.0 mmol L^{-1} Mg^{2+} in a Balance A 4.25/1.75 solution within a period of about 505 min

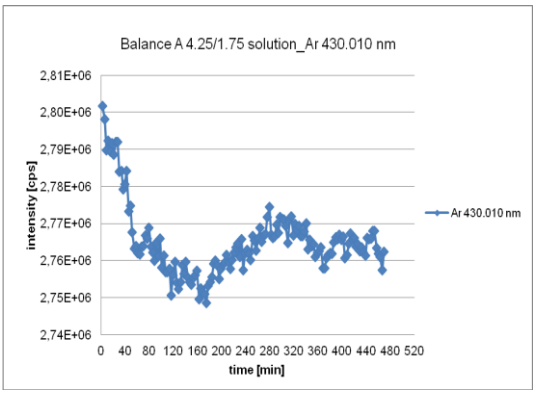

Figure 9-61: The intensity of Ar 430.010 nm by the determination of 1.0 mmol L^{-1} Mg^{2+} in a Balance A 4.25/1.75 solution within a period of about 505 min

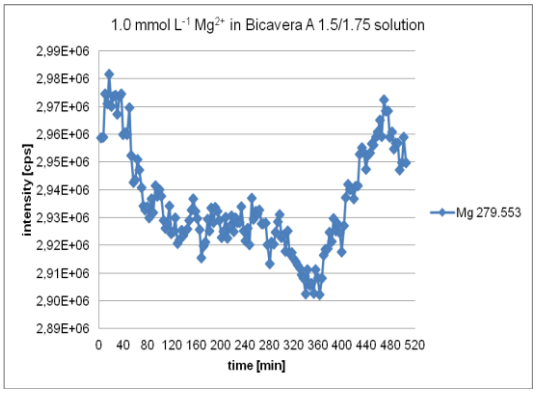

Figure 9-62: The intensity of Mg 279.553 nm by the determination of 1.0 mmol L^{-1} Mg^{2+} in a Bicavera A 1.5/1.75 solution within a period of about 505 min

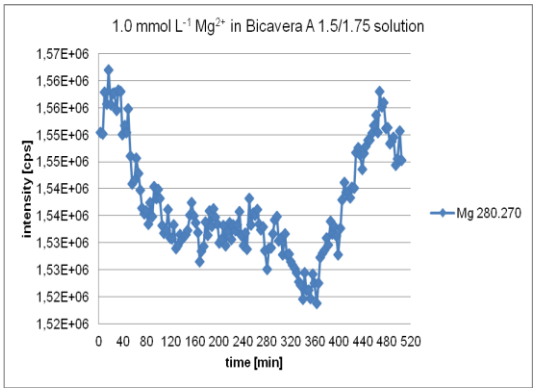

Figure 9-63: The intensity of Mg 280.270 nm by the determination of 1.0 mmol L^{-1} Mg^{2+} in a Bicavera A 1.5/1.75 solution within a period of about 505 min

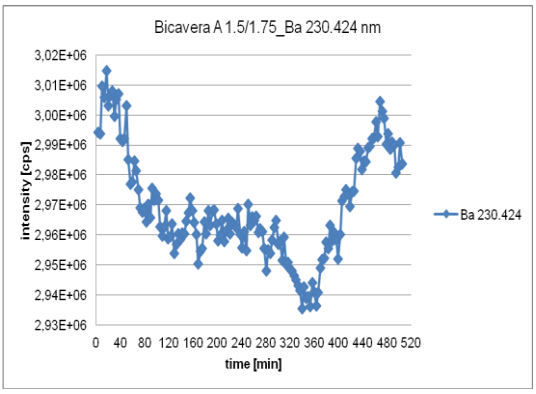

Figure 9-64: The intensity of Ba 230.424 nm by the determination of 1.0 mmol L^{-1} Mg^{2+} in a Bicavera A 1.5/1.75 solution within a period of about 505 min

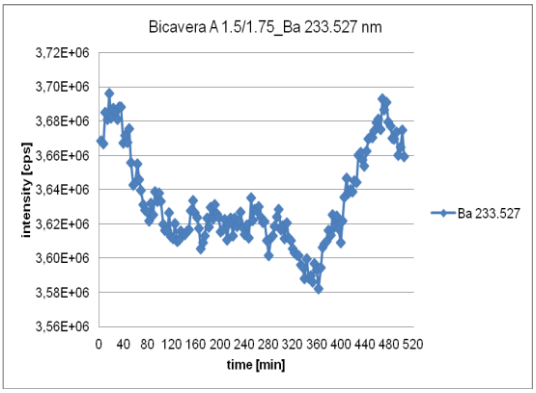

Figure 9-65: The intensity of Ba 233.527 nm by the determination of 1.0 mmol L^{-1} Mg^{2+} in a Bicavera A 1.5/1.75 solution within a period of about 505 min

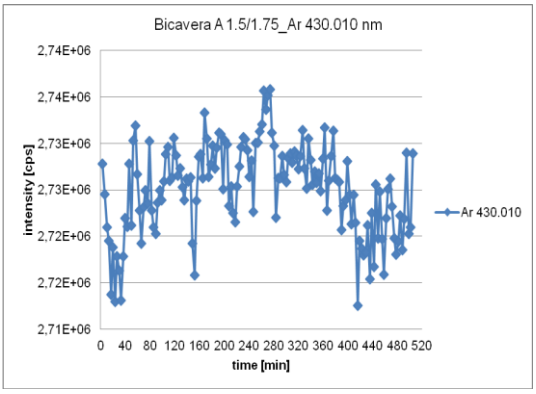

Figure 9-66: The intensity of Ar 430.010 nm by the determination of 1.0 mmol L^{-1} Mg^{2+} in a Bicavera A 1.5/1.75 solution within a period of about 505 min

9.4 Attachments on the study of the long-term stability of the determination of potassium by ICP-OES

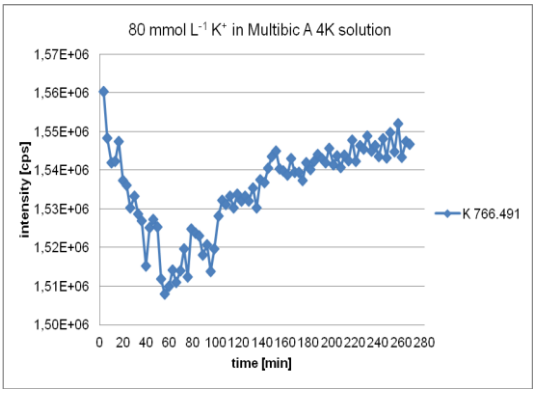

Figure 9-67: The intensity of K 766.491 nm by the determination of 80.0 mmol L^{-1} K^+ in a Multibic A 4K solution within a period of about 267 min

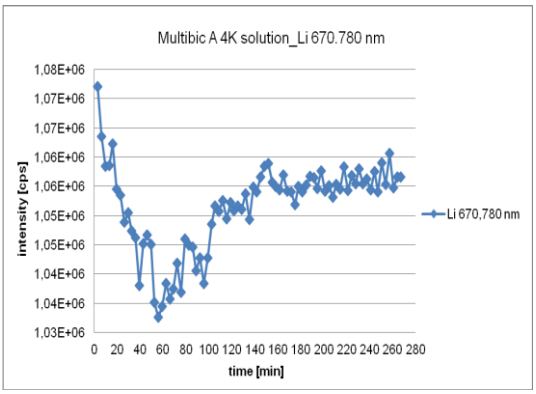

Figure 9-68: The intensity of Li 670.780 nm by the determination of 80.0 mmol L^{-1} K^+ in a Multibic A 4K solution within a period of about 267 min

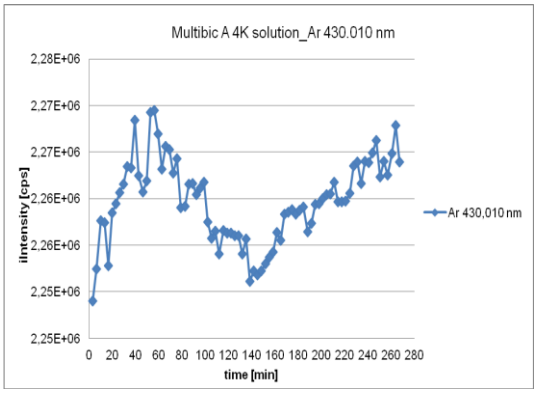

Figure 9-69: The intensity of Ar 430.010 nm by the determination of 80.0 mmol L^{-1} K^+ in a Multibic A 4K solution within a period of about 267 min

9.5 Attachments on the effect of glucose and lactate on the determination of magnesium by ICP-OES

9.5.1 Attachments on the matrix effects on the determination of the lowest magnesium concentration (0.4 mmol L^{-1})

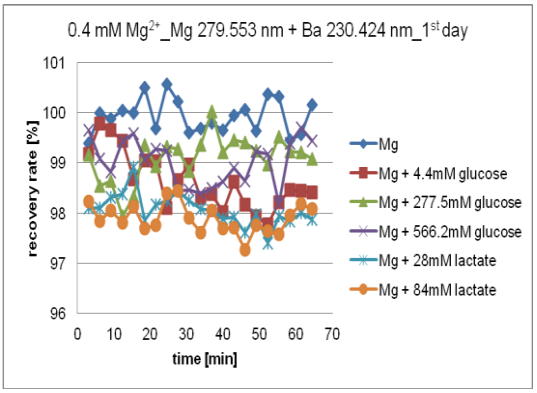

Figure 9-70: Recovery rates by the determination of 0.4 mmol L^{-1} Mg^{2+} in glucose or lactate matrices, with Mg 279.553 nm + Ba 230.424 nm (1st day)

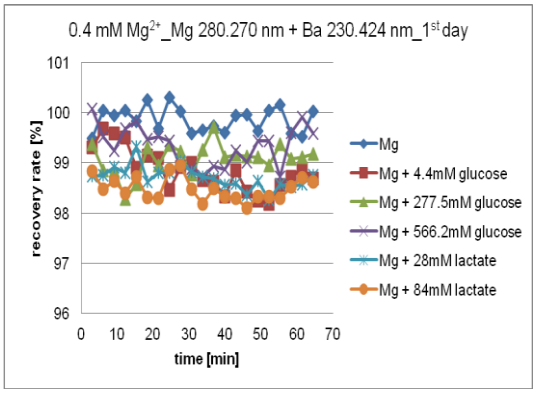

Figure 9-72: Recovery rates by the determination of 0.4 mmol L^{-1} Mg^{2+} in glucose or lactate matrices, with Mg 280.270 nm + Ba 230.424 nm (1st day)

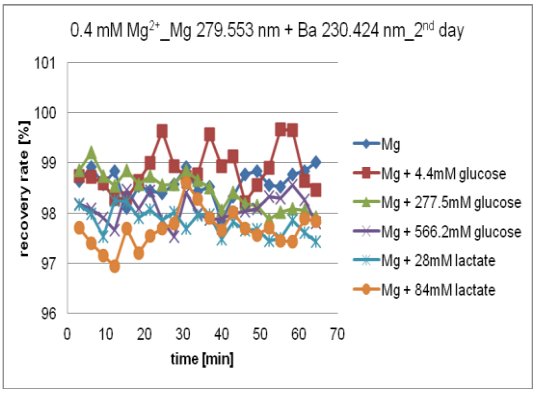

Figure 9-71: Recovery rates by the determination of 0.4 mmol L^{-1} Mg^{2+} in glucose or lactate matrices, with Mg 279.553 nm + Ba 230.424 nm(2nd day)

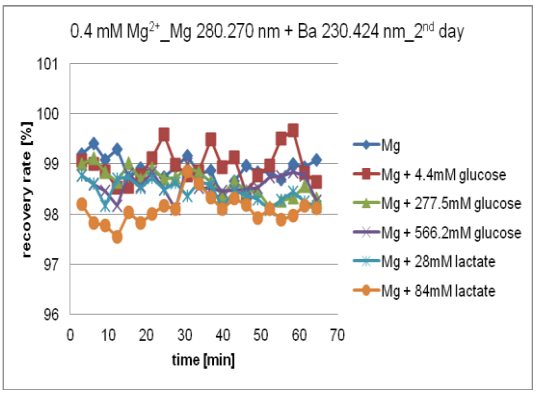

Figure 9-73: Recovery rates by the determination of 0.4 mmol L^{-1} Mg^{2+} in glucose or lactate matrices, with Mg 280.270 nm + Ba 230.424 nm (2nd day)

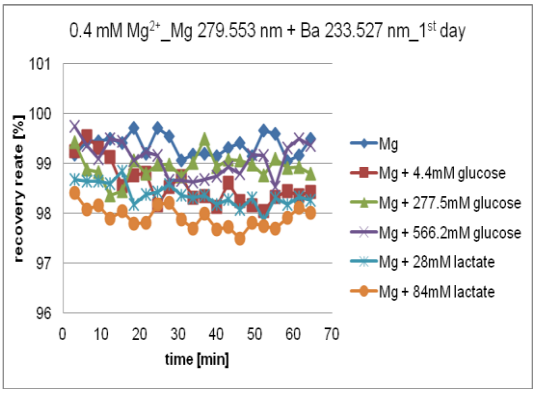

Figure 9-74: Recovery rates by the determination of 0.4 mmol L^{-1} Mg^{2+} in glucose or lactate matrices, with Mg 279.553 nm + Ba 233.527 nm (1st day)

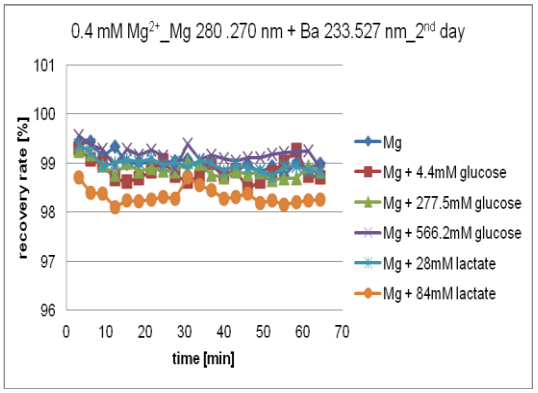

Figure 9-77: Recovery rates by the determination of 0.4 mmol L^{-1} Mg^{2+} in glucose or lactate matrices, with Mg 280.270 nm + Ba 233.527 nm (2nd day)

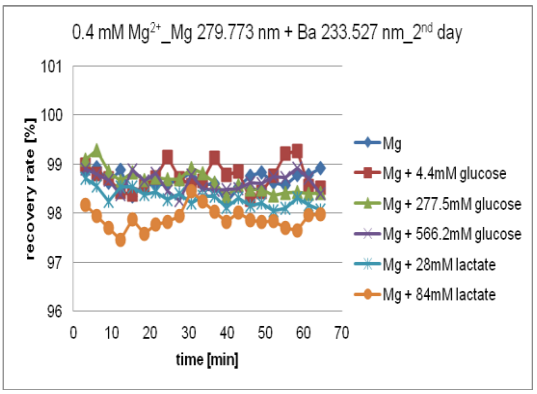

Figure 9-75: Recovery rates by the determination of 0.4 mmol L^{-1} Mg^{2+} in glucose or lactate matrices, with Mg 279.553 nm + Ba 233.527 nm (2nd day)

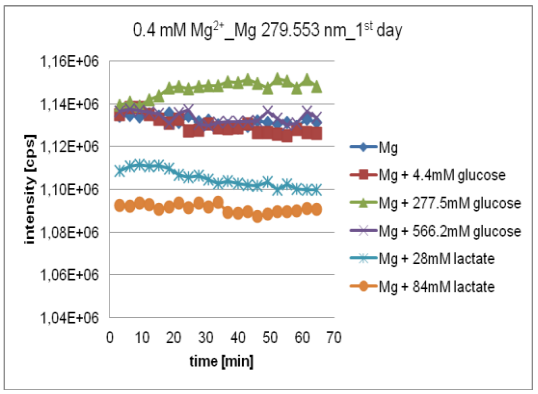

Figure 9-78: The intensity of Mg 279.553 nm by the determination of 0.4 mmol L^{-1} Mg^{2+} in glucose or lactate matrices (1st day)

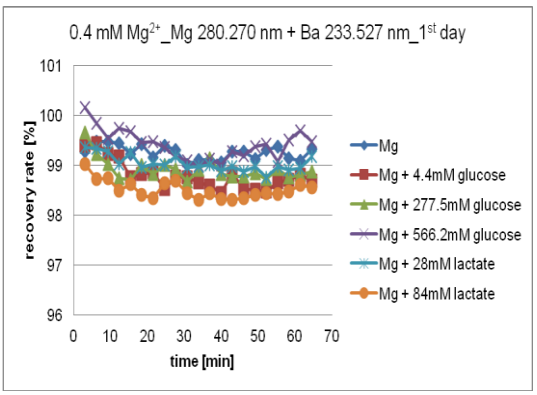

Figure 9-76: Recovery rates by the determination of 0.4 mmol L^{-1} Mg^{2+} in glucose or lactate matrices, with Mg 280.270 nm + Ba 233.527 nm (1st day)

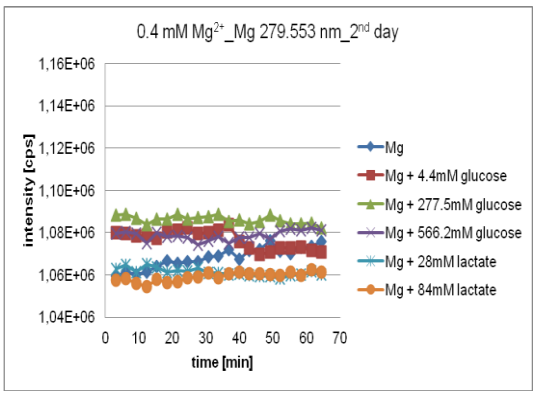

Figure 9-79: The intensity of Mg 279.553 nm by the determination of 0.4 mmol L^{-1} Mg^{2+} in glucose or lactate matrices (2nd day)

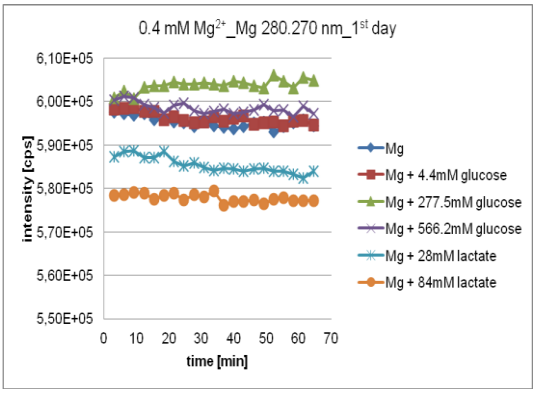

Figure 9-80: The intensity of Mg 280.270 nm by the determination of 0.4 mmol L^{-1} Mg^{2+} in glucose or lactate matrices (1st day)

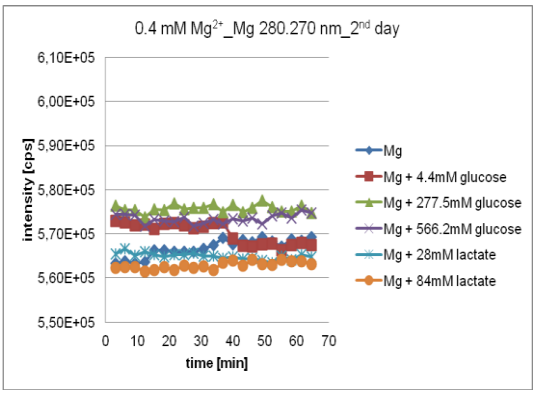

Figure 9-81: The intensity of Mg 280.270 nm by the determination of 0.4 mmol L^{-1} Mg^{2+} in glucose or lactate matrices (2nd day)

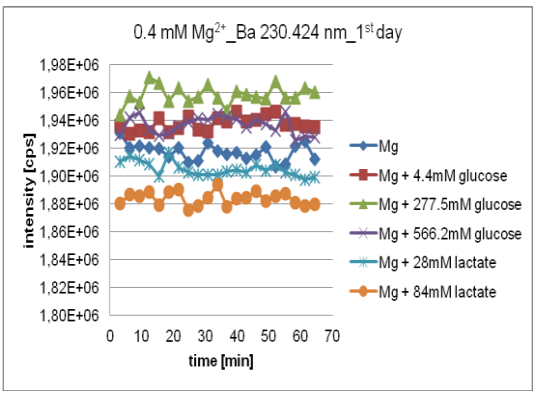

Figure 9-82: The intensity of Ba 230.424 nm by the determination of 0.4 mmol L^{-1} Mg^{2+} in glucose or lactate matrices (1st day)

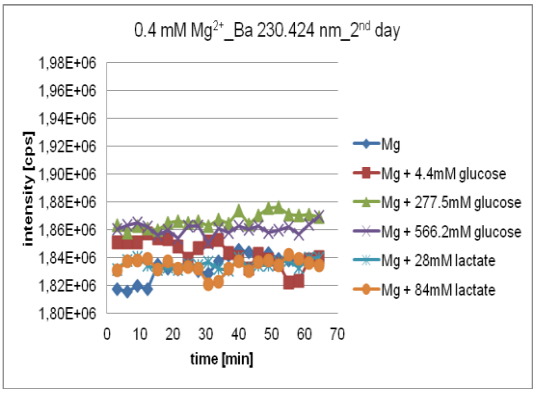

Figure 9-83: The intensity of Ba 230.424 nm by the determination of 0.4 mmol L^{-1} Mg^{2+} in glucose or lactate matrices (2nd day)

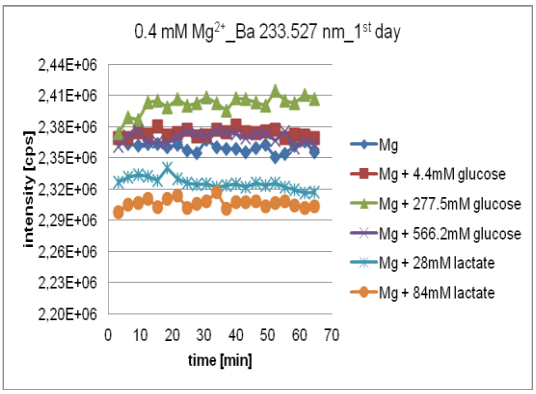

Figure 9-84: The intensity of Ba 233.527 nm by the determination of 0.4 mmol L^{-1} Mg^{2+} in glucose or lactate matrices (1st day)

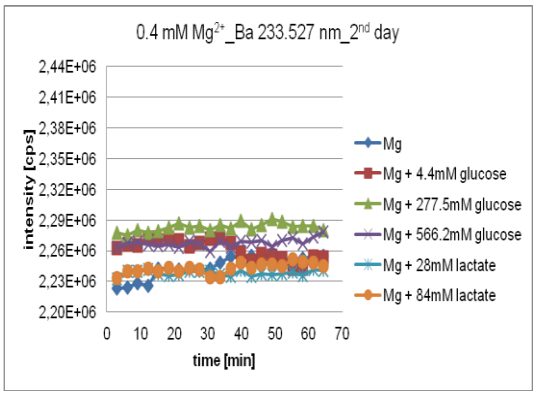

Figure 9-85: The intensity of Ba 233.527 nm by the determination of 0.4 mmol L^{-1} Mg^{2+} in glucose or lactate matrices (2nd day)

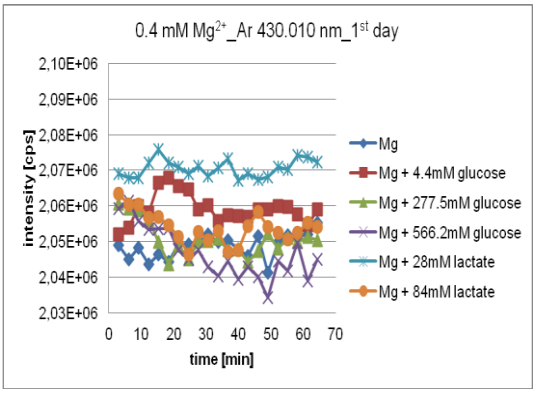

Figure 9-86: The intensity of Ar 430.010 nm by the determination of 0.4 mmol L^{-1} Mg^{2+} in glucose or lactate matrices (1st day)

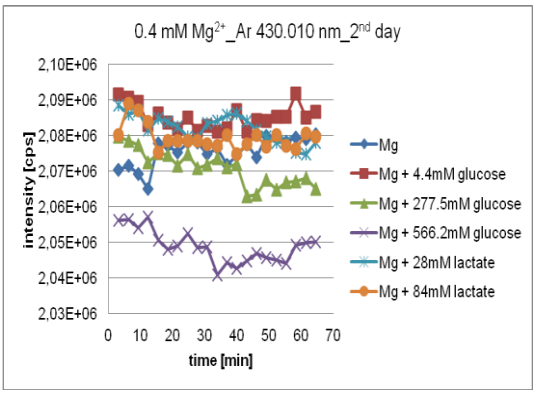

Figure 9-87: The intensity of Ar 430.010 nm by the determination of 0.4 mmol L^{-1} Mg^{2+} in glucose or lactate matrices (2nd day)

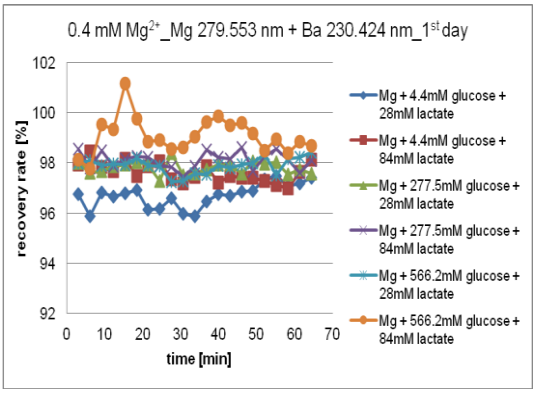

Figure 9-88: Recovery rates by the determination of 0.4 mmol L^{-1} Mg^{2+} in glucose and lactate matrices, with Mg 279.553 nm + Ba 230.424 nm (1st day)

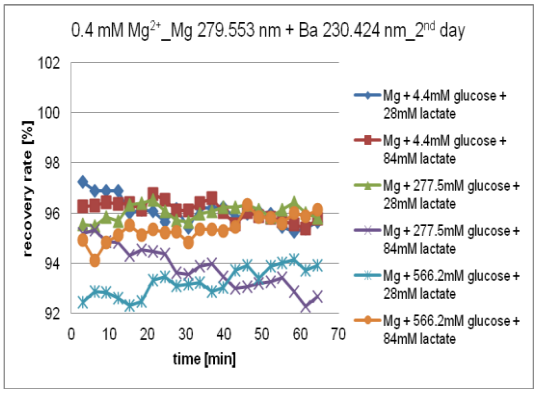

Figure 9-89: Recovery rates by the determination of 0.4 mmol L^{-1} Mg^{2+} in glucose and lactate matrices, with Mg 279.553 nm + Ba 230.424 nm (2nd day)

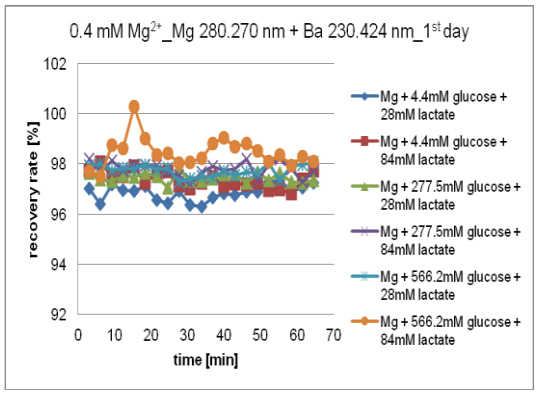

Figure 9-90: Recovery rates by the determination of 0.4 mmol L^{-1} Mg^{2+} in glucose and lactate matrices, with Mg 280.270 nm + Ba 230.424 nm (1st day)

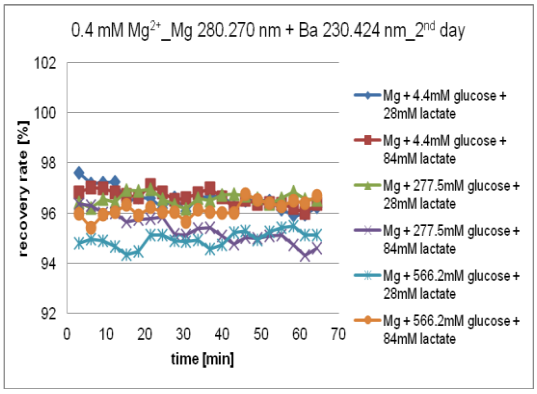

Figure 9-91: Recovery rates by the determination of 0.4 mmol L^{-1} Mg^{2+} in glucose and lactate matrices, with Mg 280.270 nm + Ba 230.424 nm (2nd day)

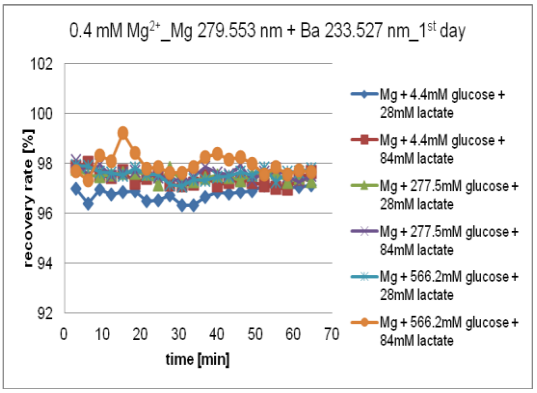

Figure 9-92: Recovery rates by the determination of 0.4 mmol L^{-1} Mg^{2+} in glucose and lactate matrices, with Mg 279.553 nm + Ba 233.527 nm (1st day)

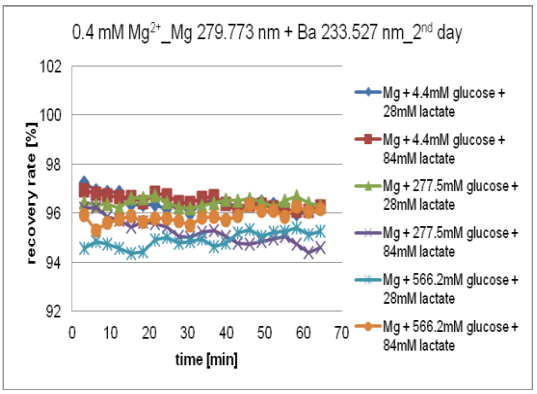

Figure 9-93: Recovery rates by the determination of 0.4 mmol L^{-1} Mg^{2+} in glucose and lactate matrices, with Mg 279.553 nm + Ba 233.527 nm (2nd day)

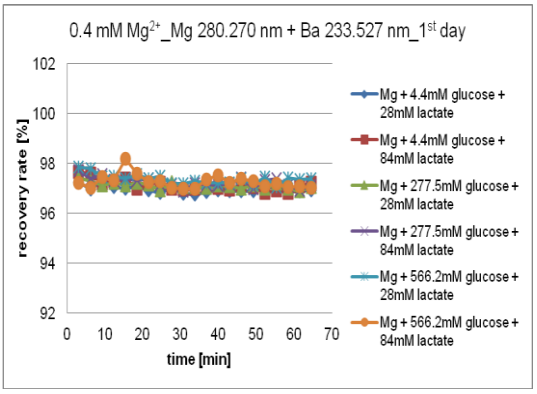

Figure 9-94: Recovery rates by the determination of 0.4 mmol L^{-1} Mg^{2+} in glucose and lactate matrices, with Mg 280.270 nm + Ba 233.527 nm (1st day)

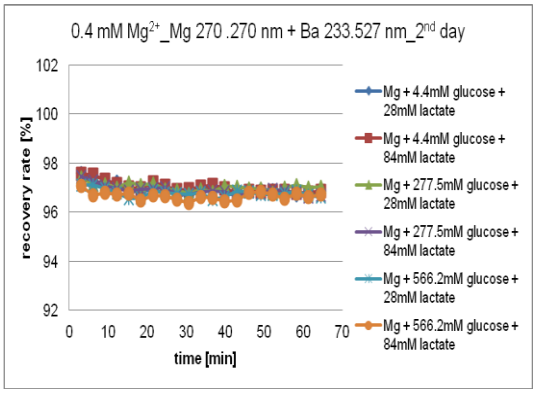

Figure 9-95: Recovery rates by the determination of 0.4 mmol L^{-1} Mg^{2+} in glucose and lactate matrices, with Mg 280.270 nm + Ba 233.527 nm (2nd day)

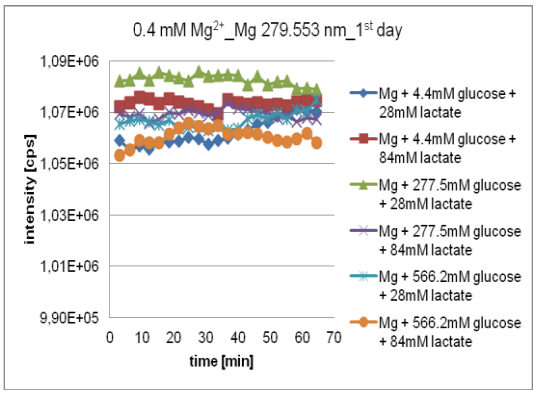

Figure 9-96: The intensity of Mg 279.553 nm by the determination of 0.4 mmol L^{-1} Mg^{2+} in glucose and lactate matrices (1st day)

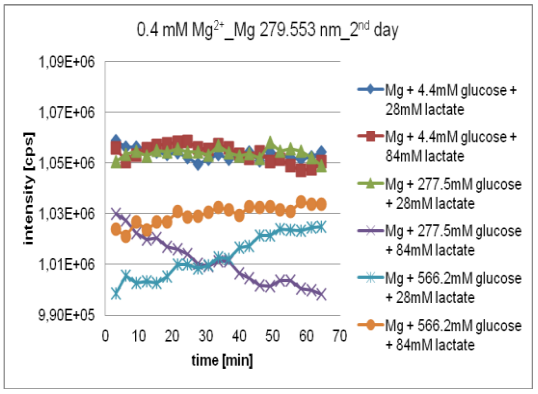

Figure 9-97: The intensity of Mg 279.553 nm by the determination of 0.4 mmol L^{-1} Mg^{2+} in glucose and lactate matrices (2nd day)

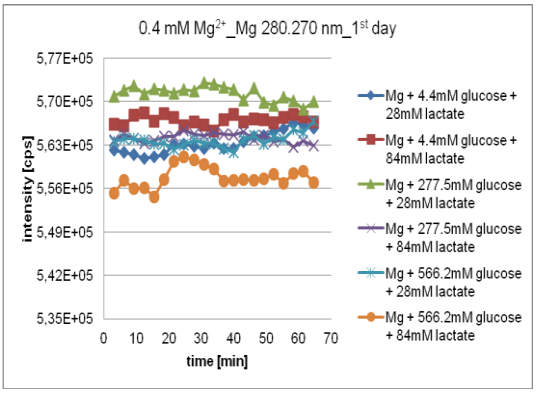

Figure 9-98: The intensity of Mg 280.270 nm by the determination of 0.4 mmol L^{-1} Mg^{2+} in glucose and lactate matrices (1st day)

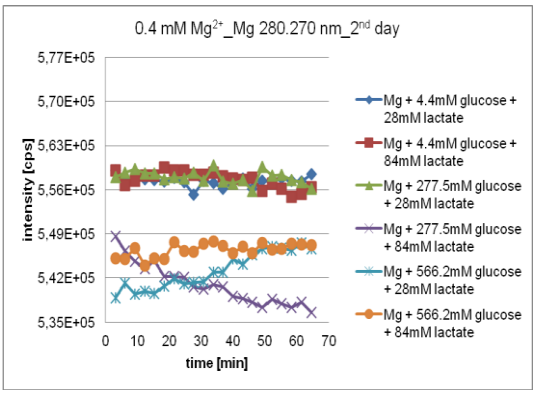

Figure 9-99: The intensity of Mg 280.270 nm by the determination of 0.4 mmol L^{-1} Mg^{2+} in glucose and lactate matrices (2nd day)

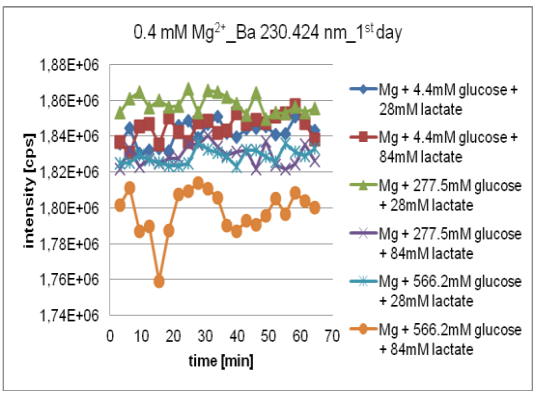

Figure 9-100: The intensity of Ba 230.424 nm by the determination of 0.4 mmol L^{-1} Mg^{2+} in glucose and lactate matrices (1st day)

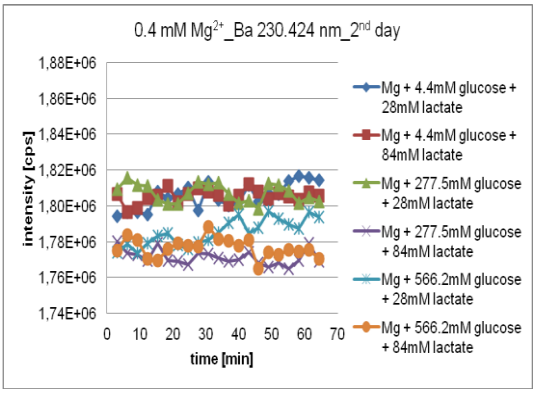

Figure 9-101: The intensity of Ba 230.424 nm by the determination of 0.4 mmol L^{-1} Mg^{2+} in glucose and lactate matrices (2nd day)

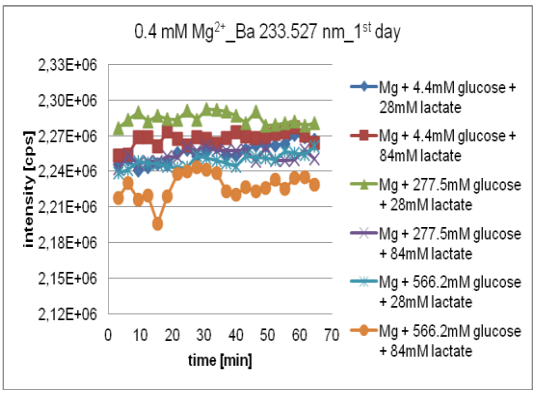

Figure 9-102: The intensity of Ba 233.527 nm by the determination of 0.4 mmol L^{-1} Mg^{2+} in glucose and lactate matrices (1st day)

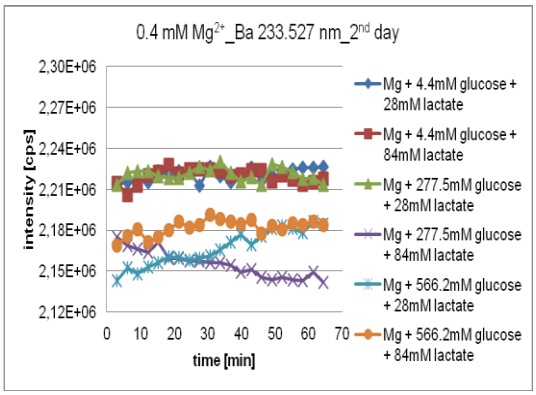

Figure 9-103: The intensity of Ba 233.527 nm by the determination of 0.4 mmol L^{-1} Mg^{2+} in glucose and lactate matrices (2nd day)

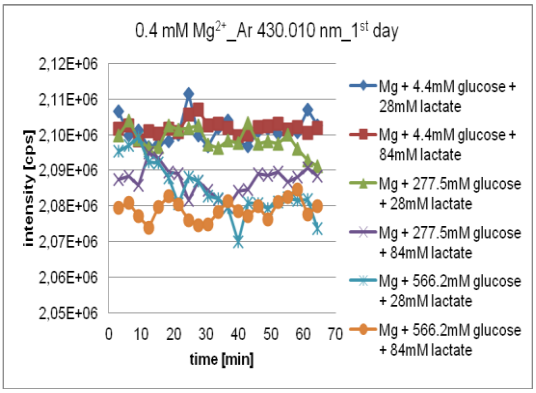

Figure 9-104: The intensity of Ar 430.010 nm by the determination of 0.4 mmol L^{-1} Mg^{2+} in glucose and lactate matrices (1st day)

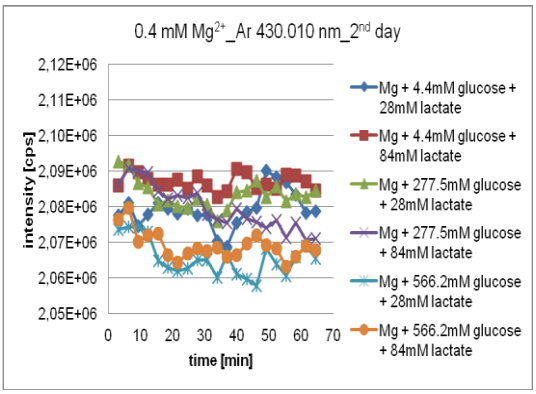

Figure 9-105: The intensity of Ar 430.010 nm by the determination of 0.4 mmol L^{-1} Mg^{2+} in glucose and lactate matrices (2nd day)

9.5.2 Attachments on the matrix effects on the determination of the highest magnesium concentration (24 mmol L^{-1})

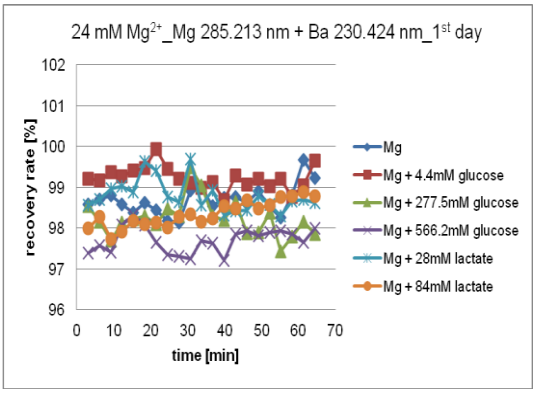

Figure 9-106: Recovery rates by the determination of 24 mmol L^{-1} Mg^{2+} in glucose or lactate matrices, with Mg 285.213 nm + Ba 230.424 nm (1st day)

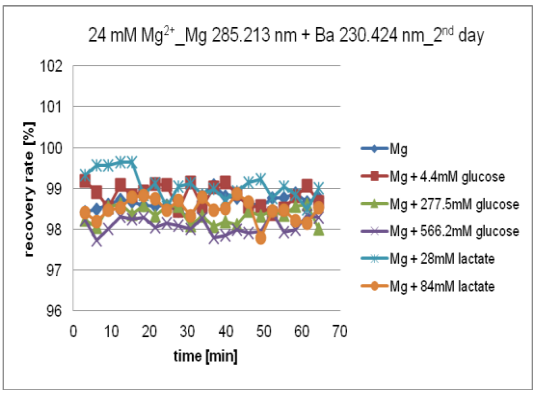

Figure 9-107: Recovery rates by the determination of 24 mmol L^{-1} Mg^{2+} in glucose or lactate matrices, with Mg 285.213 nm + Ba 230.424 nm (2nd day)

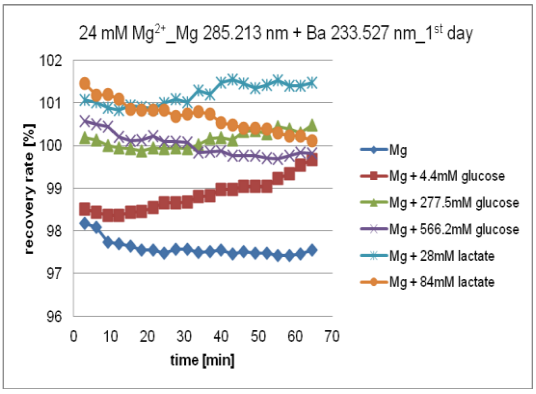

Figure 9-108: Recovery rates by the determination of 24 mmol L^{-1} Mg^{2+} in glucose or lactate matrices, with Mg 285.213 nm + Ba 233.527 nm (1st day)

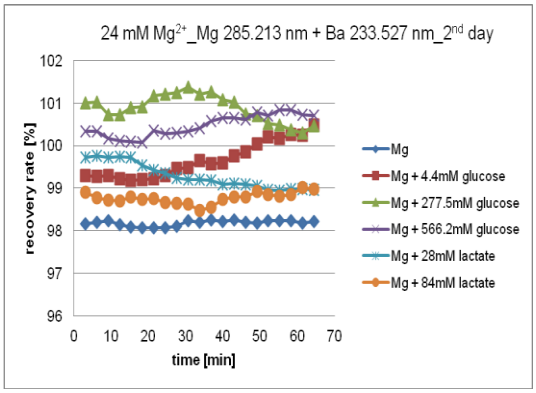

Figure 9-109: Recovery rates by the determination of 24 mmol L^{-1} Mg^{2+} in glucose or lactate matrices, with Mg 285.213 nm + Ba 233.527 nm (2nd day)

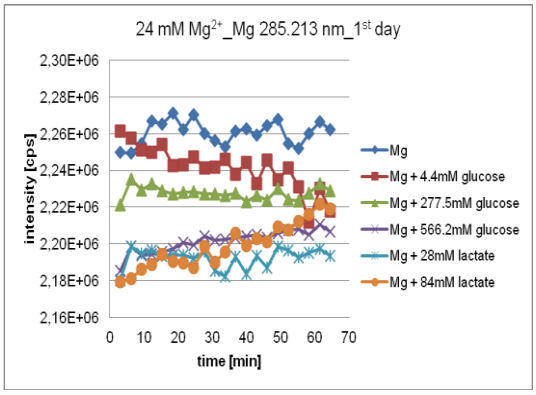

Figure 9-110: The intensity of Mg 285.213 nm by the determination of 24 mmol L^{-1} Mg^{2+} in glucose or lactate matrices (1st day)

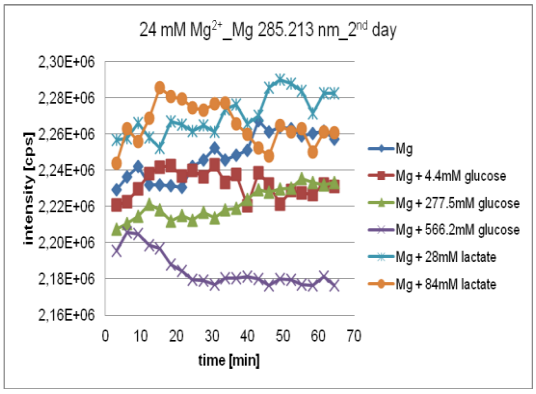

Figure 9-111: The intensity of Mg 285.213 nm by the determination of 24 mmol L^{-1} Mg^{2+} in glucose or lactate matrices (2nd day)

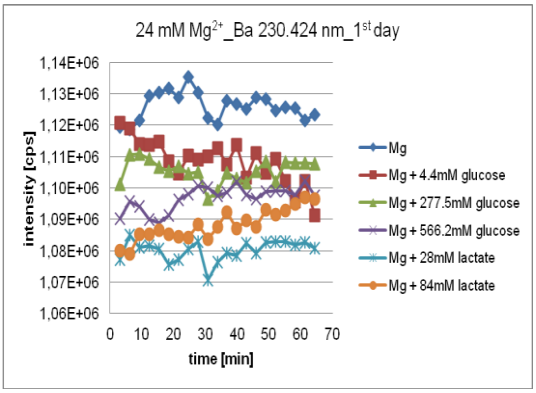

Figure 9-112: The intensity of Ba 230.424 nm by the determination of 24 mmol L^{-1} Mg^{2+} in glucose or lactate matrices (1st day)

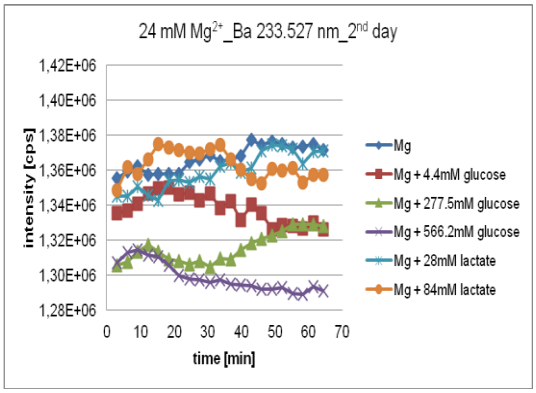

Figure 9-115: The intensity of Ba 233.527 nm by the determination of 24 mmol L^{-1} Mg^{2+} in glucose or lactate matrices (2nd day)

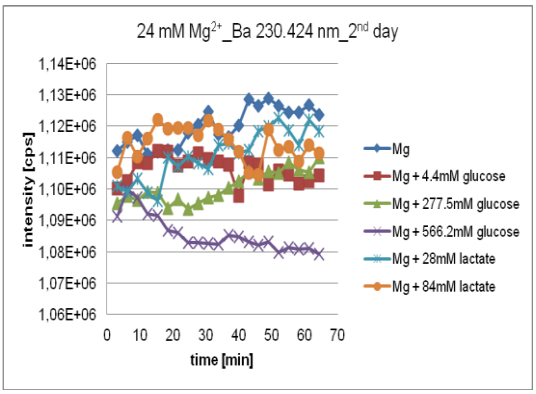

Figure 9-113: The intensity of Ba 230.424 nm by the determination of 24 mmol L^{-1} Mg^{2+} in glucose or lactate matrices (2nd day)

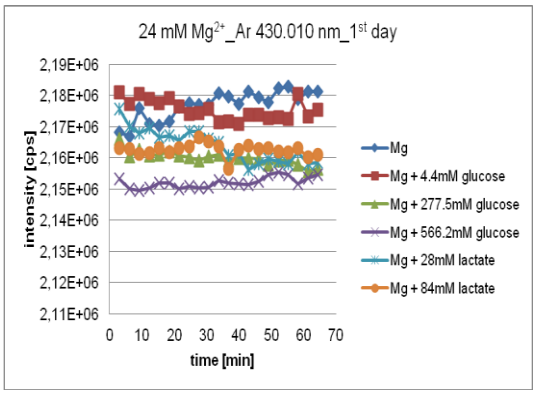

Figure 9-116: The intensity of Ar 430.010 nm by the determination of 24 mmol L^{-1} Mg^{2+} in glucose or lactate matrices (1st day)

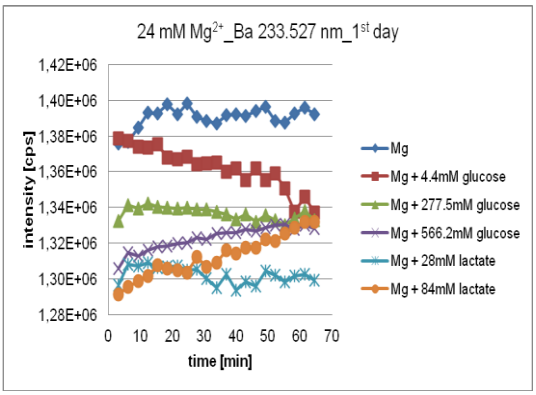

Figure 9-114: The intensity of Ba 233.527 nm by the determination of 24 mmol L^{-1} Mg^{2+} in glucose or lactate matrices (1st day)

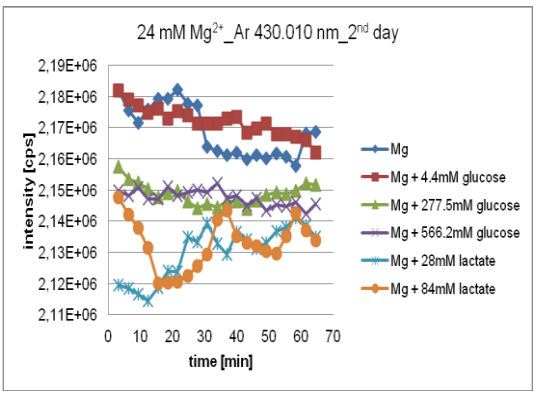

Figure 9-117: The intensity of Ar 430.010 nm by the determination of 24 mmol L^{-1} Mg^{2+} in glucose or lactate matrices (2nd day)

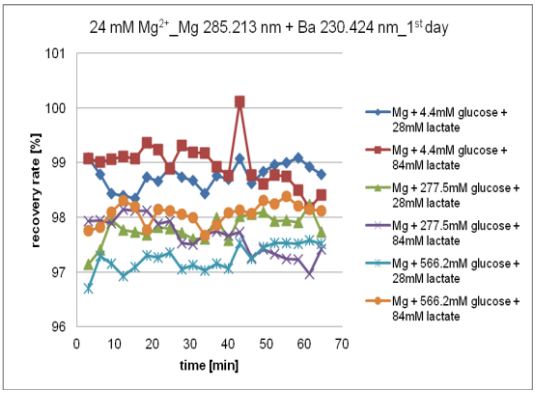

Figure 9-118: Recovery rates by the determination of 24 mmol L^{-1} Mg^{2+} in glucose and lactate matrices, with Mg 285.213 nm + Ba 230.424 nm (1st day)

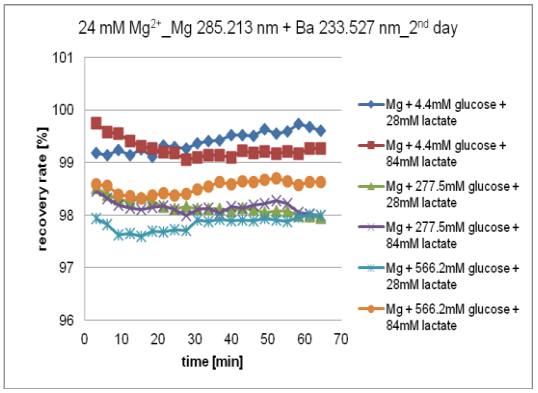

Figure 9-121: Recovery rates by the determination of 24 mmol L^{-1} Mg^{2+} in glucose and lactate matrices, with Mg 285.213 nm + Ba 233.527 nm (2nd day)

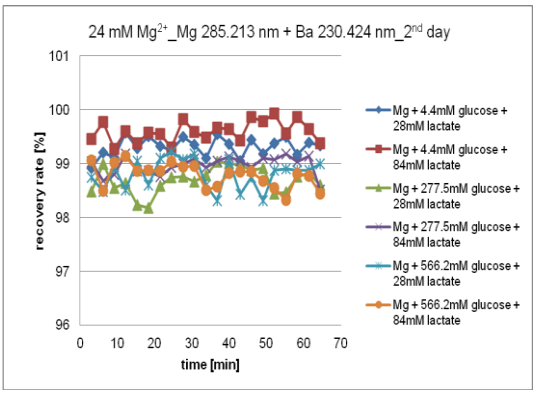

Figure 9-119: Recovery rates by the determination of 24 mmol L^{-1} Mg^{2+} in glucose and lactate matrices, with Mg 285.213 nm + Ba 230.424 nm (2nd day)

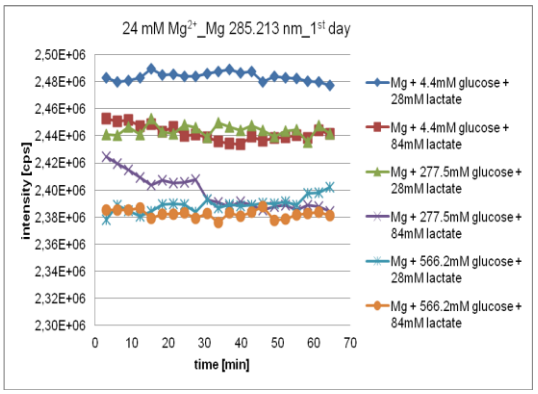

Figure 9-122: The intensity of Mg 285.213 nm by the determination of 24 mmol L^{-1} Mg^{2+} in glucose and lactate matrices (1st day)

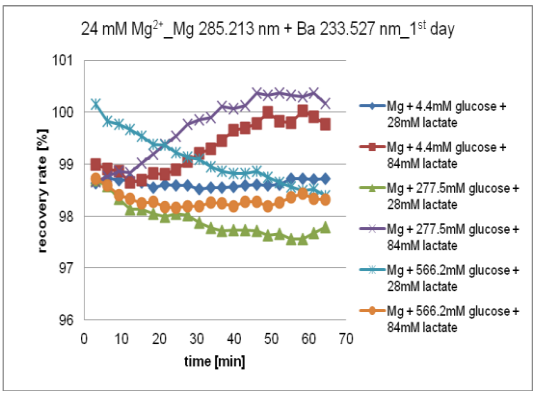

Figure 9-120: Recovery rates by the determination of 24 mmol L^{-1} Mg^{2+} in glucose and lactate matrices, with Mg 285.213 nm + Ba 233.527 nm (1st day)

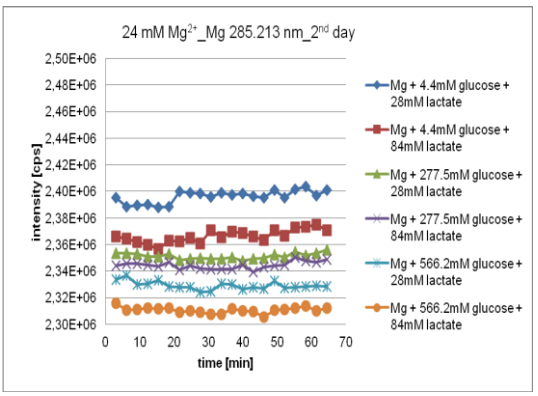

Figure 9-123: The intensity of Mg 285.213 nm by the determination of 24 mmol L^{-1} Mg^{2+} in glucose and lactate matrices (2nd day)

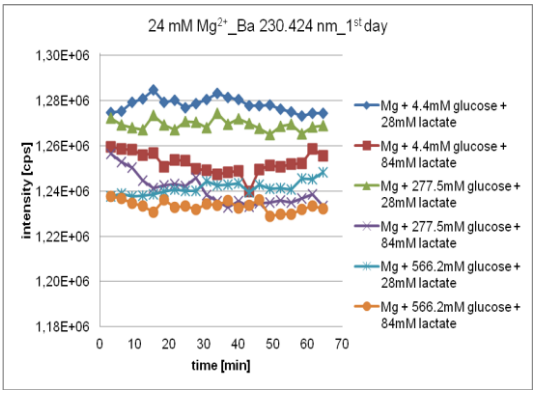

Figure 9-124: The intensity of Ba 230.424 nm by the determination of 24 mmol L^{-1} Mg^{2+} in glucose and lactate matrices (1st day)

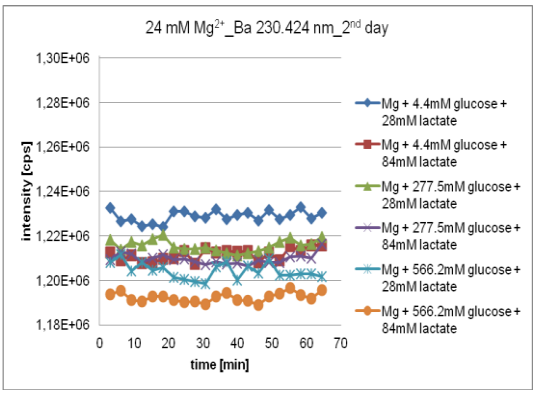

Figure 9-125: The intensity of Ba 230.424 nm by the determination of 24 mmol L^{-1} Mg^{2+} in glucose and lactate matrices (2nd day)

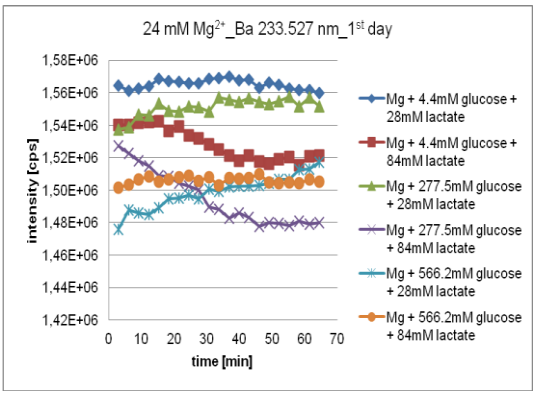

Figure 9-126: The intensity of Ba 233.527 nm by the determination of 24 mmol L^{-1} Mg^{2+} in glucose and lactate matrices (1st day)

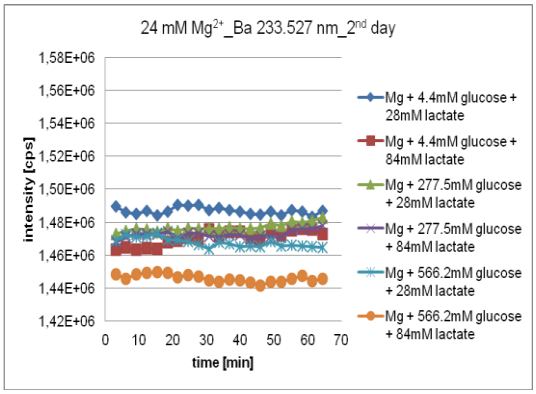

Figure 9-127: The intensity of Ba 233.527 nm by the determination of 24 mmol L^{-1} Mg^{2+} in glucose and lactate matrices (2nd day)

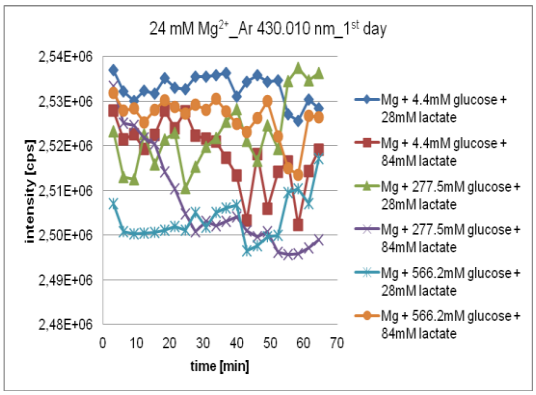

Figure 9-128: The intensity of Ar 430.010 nm by the determination of 24 mmol L^{-1} Mg^{2+} in glucose and lactate matrices (1st day)

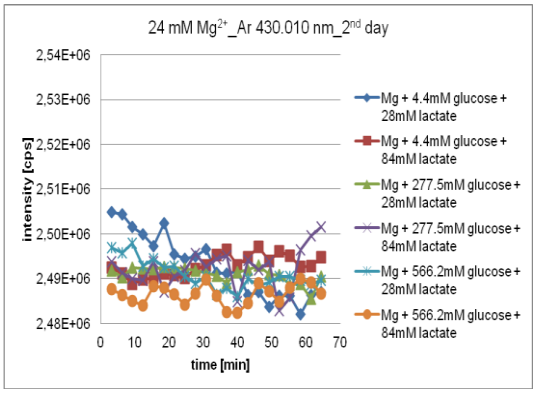

Figure 9-129: The intensity of Ar 430.010 nm by the determination of 24 mmol L^{-1} Mg^{2+} in glucose and lactate matrices (2nd day)

9.6 Attachments on the effect of glucose and lactate on the determination of calcium by ICP-OES

9.6.1 Attachments on the matrix effects on the determination of the lowest calcium concentration (0.8 mmol L^{-1})

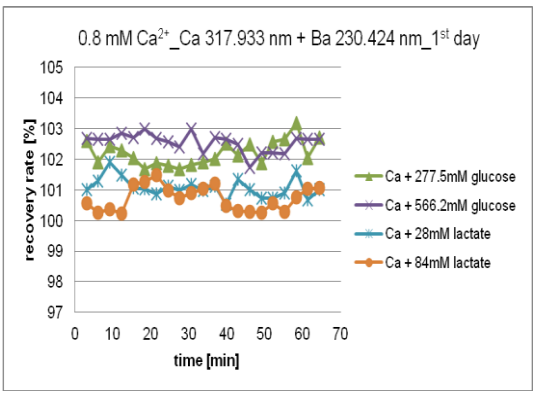

Figure 9-130: Recovery rates by the determination of 0.8 mmol L^{-1} Ca^{2+} in glucose or lactate matrices, with Ca 317.933 nm + Ba 230.424 nm (1st day)

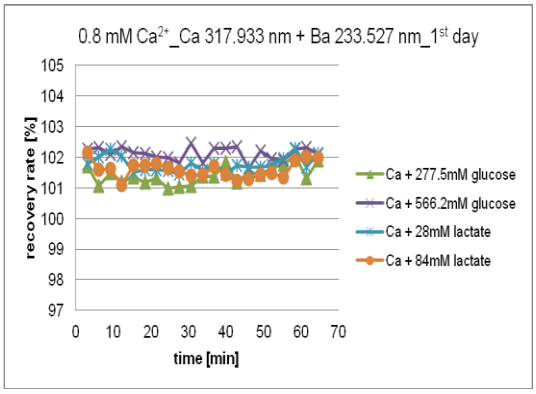

Figure 9-132: Recovery rates by the determination of 0.8 mmol L^{-1} Ca^{2+} in glucose or lactate matrices, with Ca 317.933 nm + Ba 233.527 nm (1st day)

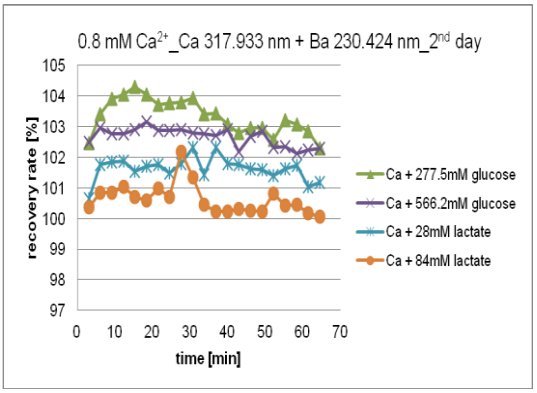

Figure 9-131: Recovery rates by the determination of 0.8 mmol L^{-1} Ca^{2+} in glucose or lactate matrices, with Ca 317.933 nm + Ba 230.424 nm (2nd day)

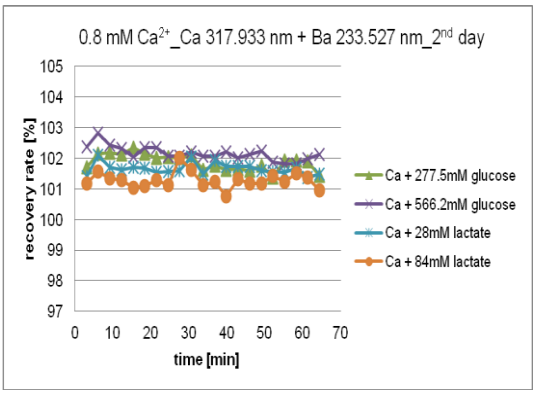

Figure 9-133: Recovery rates by the determination of 0.8 mmol L^{-1} Ca^{2+} in glucose or lactate matrices, with Ca 317.933 nm + Ba 233.527 nm (2nd day)

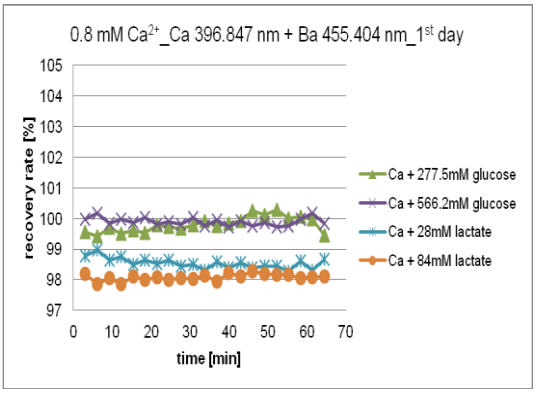

Figure 9-134: Recovery rates by the determination of 0.8 mmol L^{-1} Ca^{2+} in glucose or lactate matrices, with Ca 396.847 nm + Ba 455.404 nm (1st day)

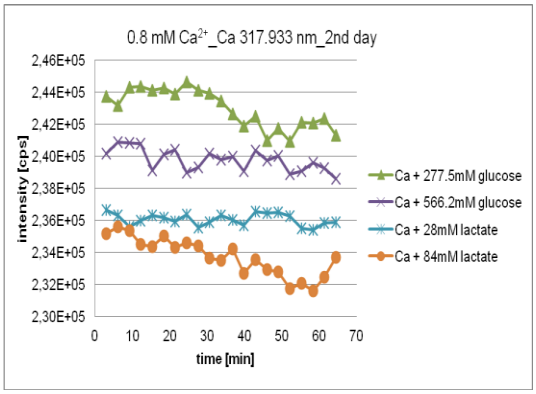

Figure 9-137: The intensity of Ca 317.933 nm by the determination of 0.8 mmol L^{-1} Ca^{2+} in glucose or lactate matrices (2nd day)

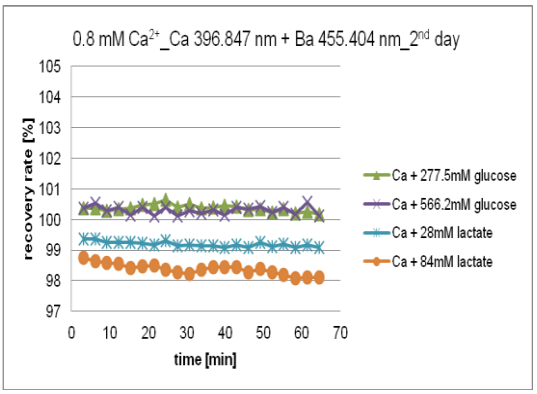

Figure 9-135: Recovery rates by the determination of 0.8 mmol L^{-1} Ca^{2+} in glucose or lactate matrices, with Ca 396.847 nm + Ba 455.404 nm (2nd day)

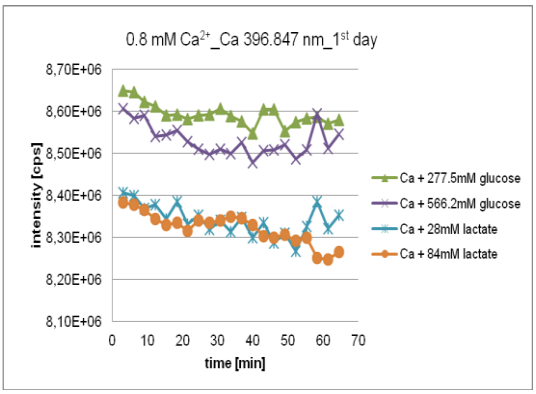

Figure 9-138: The intensity of Ca 396.847 nm by the determination of 0.8 mmol L^{-1} Ca^{2+} in glucose or lactate matrices (1st day)

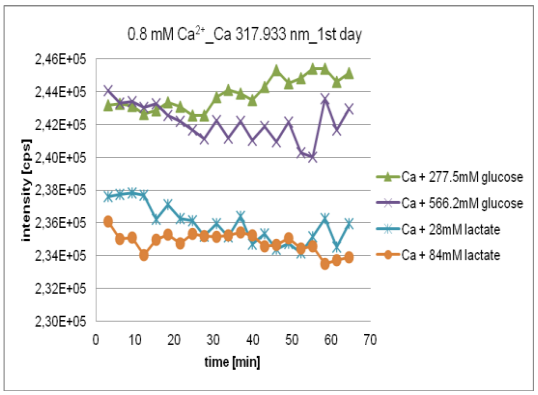

Figure 9-136: The intensity of Ca 317.933 nm by the determination of 0.8 mmol L^{-1} Ca^{2+} in glucose or lactate matrices (1st day)

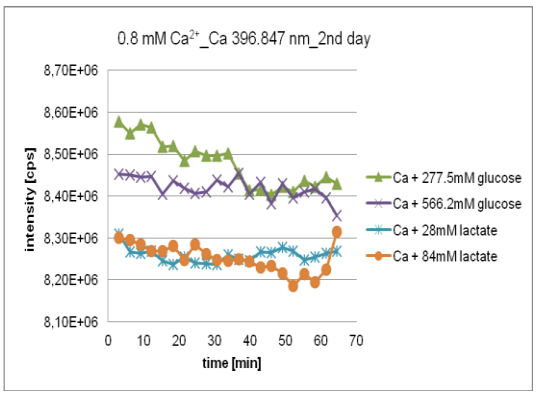

Figure 9-139: The intensity of Ca 396.847 nm by the determination of 0.8 mmol L^{-1} Ca^{2+} in glucose or lactate matrices (2nd day)

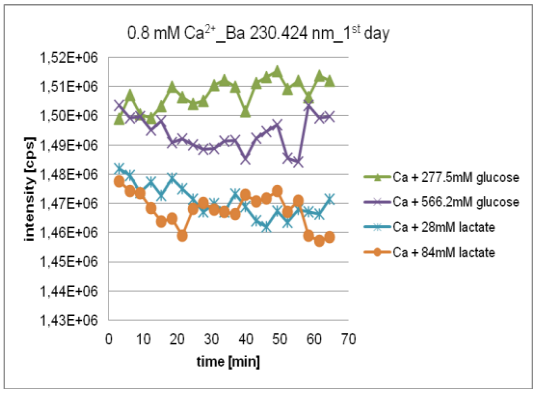

Figure 9-140: The intensity of Ba 230.424 nm by the determination of 0.8 mmol L^{-1} Ca^{2+} in glucose or lactate matrices (1st day)

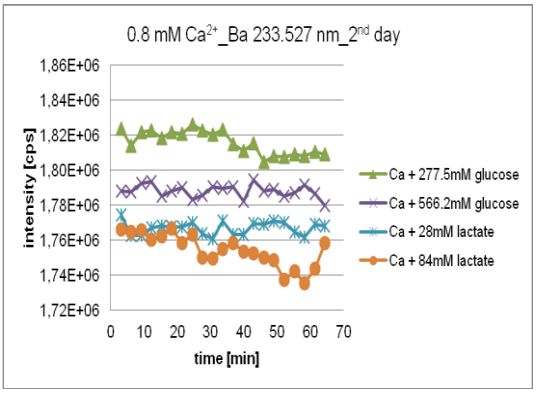

Figure 9-143: The intensity of Ba 233.527 nm by the determination of 0.8 mmol L^{-1} Ca^{2+} in glucose or lactate matrices (2nd day)

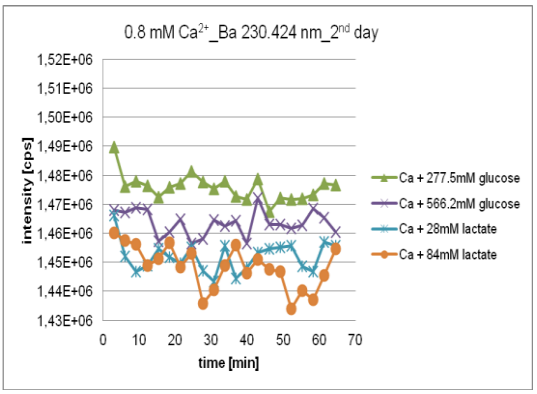

Figure 9-141: The intensity of Ba 230.424 nm by the determination of 0.8 mmol L^{-1} Ca^{2+} in glucose or lactate matrices (2nd day)

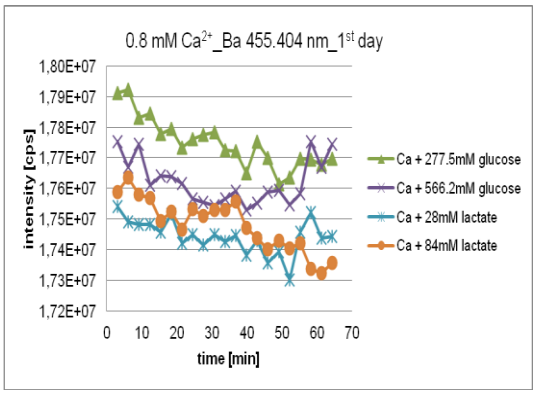

Figure 9-144: The intensity of Ba 455.404 nm by the determination of 0.8 mmol L^{-1} Ca^{2+} in glucose or lactate matrices (1st day)

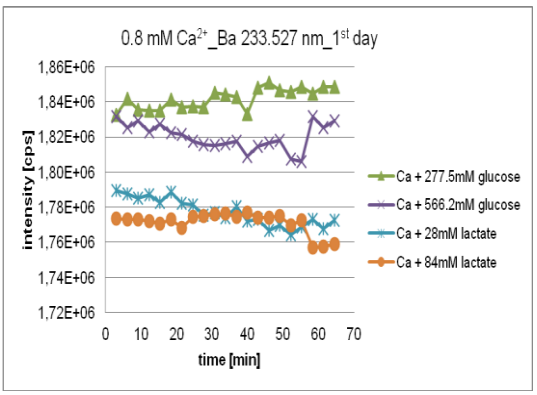

Figure 9-142: The intensity of Ba 233.527 nm by the determination of 0.8 mmol L^{-1} Ca^{2+} in glucose or lactate matrices (1st day)

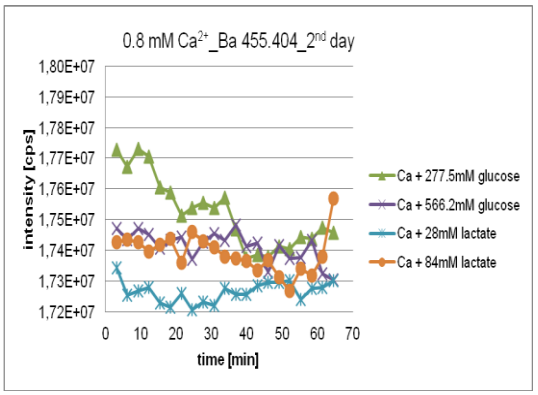

Figure 9-145: The intensity of Ba 455.404 nm by the determination of 0.8 mmol L^{-1} Ca^{2+} in glucose or lactate matrices (2nd day)

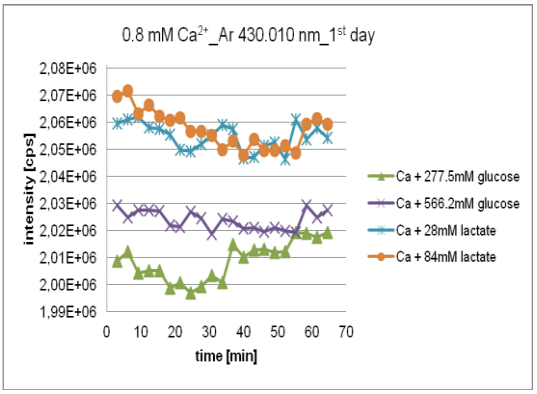

Figure 9-146: The intensity of Ar 430.010 nm by the determination of 0.8 mmol L^{-1} Ca^{2+} in glucose or lactate matrices (1st day)

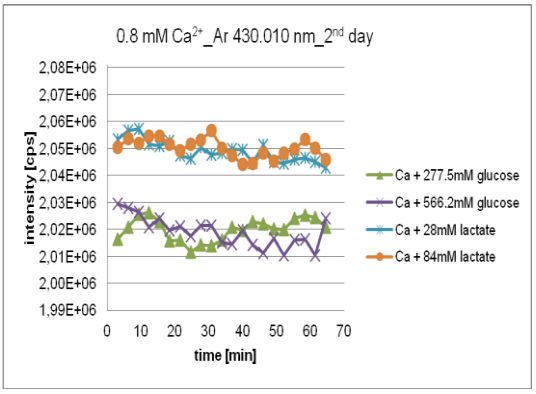

Figure 9-147: The intensity of Ar 430.010 nm by the determination of 0.8 mmol L^{-1} Ca^{2+} in glucose or lactate matrices (2nd day)

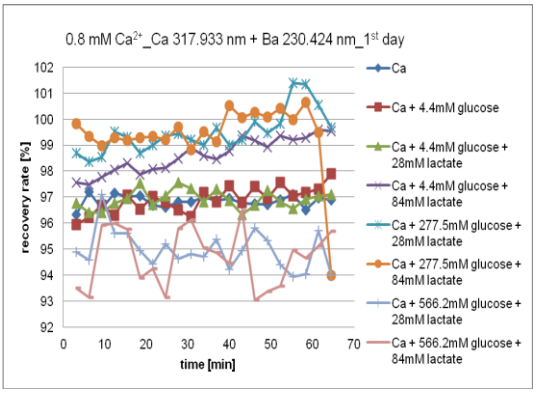

Figure 9-148: Recovery rates by the determination of 0.8 mmol L^{-1} Ca^{2+} in glucose and lactate matrices, with Ca 317.937 nm + Ba 230.424 nm (1st day)

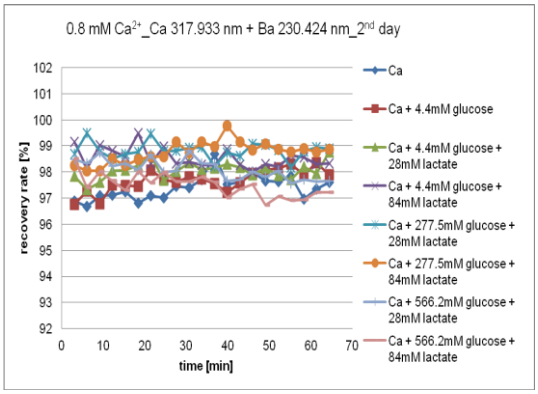

Figure 9-149: Recovery rates by the determination of 0.8 mmol L^{-1} Ca^{2+} in glucose and lactate matrices, with Ca 317.937 nm + Ba 230.424 nm (2nd day)

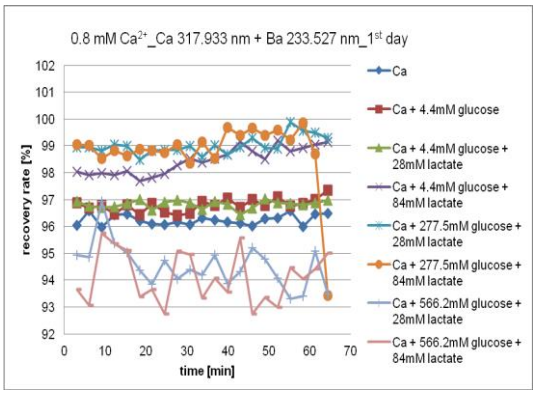

Figure 9-150: Recovery rates by the determination of 0.8 mmol L^{-1} Ca^{2+} in glucose and lactate matrices, with Ca 317.937 nm + Ba 233.527 nm (1st day)

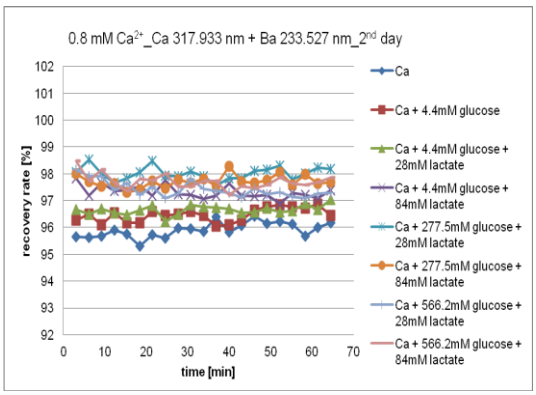

Figure 9-151: Recovery rates by the determination of 0.8 mmol L^{-1} Ca^{2+} in glucose and lactate matrices, with Ca 317.937 nm + Ba 233.527 nm (2nd day)

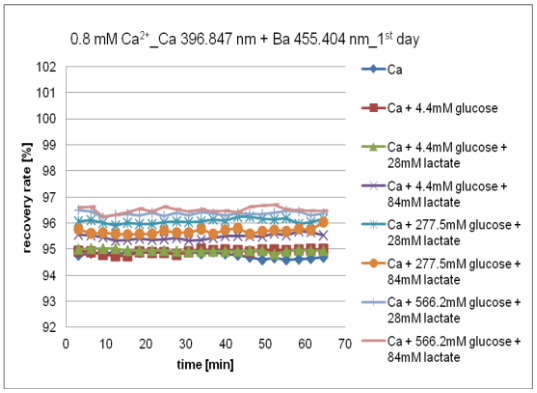

Figure 9-152: Recovery rates by the determination of 0.8 mmol L^{-1} Ca^{2+} in glucose and lactate matrices, with Ca 396.847 nm + Ba 455.404 nm (1st day)

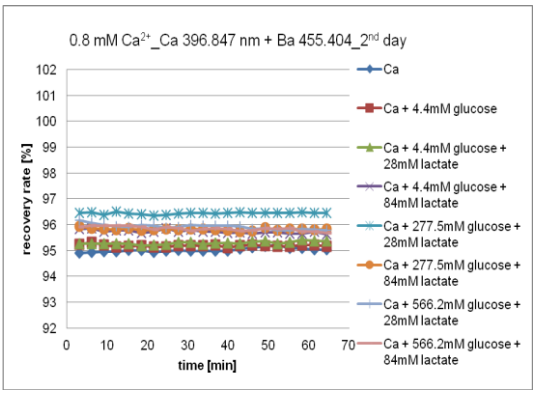

Figure 9-153: Recovery rates by the determination of 0.8 mmol L^{-1} Ca^{2+} in glucose and lactate matrices, with Ca 396.847 nm + Ba 455.404 nm (2nd day)

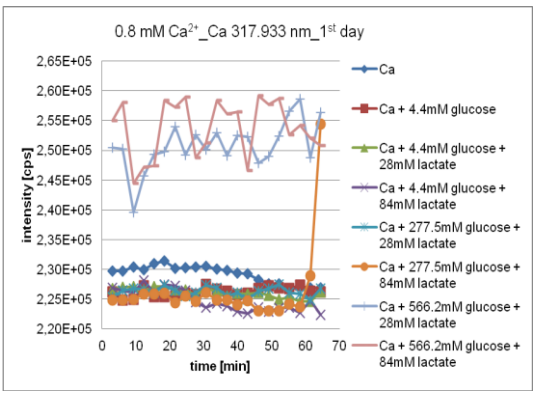

Figure 9-154: The intensity of Ca 317.933 nm by the determination of 0.8 mmol L^{-1} Ca^{2+} in glucose and lactate matrices (1st day)

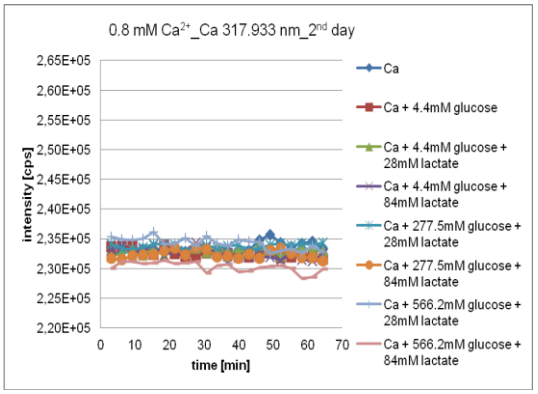

Figure 9-155: The intensity of Ca 317.933 nm by the determination of 0.8 mmol L^{-1} Ca^{2+} in glucose and lactate matrices (2nd day)

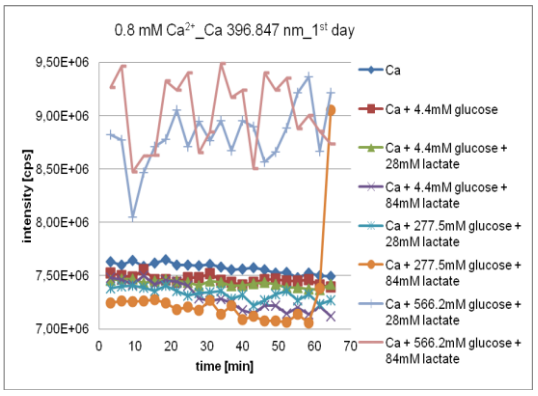

Figure 9-156: The intensity of Ca 396.847 nm by the determination of 0.8 mmol L^{-1} Ca^{2+} in glucose and lactate matrices (1st day)

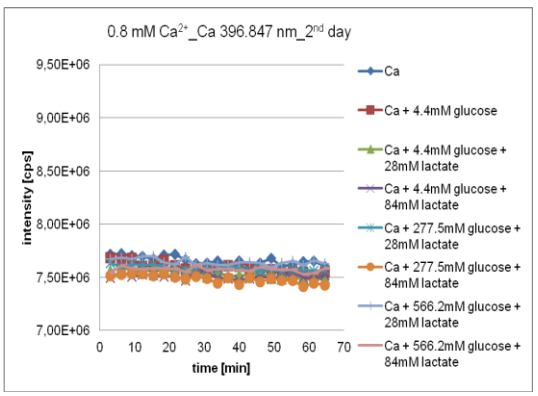

Figure 9-157: The intensity of Ca 396.847 nm by the determination of 0.8 mmol L^{-1} Ca^{2+} in glucose and lactate matrices (2nd day)

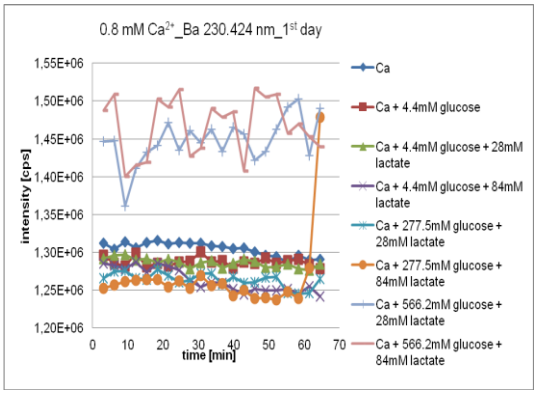

Figure 9-158: The intensity of Ba 230.424 nm by the determination of 0.8 mmol L^{-1} Ca^{2+} in glucose and lactate matrices (1st day)

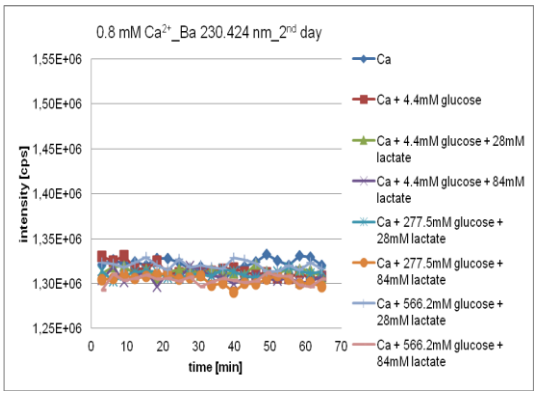

Figure 9-159: The intensity of Ba 230.424 nm by the determination of 0.8 mmol L^{-1} Ca^{2+} glucose and lactate matrices (2nd day)

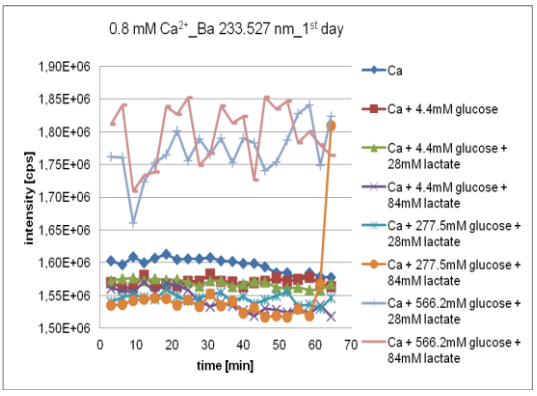

Figure 9-160: The intensity of Ba 233.527 nm by the determination of 0.8 mmol L^{-1} Ca^{2+} in glucose and lactate matrices (1st day)

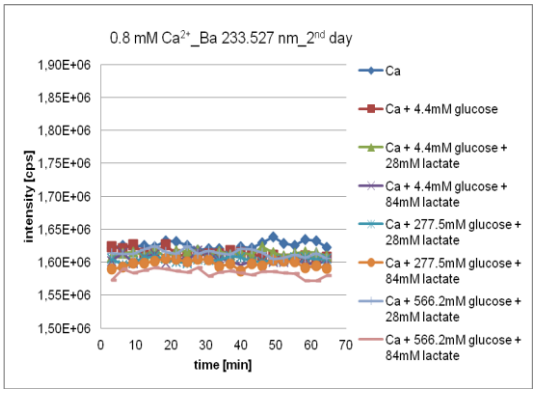

Figure 9-161: The intensity of Ba 233.527 nm by the determination of 0.8 mmol L^{-1} Ca^{2+} in glucose and lactate matrices (2nd day)

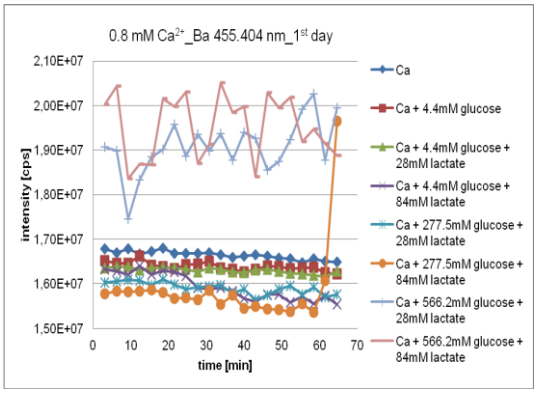

Figure 9-162: The intensity of Ba 455.404 nm by the determination of 0.8 mmol L^{-1} Ca^{2+} in glucose and lactate matrices (1st day)

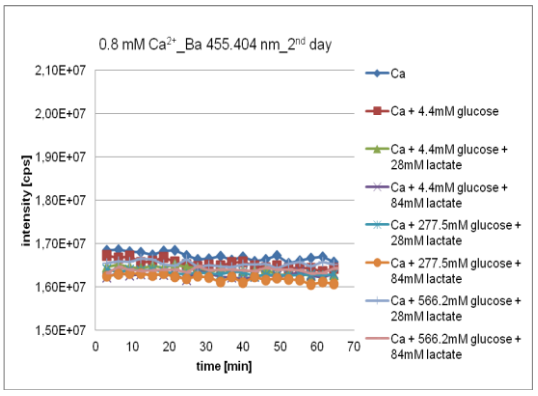

Figure 9-163: The intensity of Ba 455.404 nm by the determination of 0.8 mmol L^{-1} Ca^{2+} in glucose and lactate matrices (2nd day)

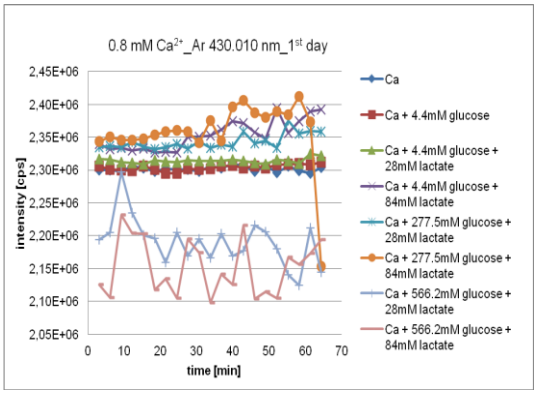

Figure 9-164: The intensity of Ar 430.010 nm by the determination of 0.8 mmol L^{-1} Ca^{2+} in glucose and lactate matrices (1st day)

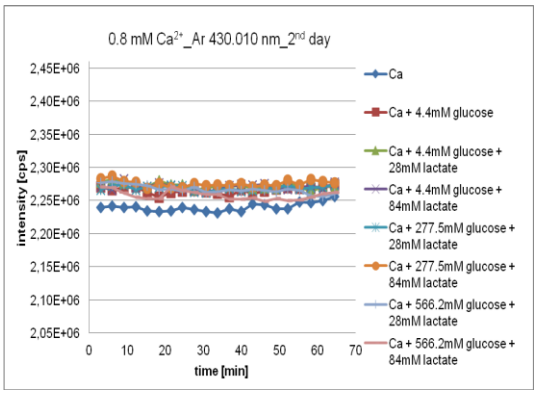

Figure 9-165: The intensity of Ar 430.010 nm by the determination of 0.8 mmol L^{-1} Ca^{2+} in glucose and lactate matrices (2nd day)

9.6.2 Attachments on the matrix effects on the determination of the highest calcium concentration (36 mmol L^{-1})

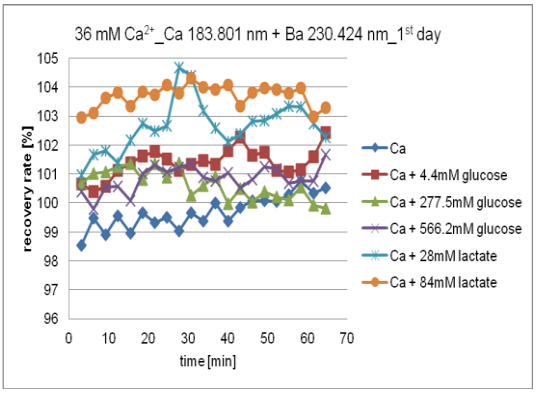

Figure 9-166: Recovery rates by the determination of 36 mmol L^{-1} Ca^{2+} in glucose or lactate matrices, with Ca 183.801 nm + Ba 230.424 nm (1st day)

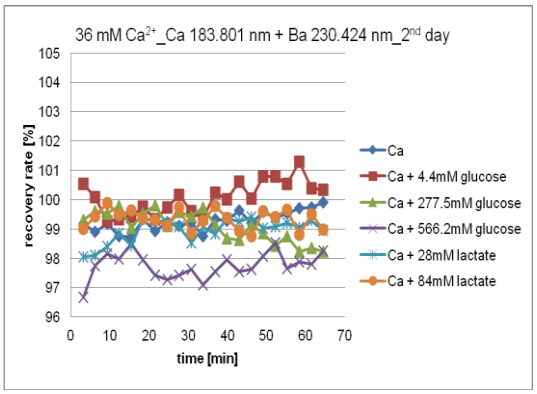

Figure 9-167: Recovery rates by the determination of 36 mmol L^{-1} Ca^{2+} in glucose or lactate matrices, with Ca 183.801 nm + Ba 230.424 nm (2nd day)

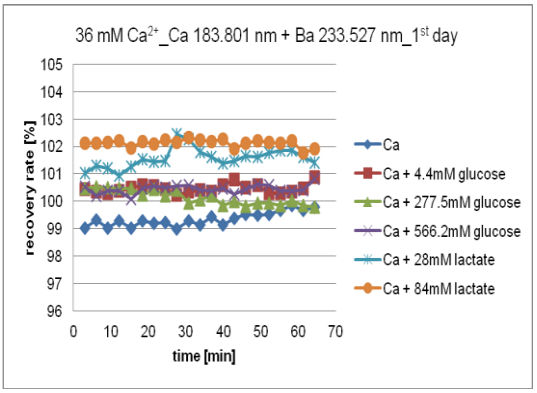

Figure 9-168: Recovery rates by the determination of 36 mmol L^{-1} Ca^{2+} in glucose or lactate matrices, with Ca 183.801 nm + Ba 233.527 nm (1st day)

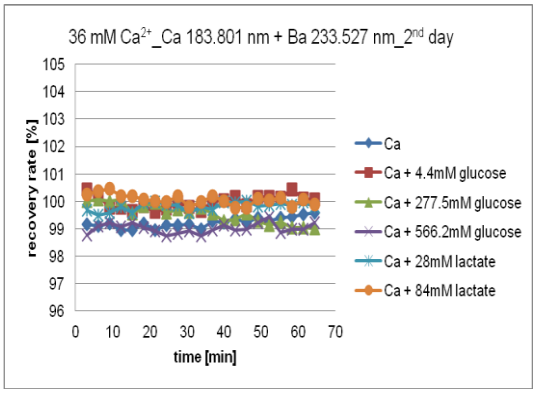

Figure 9-169: Recovery rates by the determination of 36 mmol L^{-1} Ca^{2+} in glucose or lactate matrices, with Ca 183.801 nm + Ba 233.527 nm (2nd day)

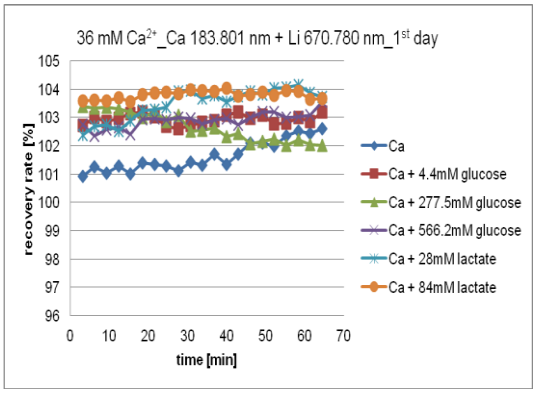

Figure 9-170: Recovery rates by the determination of 36 mmol L^{-1} Ca^{2+} in glucose or lactate matrices, with Ca 183.801 nm + Li 670.780 nm (1st day)

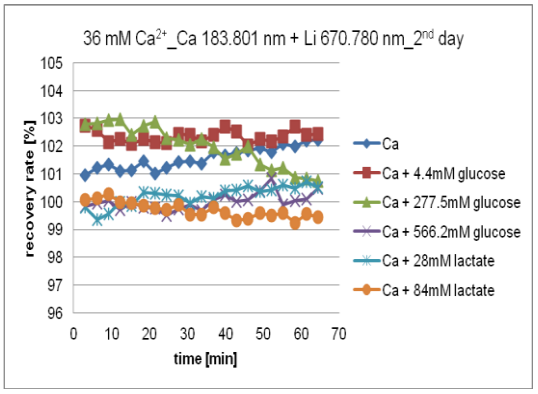

Figure 9-171: Recovery rates by the determination of 36 mmol L^{-1} Ca^{2+} in glucose or lactate matrices, with Ca 183.801 nm + Li 670.780 nm (2nd day)

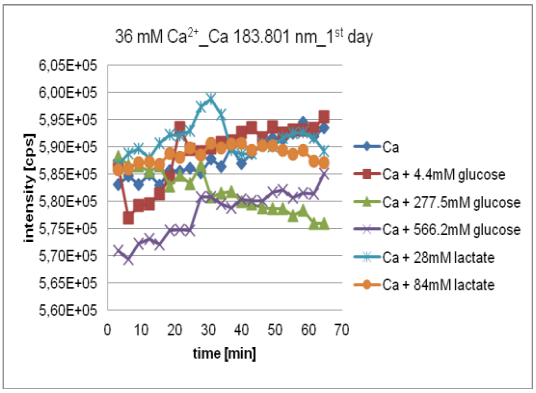

Figure 9-172: The intensity of Ca 183.801 nm by the determination of 36 mmol L^{-1} Ca^{2+} in glucose or lactate matrices (1st day)

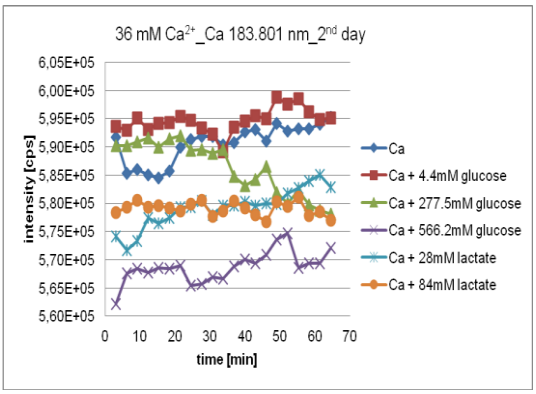

Figure 9-173: The intensity of Ca 183.801 nm by the determination of 36 mmol L^{-1} Ca^{2+} in glucose or lactate matrices (2nd day)

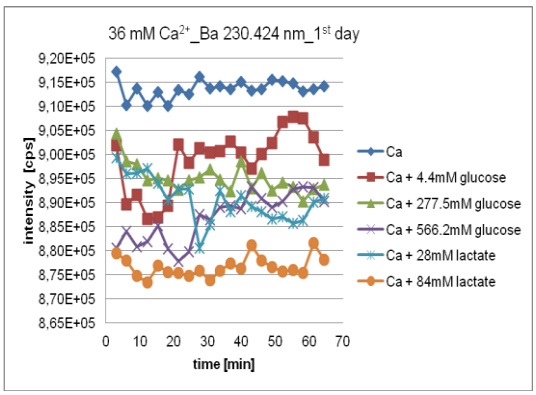

Figure 9-174: The intensity of Ba 230.424 nm by the determination of 36 mmol L^{-1} Ca^{2+} in glucose or lactate matrices (1st day)

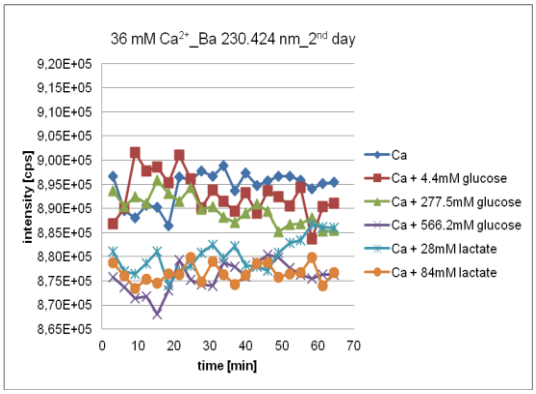

Figure 9-175: The intensity of Ba 230.424 nm by the determination of 36 mmol L^{-1} Ca^{2+} in glucose or lactate matrices (2nd day)

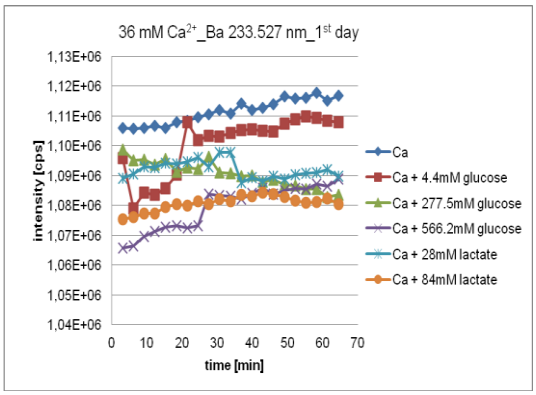

Figure 9-176: The intensity of Ba 233.527 nm by the determination of 36 mmol L^{-1} Ca^{2+} in glucose or lactate matrices (1st day)

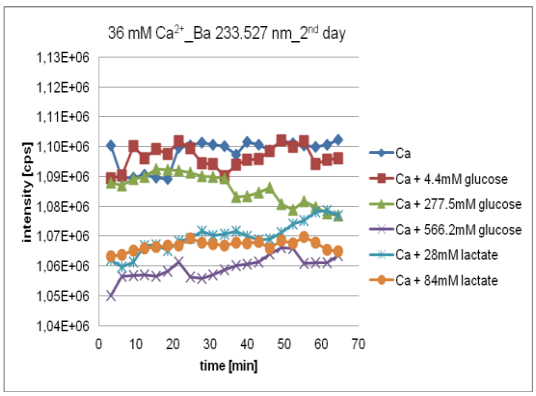

Figure 9-177: The intensity of Ba 233.527 nm by the determination of 36 mmol L^{-1} Ca^{2+} in glucose or lactate matrices (2nd day)

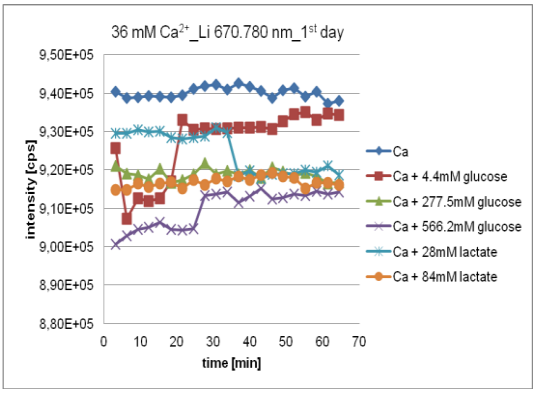

Figure 9-178: The intensity of Li 670.780 nm by the determination of 36 mmol L^{-1} Ca^{2+} in glucose or lactate matrices (1st day)

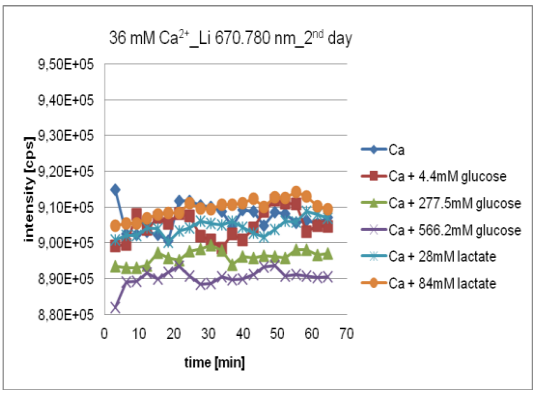

Figure 9-179: The intensity of Li 670.780 nm by the determination of 36 mmol L^{-1} Ca^{2+} in glucose or lactate matrices (2nd day)

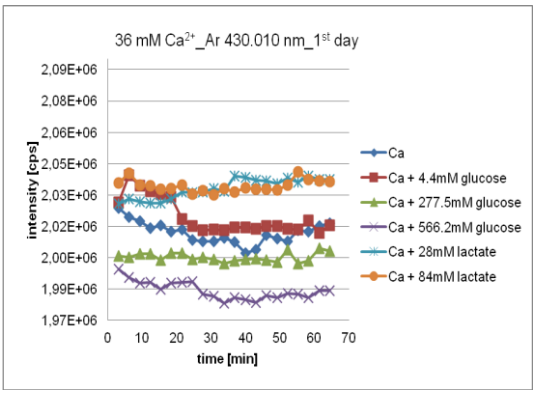

Figure 9-180: The intensity of Ar 430.010 nm by the determination of 36 mmol L^{-1} Ca^{2+} in glucose or lactate matrices (1st day)

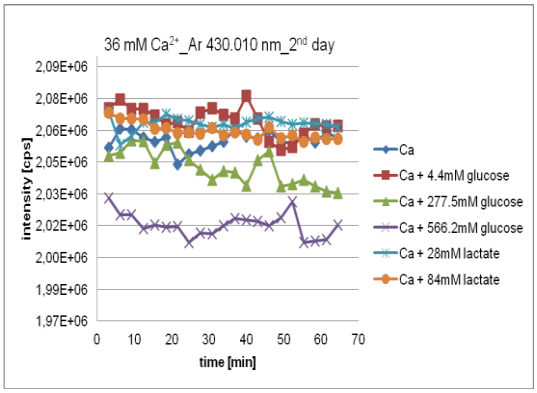

Figure 9-181: The intensity of Ar 430.010 nm by the determination of 36 mmol L^{-1} Ca^{2+} in glucose or lactate matrices (2nd day)

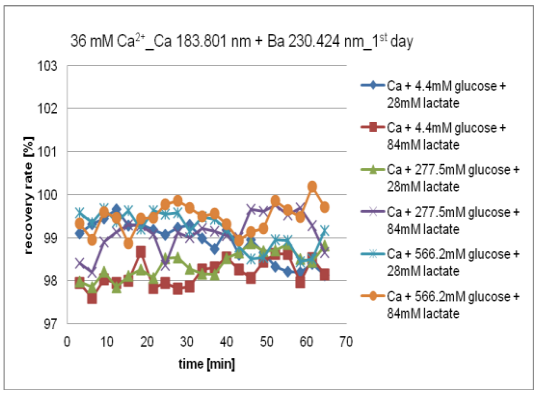

Figure 9-182: Recovery rates by the determination of 36 mmol L^{-1} Ca^{2+} in glucose and lactate matrices, with Ca 183.801 nm + Ba 230.424 nm (1st day)

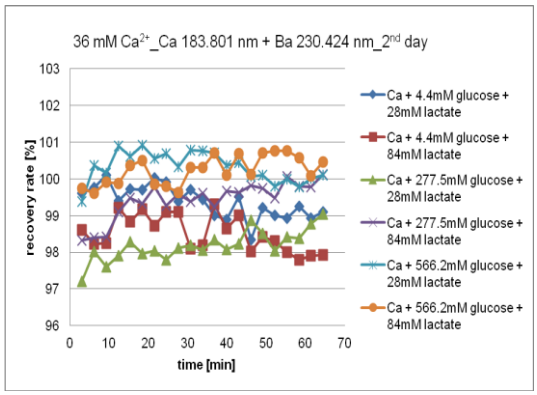

Figure 9-183: Recovery rates by the determination of 36 mmol L^{-1} Ca^{2+} in glucose and lactate matrices, with Ca 183.801 nm + Ba 230.424 nm (2nd day)

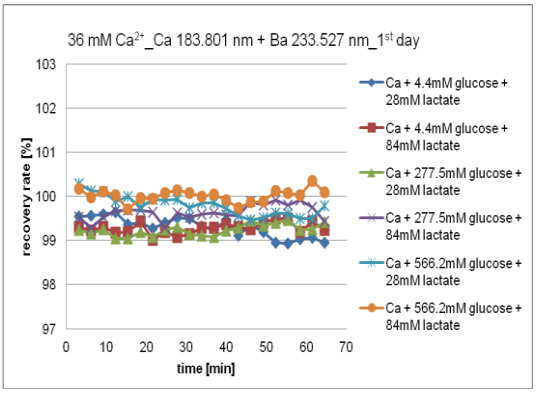

Figure 9-184: Recovery rates by the determination of 36 mmol L^{-1} Ca^{2+} in glucose and lactate matrices, with Ca 183.801 nm + Ba 233.527 nm (1st day)

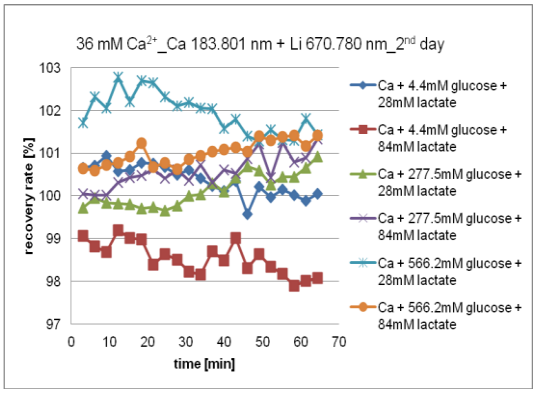

Figure 9-187: Recovery rates by the determination of 36 mmol L^{-1} Ca^{2+} in glucose and lactate matrices, with Ca 183.801 nm + Li 670.780 nm (2nd day)

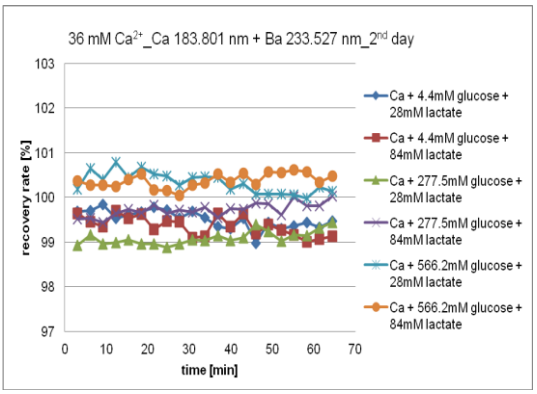

Figure 9-185: Recovery rates by the determination of 36 mmol L^{-1} Ca^{2+} in glucose and lactate matrices, with Ca 183.801 nm + Ba 233.527 nm (2nd day)

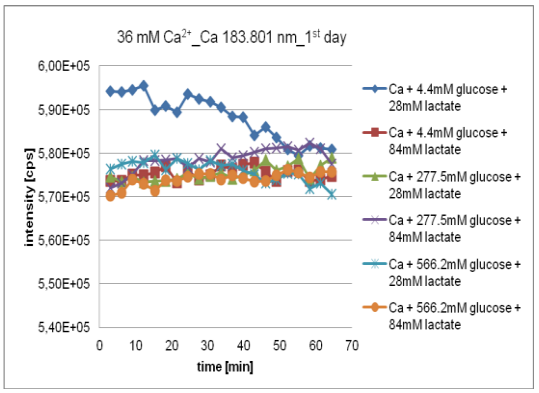

Figure 9-188: The intensity of Ca 183.801 nm by the determination of 36 mmol L^{-1} Ca^{2+} in glucose and lactate matrices (1st day)

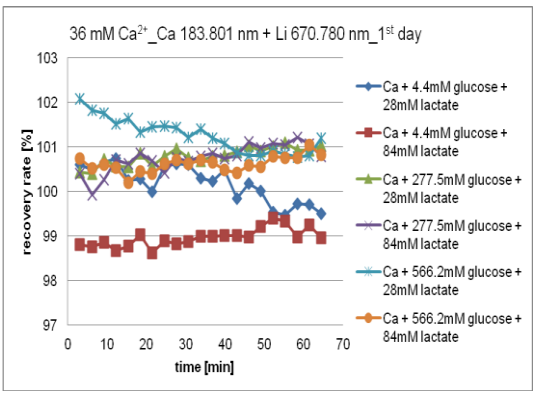

Figure 9-186: Recovery rates by the determination of 36 mmol L^{-1} Ca^{2+} in glucose and lactate matrices, with Ca 183.801 nm + Li 670.780 nm (1st day)

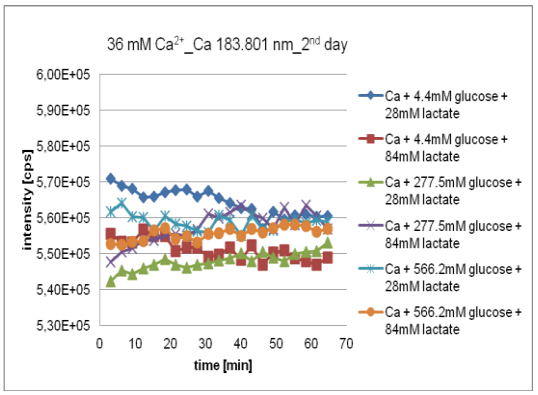

Figure 9-189: The intensity of Ca 183.801 nm by the determination of 36 mmol L^{-1} Ca^{2+} in glucose and lactate matrices (2nd day)

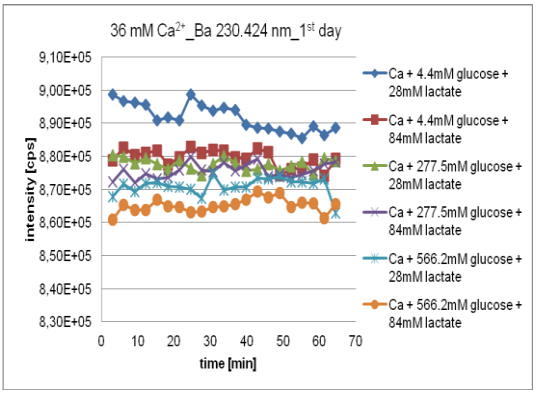

Figure 9-190: The intensity of Ba 230.424 nm by the determination of 36 mmol L^{-1} Ca^{2+} in glucose and lactate matrices (1st day)

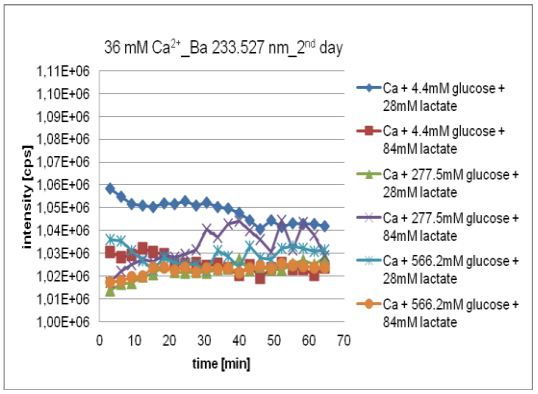

Figure 9-193: The intensity of Ba 233.527 nm by the determination of 36 mmol L^{-1} Ca^{2+} in glucose and lactate matrices (2nd day)

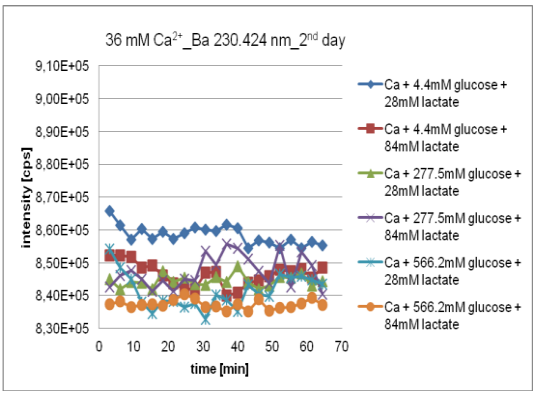

Figure 9-191: The intensity of Ba 230.424 nm by the determination of 36 mmol L^{-1} Ca^{2+} in glucose and lactate matrices (2nd day)

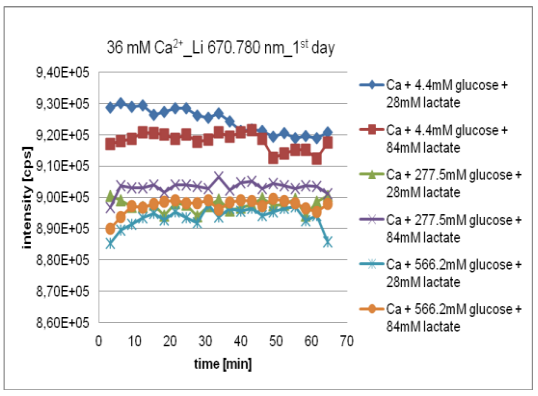

Figure 9-194: The intensity of Li 670.780 nm by the determination of 36 mmol L^{-1} Ca^{2+} in glucose and lactate matrices (1st day)

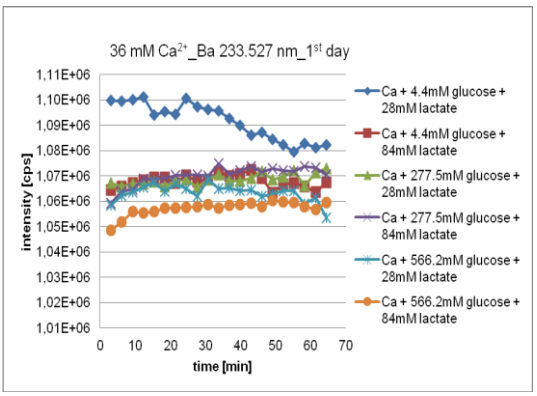

Figure 9-192: The intensity of Ba 233.527 nm by the determination of 36 mmol L^{-1} Ca^{2+} in glucose and lactate matrices (1st day)

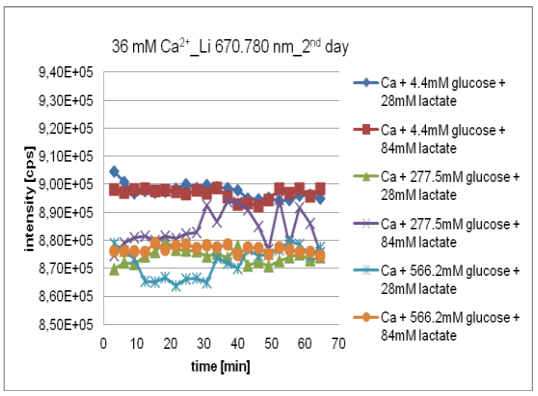

Figure 9-195: The intensity of Li 670.780 nm by the determination of 36 mmol L^{-1} Ca^{2+} in glucose and lactate matrices (2nd day)

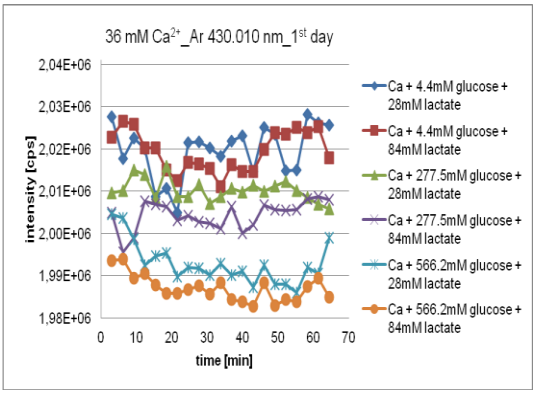

Figure 9-196:The intensity of Ar 430.010 nm by the determination of 36 mmol L^{-1} Ca^{2+} in glucose and lactate matrices (1^{st} day)

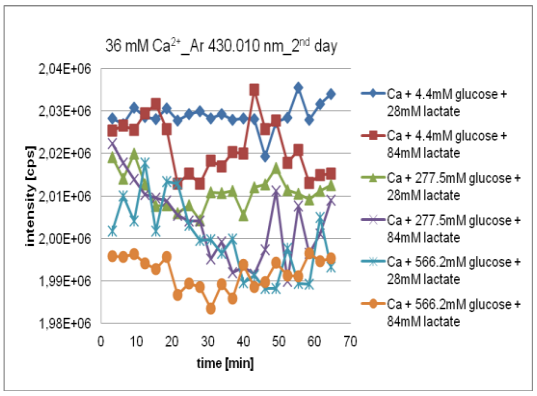

Figure 9-197: The intensity of Ar 430.010 nm by the determination of 36 mmol L^{-1} Ca^{2+} in glucose and lactate matrices (2^{nd} day)

9.7 Attachments on comparing the effect of lactate and some other α-hydroxy-carboxylates on the determination of calcium by ICP OES

9.7.1 Attachments on the effect of α-hydroxy-carboxylates on the determination of the lowest calcium concentration (0.8 mmol L^{-1})

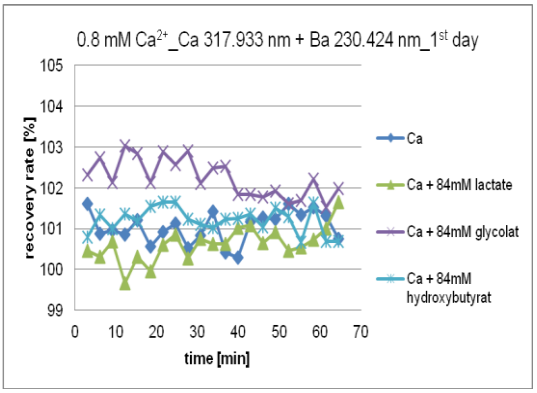

Figure 9-198: Recovery rates by the determination of 0.8 mmol L^{-1} Ca^{2+} in different α-hydroxy-carboxylate matrices, with Ca 317.933 nm + Ba 230.424 nm (1st day)

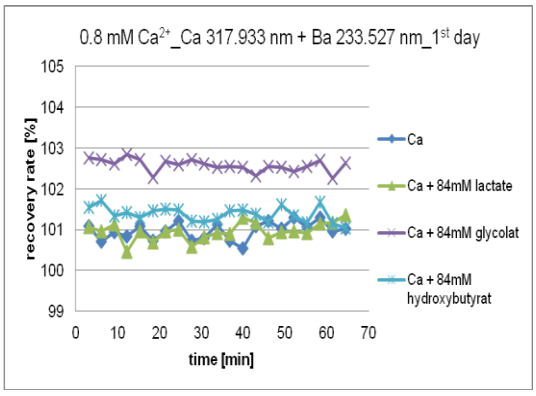

Figure 9-200: Recovery rates by the determination of 0.8 mmol L^{-1} Ca^{2+} in different α-hydroxy-carboxylate matrices, with Ca 317.933 nm + Ba 233.527 nm (1st day)

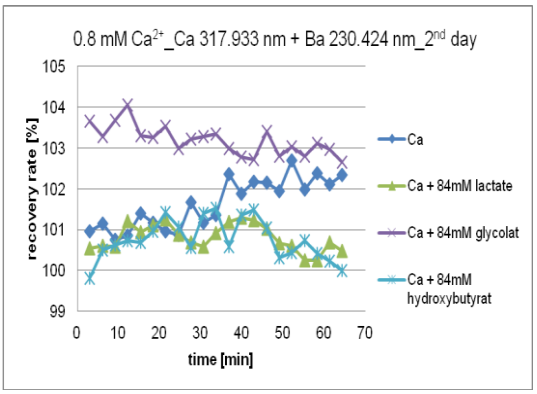

Figure 9-199: Recovery rates by the determination of 0.8 mmol L^{-1} Ca^{2+} in different α-hydroxy-carboxylate matrices, with Ca 317.933 nm + Ba 230.424 nm (2nd day)

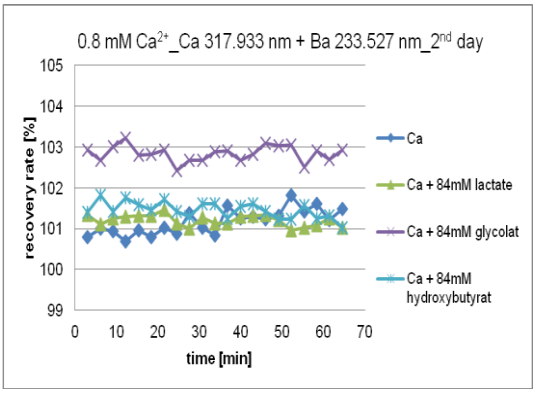

Figure 9-201: Recovery rates by the determination of 0.8 mmol L^{-1} Ca^{2+} in different α-hydroxy-carboxylate matrices, with Ca 317.933 nm + Ba 233.527 nm (2nd day)

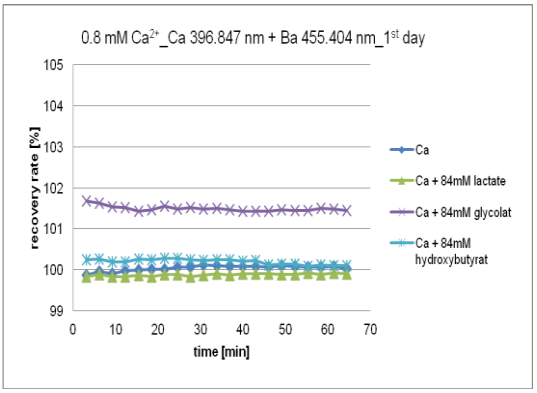

Figure 9-202: Recovery rates by the determination of 0.8 mmol L^{-1} Ca^{2+} in different α-hydroxy-carboxylate matrices, with Ca 396.847 nm + Ba 455.404 nm (1st day)

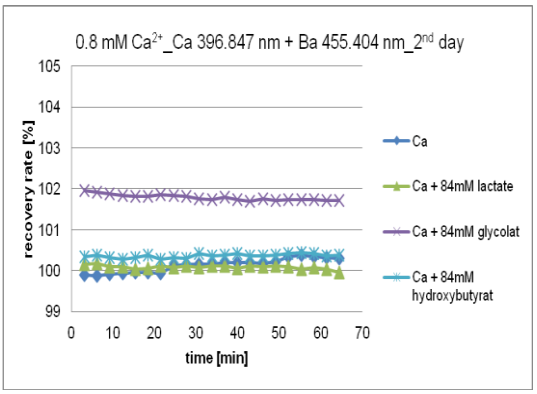

Figure 9-203: Recovery rates by the determination of 0.8 mmol L^{-1} Ca^{2+} in different α-hydroxy-carboxylate matrices, with Ca 396.847 nm + Ba 455.404 nm (2nd day)

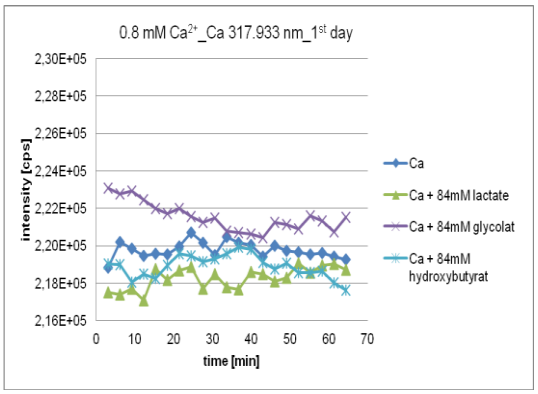

Figure 9-204: The intensity of Ca 317.933 nm by the determination of 0.8 mmol L^{-1} Ca^{2+} in different α-hydroxy-carboxylate matrices (1st day)

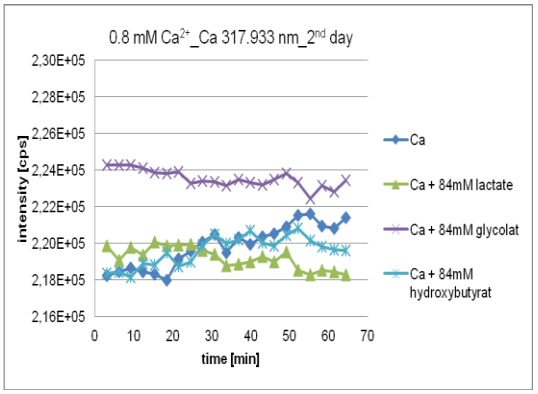

Figure 9-205: The intensity of Ca 317.933 nm by the determination of 0.8 mmol L^{-1} Ca^{2+} in different α-hydroxy-carboxylate matrices (2nd day)

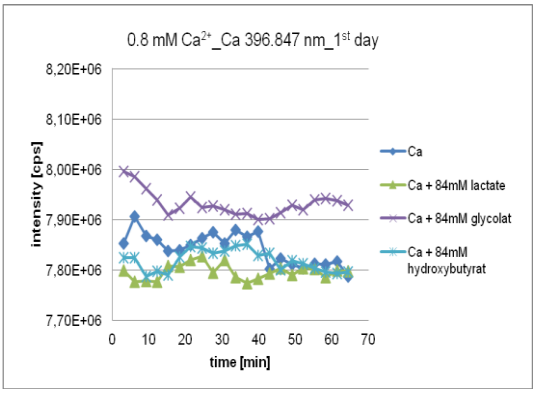

Figure 9-206: The intensity of Ca 396.847 nm by the determination of 0.8 mmol L^{-1} Ca^{2+} in different α-hydroxy-carboxylate matrices (1st day)

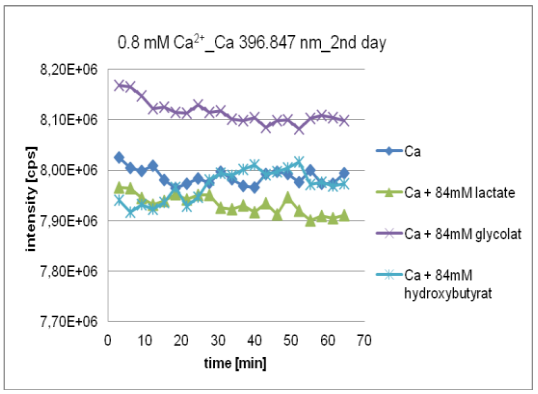

Figure 9-207: The intensity of Ca 396.847 nm by the determination of 0.8 mmol L^{-1} Ca^{2+} in different α-hydroxy-carboxylate matrices (2nd day)

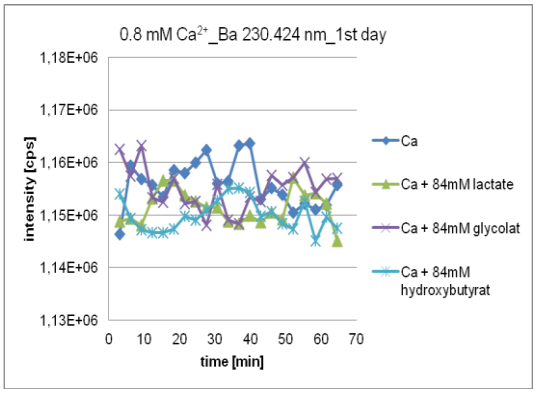

Figure 9-208: The intensity of Ba 230.424 nm by the determination of 0.8 mmol L^{-1} Ca^{2+} in different α-hydroxy-carboxylate matrices (1st day)

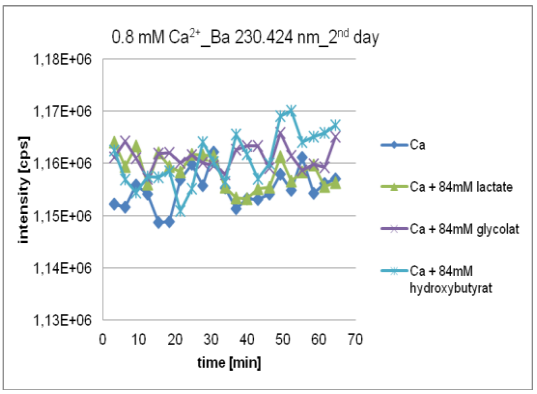

Figure 9-209: The intensity of Ba 230.424 nm by the determination of 0.8 mmol L^{-1} Ca^{2+} in different α-hydroxy-carboxylate matrices (2nd day)

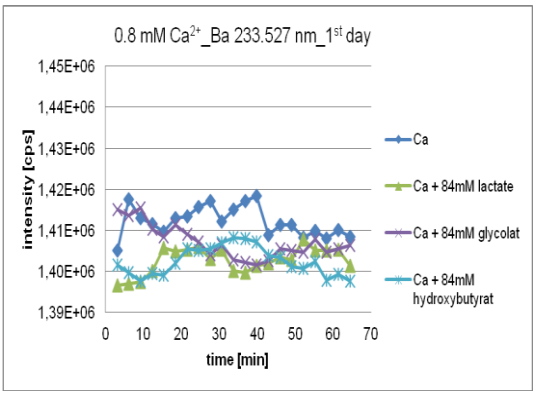

Figure 9-210: The intensity of Ba 233.527 nm by the determination of 0.8 mmol L^{-1} Ca^{2+} in different α-hydroxy-carboxylate matrices (1st day)

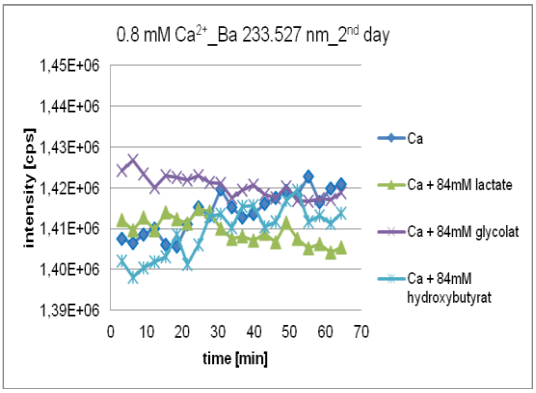

Figure 9-211: The intensity of Ba 233.527 nm by the determination of 0.8 mmol L^{-1} Ca^{2+} in different α-hydroxy-carboxylate matrices (2nd day)

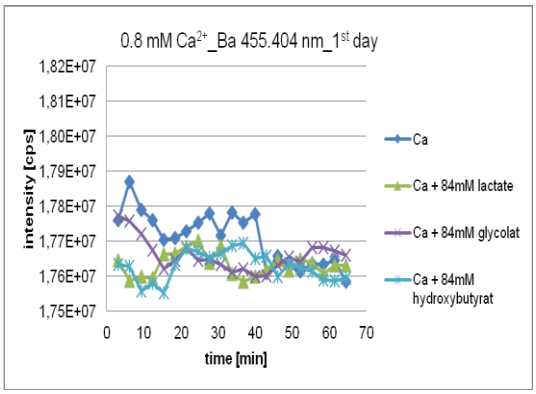

Figure 9-212: The intensity of Ba 455.404 nm by the determination of 0.8 mmol L^{-1} Ca^{2+} in different α-hydroxy-carboxylate matrices (1st day)

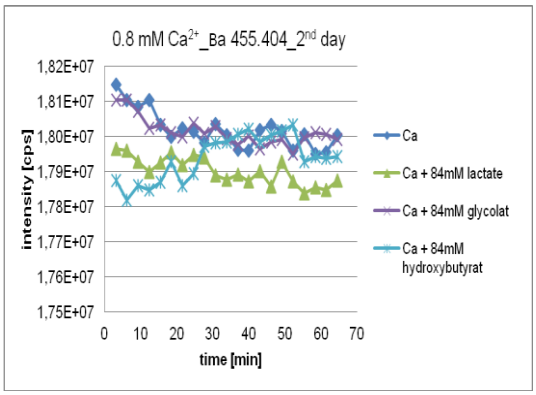

Figure 9-213: The intensity of Ba 455.404 nm by the determination of 0.8 mmol L^{-1} Ca^{2+} in different α-hydroxy-carboxylate matrices (2nd day)

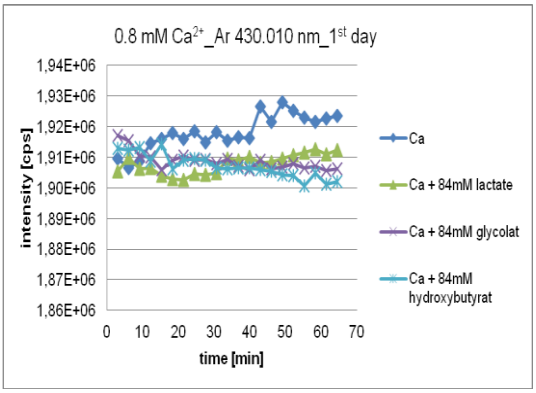

Figure 9-214: The intensity of Ar 430.010 nm by the determination of 0.8 mmol L^{-1} Ca^{2+} in different α-hydroxy-carboxylate matrices (1st day)

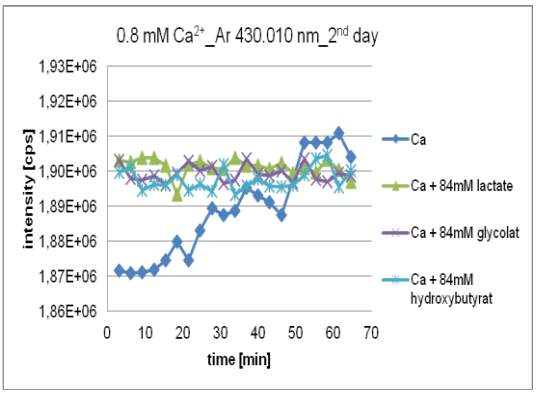

Figure 9-215: The intensity of Ar 430.010 nm by the determination of 0.8 mmol L^{-1} Ca^{2+} in different α-hydroxy-carboxylate matrices (2nd day)

9.7.2 Attachments on the effect of α-hydroxy-carboxylates on the determination of the highest calcium concentration (36 mmol L^{-1})

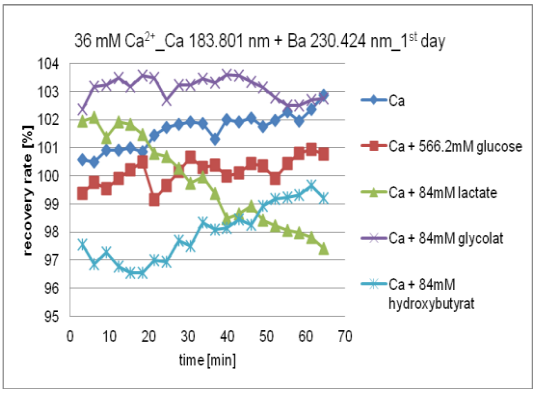

Figure 9-216: Recovery rates by the determination of 36 mmol L^{-1} Ca^{2+} in glucose and different α-hydroxy-carboxylate matrices, with Ca 183.801 nm + Ba 230.424 nm (1st day)

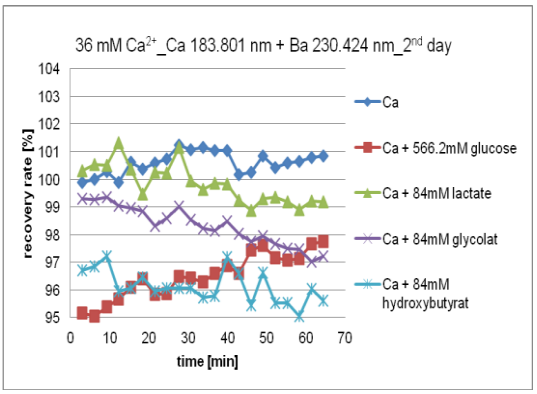

Figure 9-217: Recovery rates by the determination of 36 mmol L^{-1} Ca^{2+} in glucose and different α-hydroxy-carboxylate matrices, with Ca 183.801 nm + Ba 230.424 nm (2nd day)

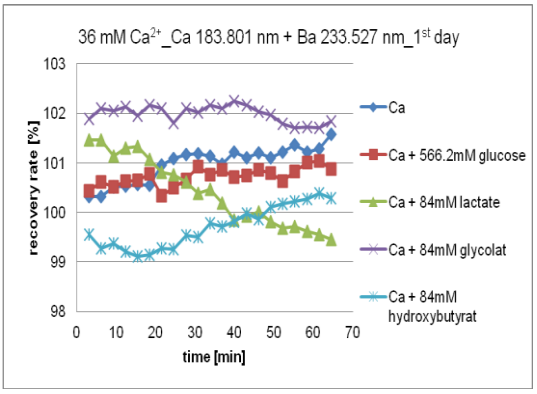

Figure 9-218: Recovery rates by the determination of 36 mmol L^{-1} Ca^{2+} in glucose and different α-hydroxy-carboxylate matrices, with Ca 183.801 nm + Ba 233.527 nm (1st day)

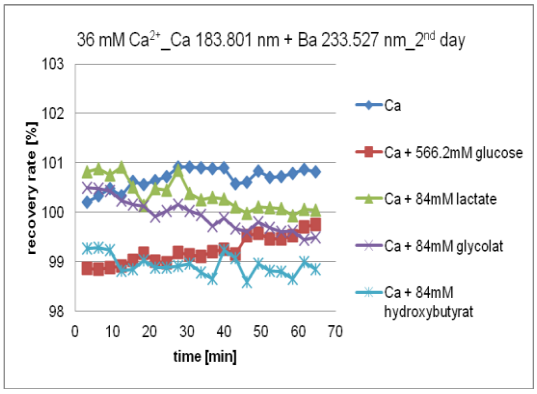

Figure 9-219: Recovery rates by the determination of 36 mmol L^{-1} Ca^{2+} in glucose and different α-hydroxy-carboxylate matrices, with Ca 183.801 nm + Ba 233.527 nm (2nd day)

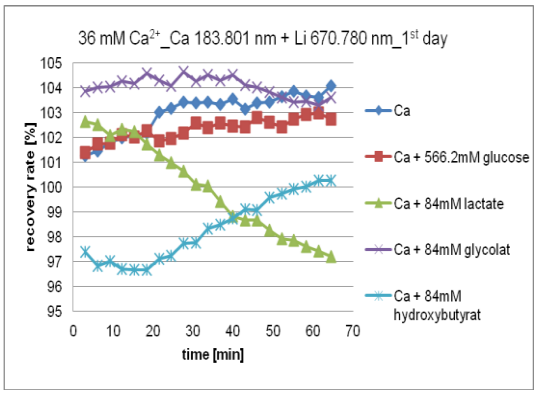

Figure 9-220: Recovery rates by the determination of 36 mmol L^{-1} Ca^{2+} in glucose and different α-hydroxy-carboxylate matrices, with Ca 183.801 nm + Li 670.780 nm (1st day)

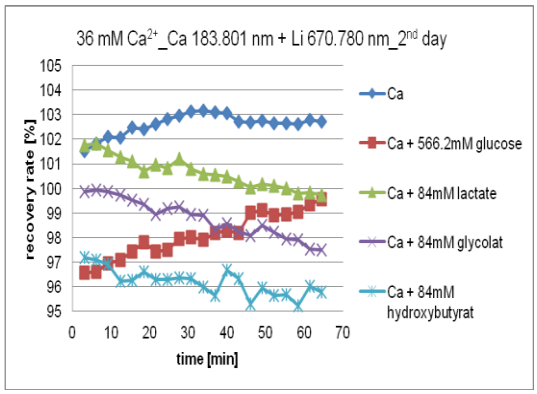

Figure 9-221: Recovery rates by the determination of 36 mmol L^{-1} Ca^{2+} in glucose and different α-hydroxy-carboxylate matrices, with Ca 183.801 nm + Li 670.780 nm (2nd day)

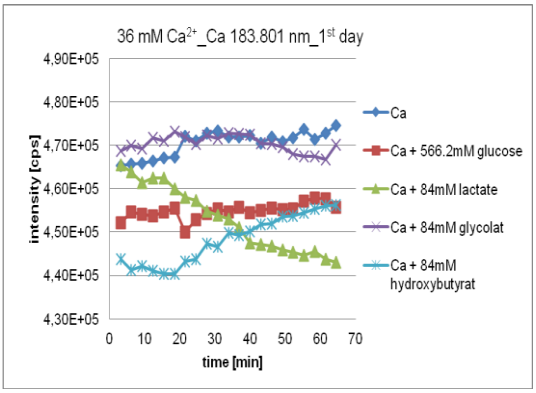

Figure 9-222: The intensity of Ca 183.801 nm by the determination of 36 mmol L^{-1} Ca^{2+} in glucose and different α-hydroxy-carboxylate matrices (1st day)

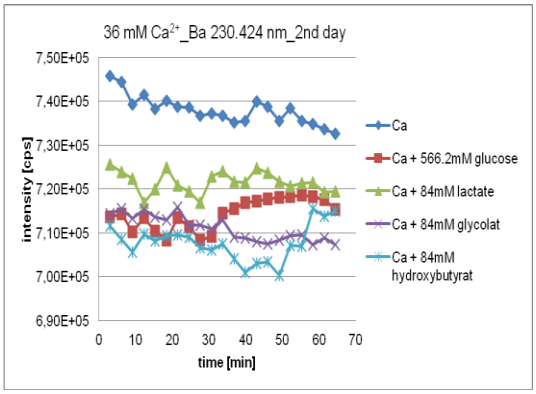

Figure 9-225: The intensity of Ba 230.424 nm by the determination of 36 mmol L^{-1} Ca^{2+} in glucose and different α-hydroxy-carboxylate matrices (2nd day)

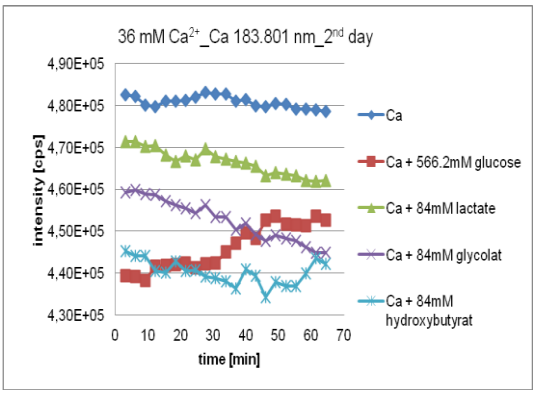

Figure 9-223: The intensity of Ca 183.801 nm by the determination of 36 mmol L^{-1} Ca^{2+} in glucose and different α-hydroxy-carboxylate matrices (2nd day)

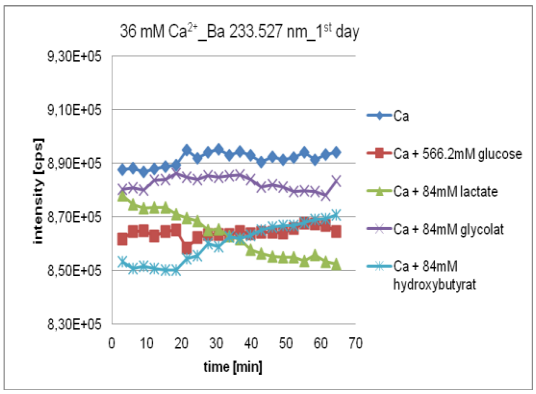

Figure 9-226: The intensity of Ba 233.527 nm by the determination of 36 mmol L^{-1} Ca^{2+} in glucose and different α-hydroxy-carboxylate matrices (1st day)

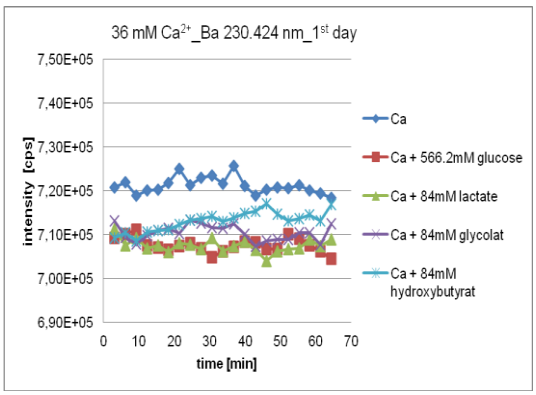

Figure 9-224: The intensity of Ba 230.424 nm by the determination of 36 mmol L^{-1} Ca^{2+} in glucose and different α-hydroxy-carboxylate matrices (1st day)

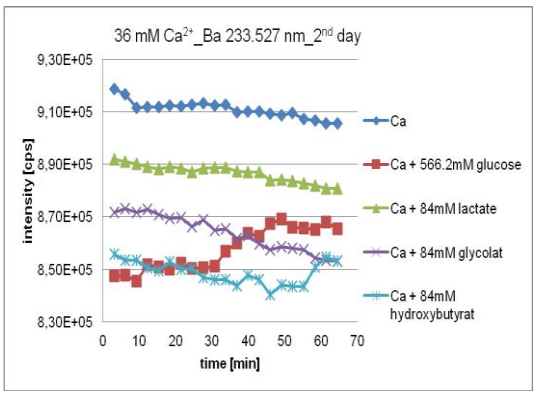

Figure 9-227: The intensity of Ba 233.527 nm by the determination of 36 mmol L^{-1} Ca^{2+} in glucose and different α-hydroxy-carboxylate matrices (2nd day)

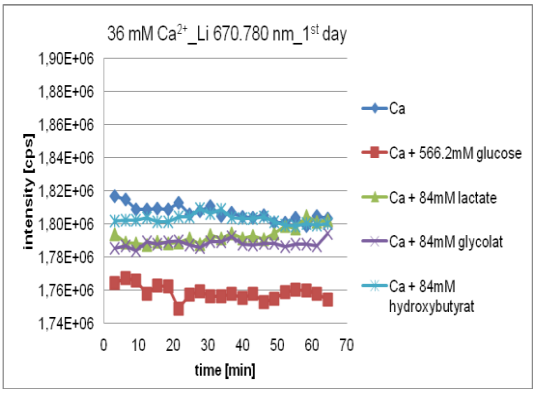

Figure 9-228: The intensity of Li 670.780 nm by the determination of 36 mmol L^{-1} Ca^{2+} in glucose and different α-hydroxy-carboxylate matrices (1st day)

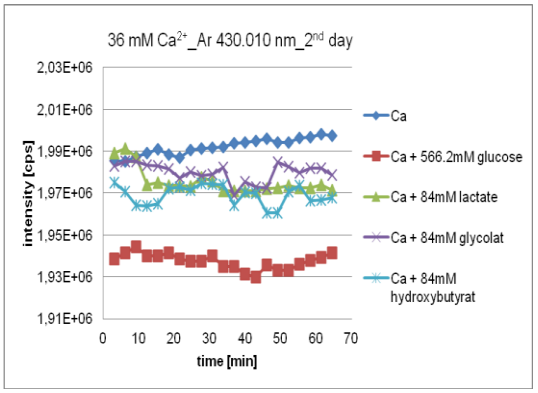

Figure 9-231: The intensity of Ar 430.010 nm by the determination of 36 mmol L^{-1} Ca^{2+} in glucose and different α-hydroxy-carboxylate matrices (2nd day)

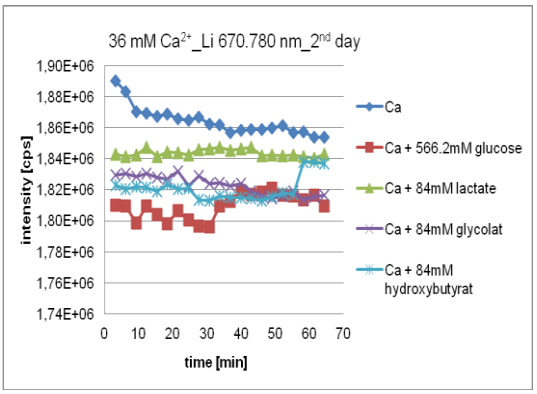

Figure 9-229: The intensity of Li 670.780 nm by the determination of 36 mmol L^{-1} Ca^{2+} in glucose and different α-hydroxy-carboxylate matrices (2nd day)

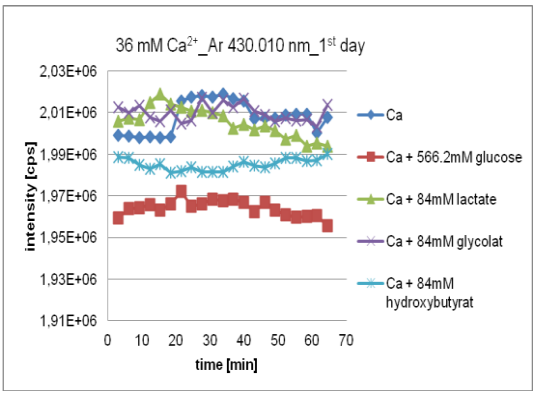

Figure 9-230: The intensity of Ar 430.010 nm by the determination of 36 mmol L^{-1} Ca^{2+} in glucose and different α-hydroxy-carboxylate matrices (1st day)

9.8 Attachments on the effect of glucose and lactate on the determination of potassium by ICP-OES

9.8.1 Attachments on the matrix effects on the determination of the lowest potassium concentration (0.8 mmol L^{-1})

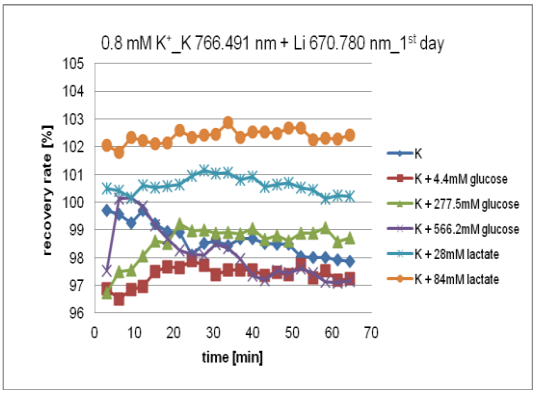

Figure 9-232: Recovery rates by the determination of 0.8 mmol L^{-1} K^+ in glucose or lactate matrices, with K 766.491 + Li 670.780 nm (1st day)

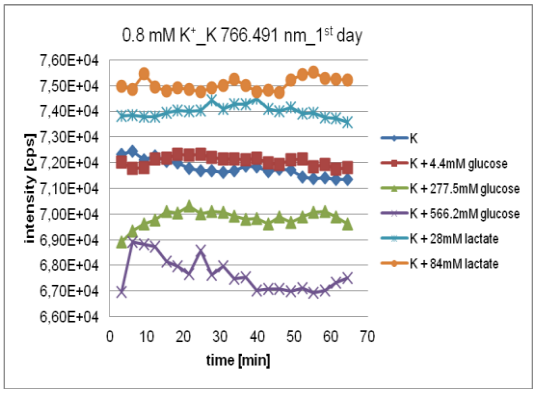

Figure 9-234: The intensity of K 766.491 nm by the determination of 0.8 mmol L^{-1} K^+ in glucose or lactate matrices (1st day)

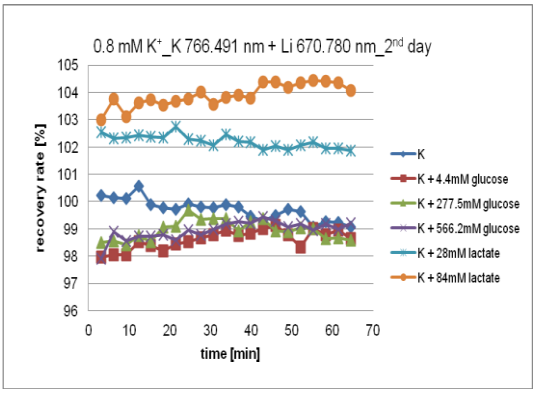

Figure 9-233: Recovery rates by the determination of 0.8 mmol L^{-1} K^+ in glucose or lactate matrices, with K 766.491 + Li 670.780 nm (2nd day)

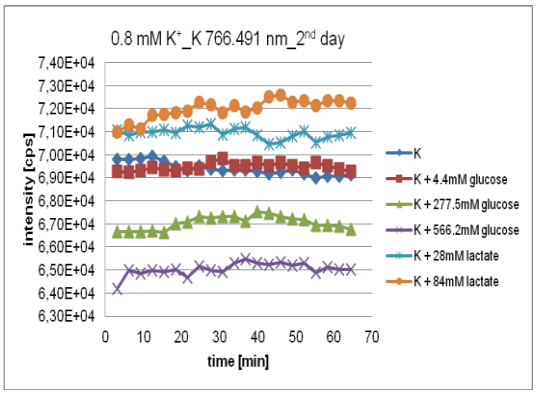

Figure 9-235: The intensity of K 766.491 nm by the determination of 0.8 mmol L^{-1} K^+ in glucose or lactate matrices (2nd day)

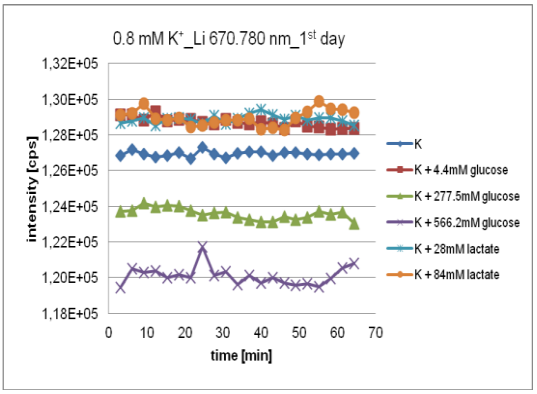

Figure 9-236: The intensity of Li 670.780 nm by the determination of 0.8 mmol L^{-1} K^+ glucose or lactate matrices (1st day)

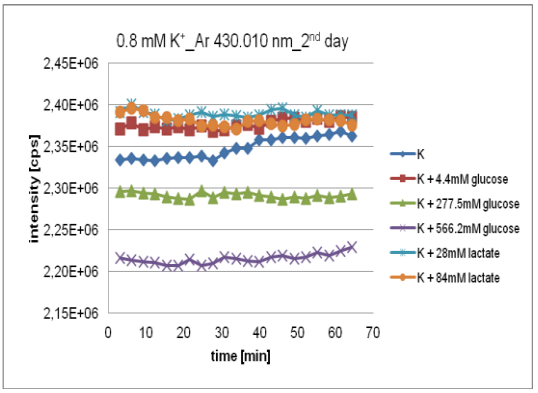

Figure 9-239: The intensity of Ar 430.010 nm by the determination of 0.8 mmol L^{-1} K^+ glucose or lactate matrices (2nd day)

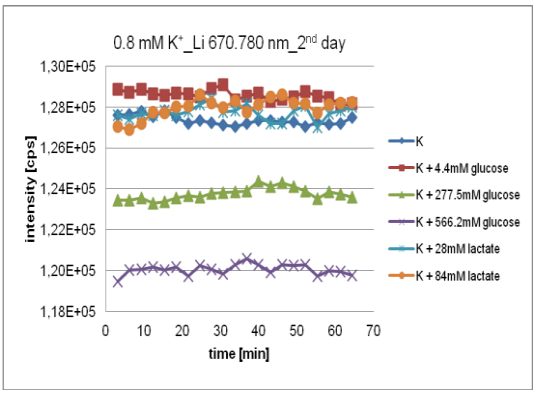

Figure 9-237: The intensity of Li 670.780 nm by the determination of 0.8 mmol L^{-1} K^+ in glucose or lactate matrices (2nd day)

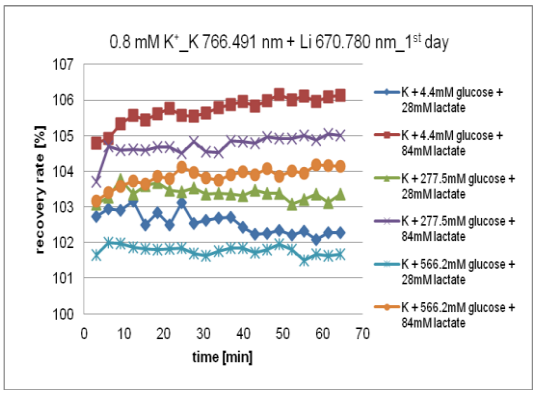

Figure 9-240: Recovery rates by the determination of 0.8 mmol L^{-1} K^+ in glucose and lactate matrices, with K 766.491 + Li 670.780 nm (1st day)

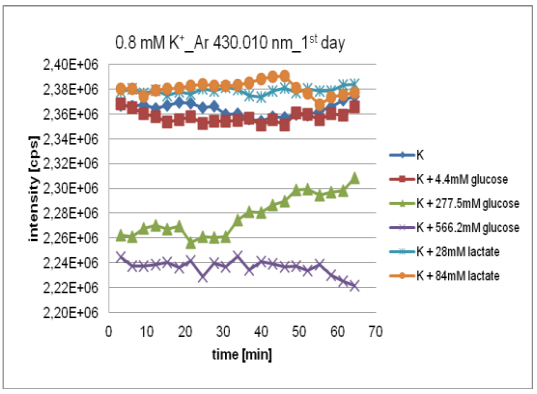

Figure 9-238: The intensity of Ar 430.010 nm by the determination of 0.8 mmol L^{-1} K^+ in glucose or lactate matrices (1st day)

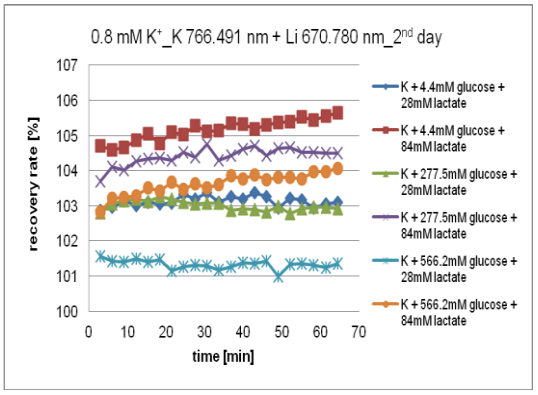

Figure 9-241: Recovery rates by the determination of 0.8 mmol L^{-1} K^+ in glucose and lactate matrices, with K 766.491 + Li 670.780 nm (2nd day)

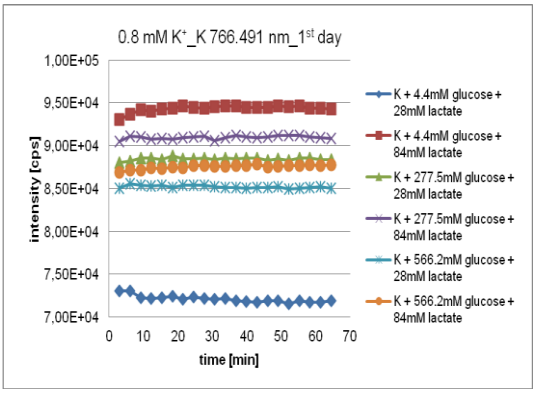

Figure 9-242: The intensity of K 766.491 nm by the determination of 0.8 mmol L^{-1} K^+ in glucose and lactate matrices (1st day)

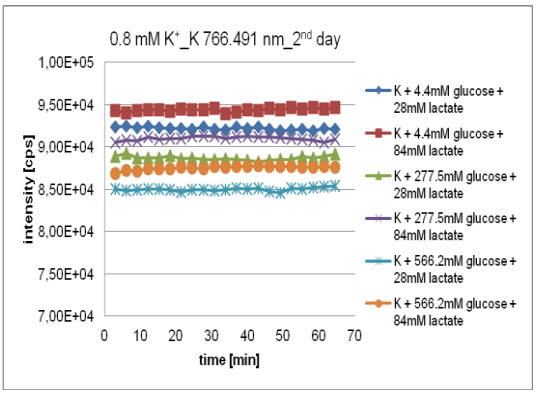

Figure 9-243: The intensity of K 766.491 nm by the determination of 0.8 mmol L^{-1} K^+ in glucose and lactate matrices (2nd day)

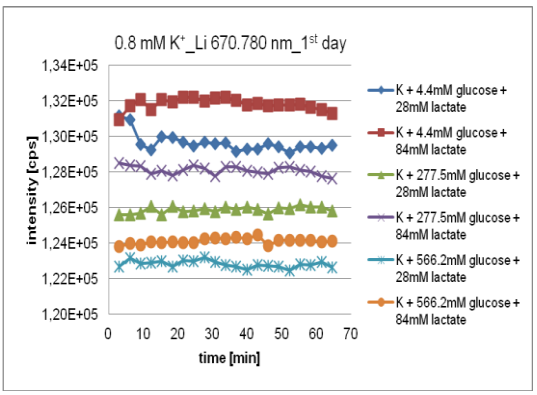

Figure 9-244: The intensity of Li 670.780 nm by the determination of 0.8 mmol L^{-1} K^+ in glucose and lactate matrices (1st day)

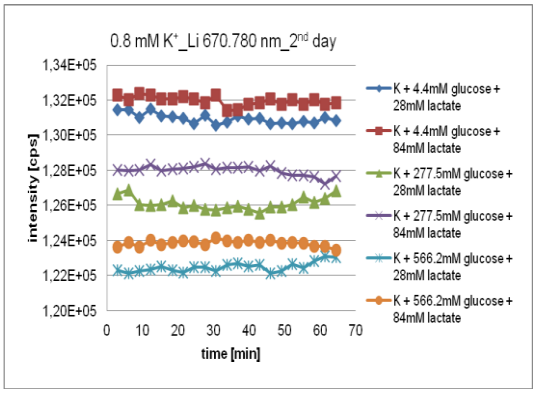

Figure 9-245: The intensity of Li 670.780 nm by the determination of 0.8 mmol L^{-1} K^+ in glucose and lactate matrices (2nd day)

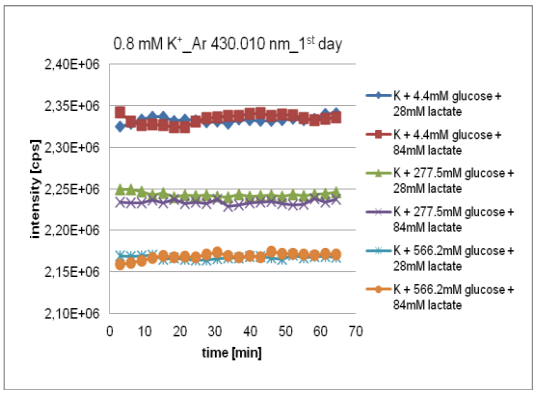

Figure 9-246: The intensity of Ar 430.010 nm by the determination of 0.8 mmol L^{-1} K^+ in glucose and lactate matrices (1st day)

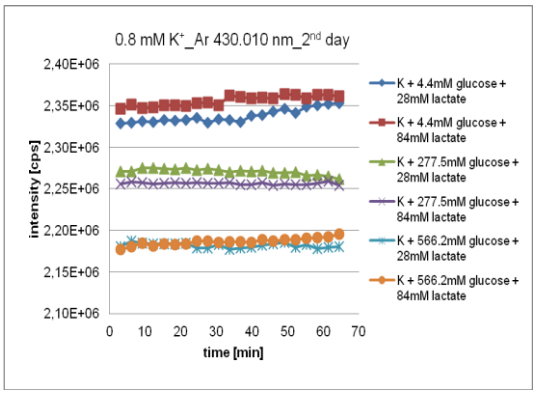

Figure 9-247: The intensity of Ar 430.010 nm by the determination of 0.8 mmol L^{-1} K^+ in glucose and lactate matrices (2nd day)

9.8.2 Attachments on the matrix effects on the determination of the highest potassium concentration (96 mmol L^{-1})

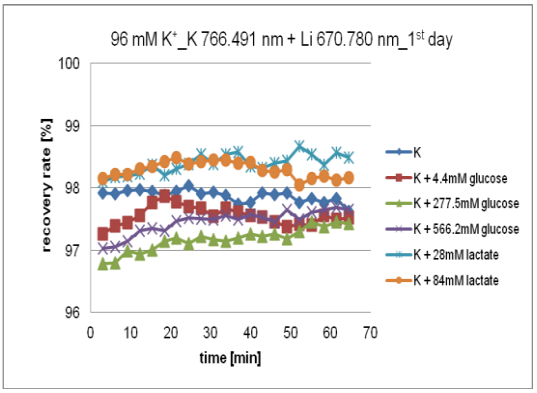

Figure 9-248: Recovery rates by the determination of 96 mmol L^{-1} K^+ in glucose or lactate matrices, with K 766.491 + Li 670.780 nm (1st day)

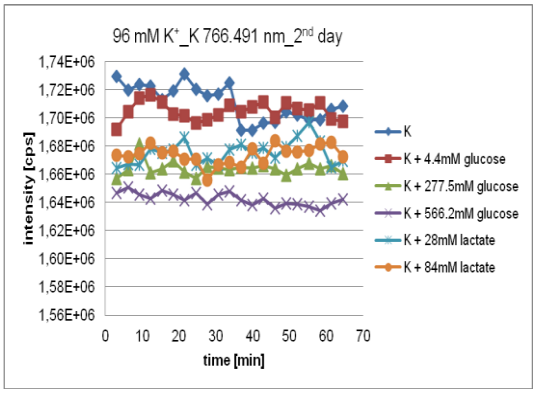

Figure 9-251: The intensity of K 766.491 nm by the determination of 96 mmol L^{-1} K^+ in glucose or lactate matrices (2nd day)

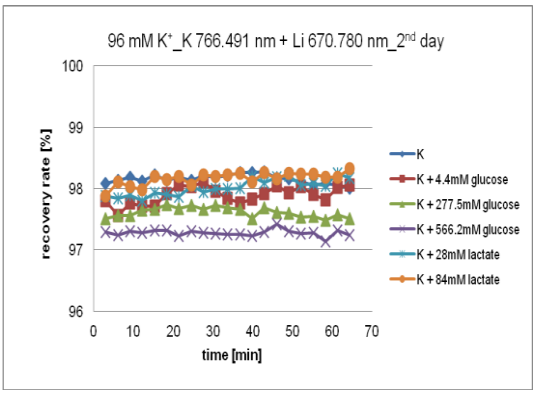

Figure 9-249: Recovery rates by the determination of 96 mmol L^{-1} K^+ in glucose or lactate matrices, with K 766.491 + Li 670.780 nm (2nd day)

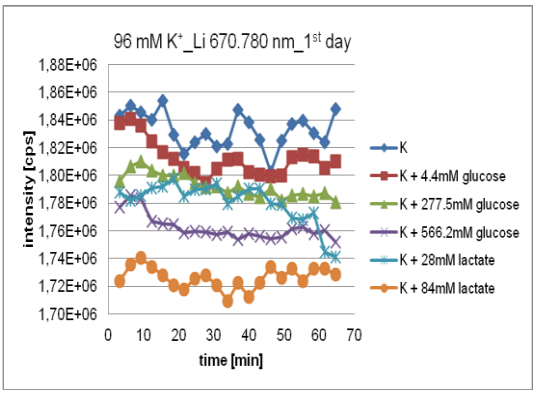

Figure 9-252: The intensity of Li 670.780 nm by the determination of 96 mmol L^{-1} K^+ in glucose or lactate matrices (1st day)

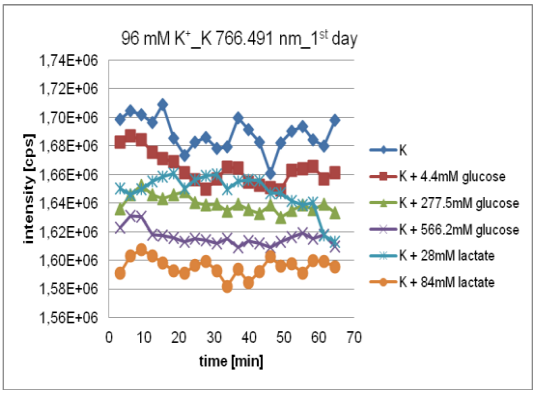

Figure 9-250: The intensity of K 766.491 nm by the determination of 96 mmol L^{-1} K^+ in glucose or lactate matrices (1st day)

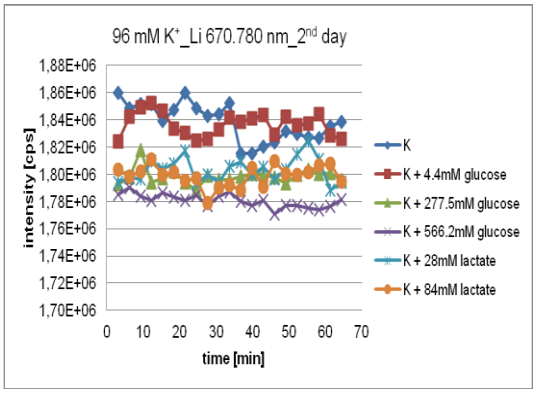

Figure 9-253: The intensity of Li 670.780 nm by the determination of 96 mmol L^{-1} K^+ in glucose or lactate matrices (2nd day)

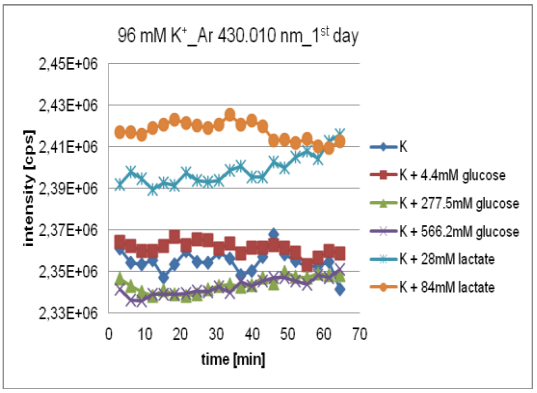

Figure 9-254: The intensity of Ar 430.010 nm by the determination of 96 mmol L^{-1} K^+ in glucose or lactate matrices (1st day)

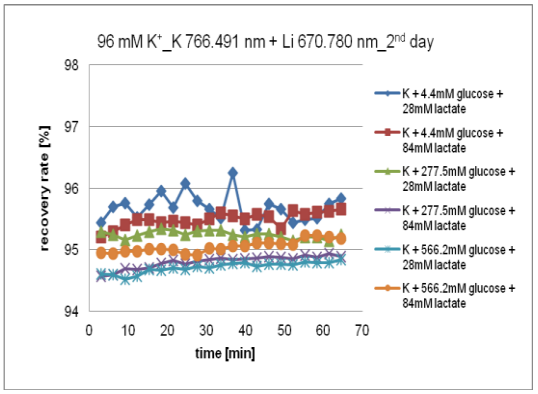

Figure 9-257: Recovery rates by the determination of 96 mmol L^{-1} K^+ in glucose and lactate matrices, with K 766.491 + Li 670.780 nm (2nd day)

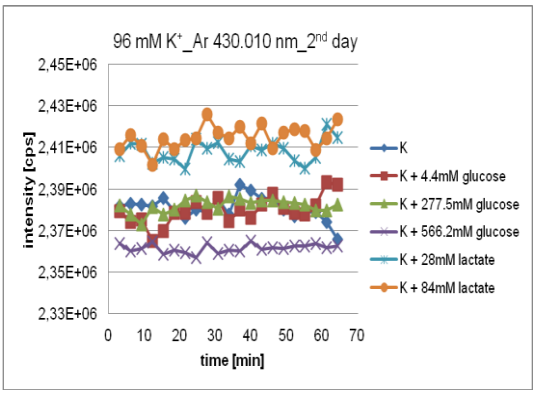

Figure 9-255: The intensity of Ar 430.010 nm by the determination of 96 mmol L^{-1} K^+ in glucose or lactate matrices (2nd day)

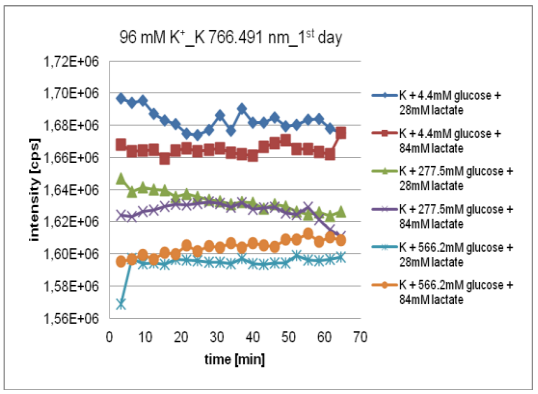

Figure 9-258: The intensity of K 766.491 nm by the determination of 96 mmol L^{-1} K^+ in glucose and lactate matrices (1st day)

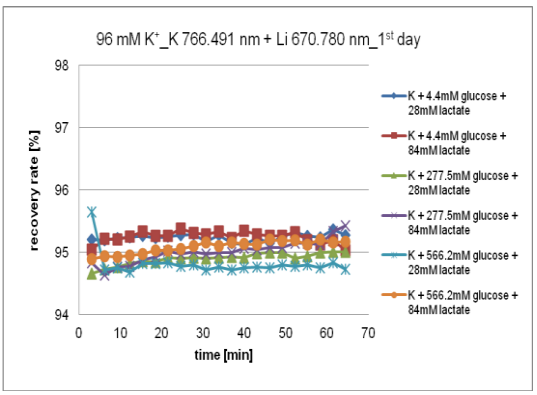

Figure 9-256: Recovery rates by the determination of 96 mmol L^{-1} K^+ in glucose and lactate matrices, with K 766.491 + Li 670.780 nm (1st day)

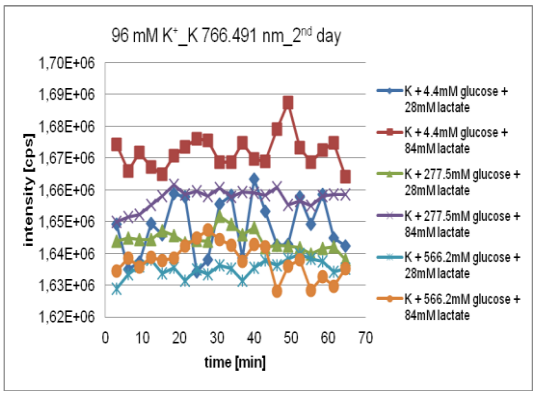

Figure 9-259: The intensity of K 766.491 nm by the determination of 96 mmol L^{-1} K^+ in glucose and lactate matrices (2nd day)

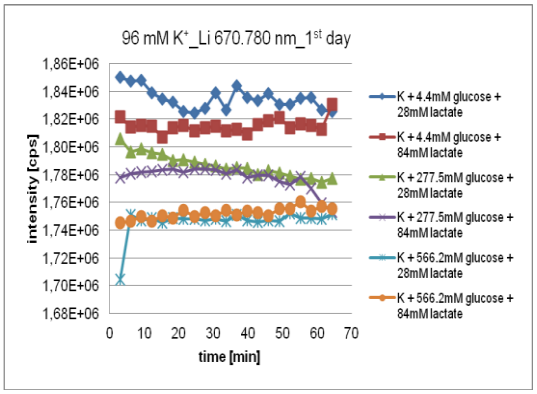

Figure 9-260: The intensity of Li 670.780 nm by the determination of 96 mmol L^{-1} K^+ in glucose and lactate matrices (1st day)

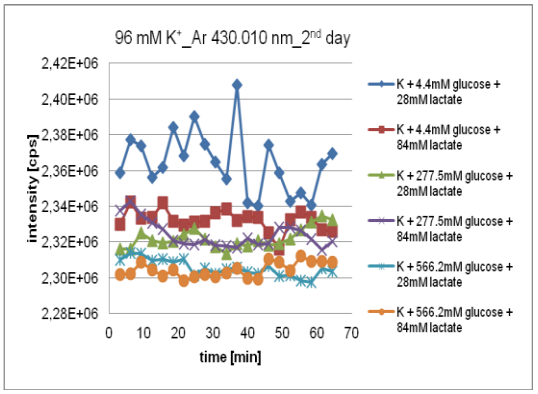

Figure 9-263: The intensity of Ar 430.010 nm by the determination of 96 mmol L^{-1} K^+ in glucose and lactate matrices (2nd day)

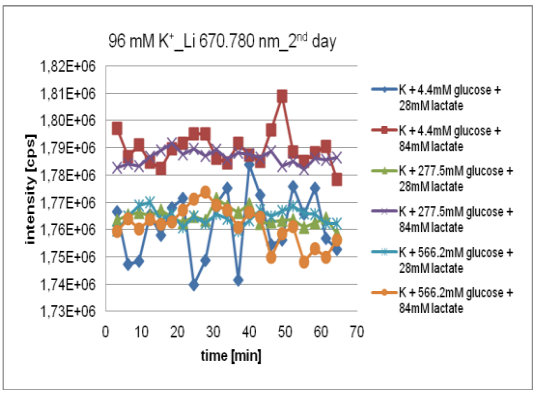

Figure 9-261: The intensity of Li 670.780 nm by the determination of 96 mmol L^{-1} K^+ in glucose and lactate matrices (2nd day)

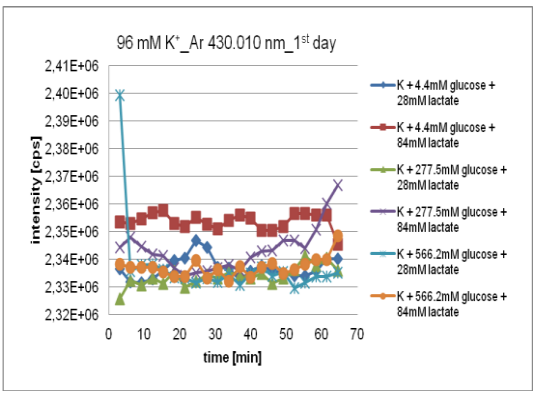

Figure 9-262: The intensity of Ar 430.010 nm by the determination of 96 mmol L^{-1} K^+ in glucose and lactate matrices (1st day)

9.9 Attachments on the effect of glucose and lactate on the determination of sodium by ICP-OES

9.9.1 Attachments on the matrix effects on the determination of the average sodium concentration (140 mmol L^{-1})

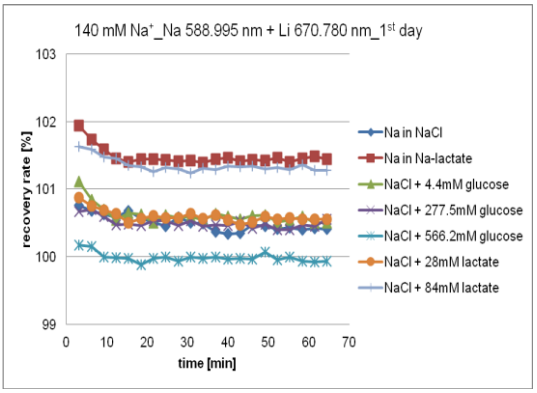

Figure 9-264: Recovery rates by the determination of 140 mmol L^{-1} Na^+ in NaCl solutions with glucose or Na-lactate, with Na 588.995 + Li 670.780 nm (1st day)

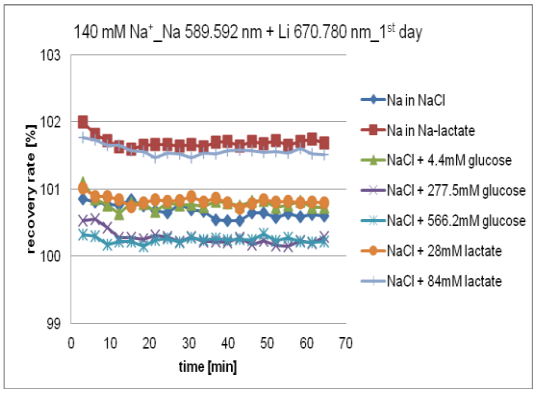

Figure 9-266: Recovery rates by the determination of 140 mmol L^{-1} Na^+ in NaCl solutions with glucose or Na-lactate, with Na 589.592 + Li 670.780 nm (1st day)

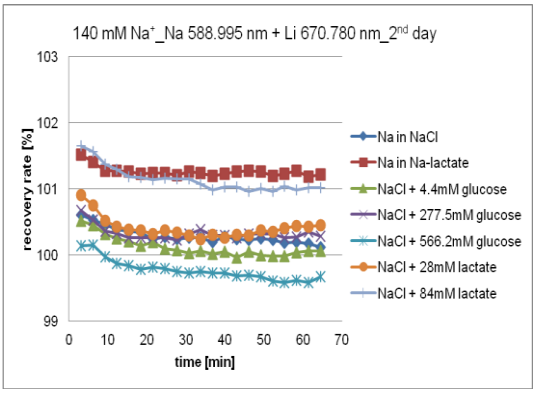

Figure 9-265: Recovery rates by the determination of 140 mmol L^{-1} Na^+ in NaCl solutions with glucose or Na-lactate, with Na 588.995 + Li 670.780 nm (2nd day)

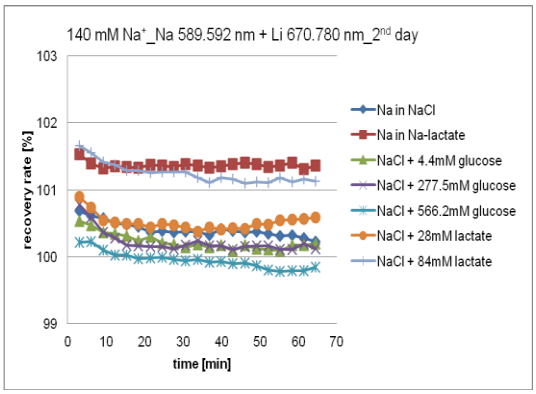

Figure 9-267: Recovery rates by the determination of 140 mmol L^{-1} Na^+ in NaCl solutions with glucose or Na-lactate, with Na 589.592 + Li 670.780 nm (2nd day)

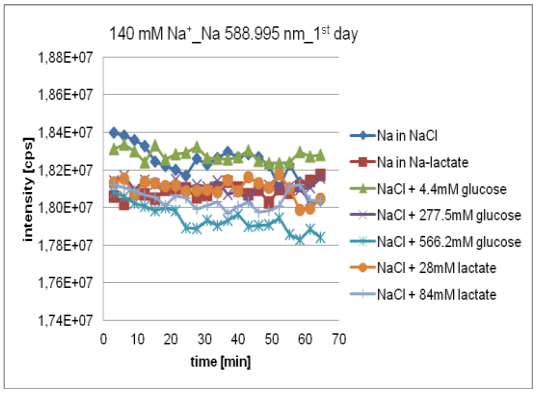

Figure 9-268: The intensity of Na 588.995 nm by the determination of 140 mmol L^{-1} Na^+ in NaCl solutions with glucose or Na-lactate (1st day)

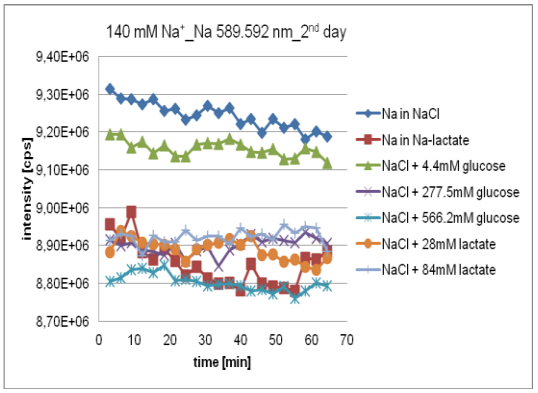

Figure 9-271: The intensity of Na 589.592 nm by the determination of 140 mmol L^{-1} Na^+ in NaCl solutions with glucose or Na-lactate (2nd day)

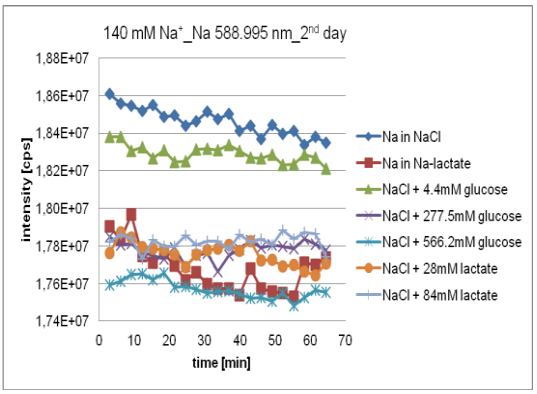

Figure 9-269: The intensity of Na 588.995 nm by the determination of 140 mmol L^{-1} Na^+ in NaCl solutions with glucose or Na-lactate (2nd day)

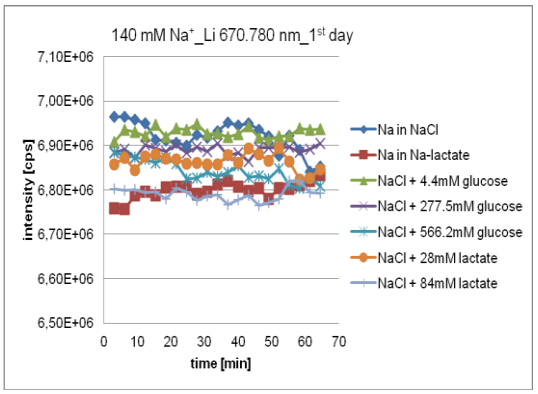

Figure 9-272: The intensity of Li 670.780 nm by the determination of 140 mmol L^{-1} Na^+ in NaCl solutions with glucose or Na-lactate (1st day)

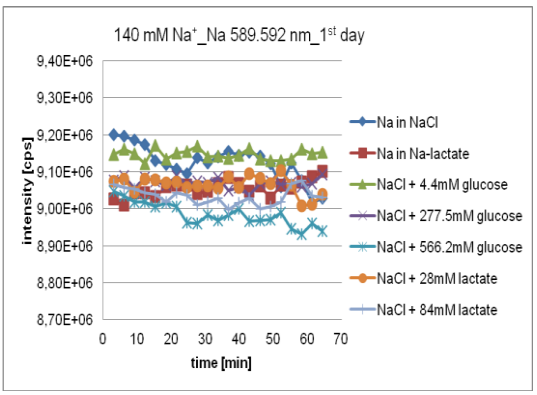

Figure 9-270: The intensity of Na 589.592 nm by the determination of 140 mmol L^{-1} Na^+ in NaCl solutions with glucose or Na-lactate (1st day)

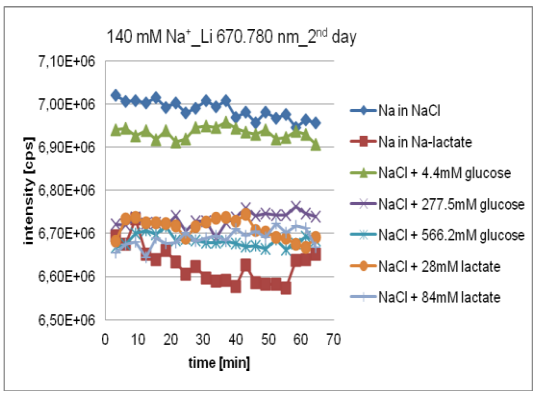

Figure 9-273: The intensity of Li 670.780 nm by the determination of 140 mmol L^{-1} Na^+ in NaCl solutions with glucose or Na-lactate (2nd day)

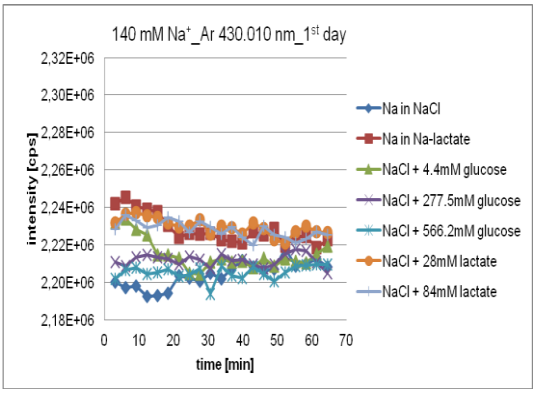

Figure 9-274: The intensity of Ar 430.010 nm by the determination of 140 mmol L^{-1} Na^+ in NaCl solutions with glucose or Na-lactate (1st day)

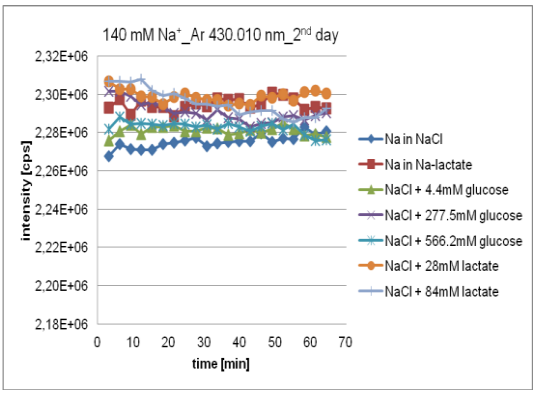

Figure 9-275: The intensity of Ar 430.010 nm by the determination of 140 mmol L^{-1} Na^+ in NaCl solutions with glucose or Na-lactate (2nd day)

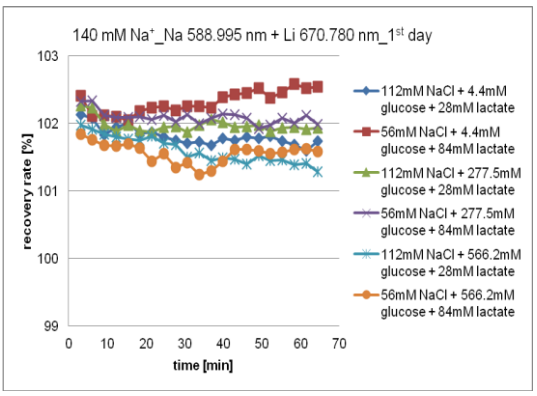

Figure 9-276: Recovery rates by the determination of 140 mmol L^{-1} Na^+ in NaCl solutions with glucose and Na-lactate, with Na 588.995 + Li 670.780 nm (1st day)

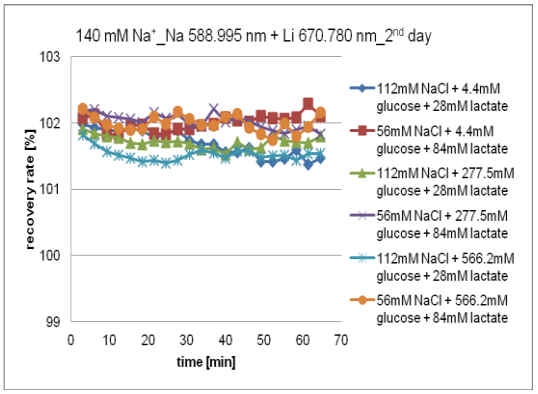

Figure 9-277: Recovery rates by the determination of 140 mmol L^{-1} Na^+ in NaCl solutions with glucose and Na-lactate, with Na 588.995 + Li 670.780 nm (2nd day)

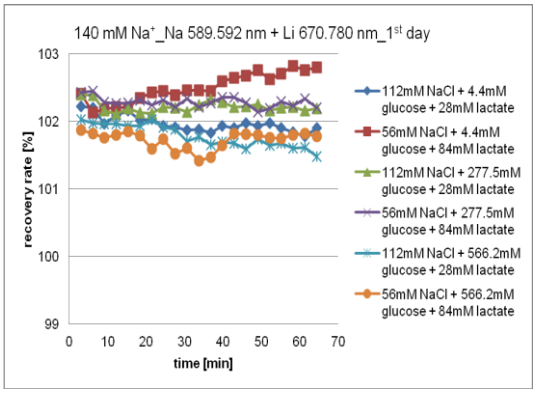

Figure 9-278: Recovery rates by the determination of 140 mmol L^{-1} Na^+ in NaCl solutions with glucose and Na-lactate, with Na 589.592 + Li 670.780 nm (1st day)

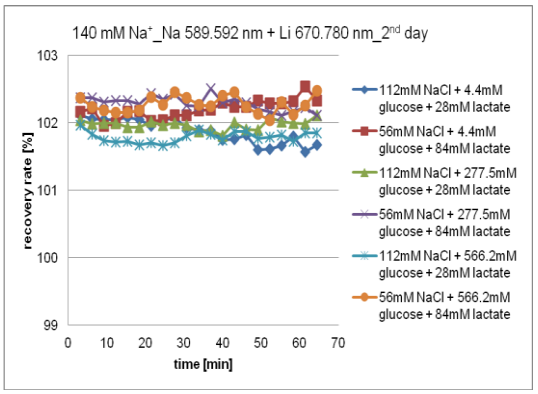

Figure 9-279: Recovery rates by the determination of 140 mmol L^{-1} Na^+ in NaCl solutions with glucose and Na-lactate, with Na 589.592 + Li 670.780 nm (2nd day)

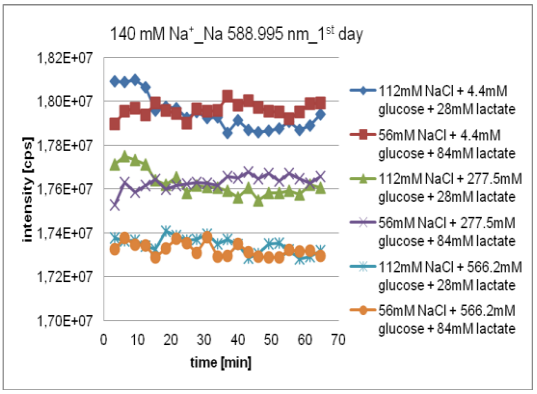

Figure 9-280: The intensity of Na 588.995 nm by the determination of 140 mmol L^{-1} Na^+ in NaCl solutions with glucose and Na-lactate (1st day)

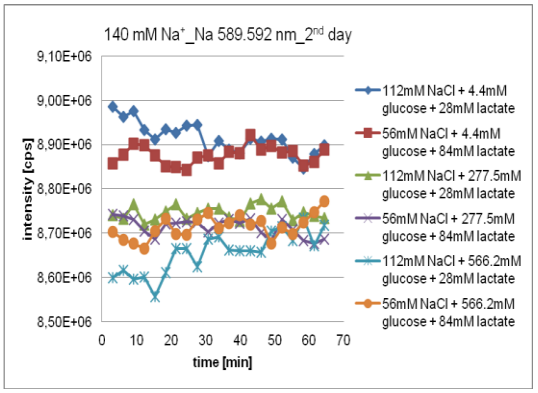

Figure 9-283: The intensity of Na 589.592 nm by the determination of 140 mmol L^{-1} Na^+ in NaCl solutions with glucose and Na-lactate (2nd day)

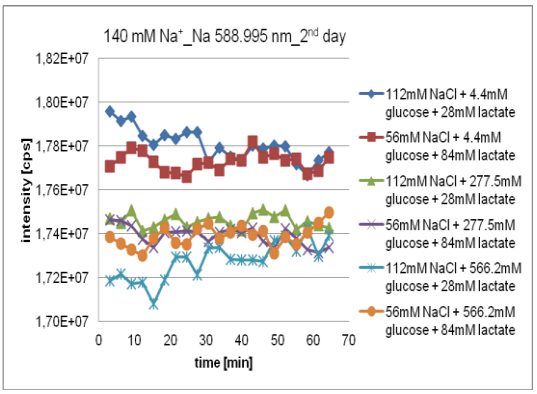

Figure 9-281: The intensity of Na 588.995 nm by the determination of 140 mmol L^{-1} Na^+ in NaCl solutions with glucose and Na-lactate (2nd day)

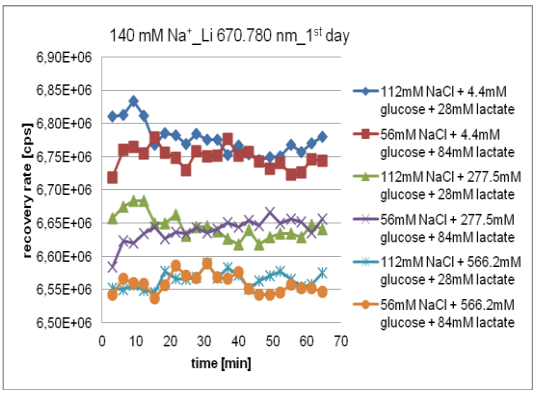

Figure 9-284: The intensity of Li 670.780 nm by the determination of 140 mmol L^{-1} Na^+ in NaCl solutions with glucose and Na-lactate (1st day)

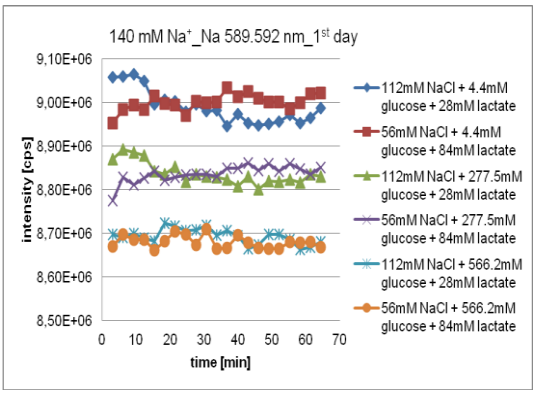

Figure 9-282: The intensity of Na 589.592 nm by the determination of 140 mmol L^{-1} Na^+ in NaCl solutions with glucose and Na-lactate (1st day)

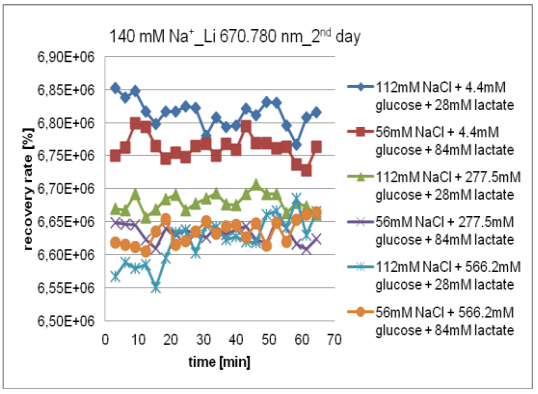

Figure 9-285: The intensity of Li 670.780 nm by the determination of 140 mmol L^{-1} Na^+ in NaCl solutions with glucose and Na-lactate (2nd day)

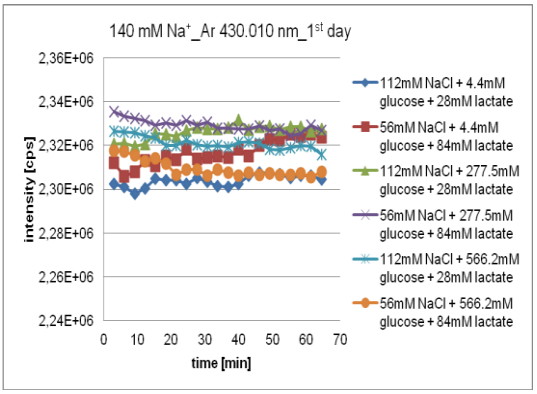

Figure 9-286: The intensity of Ar 430.010 nm by the determination of 140 mmol L^{-1} Na^+ in NaCl solutions with glucose and Na-lactate (1st day)

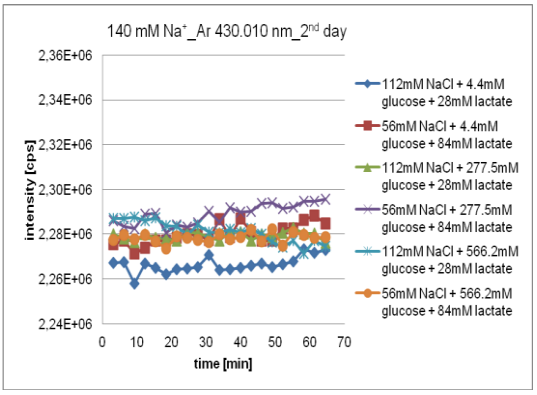

Figure 9-287: The intensity of Ar 430.010 nm by the determination of 140 mmol L^{-1} Na^+ in NaCl solutions with glucose and Na-lactate (2nd day)

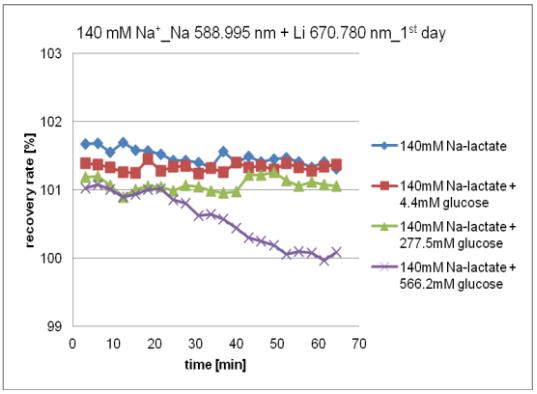

Figure 9-288: Recovery rates by the determination of 140 mmol L^{-1} Na^+ in Na-lactate and glucose matrices, with Na 588.995 + Li 670.780 nm (1st day)

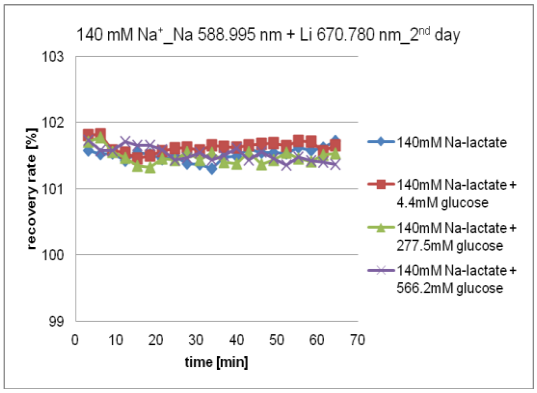

Figure 9-289: Recovery rates by the determination of 140 mmol L^{-1} Na^+ in Na-lactate and glucose matrices, with Na 588.995 + Li 670.780 nm (2nd day)

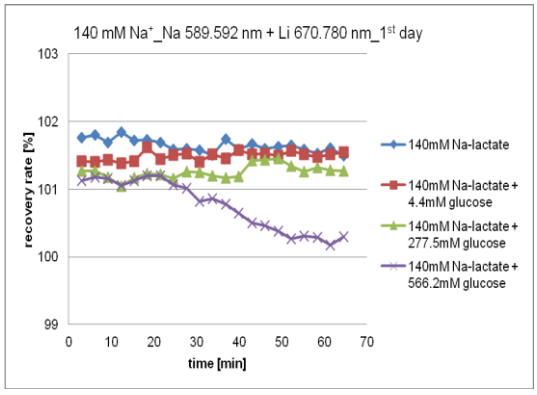

Figure 9-290: Recovery rates by the determination of 140 mmol L^{-1} Na^+ in Na-lactate and glucose matrices, with Na 589.592 + Li 670.780 nm (1st day)

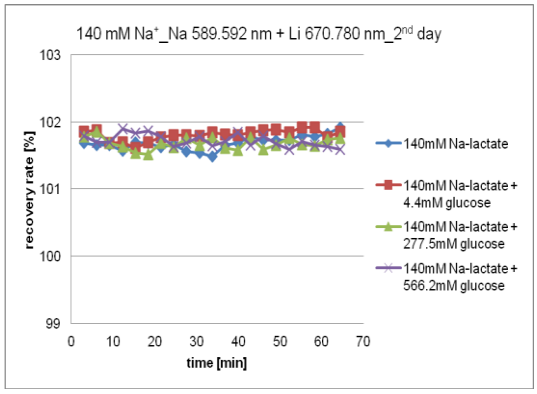

Figure 9-291: Recovery rates by the determination of 140 mmol L^{-1} Na^+ in Na-lactate and glucose matrices, with Na 589.592 + Li 670.780 nm (2nd day)

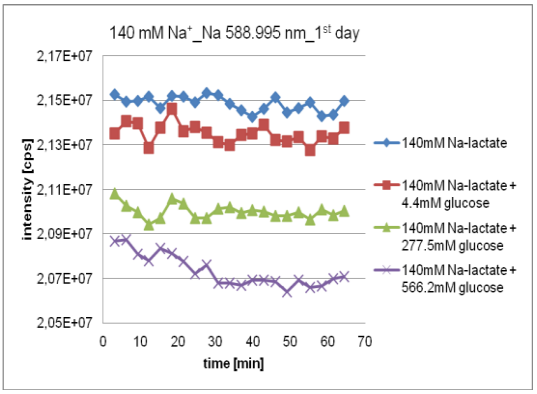

Figure 9-292: The intensity of Na 588.995 nm by the determination of 140 mmol L^{-1} Na^+ in Na-lactate and glucose matrices (1st day)

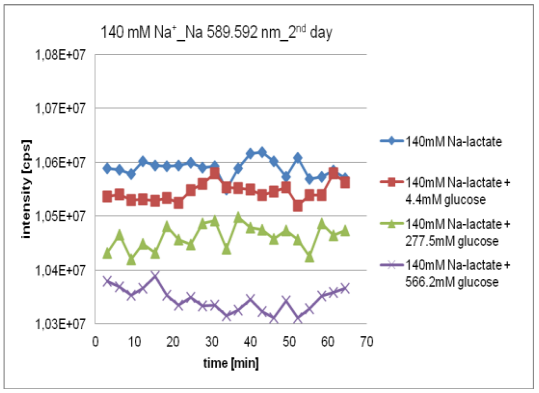

Figure 9-295: The intensity of Na 589.592 nm by the determination of 140 mmol L^{-1} Na^+ in Na-lactate and glucose matrices (2nd day)

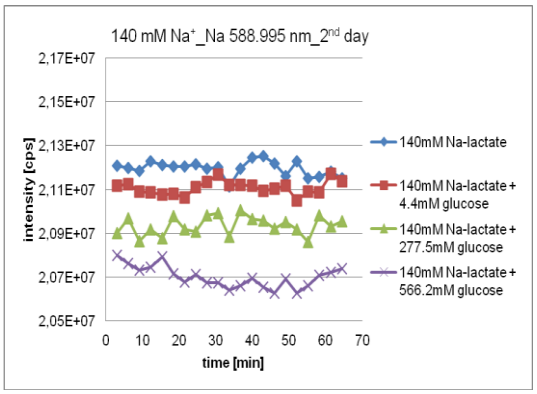

Figure 9-293: The intensity of Na 588.995 nm by the determination of 140 mmol L^{-1} Na^+ in Na-lactate and glucose matrices (2nd day)

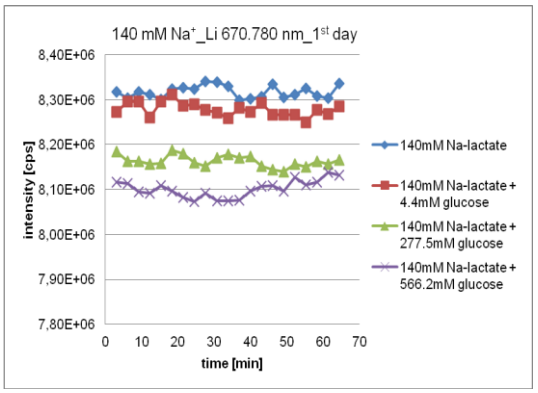

Figure 9-296: The intensity of Li 670.780 nm by the determination of 140 mmol L^{-1} Na^+ in Na-lactate and glucose matrices (1st day)

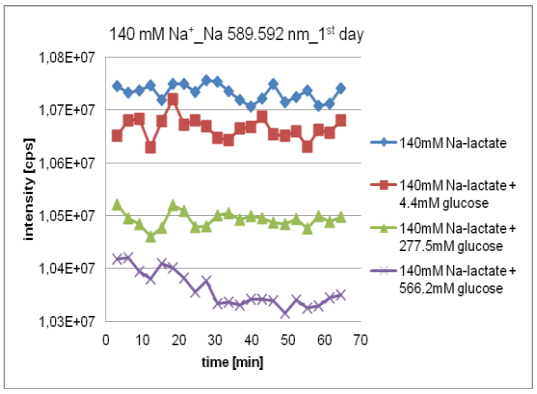

Figure 9-294: The intensity of Na 589.592 nm by the determination of 140 mmol L^{-1} Na^+ in Na-lactate and glucose matrices (1st day)

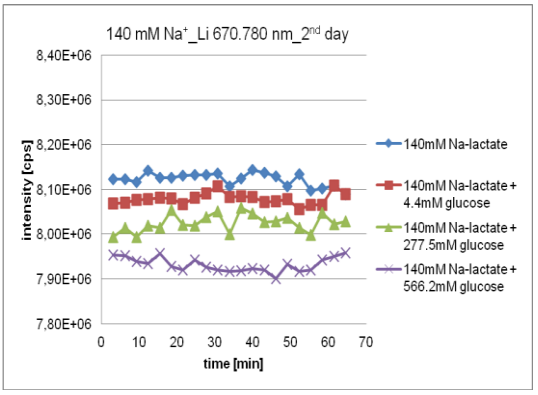

Figure 9-297: The intensity of Li 670.780 nm by the determination of 140 mmol L^{-1} Na^+ in Na-lactate and glucose matrices (2nd day)

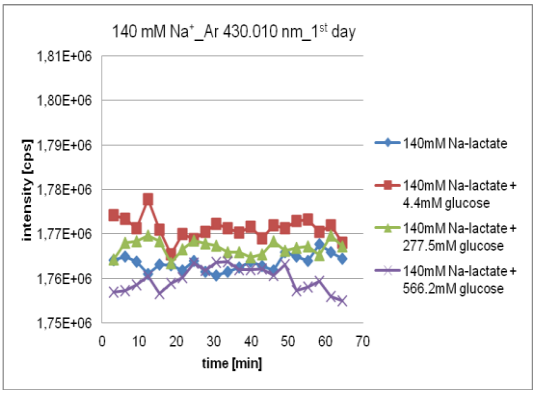

Figure 9-298: The intensity of Ar 430.010 nm by the determination of 140 mmol L^{-1} Na^+ in Na-lactate and glucose matrices (1st day)

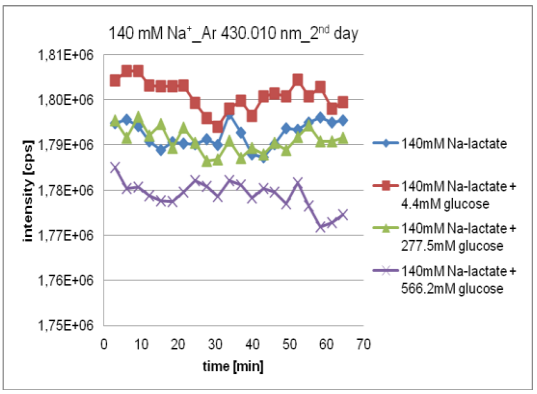

Figure 9-299: The intensity of Ar 430.010 nm by the determination of 140 mmol L^{-1} Na^+ in Na-lactate and glucose matrices (2nd day)

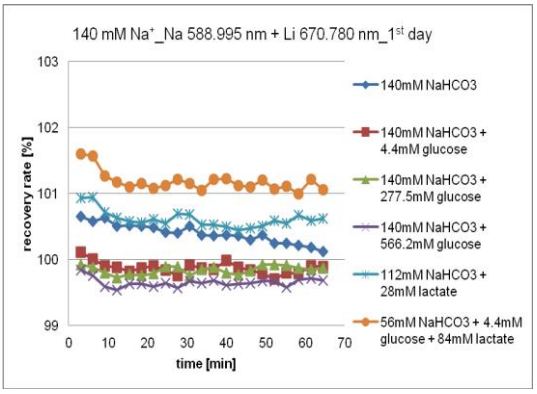

Figure 9-300: Recovery rates by the determination of 140 mmol L^{-1} Na^+ in $NaHCO_3$ solutions with glucose and/or Na-lactate, with Na 588.995 + Li 670.780 nm (1st day)

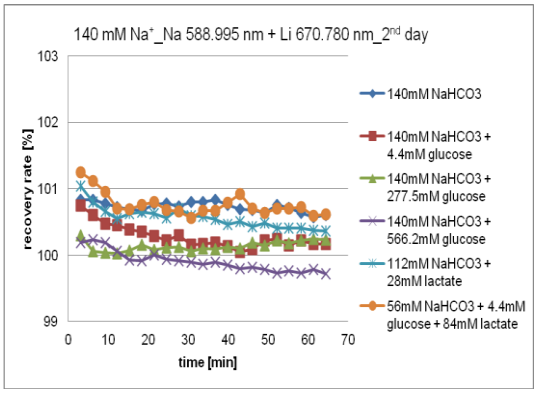

Figure 9-301: Recovery rates by the determination of 140 mmol L^{-1} Na^+ in $NaHCO_3$ solutions with glucose and/or Na-lactate, with Na 588.995 + Li 670.780 nm (2nd day)

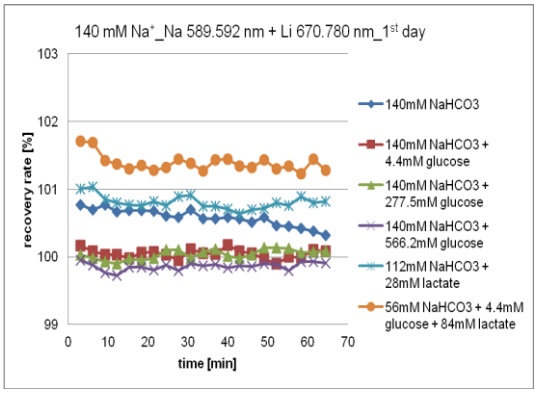

Figure 9-302: Recovery rates by the determination of 140 mmol L^{-1} Na^+ in $NaHCO_3$ solutions with glucose and/or Na-lactate, with Na 589.592 + Li 670.780 nm (1st day)

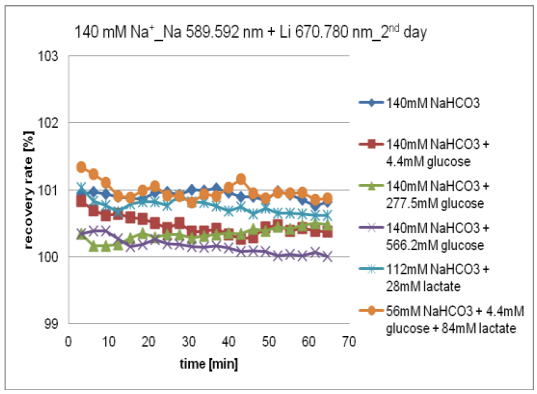

Figure 9-303: Recovery rates by the determination of 140 mmol L^{-1} Na^+ in $NaHCO_3$ solutions with glucose and/or Na-lactate, with Na 589.592 + Li 670.780 nm (2nd day)

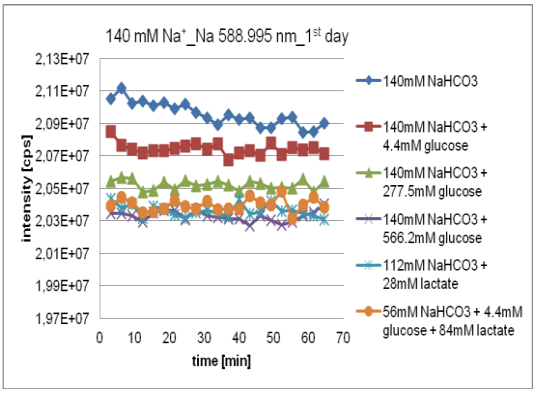

Figure 9-304: The intensity of Na 588.995 nm by the determination of 140 mmol L^{-1} Na^+ in $NaHCO_3$ solutions with glucose and/or Na-lactate (1st day)

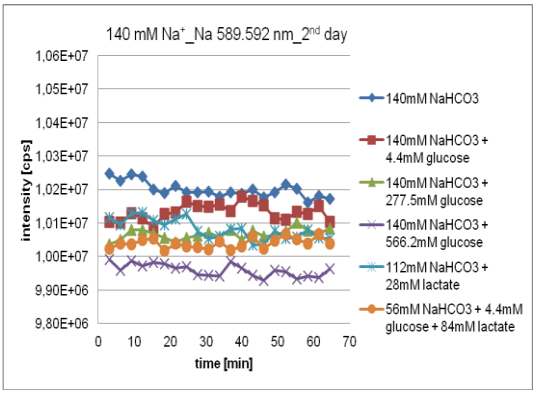

Figure 9-307: The intensity of Na 589.592 nm by the determination of 140 mmol L^{-1} Na^+ in $NaHCO_3$ solutions with glucose and/or Na-lactate (2nd day)

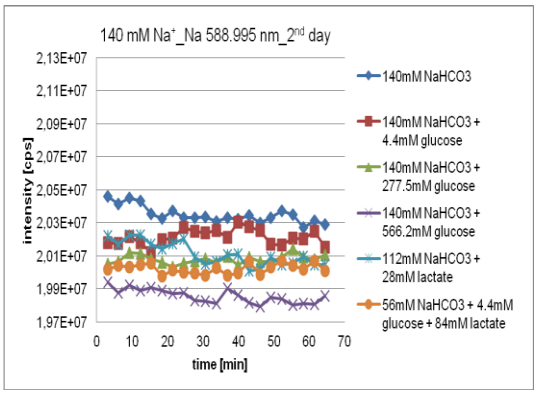

Figure 9-305: The intensity of Na 588.995 nm by the determination of 140 mmol L^{-1} Na^+ in $NaHCO_3$ solutions with glucose and/or Na-lactate (2nd day)

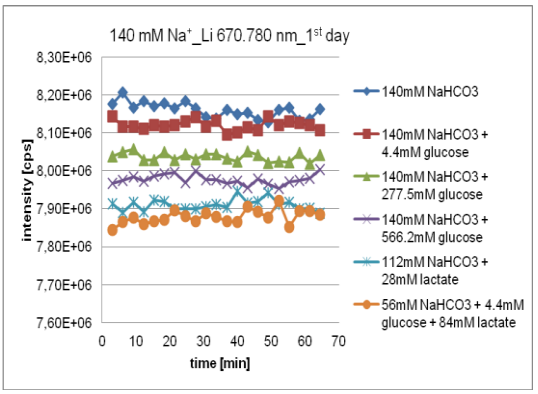

Figure 9-308: The intensity of Li 670.780 nm by the determination of 140 mmol L^{-1} Na^+ in $NaHCO_3$ solutions with glucose and/or Na-lactate (1st day)

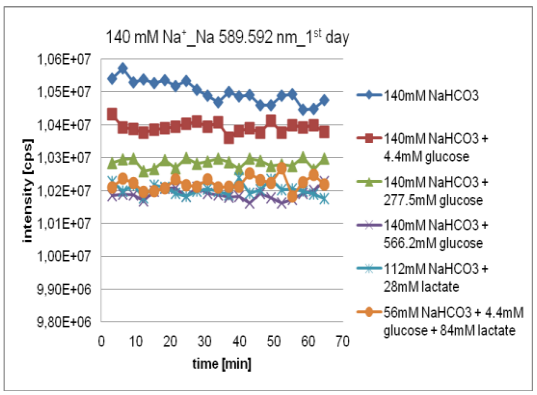

Figure 9-306: The intensity of Na 589.592 nm by the determination of 140 mmol L^{-1} Na^+ in $NaHCO_3$ solutions with glucose and/or Na-lactate (1st day)

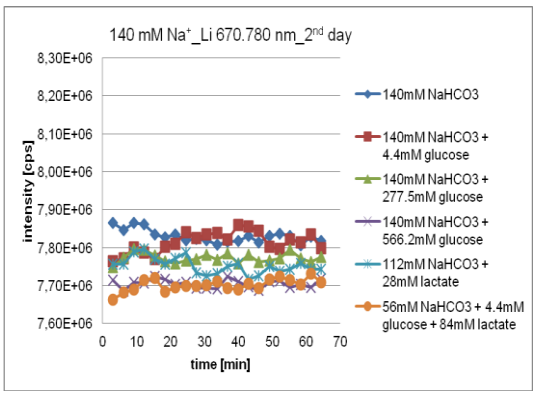

Figure 9-309: The intensity of Li 670.780 nm by the determination of 140 mmol L^{-1} Na^+ in $NaHCO_3$ solutions with glucose and/or Na-lactate (2nd day)

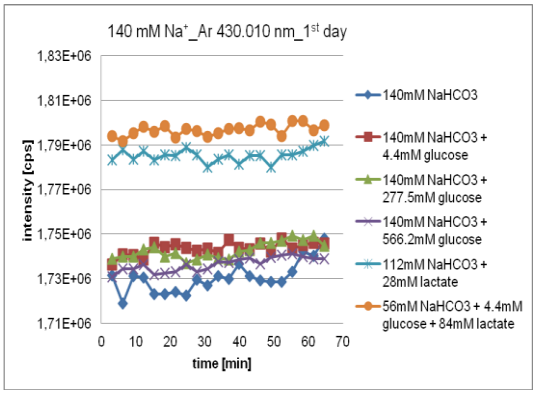

Figure 9-310: The intensity of Ar 430.010 nm by the determination of 140 mmol L^{-1} Na^+ in $NaHCO_3$ solutions with glucose and/or Na-lactate (1st day)

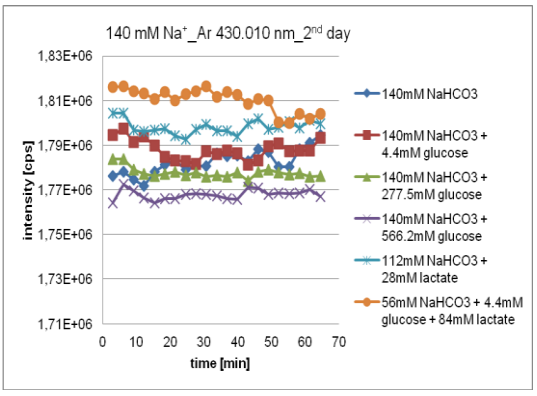

Figure 9-311: The intensity of Ar 430.010 nm by the determination of 140 mmol L^{-1} Na^+ in $NaHCO_3$ solutions with glucose and/or Na-lactate (2nd day)

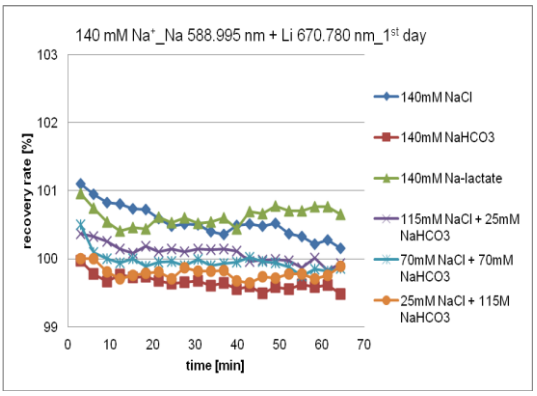

Figure 9-312: Recovery rates by the determination of 140 mmol L^{-1} Na^+ in NaCl, $NaHCO_3$ and Na-lactate solutions, with Na 588.995 + Li 670.780 nm (1st day)

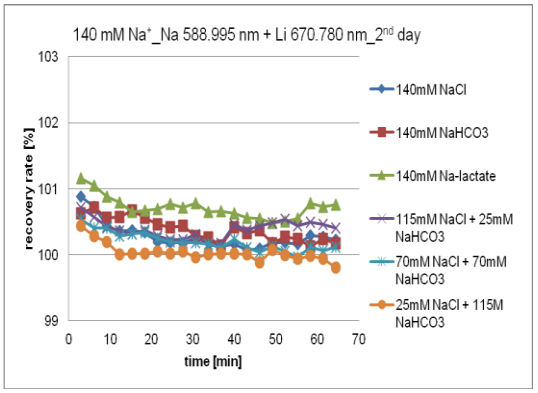

Figure 9-313: Recovery rates by the determination of 140 mmol L^{-1} Na^+ in NaCl, $NaHCO_3$ and Na-lactate solutions, with Na 588.995 + Li 670.780 nm (2nd day)

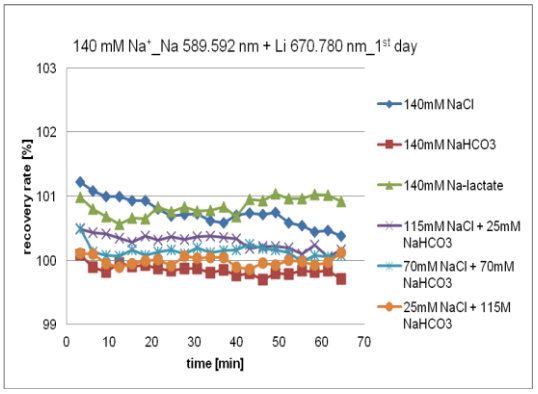

Figure 9-314: Recovery rates by the determination of 140 mmol L^{-1} Na^+ in NaCl, $NaHCO_3$ and Na-lactate solutions, with Na 589.592 + Li 670.780 nm (1st day)

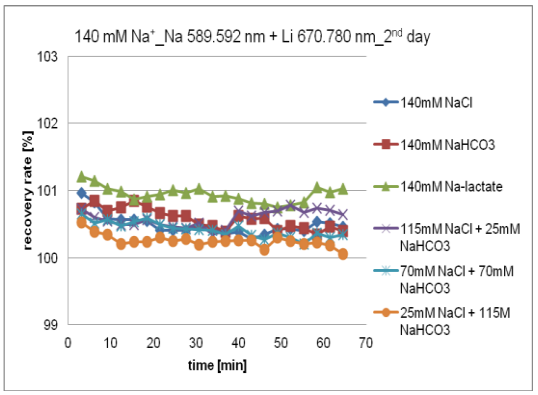

Figure 9-315: Recovery rates by the determination of 140 mmol L^{-1} Na^+ in NaCl, $NaHCO_3$ and Na-lactate solutions, with Na 589.592 + Li 670.780 nm (2nd day)

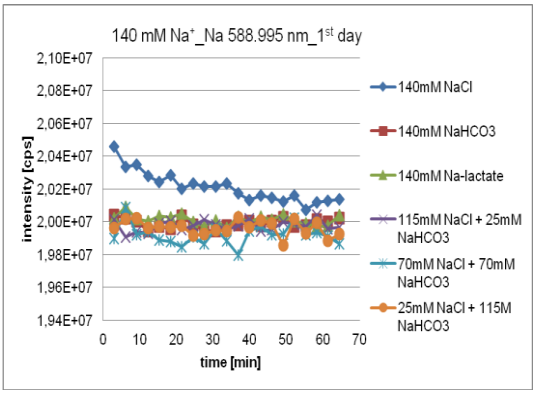

Figure 9-316: The intensity of Na 588.995 nm by the determination of 140 mmol L^{-1} Na^+ in NaCl, $NaHCO_3$ and Na-lactate solutions (1st day)

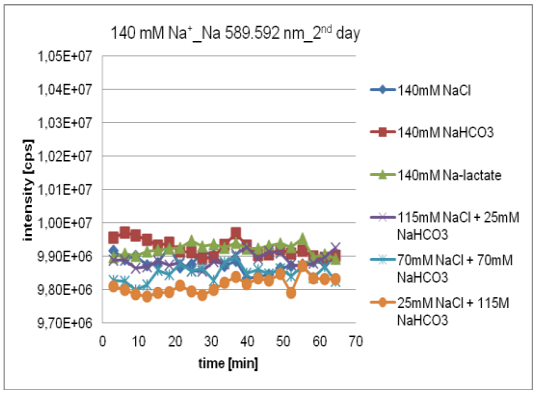

Figure 9-319: The intensity of Na 589.592 nm by the determination of 140 mmol L^{-1} Na^+ in NaCl, $NaHCO_3$ and Na-lactate solutions (2nd day)

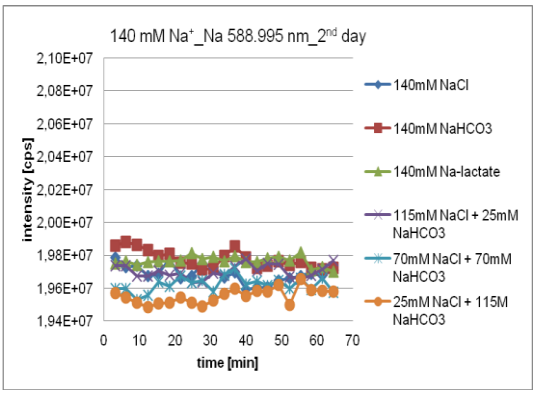

Figure 9-317: The intensity of Na 588.995 nm by the determination of 140 mmol L^{-1} Na^+ in NaCl, $NaHCO_3$ and Na-lactate solutions (2nd day)

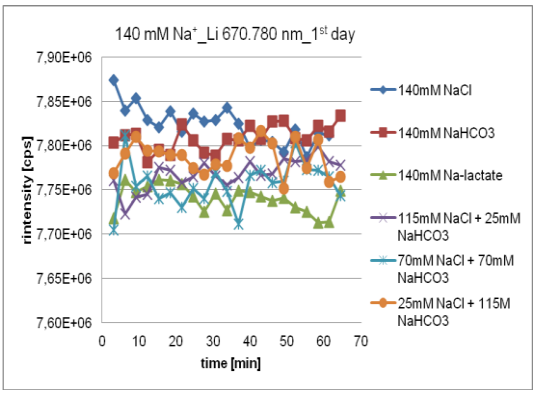

Figure 9-320: The intensity of Li 670.780 nm by the determination of 140 mmol L^{-1} Na^+ in NaCl, $NaHCO_3$ and Na-lactate solutions (1st day)

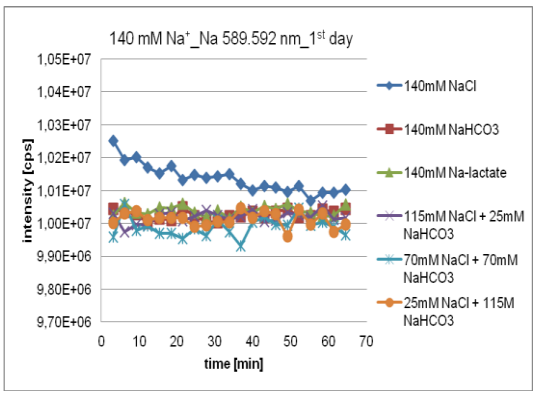

Figure 9-318: The intensity of Na 589.592 nm by the determination of 140 mmol L^{-1} Na^+ in NaCl, $NaHCO_3$ and Na-lactate solutions (1st day)

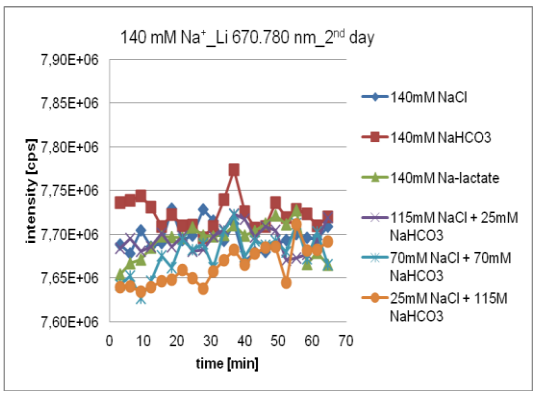

Figure 9-321: The intensity of Li 670.780 nm by the determination of 140 mmol L^{-1} Na^+ in NaCl, $NaHCO_3$ and Na-lactate solutions (2nd day)

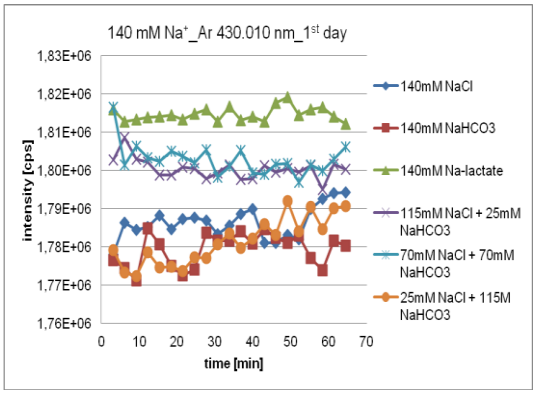

Figure 9-322: The intensity of Ar 430.010 nm by the determination of 140 mmol L^{-1} Na^+ in NaCl, $NaHCO_3$ and Na-lactate solutions (1st day)

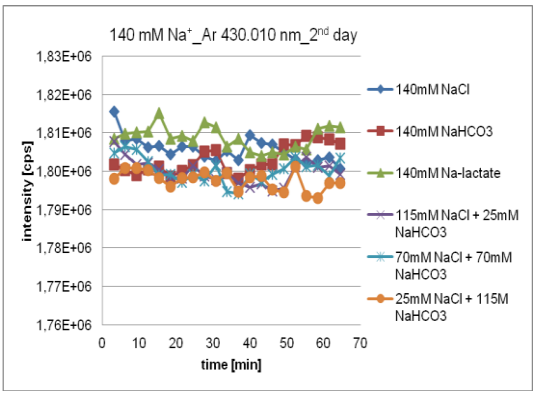

Figure 9-323: The intensity of Ar 430.010 nm by the determination of 140 mmol L^{-1} Na^+ in NaCl, $NaHCO_3$ and Na-lactate solutions (2nd day)

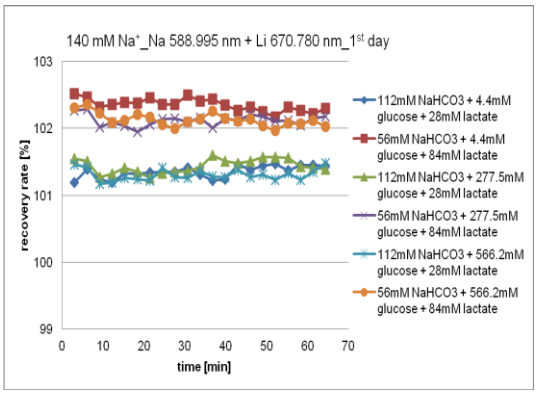

Figure 9-324: Recovery rates by the determination of 140 mmol L^{-1} Na^+ in $NaHCO_3$, Na-lactate and glucose solutions, with Na 588.995 + Li 670.780 nm (1st day)

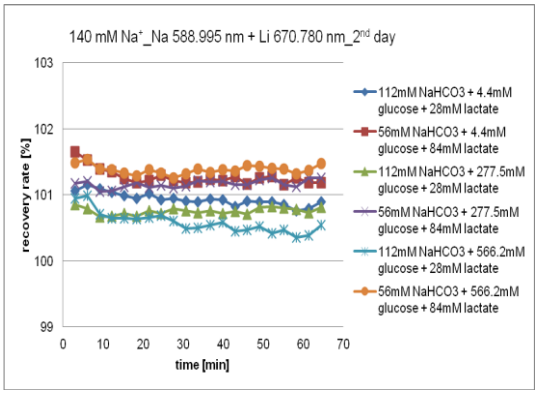

Figure 9-325: Recovery rates by the determination of 140 mmol L^{-1} Na^+ in $NaHCO_3$, Na-lactate and glucose solutions, with Na 588.995 + Li 670.780 nm (2nd day)

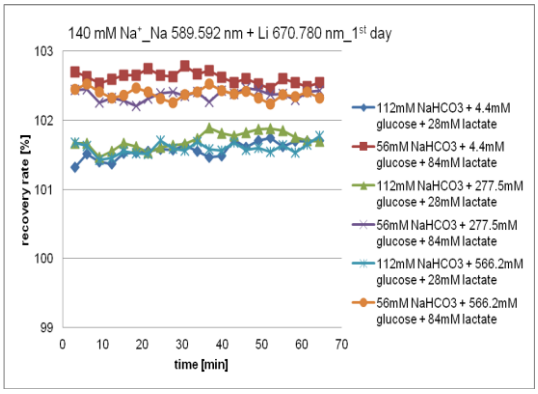

Figure 9-326: Recovery rates by the determination of 140 mmol L^{-1} Na^+ in $NaHCO_3$, Na-lactate and glucose solutions, with Na 589.592 + Li 670.780 nm (1st day)

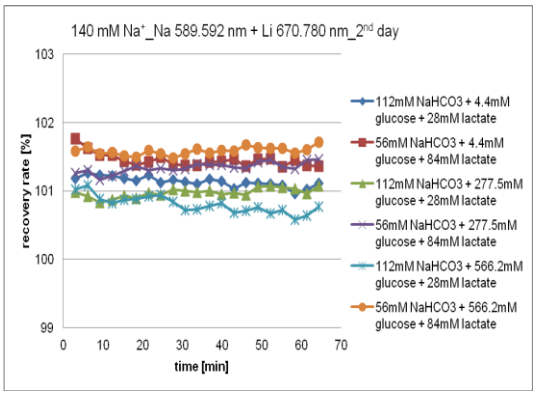

Figure 9-327: Recovery rates by the determination of 140 mmol L^{-1} Na^+ in $NaHCO_3$, Na-lactate and glucose solutions, with Na 589.592 + Li 670.780 nm (2nd day)

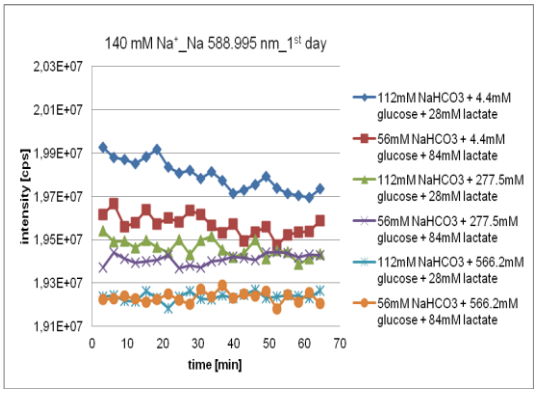

Figure 9-328: The intensity of Na 588.995 nm by the determination of 140 mmol L^{-1} Na^+ in $NaHCO_3$, Na-lactate and glucose solutions (1st day)

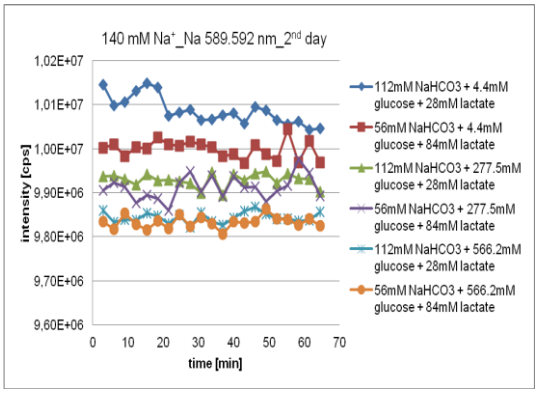

Figure 9-331: The intensity of Na 589.592 nm by the determination of 140 mmol L^{-1} Na^+ in $NaHCO_3$, Na-lactate and glucose solutions (2nd day)

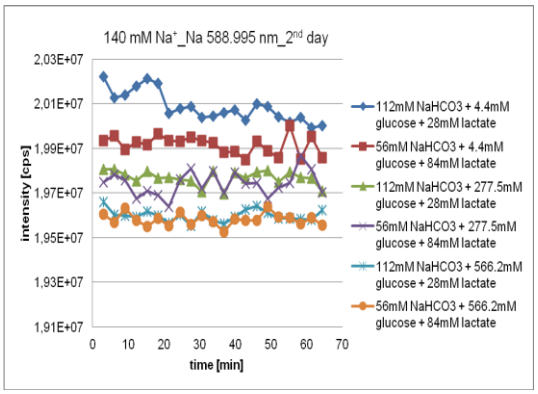

Figure 9-329: The intensity of Na 588.995 nm by the determination of 140 mmol L^{-1} Na^+ in $NaHCO_3$, Na-lactate and glucose solutions (2nd day)

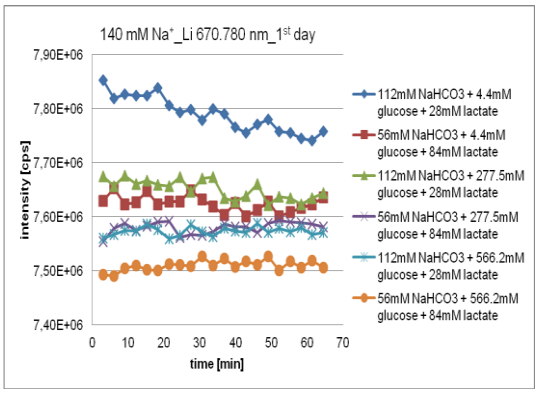

Figure 9-332: The intensity of Li 670.780 nm by the determination of 140 mmol L^{-1} Na^+ in $NaHCO_3$, Na-lactate and glucose solutions (1st day)

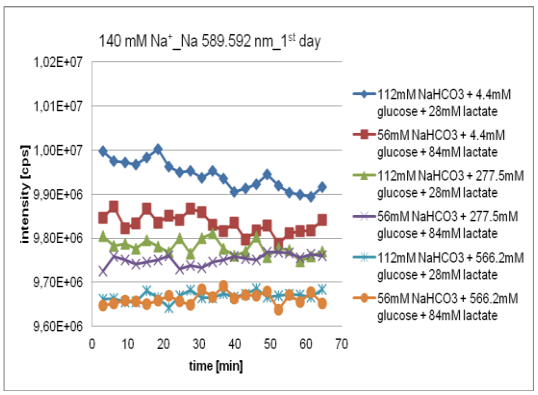

Figure 9-330: The intensity of Na 589.592 nm by the determination of 140 mmol L^{-1} Na^+ in $NaHCO_3$, Na-lactate and glucose solutions (1st day)

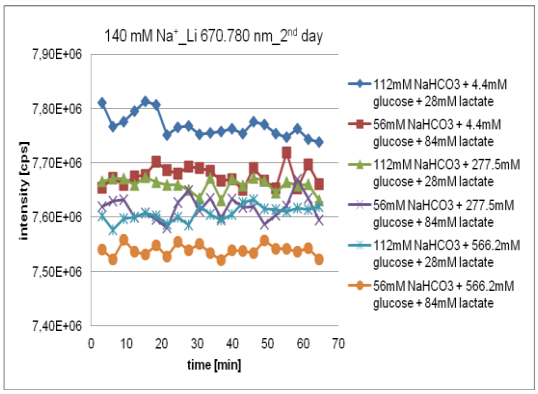

Figure 9-333: The intensity of Li 670.780 nm by the determination of 140 mmol L^{-1} Na^+ in $NaHCO_3$, Na-lactate and glucose solutions (2nd day)

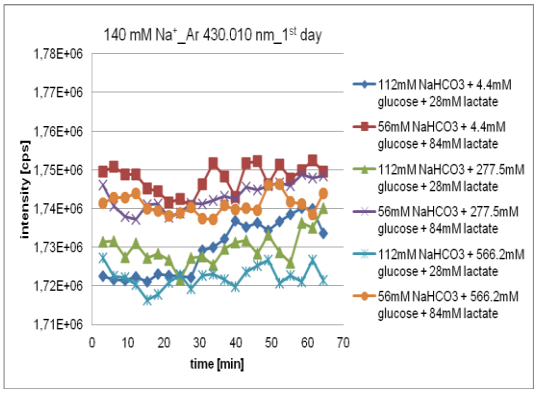

Figure 9-334: The intensity of Ar 430.010 nm by the determination of 140 mmol L^{-1} Na^+ in $NaHCO_3$, Na-lactate and glucose solutions (1st day)

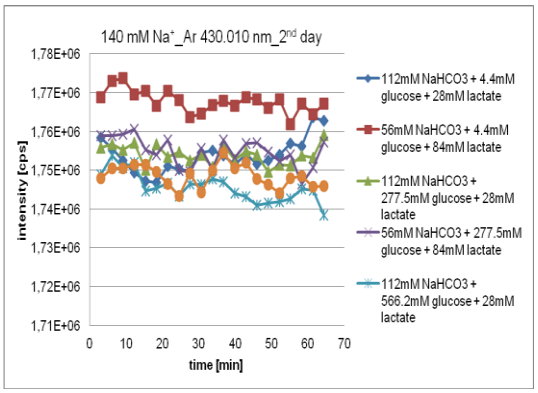

Figure 9-335: The intensity of Ar 430.010 nm by the determination of 140 mmol L^{-1} Na^+ in $NaHCO_3$, Na-lactate and glucose solutions (2nd day)

9.9.2 Attachments on the matrix effects on the determination of the highest sodium concentration (235 mmol L^{-1})

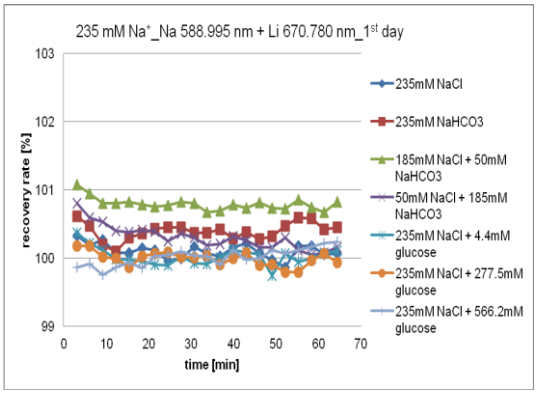

Figure 9-336: Recovery rates by the determination of 235 mmol L^{-1} Na^+ in NaCl, $NaHCO_3$ and glucose solutions, with Na 588.995 + Li 670.780 nm (1st day)

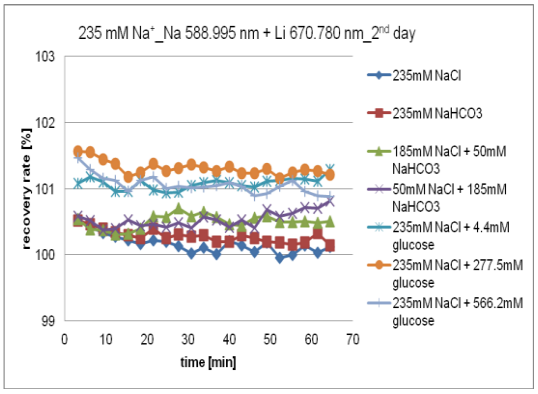

Figure 9-337: Recovery rates by the determination of 235 mmol L^{-1} Na^+ in NaCl, $NaHCO_3$ and glucose solutions, with Na 588.995 + Li 670.780 nm (2nd day)

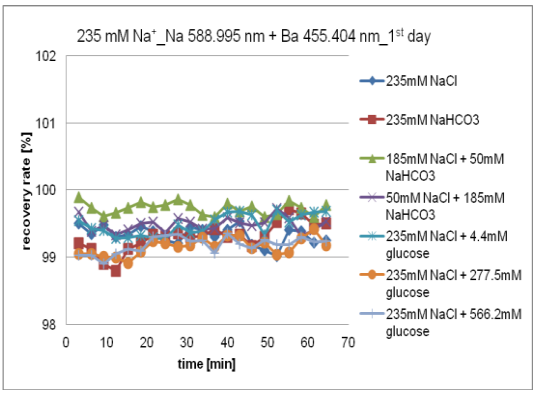

Figure 9-338: Recovery rates by the determination of 235 mmol L^{-1} Na^+ in NaCl, $NaHCO_3$ and glucose solutions, with Na 588.995 + Ba 455.404 (1st day)

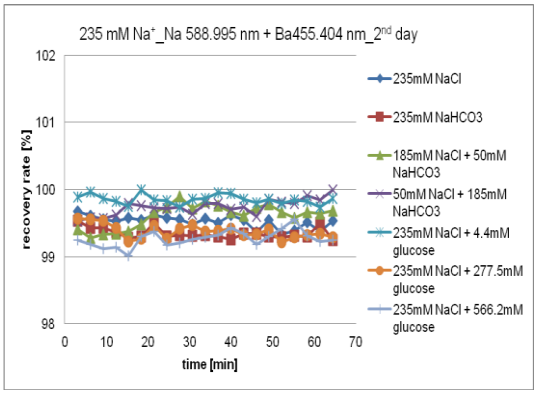

Figure 9-339: Recovery rates by the determination of 235 mmol L^{-1} Na^+ in NaCl, $NaHCO_3$ and glucose solutions, with Na 588.995 + Ba 455.404 (2nd day)

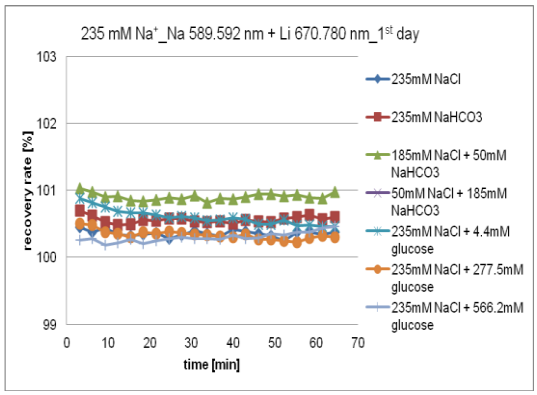

Figure 9-340: Recovery rates by the determination of 235 mmol L^{-1} Na^+ in NaCl, $NaHCO_3$ and glucose solutions, with Na 589.592 + Li 670.780 (1st day)

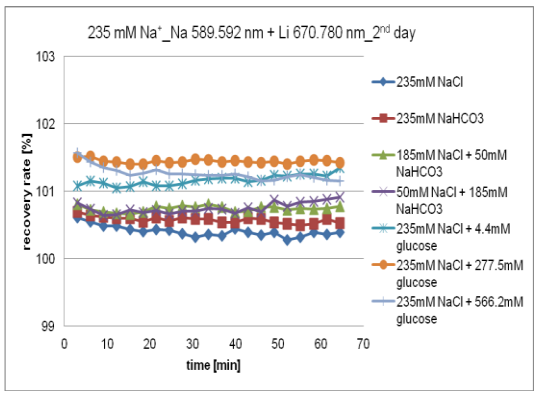

Figure 9-341: Recovery rates by the determination of 235 mmol L^{-1} Na^+ in NaCl, $NaHCO_3$ and glucose solutions, with Na 589.592 + Li 670.780 (2nd day)

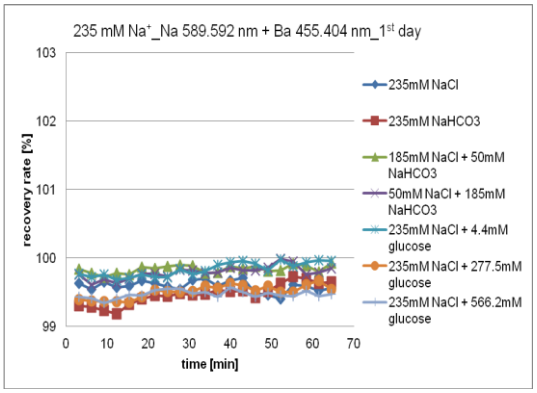

Figure 9-342: Recovery rates by the determination of 235 mmol L^{-1} Na^+ in NaCl, $NaHCO_3$ and glucose solutions, with Na 589.592 + Ba 455.404 (1st day)

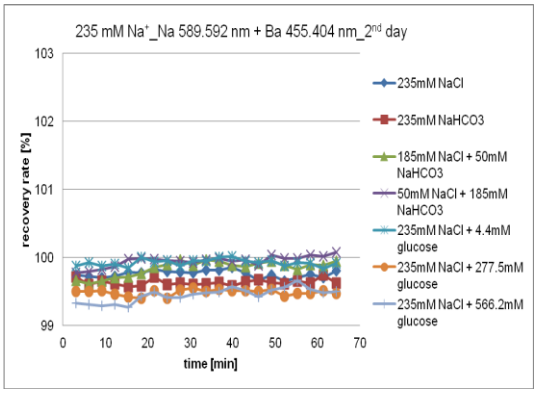

Figure 9-343: Recovery rates by the determination of 235 mmol L^{-1} Na^+ in NaCl, $NaHCO_3$ and glucose solutions, with Na 589.592 + Ba 455.404 (2nd day)

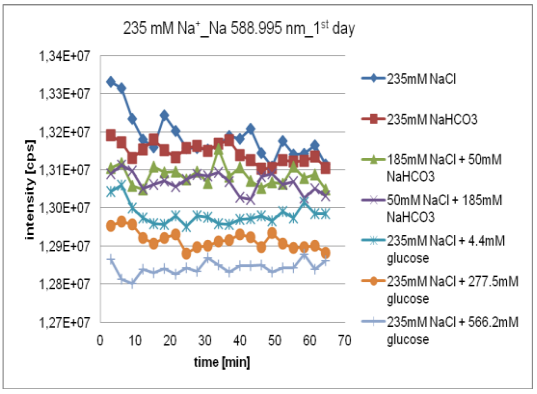

Figure 9-344: The intensity of Na 588.995 nm by the determination of 235 mmol L^{-1} Na^+ in NaCl, $NaHCO_3$ and glucose solutions (1st day)

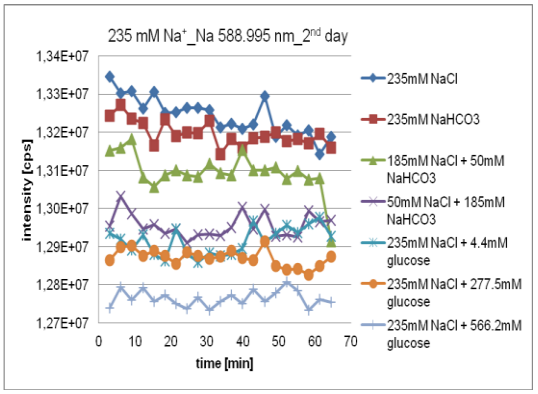

Figure 9-345: The intensity of Na 588.995 nm by the determination of 235 mmol L^{-1} Na^+ in NaCl, $NaHCO_3$ and glucose solutions (2nd day)

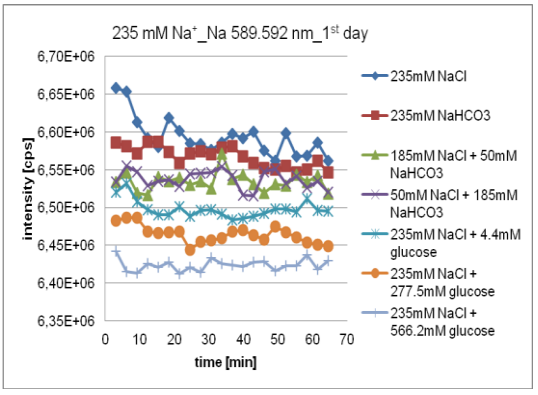

Figure 9-346: The intensity of Na 589-592 nm by the determination of 235 mmol L^{-1} Na^+ in NaCl, $NaHCO_3$ and glucose solutions (1st day)

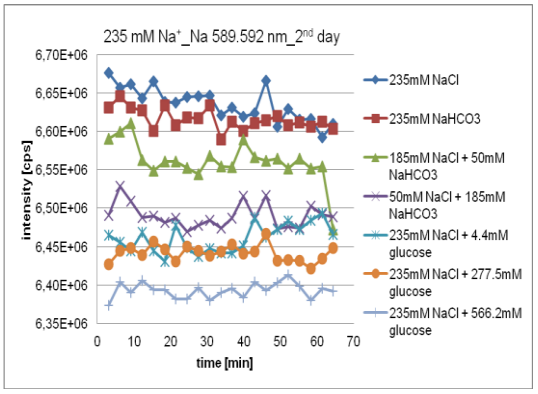

Figure 9-347: The intensity of Na 589-592 nm by the determination of 235 mmol L^{-1} Na^+ in NaCl, $NaHCO_3$ and glucose solutions (2nd day)

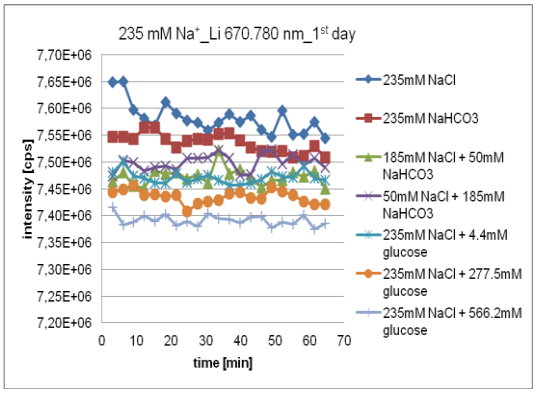

Figure 9-348: The intensity of Li 670.780 nm by the determination of 235 mmol L^{-1} Na^+ in NaCl, $NaHCO_3$ and glucose solutions (1st day)

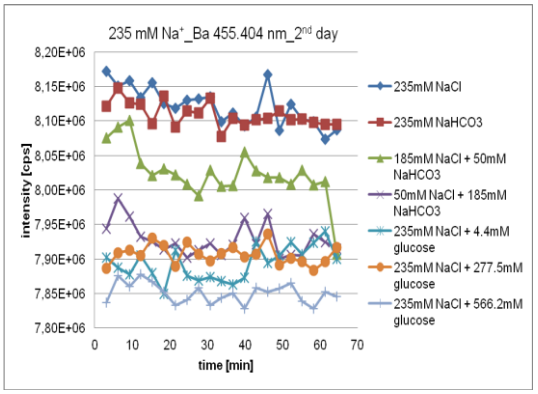

Figure 9-351: The intensity of Ba 455.404 nm by the determination of 235 mmol L^{-1} Na^+ in NaCl, $NaHCO_3$ and glucose solutions (2nd day)

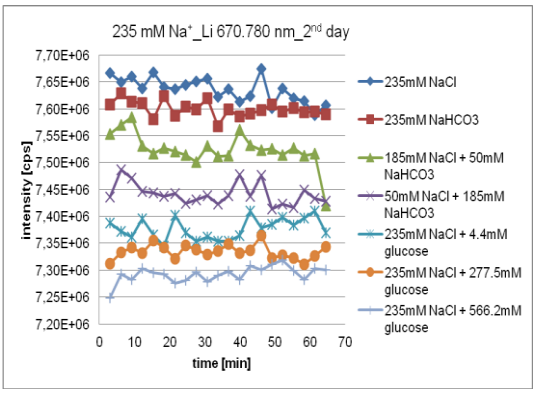

Figure 9-349: The intensity of Li 670.780 nm by the determination of 235 mmol L^{-1} Na^+ in NaCl, $NaHCO_3$ and glucose solutions (2nd day)

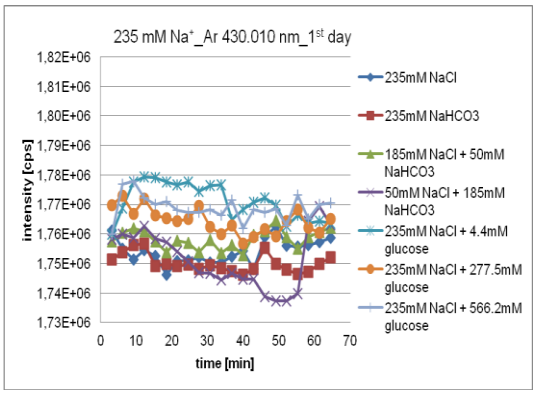

Figure 9-352: The intensity of Ar 430.010 nm by the determination of 235 mmol L^{-1} Na^+ in NaCl, $NaHCO_3$ and glucose solutions (1st day)

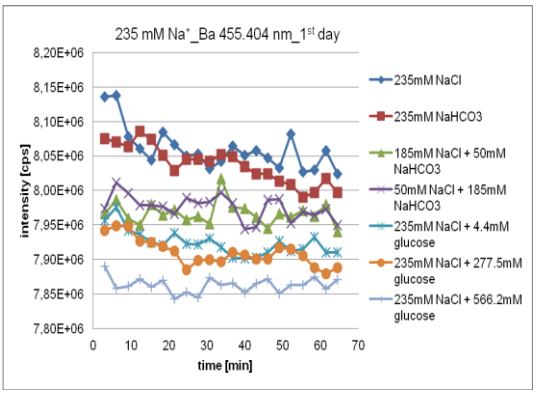

Figure 9-350: The intensity of Ba 455.404 nm by the determination of 235 mmol L^{-1} Na^+ in NaCl, $NaHCO_3$ and glucose solutions (1st day)

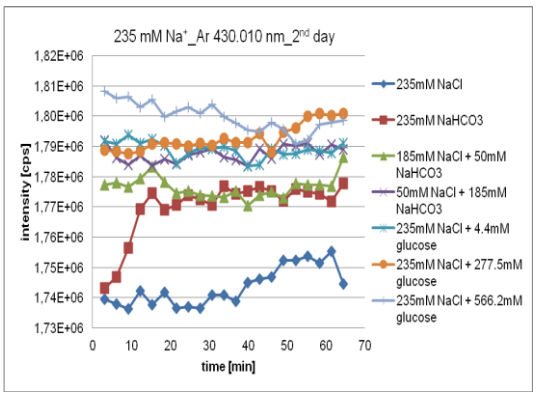

Figure 9-353: The intensity of Ar 430.010 nm by the determination of 235 mmol L^{-1} Na^+ in NaCl, $NaHCO_3$ and glucose solutions (2nd day)

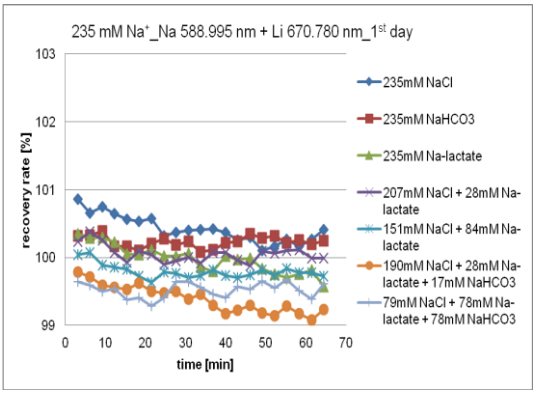

Figure 9-354: Recovery rates by the determination of 235 mmol L^{-1} Na^+ in NaCl, $NaHCO_3$ and Na-lactate solutions, with Na 588.995 + Li 670.780 (1st day)

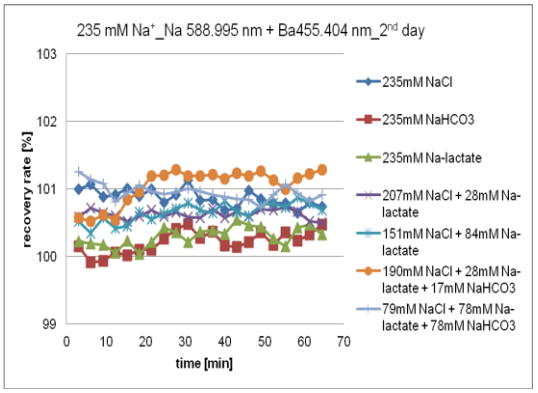

Figure 9-357: Recovery rates by the determination of 235 mmol L^{-1} Na^+ in NaCl, $NaHCO_3$ and Na-lactate solutions, with Na 588.995 + Ba 455.404 (2nd day)

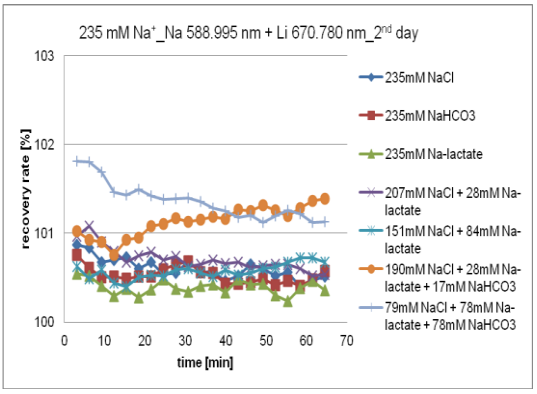

Figure 9-355: Recovery rates by the determination of 235 mmol L^{-1} Na^+ in NaCl, $NaHCO_3$ and Na-lactate solutions, with Na 588.995 + Li 670.780 (2nd day)

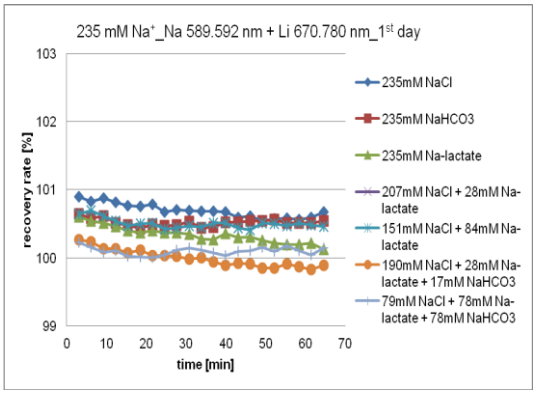

Figure 9-358: Recovery rates by the determination of 235 mmol L^{-1} Na^+ in NaCl, $NaHCO_3$ and Na-lactate solutions, with Na 589.592 + Li 670.780 (1st day)

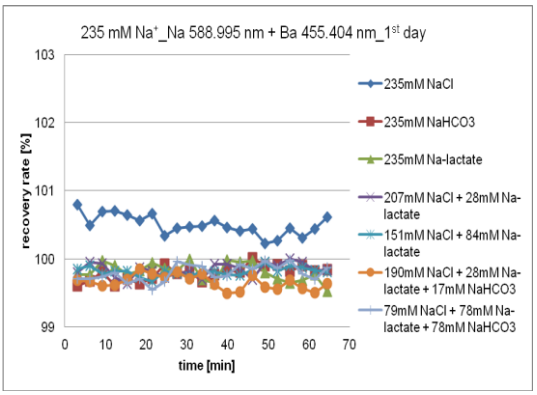

Figure 9-356: Recovery rates by the determination of 235 mmol L^{-1} Na^+ in NaCl, $NaHCO_3$ and Na-lactate solutions, with Na 588.995 + Ba 455.404 (1st day)

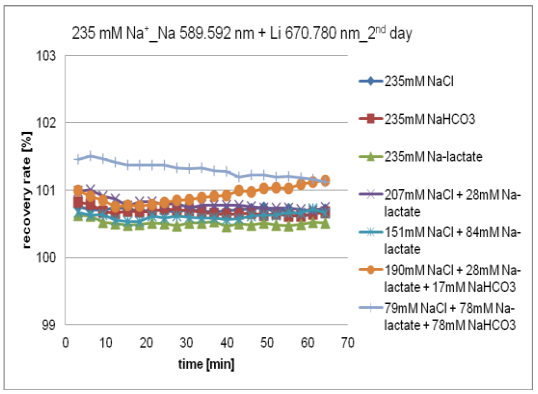

Figure 9-359: Recovery rates by the determination of 235 mmol L^{-1} Na^+ in NaCl, $NaHCO_3$ and Na-lactate solutions, with Na 589.592 + Li 670.780 (2nd day)

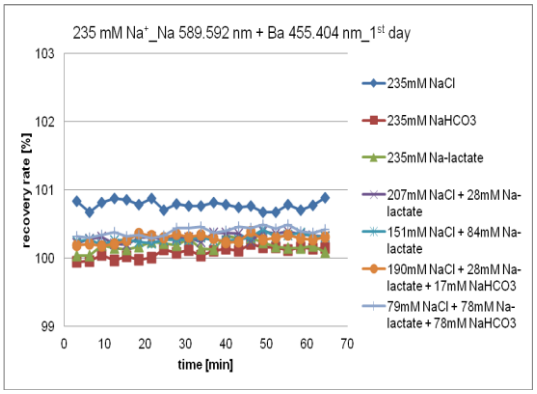

Figure 9-360: Recovery rates by the determination of 235 mmol L^{-1} Na^+ in NaCl, $NaHCO_3$ and Na-lactate solutions, with Na 589.592 + Ba 455.404 (1st day)

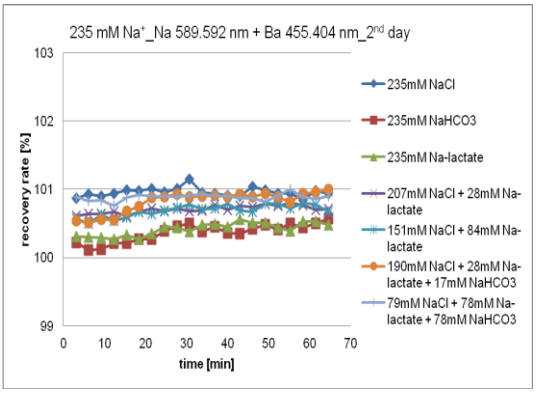

Figure 9-361: Recovery rates by the determination of 235 mmol L^{-1} Na^+ in NaCl, $NaHCO_3$ and Na-lactate solutions, with Na 589.592 + Ba 455.404 (2nd day)

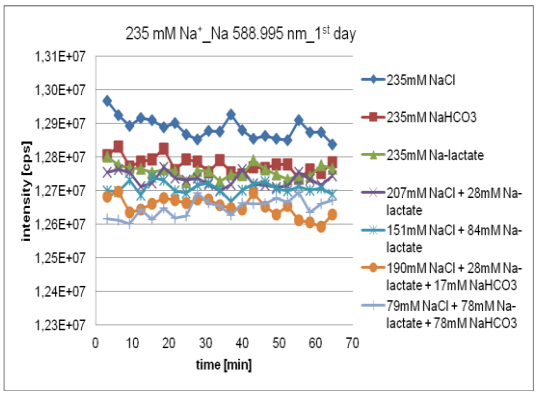

Figure 9-362: The intensity of Na 588.995 nm by the determination of 235 mmol L^{-1} Na^+ in NaCl, $NaHCO_3$ and Na-lactate solutions (1st day)

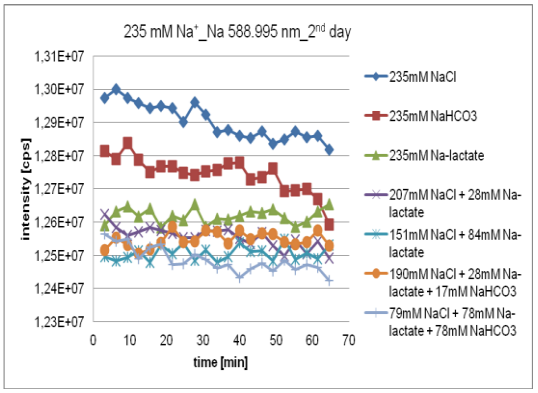

Figure 9-363: The intensity of Na 588.995 nm by the determination of 235 mmol L^{-1} Na^+ in NaCl, $NaHCO_3$ and Na-lactate solutions (2nd day)

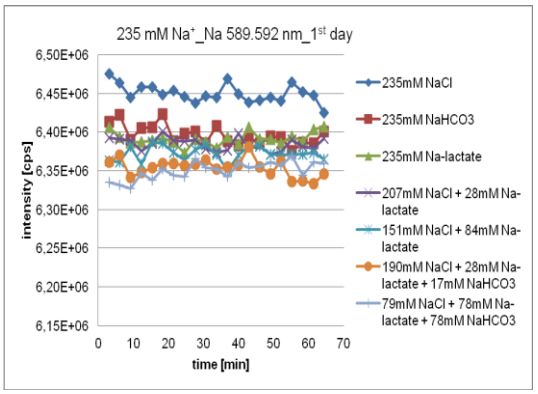

Figure 9-364: The intensity of Na 589.592 nm by the determination of 235 mmol L^{-1} Na^+ in NaCl, $NaHCO_3$ and Na-lactate solutions (1st day)

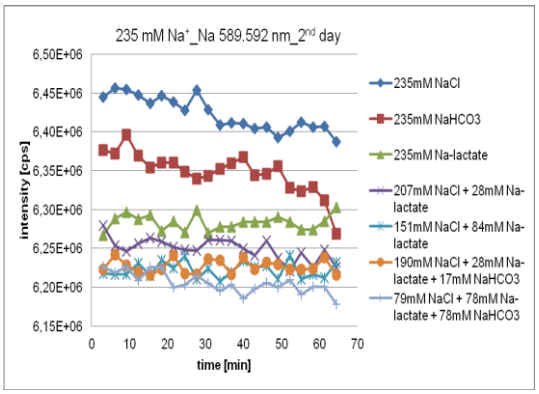

Figure 9-365: The intensity of Na 589.592 nm by the determination of 235 mmol L^{-1} Na^+ in NaCl, $NaHCO_3$ and Na-lactate solutions (2nd day)

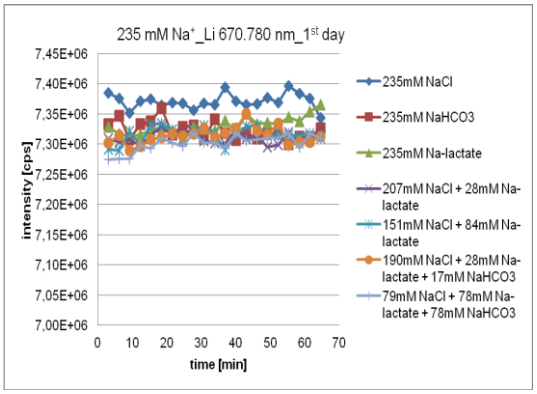

Figure 9-366: The intensity of Li 670.780 nm by the determination of 235 mmol L^{-1} Na^+ in NaCl, $NaHCO_3$ and Na-lactate solutions (1st day)

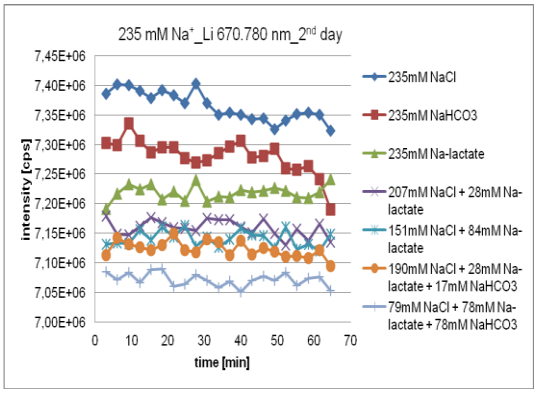

Figure 9-367: The intensity of Li 670.780 nm by the determination of 235 mmol L^{-1} Na^+ in NaCl, $NaHCO_3$ and Na-lactate solutions (2nd day)

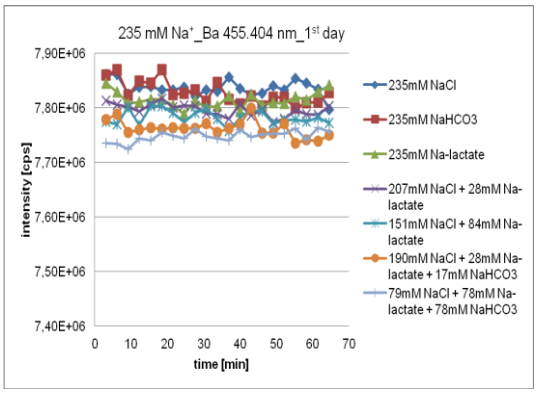

Figure 9-368: The intensity of Ba 455.404 nm by the determination of 235 mmol L^{-1} Na^+ in NaCl, $NaHCO_3$ and Na-lactate solutions (1st day)

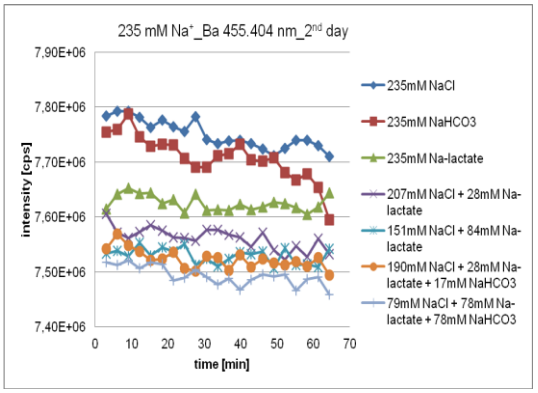

Figure 9-369: The intensity of Ba 455.404 nm by the determination of 235 mmol L^{-1} Na^+ in NaCl, $NaHCO_3$ and Na-lactate solutions (2nd day)

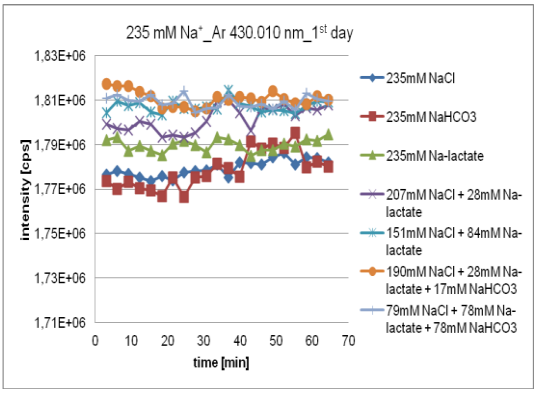

Figure 9-370: The intensity of Ar 430.010 nm by the determination of 235 mmol L^{-1} Na^+ in NaCl, $NaHCO_3$ and Na-lactate solutions (1st day)

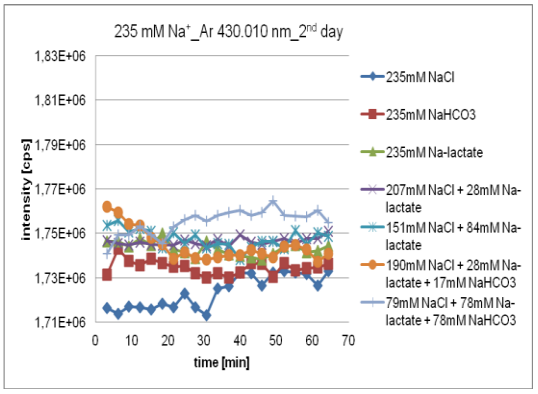

Figure 9-371: The intensity of Ar 430.010 nm by the determination of 235 mmol L^{-1} Na^+ in NaCl, $NaHCO_3$ and Na-lactate solutions (2nd day)

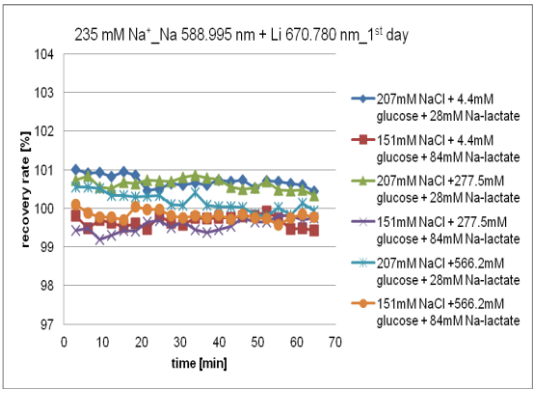

Figure 9-372: Recovery rates by the determination of 235 mmol L^{-1} Na^+ in NaCl, Na-lactate and glucose solutions, with Na 588.995 + Li 670.780 (1st day)

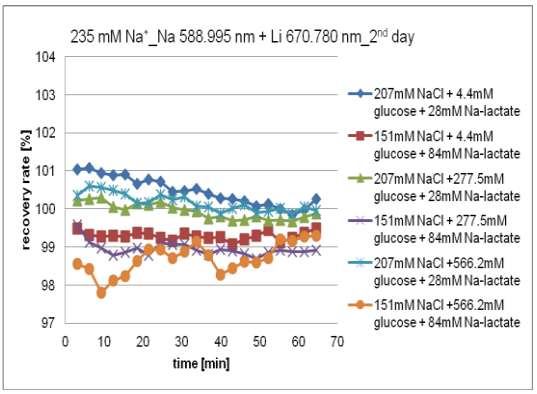

Figure 9-373: Recovery rates by the determination of 235 mmol L^{-1} Na^+ in NaCl, Na-lactate and glucose solutions, with Na 588.995 + Li 670.780 (2nd day)

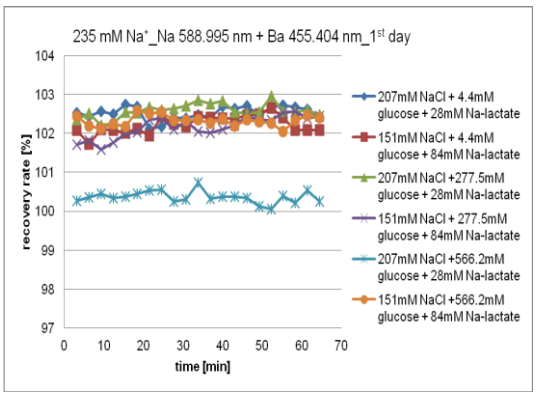

Figure 9-374: Recovery rates by the determination of 235 mmol L^{-1} Na^+ in NaCl, Na-lactate and glucose solutions, with Na 588.995 + Ba 455.404 (1st day)

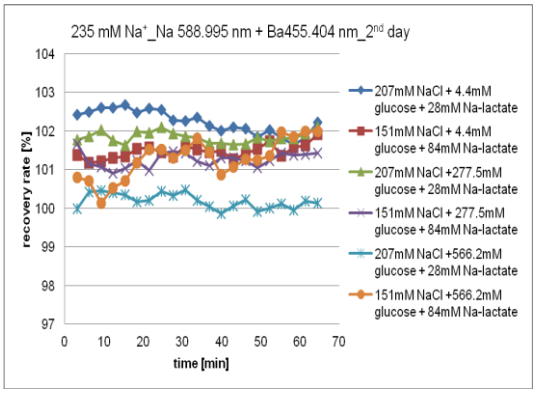

Figure 9-375: Recovery rates by the determination of 235 mmol L^{-1} Na^+ in NaCl, Na-lactate and glucose solutions, with Na 588.995 + Ba 455.404 (2nd day)

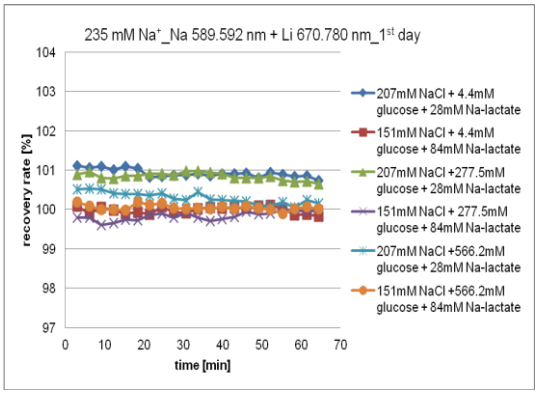

Figure 9-376: Recovery rates by the determination of 235 mmol L^{-1} Na^+ in NaCl, Na-lactate and glucose solutions, with Na 589.592 + Li 670.780 (1st day)

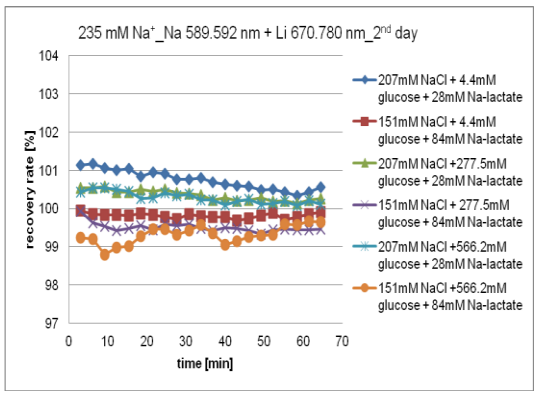

Figure 9-377: Recovery rates by the determination of 235 mmol L^{-1} Na^+ in NaCl, Na-lactate and glucose solutions, with Na 589.592 + Li 670.780 (2nd day)

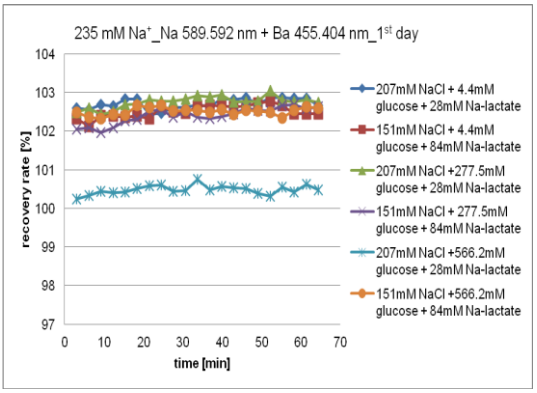

Figure 9-378: Recovery rates by the determination of 235 mmol L^{-1} Na^+ in NaCl, Na-lactate and glucose solutions, with Na 589.592 + Ba 455.404 (1st day)

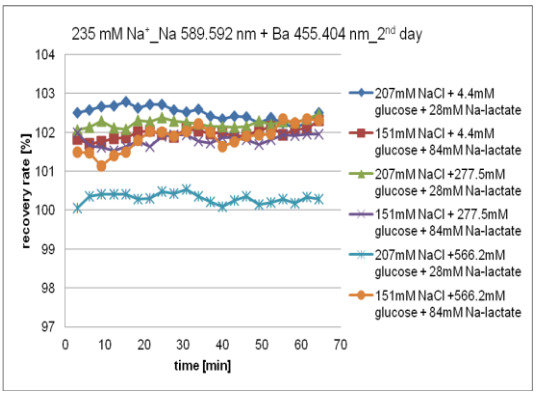

Figure 9-379: Recovery rates by the determination of 235 mmol L^{-1} Na^+ in NaCl, Na-lactate and glucose solutions, with Na 589.592 + Ba 455.404 (2nd day)

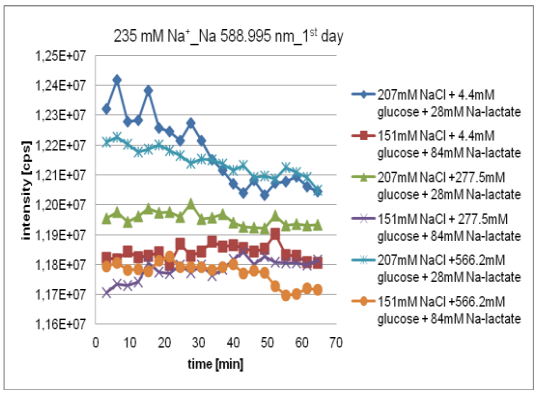

Figure 9-380: The intensity of Na 588.995 nm by the determination of 235 mmol L^{-1} Na^+ in NaCl, Na-lactate and glucose solutions (1st day)

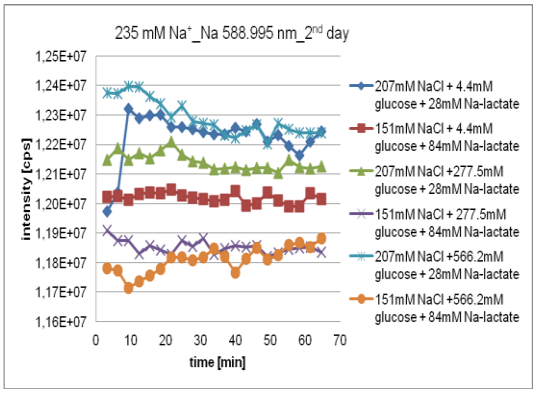

Figure 9-381: The intensity of Na 588.995 nm by the determination of 235 mmol L^{-1} Na^+ in NaCl, Na-lactate and glucose solutions (2nd day)

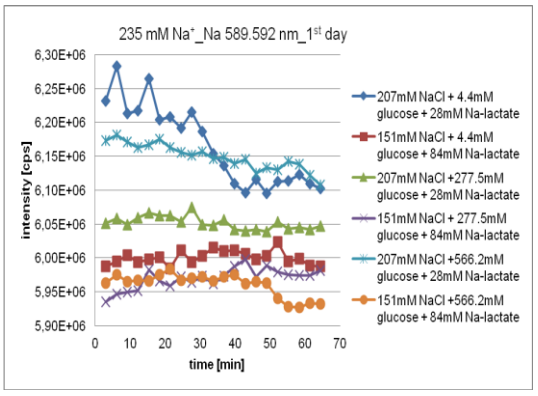

Figure 9-382: The intensity of Na 589.592 nm by the determination of 235 mmol L^{-1} Na^+ in NaCl, Na-lactate and glucose solutions (1st day)

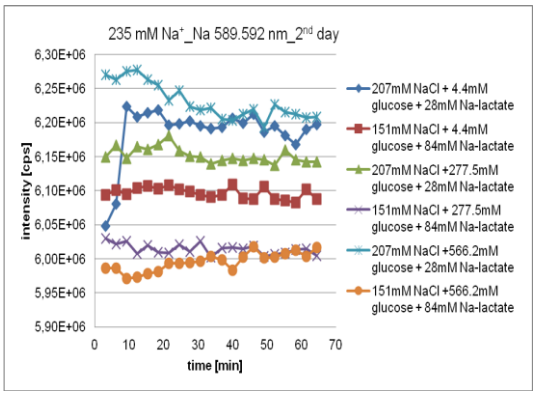

Figure 9-383: The intensity of Na 589.592 nm by the determination of 235 mmol L^{-1} Na^+ in NaCl, Na-lactate and glucose solutions (2nd day)

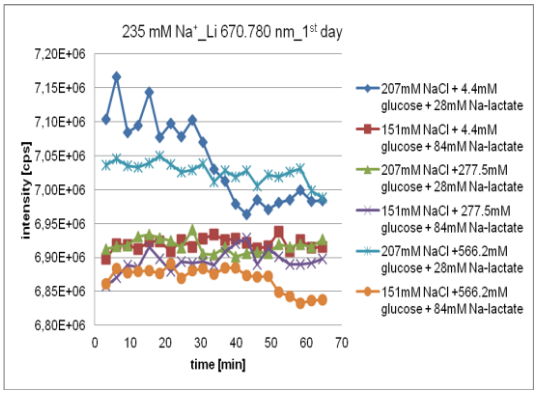

Figure 9-384: The intensity of Li 670.780 nm by the determination of 235 mmol L^{-1} Na^+ in NaCl, Na-lactate and glucose solutions (1st day)

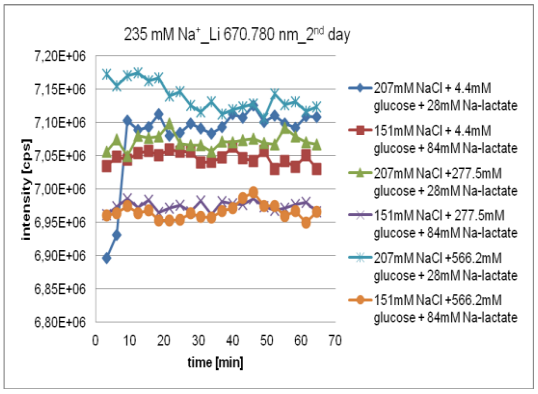

Figure 9-385: The intensity of Li 670.780 nm by the determination of 235 mmol L^{-1} Na^+ in NaCl, Na-lactate and glucose solutions (2nd day)

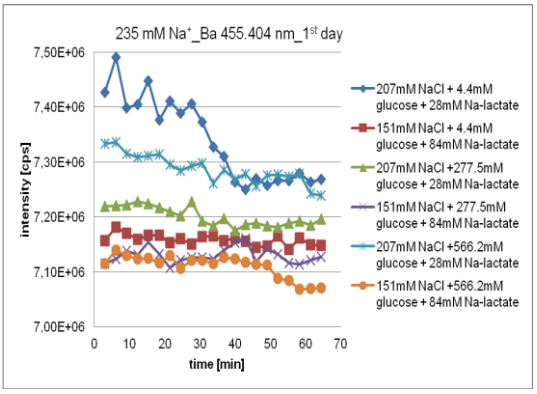

Figure 9-386: The intensity of Ba 455.404 nm by the determination of 235 mmol L^{-1} Na^+ in NaCl, Na-lactate and glucose solutions (1st day)

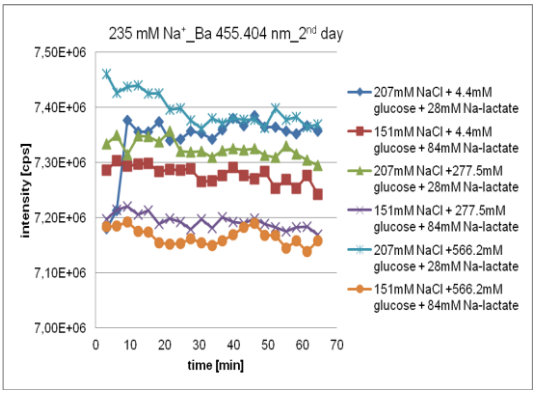

Figure 9-387: The intensity of Ba 455.404 nm by the determination of 235 mmol L^{-1} Na^+ in NaCl, Na-lactate and glucose solutions (2nd day)

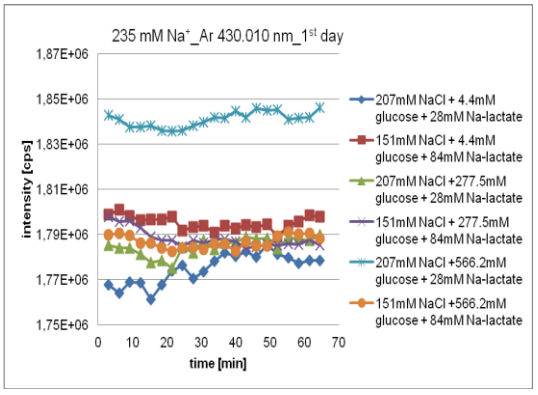

Figure 9-388: The intensity of Ar 430.010 nm by the determination of 235 mmol L^{-1} Na^+ in NaCl, Na-lactate and glucose solutions (1st day)

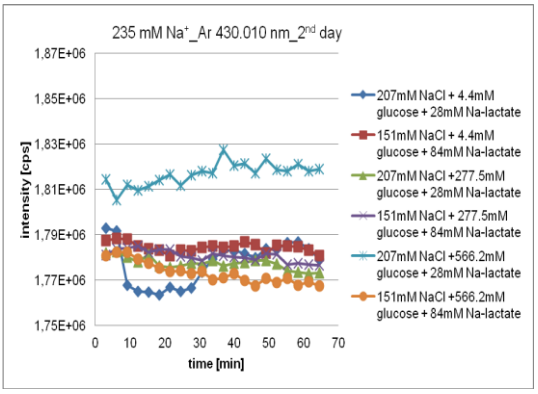

Figure 9-389: The intensity of Ar 430.010 nm by the determination of 235 mmol L^{-1} Na^+ in NaCl, Na-lactate and glucose solutions (2nd day)

9.10 Attachments on the results of the on-line process analysis system

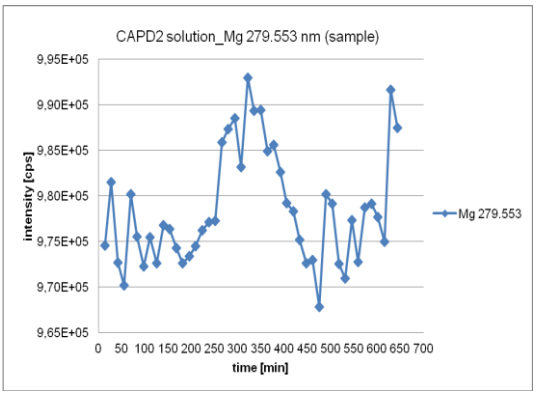

Figure 9-390: The intensity of Mg 279.553 nm by the determination of Na, Ca and Mg in CAPD2 solution, as sample, prepared with the left loop and in the left vessel (see Figure 4-2)

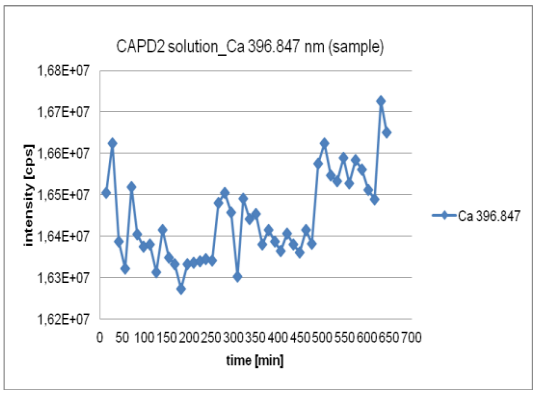

Figure 9-393: The intensity of Ca 396.847 nm by the determination of Na, Ca and Mg in CAPD2 solution, as sample, prepared with the left loop and in the left vessel (see Figure 4-2)

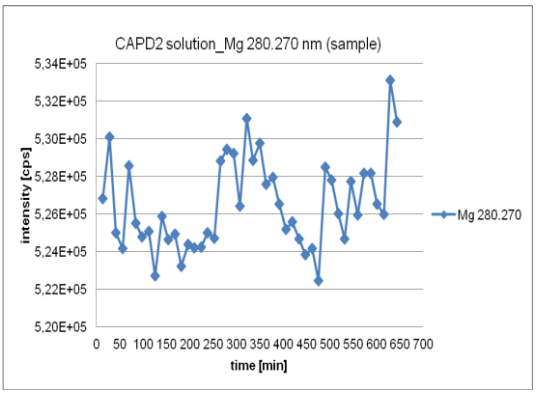

Figure 9-391: The intensity of Mg 280.270 nm by the determination of Na, Ca and Mg in CAPD2 solution, as sample, prepared with the left loop and in the left vessel (see Figure 4-2)

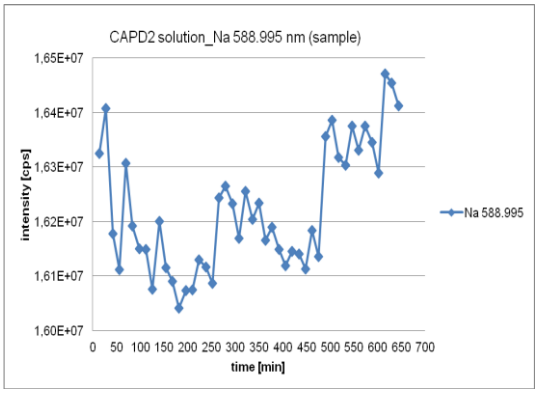

Figure 9-394: The intensity of Na 588.995 nm by the determination of Na, Ca and Mg in CAPD2 solution, as sample, prepared with the left loop and in the left vessel (see Figure 4-2)

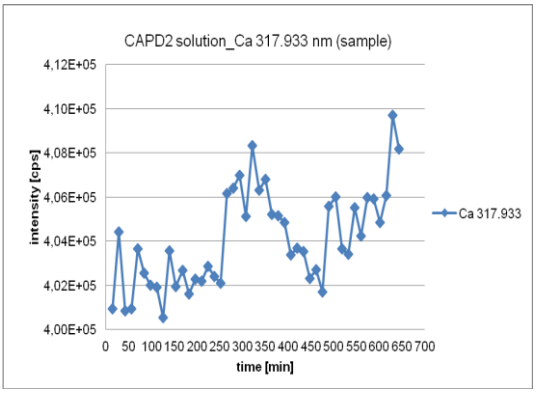

Figure 9-392: The intensity of Ca 317.933 nm by the determination of Na, Ca and Mg in CAPD2 solution, as sample, prepared with the left loop and in the left vessel (see Figure 4-2)

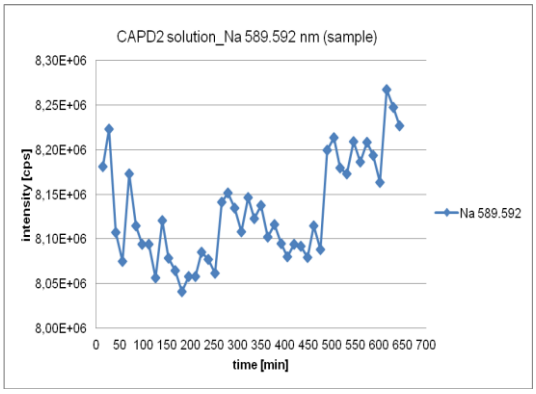

Figure 9-395: The intensity of Na 589.592 nm by the determination of Na, Ca and Mg in CAPD2 solution, as sample, prepared with the left loop and in the left vessel (see Figure 4-2)

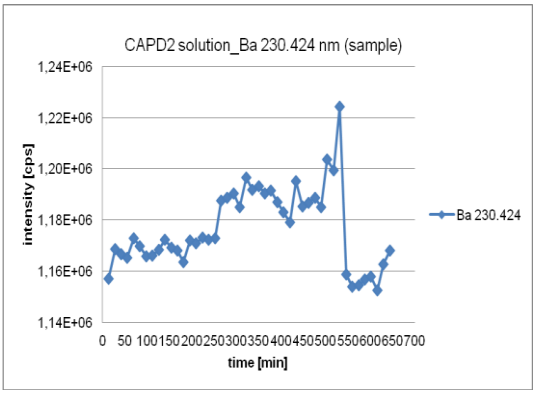

Figure 9-396: The intensity of Ba 230.424 nm by the determination of Na, Ca and Mg in CAPD2 solution, as sample, prepared with the left loop and in the left vessel (see Figure 4-2)

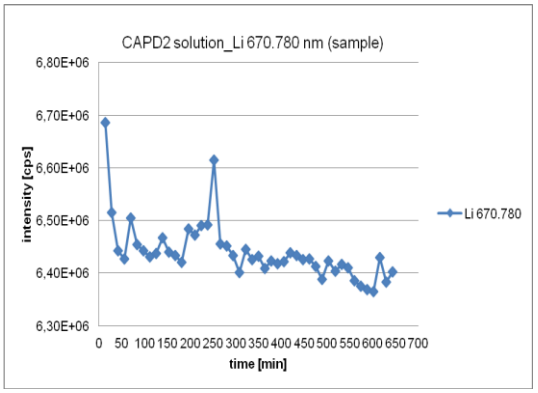

Figure 9-399: The intensity of Li 670.780 nm by the determination of Na, Ca and Mg in CAPD2 solution, as sample, prepared with the left loop and in the left vessel (see Figure 4-2)

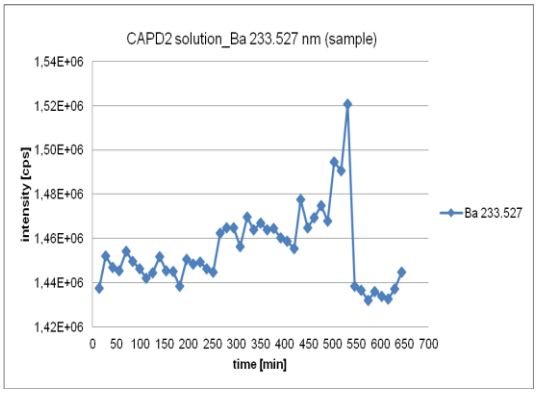

Figure 9-397: The intensity of Ba 3233.527 nm by the determination of Na, Ca and Mg in CAPD2 solution, as sample, prepared with the left loop and in the left vessel (see Figure 4-2)

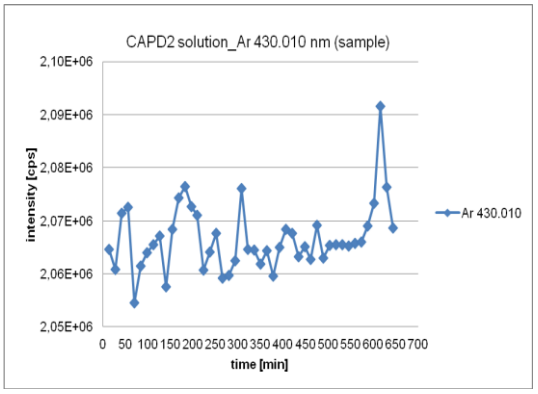

Figure 9-400: The intensity of Ar 430.010 nm by the determination of Na, Ca and Mg in CAPD2 solution, as sample, prepared with the left loop and in the left vessel (see Figure 4-2)

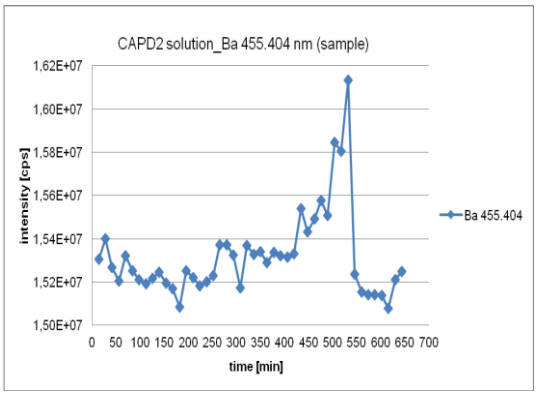

Figure 9-398: The intensity of Ba 455.404 nm by the determination of Na, Ca and Mg in CAPD2 solution, as sample, prepared with the left loop and in the left vessel (see Figure 4-2)

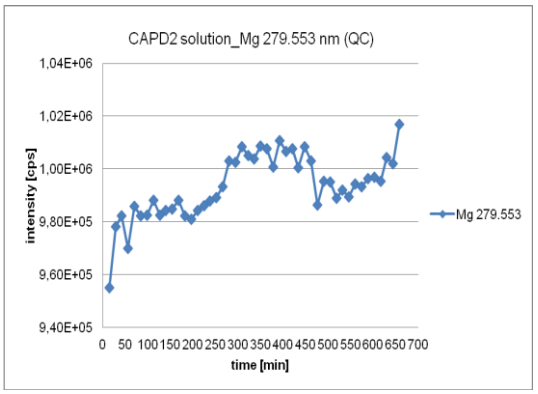

Figure 9-401: The intensity of Mg 279.553 nm by the determination of Na, Ca and Mg in CAPD2 solution, as QC, prepared with the left loop and in the left vessel (see Figure 4-2)

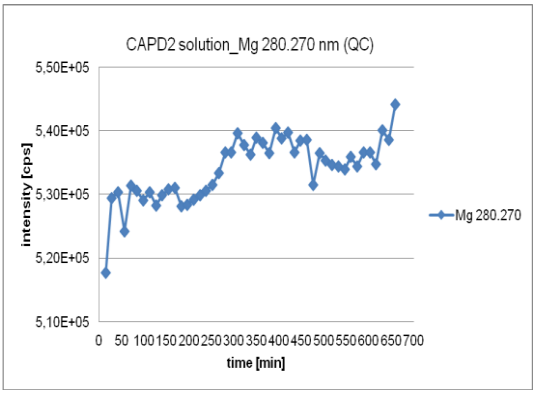

Figure 9-402: The intensity of Mg 280.270 nm by the determination of Na, Ca and Mg in CAPD2 solution, as QC, prepared with the left loop and in the left vessel (see Figure 4-2)

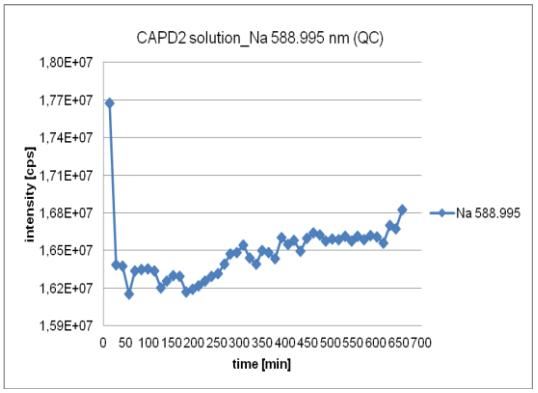

Figure 9-405: The intensity of Na 588.995 nm by the determination of Na, Ca and Mg in CAPD2 solution, as QC, prepared with the left loop and in the left vessel (see Figure 4-2)

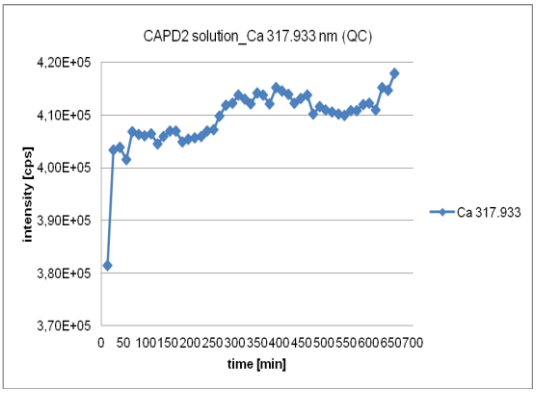

Figure 9-403: The intensity of Ca 317.933 nm by the determination of Na, Ca and Mg in CAPD2 solution, as QC, prepared with the left loop and in the left vessel (see Figure 4-2)

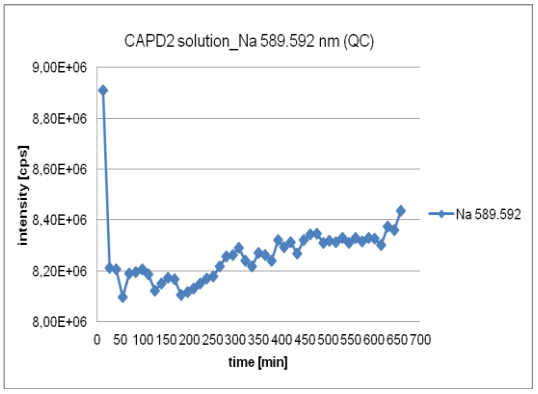

Figure 9-406: The intensity of Na 589.592 nm by the determination of Na, Ca and Mg in CAPD2 solution, as QC, prepared with the left loop and in the left vessel (see Figure 4-2)

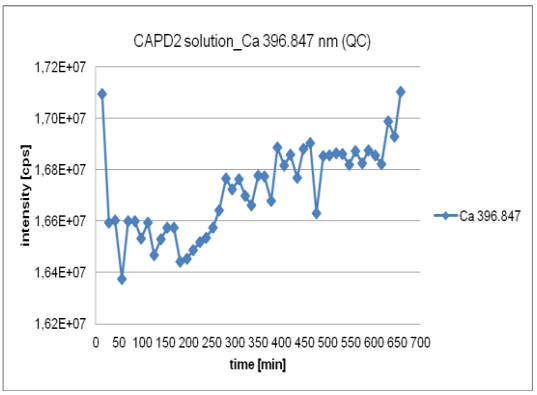

Figure 9-404: The intensity of Ca 396.847 nm by the determination of Na, Ca and Mg in CAPD2 solution, as QC, prepared with the left loop and in the left vessel (see Figure 4-2)

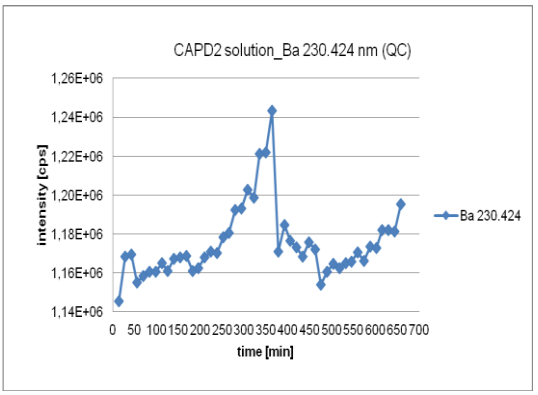

Figure 9-407: The intensity of Ba 230.424 nm by the determination of Na, Ca and Mg in CAPD2 solution, as QC, prepared with the left loop and in the left vessel (see Figure 4-2)

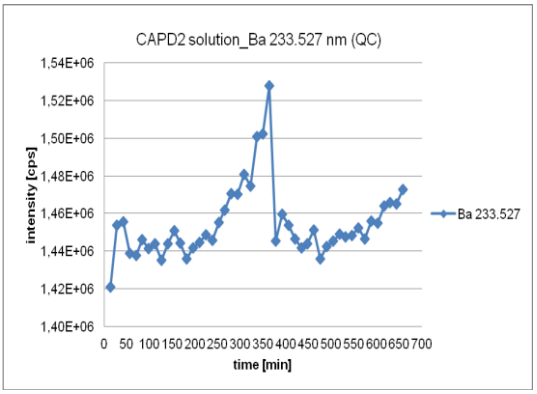

Figure 9-408: The intensity of Ba 233.527 nm by the determination of Na, Ca and Mg in CAPD2 solution, as QC, prepared with the left loop and in the left vessel (see Figure 4-2)

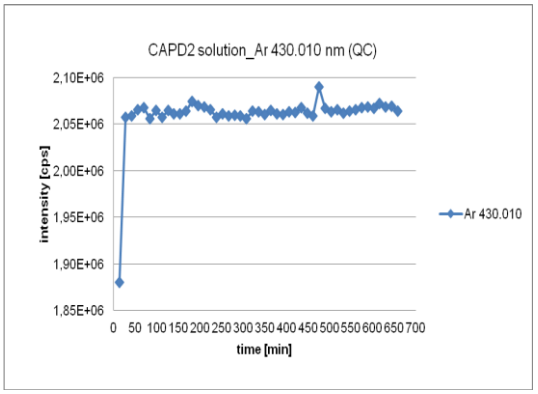

Figure 9-411: The intensity of Ar 430.010 nm by the determination of Na, Ca and Mg in CAPD2 solution, as QC, prepared with the left loop and in the left vessel (see Figure 4-2

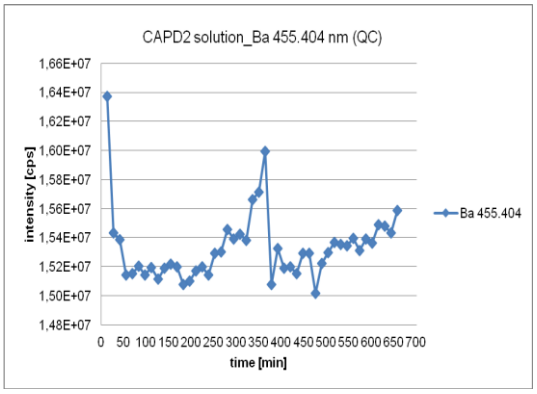

Figure 9-409: The intensity of Ba 455.404 nm by the determination of Na, Ca and Mg in CAPD2 solution, as QC, prepared with the left loop and in the left vessel (see Figure 4-2)

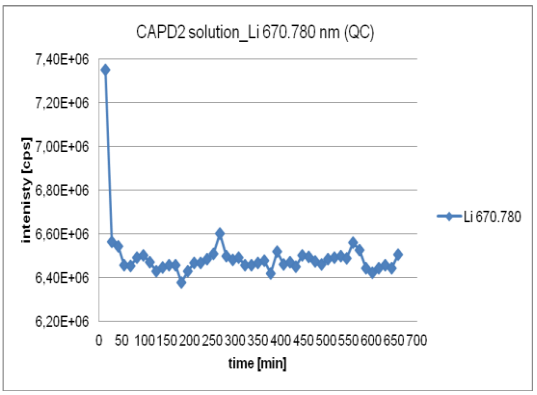

Figure 9-410: The intensity of Li 670.780 nm by the determination of Na, Ca and Mg in CAPD2 solution, as QC, prepared with the left loop and in the left vessel (see Figure 4-2)